



HAL
open science

Lab-in-Droplets platform for glycoprotein biomarker discovery : from instrument conception to diagnostic application

Théo Liénard–Mayor

► **To cite this version:**

Théo Liénard–Mayor. Lab-in-Droplets platform for glycoprotein biomarker discovery : from instrument conception to diagnostic application. Analytical chemistry. Université Paris-Saclay, 2022. English. NNT : 2022UPASF083 . tel-04839399

HAL Id: tel-04839399

<https://theses.hal.science/tel-04839399v1>

Submitted on 16 Dec 2024

HAL is a multi-disciplinary open access archive for the deposit and dissemination of scientific research documents, whether they are published or not. The documents may come from teaching and research institutions in France or abroad, or from public or private research centers.

L'archive ouverte pluridisciplinaire **HAL**, est destinée au dépôt et à la diffusion de documents scientifiques de niveau recherche, publiés ou non, émanant des établissements d'enseignement et de recherche français ou étrangers, des laboratoires publics ou privés.

Lab-in-Droplets platform for glycoprotein biomarker discovery: from instrument conception to diagnostic application

Plate-forme du Lab-en-Gouttes pour la découverte de biomarqueurs de glycoprotéines : de la conception de l'appareil à l'application en diagnostique

Thèse de doctorat de l'université Paris-Saclay

École doctorale n° 571 - sciences chimiques : molécules, matériaux, instrumentation et biosystèmes (2MIB)
Spécialité de doctorat : Chimie
Graduate School : Chimie. Référent : Faculté des Sciences d'Orsay

Thèse préparée à l'**Institut Galien Paris-Saclay** (Université Paris-Saclay, CNRS),
sous la direction de **Myriam TAVERNA**, Professeure,
et le co-encadrement de **Thanh Duc MAI**, Maître de conférences

Thèse soutenue à Paris-Saclay, le 15 décembre 2022, par

Théo LIENARD--MAYOR

Composition du Jury

Membres du jury avec voix délibérative

François FENAILLE Ingénieur-Chercheur,CEA, UPSaclay (SPI, LEMM)	Président
Jacques FATTACCIOLI Professeur, Ecole Normale Supérieure (UMR CNRS 8640)	Rapporteur & Examineur
Marianne FILLET Professeure, Université de Liège (Laboratory for the analysis of Medicines)	Rapporteuse & Examinatrice

Titre : Plate-forme du Lab-en-Gouttes pour la découverte de biomarqueurs de glycoprotéines : de la conception de l'appareil à l'application en diagnostique.

Mots clés : Microfluidique, Lab On Chip, Electrophorèse Capillaire, Glycanes, Biomarqueurs

Résumé : Les glycanes sont des biomarqueurs des maladies congénitales glycosylation (CDG) dont le dépistage est rendu difficile par leur nombre élevé (plus de 150), et les symptômes variés affectant plusieurs organes. Une puissante technique utilisée pour leur analyse est l'électrophorèse capillaire avec détection par fluorescence induite par laser (CE-LiF) mais elle nécessite des étapes de préparation d'échantillon conséquentes.

Dans un premier temps, nous présentons l'élaboration d'une nouvelle méthode CE-LiF basée sur un nouveau tampon à forte force ionique et sur de la préconcentration électrocinétique.

Nous présentons également notre adaptation du protocole de préparation des glycanes en format de gouttes microfluidiques.

Dans un second temps, nous montrons la construction d'un système CE-LiF fait à partir de modules microfluidiques, optiques et d'électrophorèse fait pour la séparation de glycanes. Un deuxième système, imaginé pour être couplé avec le protocole en goutte, est présenté pour l'injection de gouttes de 1 μL d'échantillon non dilué.

Title : Lab-in-Droplets platform for glycoprotein biomarker discovery: from instrument conception to diagnostic application.

Keywords : Microfluidics, Lab On Chip, Capillary Electrophoresis, Glycans, Biomarkers

Abstract : Glycans are biomarkers of congenital disorders of glycosylation (CDG) which are difficult to screen due to their high number (more than 150) and the varied symptoms affecting several organs. A powerful technique used for their analysis is capillary electrophoresis with laser-induced fluorescence detection (CE-LiF) which requires intensive preparation steps.

First, we present the elaboration of a new CE-LiF method based on a new buffer with high ionic strength and electrokinetic preconcentration.

We also present our work in adapting the glycan preparation protocol in a microfluidic droplet format.

Second, we showcase our conception of a CE-LiF system created from microfluidic, optic and electrophoresis modules and made for separation and detection of glycanes. A second system, designed to be coupled with the droplet protocol, is presented for the injection of 1 μL droplet of undiluted sample.

Résumé de la thèse en français

Les maladies congénitales de la glycosylation (CDG) forment un groupe de maladie génétique qui affectent la glycosylation des protéines (sites de glycosylation inoccupés, antennes de glycanes tronquées, changement dans la proportion des glycoforms) qui sont classifiées en types et sous-types et causées par des défauts dans la synthèse et l'attachement des glycanes de glycoprotéines. Leur nombre ne faisant que croître (plus de 150 différentes CDG) et les symptômes variés affectant plusieurs organes rendent leur dépistage compliqué. Pour une CDG donnée, et même au sein d'une même famille, le pronostic et la sévérité de la maladie peut varier. De plus, certaines CDG rares n'ont été diagnostiquées que pour une poignée de patient, ce qui rend difficile pour le praticien d'associer des symptômes et un pronostic. Il n'existe pas de traitement spécifique pour les CDG, les symptômes sont à la place traités pour faciliter la vie du patient. Plusieurs glycoprotéines sont des biomarqueurs pour le dépistage des CDG. Actuellement, le premier biomarqueur analysé pour le dépistage des CDG est la Transferrine (Trf) qui est séparée et analysée par focalisation isoélectrique, suivie d'une immunofixation et d'un marquage. Bien que très résolutive, cette technique est très chronophage (~48h), requiert beaucoup de manipulations, est peu reproductible et peu quantitative. L'analyse des glycoprotéines peut se faire à plusieurs niveaux : glycoprotéine intacte, glycopeptides libérés, glycanes libérés ou les monosaccharides composants les glycanes.

Chaque approche apporte des informations différentes mais complémentaires, et les différentes approches sont parfois utilisées ensemble. Dans ce manuscrit, nous nous intéressons à l'analyse de glycanes libérés dont le changement de structure peut être analysé pour donner des informations sur la micro-hétérogénéité des glycanes: famille de glycanes, structure, et type de liaison glycosidique. L'analyse des glycanes libérés peut être utilisée pour obtenir des informations pour le diagnostic et possiblement différencier des sous-types de CDG. Une technique de choix pour l'analyse des glycanes est l'électrophorèse capillaire avec détection par fluorescence induite par laser (CE-LiF). C'est une technique puissante, versatile, résolutive et très sensitive. L'analyse de glycane par CE-LiF nécessite des étapes de préparation d'échantillon, en premier lieu pour libérer les glycanes des glycoprotéines, puis pour attacher un fluorophore aux glycanes pour qu'ils puissent être détectés. Malgré cela, certains glycanes qui pourraient donner des informations cruciales pour le dépistage de CDG ne sont pas présents en quantité suffisante et sont difficilement détectables. L'objectif de cette thèse est de développer des nouvelles approches pour améliorer la détection des glycanes et se base sur deux approches complémentaires.

La première approche vise à améliorer la méthode d'analyse des glycanes par CE-LiF. Dans un premier temps, nous avons amélioré les conditions d'analyse en utilisant un nouveau tampon d'électrolyse à très forte force ionique basé sur des espèces organiques peu chargées. Grâce à la haute force ionique du tampon, la sensibilité de la détection a été augmentée tout en conservant une résolution suffisante comparé à la méthode standard. Notre nouveau tampon a également été utilisé pour faire de la préconcentration électrocinétique, ce qui a permis d'augmenter la sensibilité de notre méthode par un facteur d'environ 150. Dans un deuxième temps, le protocole de libération et de marquage des glycanes pour l'analyse par CE-LiF a été adapté en format de gouttes microfluidiques. Notre approche est basée sur la technologie des pinces magnétiques qui permet de faire de l'extraction solide-liquide de nos glycanes dans des gouttes microfluidiques. Nous avons pu augmenter l'efficacité du marquage par un facteur 2, réduire la consommation de réactifs par un facteur 10, réduire le temps d'opérations d'un facteur 3 et traiter des échantillons complexes de sérums humains de manière automatisée.

Notre deuxième approche a pour but d'améliorer l'instrumentation de CE-LiF et de construire des systèmes adaptés et complémentaires avec notre nouvelle méthodologie pour l'analyse de glycanes. Dans un premier temps, nous avons construit un système à base de modules microfluidiques, optiques et d'électrophorèse. Ce système peut être construit de manière standardisée dans n'importe quel environnement sans avoir besoin d'équipements ou de connaissances spécifiques et présente une alternative aux machines CE commerciales. Nous montrons la séparation et l'analyse avec ce système d'échantillons d'oligosaccharides standards avec une robustesse satisfaisante. Dans un deuxième temps, nous présentons un deuxième système CE désigné pour être couplé avec notre nouvelle approche pour le traitement des glycanes en goutte. Dans ce système, la goutte de 1 μL d'échantillon de glycanes fluorescent est amené en face d'un capillaire classique grâce à une interface microfluidique pour y être injecté sans être dilué (avec la méthode CE classique, l'échantillon est suspendu dans au moins 10 μL d'eau) ce qui permettra une meilleure sensibilité lors de l'analyse de glycanes.

En conclusion, ces travaux contribuent à l'amélioration du dépistage des CDG en améliorant deux aspects complémentaires : méthodologie et instrumentation.

Acknowledgments

First and foremost, my thanks go to my PhD supervisors, Professor Myriam Taverna and Doctor Thanh Duc Mai. Thanks to their teaching and guidance I was able to learn a lot during these 3 years. Thank you for your kindness, optimism, and patience. You helped me through the most difficult times of the thesis when I thought I could not do it. I am grateful for my time spent in your lab.

I thank the members of the jury: Professor Marianne Fillet, Professor Jacques Fattaccioli and Doctor François Fenaille for accepting to examine my thesis. Thank you for your availability. I also thank Professor Stéphanie Descroix for being the external member of my thesis committee and following up on my project throughout the years.

I want to thank Doctor Arnaud Bruneel for his collaboration and his help regarding the CDG part of the thesis. Thank you for your kindness, enthusiasm, and fruitful discussions.

I also thank Professor Peter C. Hauser and his student Doctor Jasmine S. Furter for their collaboration and providing a homemade LiF system for our Lego CE.

Thanks to Professor András Guttman for receiving me in his lab in Debrecen and for his collaboration regarding the glycan sample treatment protocol part of the thesis. Thanks also to his student for their warm welcome and their teachings during my stay.

Thank you to the members of the French start-up Inorevia Doctor Amel Bendali, Camille Soucies and Doctor David Gosselin for providing and assisting us with a custom Magelia machine for our experiments.

I would like to thank the other permanent members of my team PNAS (Proteins and Nanotechnology in Analytical Sciences) for three years of mentoring and friendship. Thank you, Doctor Thuy Tran-Maignan, for your precious teachings on glycochemistry. Thank you, Professor Claire Smadja for interesting conversations. And thank you both for your kindness. Thank you to previous team member Sylvie Liu for always laughing and smiling in the lab.

Thank you to Marie-Claud, Sylvie Z., Patricia, Fatiha, Maria and Orane for their invaluable assistance in helping me face the French administration.

I am grateful to the other students of PNAS for more than three years together, nice meals and conversations shared together. Special thanks to Camille Bricteux who was an intern working with me on the glycan droplet protocol for her persistence, dedication and for keeping on smiling when experiments were not going how we wanted them to. Thanks to Doctor Bin Yang, for many interesting conversations both friendly and scientific. Thank you to all the other students: Minh, Emilie, Etienne, Seray, Ayoub, Gregory, Van Thanh, Joanie, Cécile, Clara, Charlotte, Hakima, Sameh, Delaram and Mathilde.

Thank you to all the PNAS members for many cakes and celebrations shared over the years.

Thank you to the members of the Physical Pharmacy team of our unit for their teachings and assistance when I joined them to teach first years of medical studies. Thank you, Professor

Florence Agnely, for welcoming me in the teaching team, Doctor Nicolas Huang for precious assistance for both theoretical and experimental teachings, and Doctor Sandrine Geiger and Doctor Ghazlene Mekhloufi for their assistance for experimental teachings.

Thank you to all my friends from Villebon, Orsay, Grenoble, Bordeaux and Paris for their support and times spent together during difficult years. I am grateful for our friendship and look forward to many more years together.

Many thanks to my parents for supporting me during my studies, making it possible for me to study far from home and allowing me to come back home when things did not go the way I had hoped. Thank you for always being there for me, I am grateful. Thank you to all the Liénard--Mayors, the Liénards, the Mayors, the Chartiers and the Gillets for their presence and support.

Finally, thank you to Solweig for supporting me through all this while also going through her thesis. It has been a challenging time in our life, but I am grateful for your presence, support, advice, and love.

This manuscript is dedicated to my grandparents: Louis and Denise Mayor.

Curriculum Vitae

Education :

- **M.Sc. Fundamental physics at Université Paris-Saclay** Specialized in Microfluidics at Institut Pierre Gilles de Gennes.
- **Ph.D. at Université Paris-Saclay** Microfluidics and Analytical Chemistry, Institut Galien Paris-Saclay.

Oral communications:

- “A new concept for modular CE with LIF detection: A highlight with glycans analysis”, 36th International Symposium on Microscale Separations and Bioanalysis (**MSB2020**), online.
- “Lab-in-droplet: From glycan sample treatment toward diagnostic screening of congenital disorders of glycosylation”, 38th International Symposium on Microscale Separations and Bioanalysis (**MSB2022**), Liège, Belgium.

Publications:

- Liénard-Mayor, T., Bricteux, C., Bendali, A., Tran, N.-T., Bruneel, A., Taverna, M., & Mai, T. D. (2022). Lab-in-droplet: From glycan sample treatment toward diagnostic screening of congenital disorders of glycosylation. *Analytica Chimica Acta*, 1221, 340150.
DOI: <https://doi.org/10.1016/j.aca.2022.340150>
- Liénard-Mayor, T., Taverna, M., Descroix, S., & Mai, T. D. (2021). Droplet-interfacing strategies in microscale electrophoresis for sample treatment, separation and quantification: A review. *Analytica Chimica Acta*, 1143, 281–297.
DOI: <https://doi.org/10.1016/j.aca.2020.09.008>
- Liénard-Mayor, T., Yang, B., Tran, N. T., Bruneel, A., Guttman, A., Taverna, M., & Mai, T. D. (2021). High sensitivity capillary electrophoresis with fluorescent detection for glycan mapping. *Journal of Chromatography A*, 1657.
DOI: <https://doi.org/10.1016/j.chroma.2021.462593>.
- Liénard-Mayor, T., Furter, J. S., Taverna, M., Pham, H. V., Hauser, P. C., & Mai, T. D. (2020). Modular instrumentation for capillary electrophoresis with laser induced fluorescence detection using plug-and-play microfluidic, electrophoretic and optic modules. *Analytica Chimica Acta*, 1135, 47–54.
DOI: <https://doi.org/10.1016/j.aca.2020.08.025>

Teaching:

- Experimental teachings for 2nd and 4th year Pharmacy students.
- Physics tutorials for 1st year medical students.
- 128h in two years.

List of abbreviations

μTAS	Micro Total Analysis Systems
ACN	Acetonitrile
AD	Alzheimer's Disease
ADCC	Antibody-Dependent Cellular Cytotoxicity
AGP	α ₁ -acid glycoprotein
ALGx	Asparagine Linked Glycosylation
apoC-III	Apolipoprotein C-III
APTS	1-aminopyrene-3,6,8-trisulfonic acid
AQC	Aminoquinolyl-N-hydroxysuccinimidyl carbamate
ASGPR	Asialoglycoprotein receptor
Asn	Asparagine
BGE	Background Electrolyte
C4D	Capacitively-Coupled Contactless Conductivity Detectors
CDG	Congenital Disorders of glycosylation
CDT	Carbohydrate Deficient Transferrins
CDT%	Carbohydrate Deficient Trf percentage value
CE	Capillary Electrophoresis
CE-LiF	Capillary Electrophoresis with Laser induced Fluorescence detection
CGE	Capillary Gel Electrophoresis
COOH	Carboxyl
CZE	Capillary Zone Electrophoresis
DAQ	Data Acquisition
Dol-P-P	Dolichyl Pyrophosphate
DP	Degree of Polymerization
EOF	Electroosmotic Flow
EPO	Erythropoietin
ER	Endoplasmic Reticulum
ESI	Electrospray Ionization
Fuc	Fucose
Gal	Galactose
GalNAc	N- acetylgalactosamine
GBP	Glycan-Binding Protein
Glc	Glucose
GlcNAc	N- acetylglucosamine
GU	Glucose Unit
HILIC	Hydrophilic Interaction Liquid Chromatography
Hp	Haptoglobin
HPLC	High Performance Liquid Chromatography
HVPS	High Voltage Power Supply
IEF	Isoelectric Focusing
IgG	Immunoglobulin G
IMER	Immobilized Enzyme Reactor
LC	Liquid Chromatography
LiF	Laser induced Fluorescence
LVSEP	Large Volume Sample Stacking with Electroosmotic Pump

LVSS	Large Volume Sample Stacking
MALDI	Matrix-Assisted Laser Desorption/Ionization
Man	Mannose
MCE	microchip capillary electrophoresis
MD ladder	Maltooligosaccharide ladder
MEMS	Microelectro-Mechanical Systems
MS	Mass Spectrometry
NaBH ₃ CN	Sodium Cyanoborohydride
nanoLC	nano Liquid Chromatography
nESI-MS	nano Electrospray Ionization Mass Spectrometry
Neu5Ac	N- acetylneuraminic acid
OST	Oligosaccharyltransferase
PDMS	Polydimethylsiloxane
PEEK	Polyether Ether Ketone
PEO	Polyethylene Oxide
PGC	Porous Graphitized Carbon
PGC-LC	Porous Graphitized Carbon Liquid Chromatography
PNGase F	peptide-N ₄ -(N acetyl-beta-glucosaminyl) asparagine-amidase
PVA	Polyvinyl Alcohol
SAW	Surface Acoustic Wave
SDS	Sodium Dodecyl Sulfate
SDS-PAGE	Sodium Dodecyl Sulphate-Polyacrylamide Gel Electrophoresis
Ser	Serine
SNFG	Symbol Nomenclature for Glycans
SPE	Solid Phase Extraction
Tf	Serum Transferrin
THF	Tetrahydrofuran
Thr	Threonine
TOF	Time-of-Flight
uHPLC	ultra-High Performance Liqui Chromatography
UV	Ultraviolet
α -AAT or A1AT	alpha-1 antitrypsin

Contents

GENERAL INTRODUCTION.....	11
BIBLIOGRAPHY.....	14
I. CHAPTER 1: GLYCANS AS BIOMARKERS: GLYCOSYLATION, DISORDERS, AND ANALYSIS.	15
I.1. Protein glycosylation	15
1.1.1. Structural complexity and diversity in glycans	15
1.1.2. Physical and biological functions of glycans	21
I.2. Glycoproteins as biomarkers.....	23
1.2.1. Biomarkers of various diseases.....	23
1.2.2. Congenital disorders of glycosylation.....	24
1.2.3. Biomarkers of N-glycosylation defects	25
1.2.4. Biomarkers of O-glycosylation defects	28
I.3. Analysis of glycoproteins.....	29
1.3.1. Intact glycoprotein analysis	30
1.3.2. Released glycan analysis.....	35
I.4. N-glycan analysis workflow for CE-LiF analysis.....	41
1.4.1. Glycan release	41
1.4.2. Glycan derivatization for laser induced fluorescence detection	43
1.4.3. Purification.....	44
1.4.4. High-throughput sample preparation	45
1.4.5. CE separation and glycan structural identification	47
I.5. Conclusion	50
II. CHAPTER 2: DROPLET MICROFLUIDICS IN ANALYTICAL CHEMISTRY.....	52
II.1. Droplet microfluidics fundamentals	52
11.1.1. General microfluidic introduction.....	52
11.1.2. Droplet microfluidics.....	59
II.2. Microfluidic droplets for separation science.....	67
11.2.1. Microfluidic droplets systems for LC	68
11.2.2. Microfluidic droplets systems for MS.....	71
11.2.3. Microfluidic droplets systems for CE.....	74
II.3. Microfluidics for glycan analysis and sample treatment	75
11.3.1. Non-droplet microfluidic systems for HPLC, MS and MCE analysis of glycans	75

II.3.2.	Droplet microfluidic systems for glycan sample treatment analysis: high potential to be exploited	81
II.4.	Conclusion	83
OBJECTIVE OF THE THESIS.....		85
EXPERIMENTAL PART.....		89
III.	CHAPTER 3: DEVELOPMENT OF NEW METHODOLOGIES FOR HIGH PERFORMANCE ANALYSIS OF GLYCANS WITH CE-LIF	90
III.1.	Introduction to Capillary Electrophoresis.....	91
III.1.1.	Electrophoretic mobility	91
III.1.2.	Electroosmotic flow.....	92
III.1.3.	Capillary gel electrophoresis of glycans	95
III.1.4.	Preconcentration of glycans before CZE analysis by large volume sample stacking	96
III.2.	Development of a new strategy for high performance CE-LIF of glycans.....	97
III.3.	Development of a new droplet-based sample treatment strategy for CE-LIF of glycans	99
III.4.	Conclusion	102
IV.	CHAPTER 4: INSTRUMENTATION FOR IMPROVED DETECTION OF GLYCANS	103
IV.1.	Introduction.....	103
IV.2.	Development of the modular CE-LIF instrumentations	104
IV.3.	Development of the Droplet-interfaced CE (digital CE) system	106
IV.3.1.	Experimental setup.....	106
IV.3.2.	Interface.....	109
IV.3.3.	Results.....	113
IV.3.4.	Future perspectives	118
IV.4.	Conclusion	119
CONCLUSION AND PERSPECTIVES.....		121
REFERENCES.....		124

General introduction

Glycoproteins represent half of all secretory and human cellular proteins and play a broad range of functions depending also on their glycosylation (protein folding and stability, cellular interactions...). Altered glycosylation (unoccupied glycosylation sites, truncated glycan antennae, change in proportion of glycoforms...) is a post-translational modification that can harm the regular functioning and activity of glycoproteins [1-3]. As a matter of fact, several glycoproteins are validated biomarkers of various diseases such as cancer, cardiovascular diseases [4], chronic alcohol abuse [5] or congenital disorders of glycosylation (CDG) [6]. In particular, CDG represent a group of more than 150 inherited diseases [7] with varied symptoms affecting multiple organs. CDG are classified in types and subtypes and are caused by genetic defects in the synthesis and attachment of glycoprotein glycans. CDG usually become apparent during infancy and can be mistaken for similar diseases. For a given disease and even in the same family, severity and prognosis vary greatly. In addition, for several rare CDG subtypes, diagnoses are based only from a handful of patients, making it difficult for physicians to have a clear picture of symptoms and prognosis associated. No specific treatment exists for CDG, symptoms are instead treated to facilitate the life of the patient. Diagnosis of CDG is thus challenging but crucial and usually requires a whole arsenal of analytical techniques which bring complementary information. Currently at the hospital level, the first-line biomarker analysed for routine screening of CDG with an N-glycosylation defect is Transferrin (Trf), an abundant plasma glycoprotein. The preferred method of analysing Trf is isoelectric focusing (IEF) which separates Trf glycoforms depending on their isoelectric point, followed by immunofixation and Coomassie-blue staining. Although very resolutive, it is a time-consuming (~48h), labour-intensive, unreproducible and poorly quantitative method [6].

There are several approaches to analyse protein glycosylation, corresponding to different state of the glycoprotein: intact glycoprotein, glycopeptides after protease digestion, glycans after enzymatical release, and monosaccharides from the glycoprotein. All these approaches give complementary information and are sometimes employed together. In this manuscript, we focus on releasing glycans from the glycoprotein and then separating and analysing the mix of glycans obtained. This approach allows the investigation of the micro-heterogeneity of glycans: family of glycans, structure, and type of glycosidic bonds. It can allow monosaccharide composition determination as well. Analysing the distribution of glycans from a patient can be used to extract information to help the diagnosis and possibly differentiate subtypes of CDG. In the context of glycan analysis for CDG, methods of analysis already reported include matrix-assisted laser desorption ionization mass spectrometry (MALDI-MS) and high-performance liquid chromatography (HPLC). However, for glycans in general, capillary electrophoresis with laser induced fluorescence detection (CE-LiF) has become a staple [7-9]. It is a versatile, extremely sensitive, resolutive technique with low reagents consumption. Analysing glycans with CE-LiF requires several sample preparation steps: glycans needs to be released from the glycoprotein and a fluorophore must be attached to the glycan to make it fluorescent for LiF detection. One method for glycan sample treatment prior to CE-LiF consists in using functionalised magnetic beads as solid phase extraction support. This process performed in tubes is lengthy and requires manual handling. Furthermore, some glycans give precious

information but are present in small amounts and their detection is difficult even with a technique as sensitive as CE-LiF. Thus, improvements in the detection of glycans are desirable [10].

In a related context, droplet microfluidic has been widely employed in analytical sciences: spectroscopy, microscopy, electrochemical detection, mass spectrometry, capillary electrophoresis and sample treatment [11, 12]. Droplets are considered as microreactors, and adaptation into a droplet microfluidic format presents many advantages: reduction of volume used down to femtoliters, high-throughput generation, manipulation and analysis of analytes isolated in droplets, no dilution of the sample, no Taylor dispersion inside the droplet, limited absorption of sample on the channel surface and enhanced mixing and mass transfer inside droplet. Operations that can be performed on the droplets include merging, splitting, or sorting but one operation that proves difficult is the purification or extraction of molecules of interest from complex matrices. This operation can be implemented by suspending functionalized magnetic beads inside the droplet and using magnets to aggregate beads [13]. Even though the glycan sample treatment process presented above uses magnetic beads, until now, no microfluidic system has been developed for glycan sample treatment prior to CE-LiF. Indeed, it is difficult to down-scale the sample treatment while assuring no cross-contamination between steps because in addition to the deglycosylation step, the process requires steps such as heating during an incubation, or mixing droplets with organic solvents.

In terms of instruments, adaptation of MS, liquid chromatography (LC) and CE in droplet microfluidic format has been reported [11, 12] with the advantages cited above. In particular, CE is adapted to the microfluidic format because the capillary can easily be coupled with a microfluidic interface due to its size (375 μm outer diameter, 25-100 μm inner diameter in general). Compared to MS and LC, CE is relatively simple to build and more affordable [14]. In the context of CDG screening, providing alternatives to commercial systems would be beneficial to equip more hospital laboratories with affordable instruments [7]. Custom droplet microfluidic CE systems have been reported [15] but never for the separation and analysis of glycans.

The objective of this thesis is therefore to improve the automation of the glycoprotein sample pre-treatment and the detection of released and labelled glycans by CE-LiF by working on both the methodology of CE-LiF separation and the instrumentation of the CE-LiF instrument. Both approaches are based in part on carrying and manipulating samples in microfluidic droplets. The final goal is to create an integrated Lab in Droplet system that handles the glycan samples from their native state (i.e., attached to one or several glycoproteins in a serum or plasma medium) to their separation and detection in a droplet microfluidic format.

The **first chapter** aims at providing an overview on glycoproteins and glycans: the glycosylation of protein is explained, the structure of glycans is detailed along their physical and biological functions. The role of glycans as biomarkers for several diseases including CDG is then presented, and the arsenal of analytical techniques used for the analysis of glycoproteins and glycans are showcased. Finally, a focus is operated on the workflow necessary to release and fluorescently tag glycans for CE-LiF analysis.

The **second chapter** is dedicated to microfluidics in analytical chemistry. A general introduction on microfluidics and droplet microfluidics is provided, with an emphasis on the role microfluidic droplets play on separation science, and the role it plays for glycan analysis and sample treatment. The high potential of coupling microfluidic droplets containing functionalized magnetic beads with the CE-LiF sample treatment process is also discussed.

The experimental part of the manuscript is divided into two chapters that present the two complementary aspects of the glycan analysis process: methodology for both sample treatment and CE-LiF separation, and instrumentation for purpose-made CE-LiF instruments.

The **third chapter** first focuses on improving the CE methodology for the analysis of glycans. Investigations are performed to find new optimal background electrolytes (BGEs) and electrokinetic preconcentration methods. A new approach based on highly concentrated, weakly charged, organic ions in a high ionic strength BGE is proposed. Then, the translation of the classical in-tube protocol for glycan sample treatment prior to CE-LiF in a microfluidic droplet format is presented. The microfluidic is based on the magnetic tweezer technology and shows great synergy with the glycan protocol since the cornerstone of both systems is the use of functionalized magnetic beads.

The **fourth chapter** then proceeds to present the development of two different standardisable purpose-made CE-LiF systems for two different applications. Both systems are inspired from the Lego toy, where blocks are assembled to create a construction. The first system is aimed at providing an alternative to expensive commercial systems and combines blocks made of microfluidic, optic and electrophoresis modules. The second system is designed to be coupled with our new microfluidic droplet protocol for glycan sample treatment in order to be able to inject into the CE capillary one droplet. The goal is to inject into the CE capillary part of a 1 μL sample droplet coming from the sample treatment device.

Bibliography

I. Chapter 1: Glycans as biomarkers: glycosylation, disorders, and analysis.

Glycosylation, where carbohydrates are added to proteins or lipids with the help of enzymes is by far the most complex and most common post-translational modification. Indeed, more than half of secretory and cellular proteins are glycosylated [1-3]. Furthermore, an estimate 1% of human genes are used for this specific process [16]. In this chapter, protein glycosylation will be detailed with an emphasis on glycans: their structure, synthesis and role will be explained. Then an overview of the use of glycoprotein as biomarkers will be proposed, followed by the presentation of the arsenal of analytical techniques employed for the analysis of glycans. Finally, this chapter will focus on the preparation and analysis of glycoprotein sample before analysis by Capillary Electrophoresis with Laser induced Fluorescence detection (CE-LiF).

I.1. Protein glycosylation

Glycosylation is the binding of a monosaccharide or an oligosaccharide chain (called a glycan) to an amino acid of a protein via a glycosidic bond. Glycoproteins may have more than one glycosylation site, with the sugars representing between 1% and 90% of the total mass of the glycoprotein [17]. As glycans are synthesized using enzymes, glycoproteins are highly heterogeneous. In glycoproteins, macro-heterogeneity refers to the difference in site occupancy: one given glycoprotein can exist under several different glycoforms which can differ in [18]:

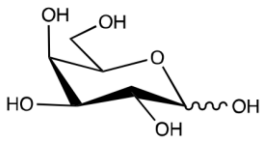
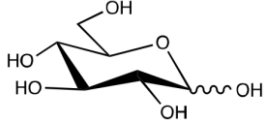
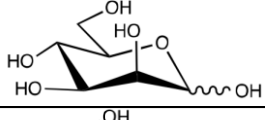
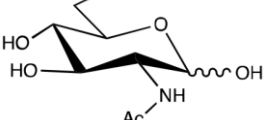
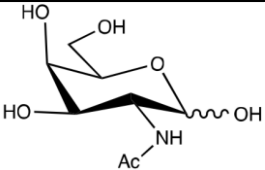
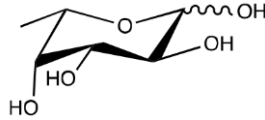
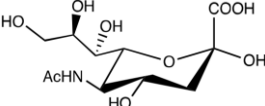
- The number and nature of glycosylation sites
- The number and structure of glycans
- The distribution of glycans on the different sites of glycosylation

Micro-heterogeneity refers to the structure diversity at a given site of glycosylation, i.e., the structure diversity and complexity in glycans, which will be our focus in this subchapter.

I.1.1. Structural complexity and diversity in glycans

More than 800 different monosaccharides exist according to the Chemical Component Dictionary (CCD) [19], but only 10 of them are found in mammals [20] and only 7 in human glycoproteins (Table 1).

Table 1 : Main monosaccharides composing glycans found in humans and their abbreviate name and formulae. [21]

Monosaccharides	Abbreviation	Structure
Galactose	Gal	
Glucose	Glc	
Mannose	Man	
N- acetylglucosamine	GlcNAc	
N- acetylgalactosamine	GalNAc	
Fucose	Fuc	
N- acetylneuraminic acid	Neu5Ac	

When linked together with glycosidic bonds, they become glycan or oligosaccharides. There is a high level of structural complexity/diversity for glycans due to (i) diversity in monosaccharides, (ii) number of hydroxyl groups in sugars, and (iii) possibility of α and β glycosidic bond.

First, the 7 different monosaccharides presented in Table 1 which can be found in human glycoproteins create a first layer of complexity due to the different combinations that can exist. For example, if we imagine a simple linear glycan composed of 5 monosaccharides, $7^5=16\ 807$ different combinations of monosaccharides exist. In reality, not all combinations are possible, but glycan structure is also more complex and glycans are often made of more than 5 sugars. Second, given the amount of hydroxyl groups existing in monosaccharides, bonding between two monosaccharides can happen at different carbon atoms (Figure 1 A)). For instance, Neu5Ac (Sialic acid) may be bound to a Gal residue via a glycosidic bond between the hydroxyl group at its n°6 carbon and the Gals hydroxyl group at the n°1 carbon (1-3 bond) or 1-6 bond, GlcNAc may be bound to a Man residue via 1-2 or 1-4 bond. Third, bonding creates a stereocenter, resulting in two different configurations: α or β (Figure 1 B)). This anomerie results in the possibility to have for instance a 1-3 bond which can be either α 1-3 or β 1-3.

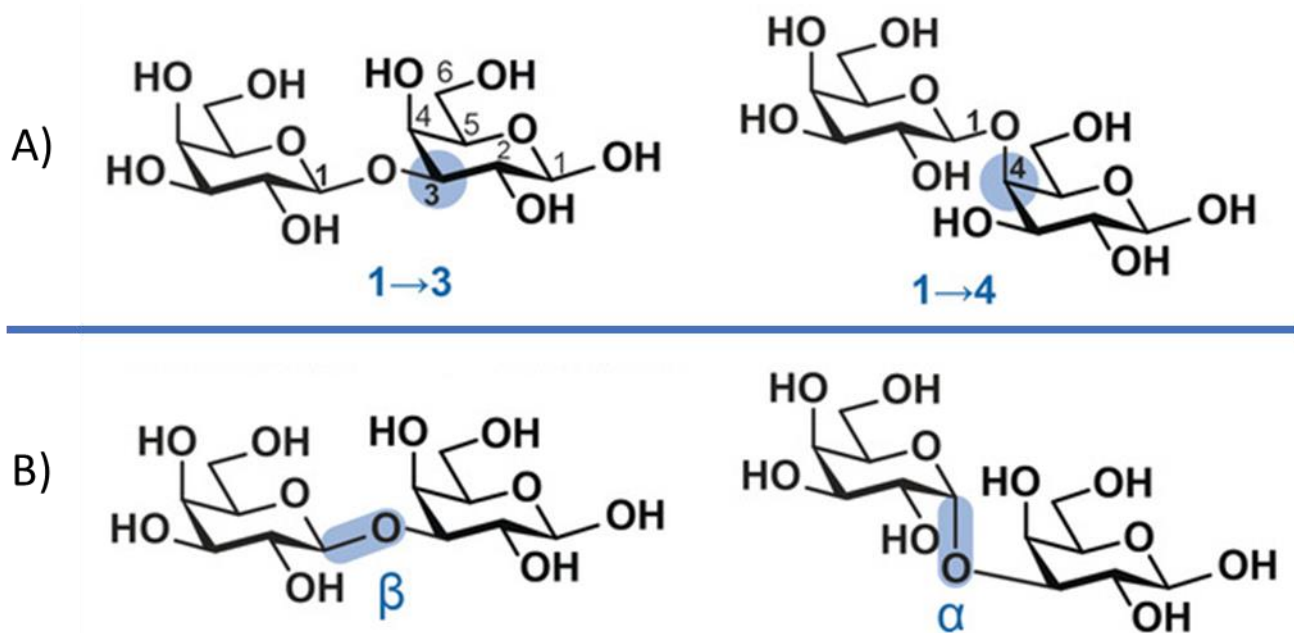


Figure 1 : A) Examples of β 1-3 and β 1-4 bonds and B) Configurations α and β of the glycosidic bond between two saccharides. From [22].

The high number of possible glycan structures has created a need for unified representations of glycans. Using precise chemical structure, although giving the most accurate representation, is not very handy for big glycans. Different representations exist, in either text or graphical format [23]. Four major glycan text formats exist: Carbank [24] and IUPAC [25] are human-readable representations of glycans while GlycoCT [26] and WURCS [27] are aimed at glycoinformaticians and are thus made to be more accurate and more complex but easily read by computers. In order to simplify the representation of glycan, two major graphical glycan formats have been created: the symbol nomenclature for glycans (SNFG) [21] which is mainly used for the representation of monosaccharides, and the Oxford system [28, 29] which includes representation of glycosidic. In this manuscript we will only be focused on the SNFG nomenclature (which can be found at this address: <https://www.ncbi.nlm.nih.gov/glycans/snfg.html>), presented in Figure 2.

Different types of glycans exist, depending on their linkage to the amino acid of their glycoprotein and their composition. N-glycans and O-glycans are two main types of glycans detailed here.

conformation is correct. If the glycoprotein is not correctly folded (approximately 30% of glycoproteins), it will be eliminated [35]. The glycoprotein is then transported in the Golgi apparatus via vesicles bearing COPII (coat protein) [36]. Figure 4 illustrates the maturation of glycoproteins going through the different networks of the Golgi apparatus, which will define its final composition. Numerous enzymes glycosidases and glycosyltransferases (ovals and rectangles in Figure 4, respectively) will modify glycan structure by trimming or addition of monosaccharides. At this step, the type of N-glycan is decided: Oligomannose, Hybrid or Complex.

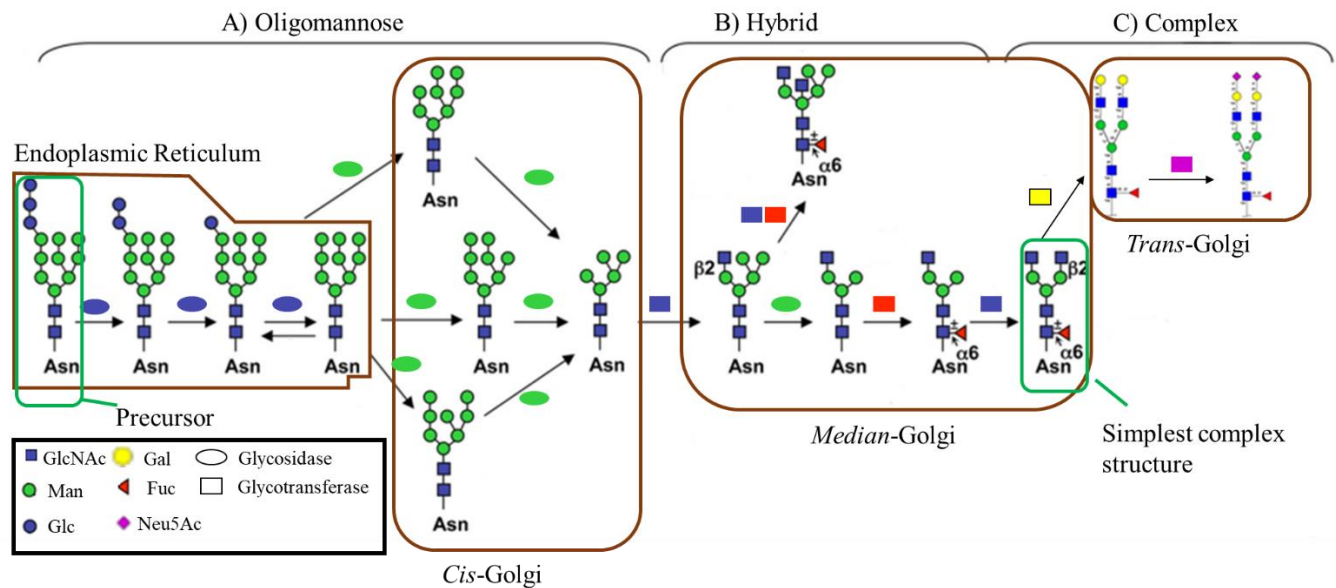


Figure 4 : Maturation of the glycoprotein in the Golgi apparatus. Enzymes are represented by ovals and rectangles with color corresponding to the related sugar. A) If some mannosidases (green oval) in the Cis-Golgi are inactive, high mannose glycan with 5 to 9 Man residues will result. B) If the mannosidases (green ovals) do not remove both Man residues, the glycan is of hybrid type. The α 1-3 antenna can then be completed with Gal or Neu5Ac, a Fuc can be attached on the first GlcNAc and a bisecting GlcNAc can be also attached. C) The simplest N-glycan complex structure is created, usually with a Fuc [37]. Other antennae can be created by GlcNAc addition, usually up to 4 in humans. Once transported in the Trans-Golgi, Gal or Neu5Ac can be added to complete the antennae. Adapted from [38]

1.1.1.2. O glycosylation

O-glycans have even more diverse structures than N-glycans, as they are built on different protein glycan linkages [39]. Contrary to N-glycans, several types of O-glycosidic bond exist. The bond is always between the alcohol function of an hydroxylized amino acid (often Serine or Threonine) and a monosaccharide. O-glycans are classified depending on the sugar involved in the bond, which can be: GalNAc, GlcNAc, Xylose, Gal, Man, Fuc or Glc [40]. More information on O-glycans structure can be found elsewhere [30, 38, 40].

O-glycans are synthesized directly in the Golgi apparatus and does not involve the use of a precursor. Depending on the type of O-glycan, the synthesis will be different. For GalNAc O-

glycans, a GalNAc is added directly onto the O-glycosylation site of the protein by a specific glycosyltransferase [41]. Then, several other specific glycosyltransferases will be employed to add more sugars on the glycan to form 4 different glycans core as seen in Figure 5 [39].

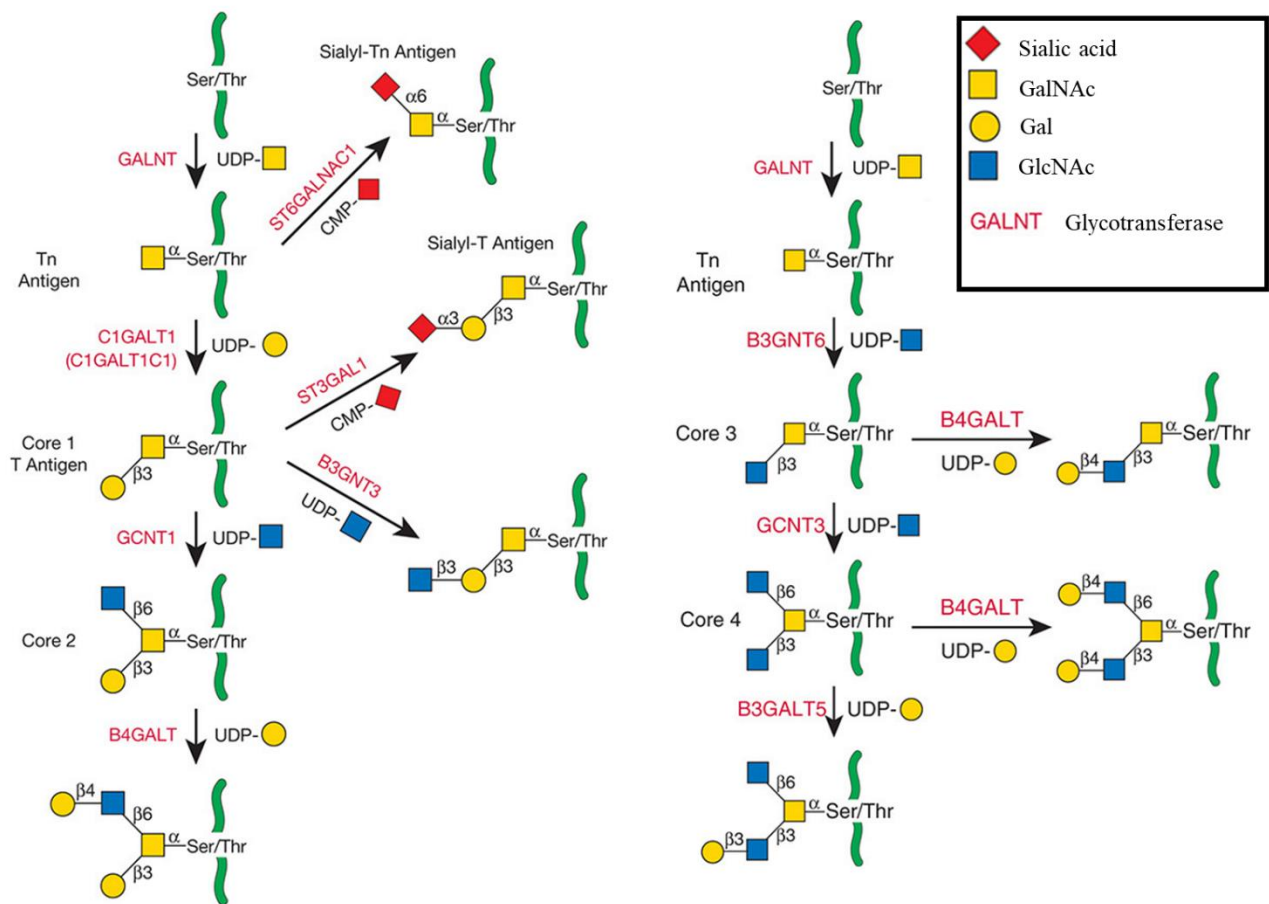


Figure 5 : Biosynthesis of GalNAc O-glycans. 4 different types of O-glycans core exist depending on the first two sugars attached to the first GalNAc. Green lines represent the glycoprotein. Adapted from [30].

1.1.2. Physical and biological functions of glycans

Depending on the glycan and the protein it is attached to, glycans can play a very broad range of roles in both physical and biological properties of glycoproteins. Some are quite subtle while others are of the foremost importance for development, growth, maintenance, or survival of the individual secreting them [30]. In many cases, the function of a glycan is not obvious. Although many theories with much evidence have been formed on the role of glycan, exceptions can often be found for each.

1.1.2.1. Protein folding and stability

It has been shown in several studies that N-glycans play a role in helping the folding of proteins, even though once folded the removal of glycans does not affect protein activity, only its stability and folding kinetics [42-44]. One early example presented in [45] involves the HIV type-1 glycoprotein 120 (HIV-1 gp 120). In the absence of a glycan in its N-glycosylation site, the protein will not fold in its active state. Nevertheless, once folded in its active state, the

removal of the N-glycan does not disrupt its biological function. This tends to show that glycans are helping the folding process of proteins without interfering with its biological functions.

As glycans are hydrophile, they tend to augment protein solubility and limit their aggregation [43, 46, 47]. When proteins are on their non-glycosylated glycoform, they can aggregate because of the hydrophobic amino acid present at the surface of the protein. It is the case with prion protein, where the presence of a glycan at Asn⁸¹ helps in preventing the formation of abnormal amyloids aggregates (responsible for Alzheimer's or Parkinson's disease for example) [48].

In some cases, glycans can form hydrogen bonds between polar amino acids or sugar residues from neighbor proteins, which results in a better resistance to thermic denaturation. In the case of partially glycosylated or deglycosylated proteins, denaturation temperature becomes lower [49]. Numerous examples have been reported, including erythropoietin (EPO), alpha-1 antitrypsine (α -AAT) or interferon beta [50]. Glycans can also help to protect proteins from proteases by masking cleavage sites [46, 51].

1.1.2.2. Biological and immunological functions

Glycans at the surface of cells are responsible for interactions with the cell's environment, meaning other cells, antibodies, viruses, or bacteria [52]. Numerous cellular interactions are regulated by homotypic and heterotypic interactions of glycan probing [53], as seen in [Figure 6](#). Glycans can also be specifically probed by "glycan-binding proteins" (GBPs) like lectins, selectins, or galectins in various biological processes: cellular adhesion, cellular growth and differentiation, apoptosis, and inflammation [30]. GBPs can also play a role in signaling or stress response [54].

An illustration of glycans interacting with GBP can be found with glycoproteins bearing sialylated glycans (terminated by Sialic Acid) circulating in serum. A GBP called asialoglycoprotein receptor (ASGPR) involved in protein clearance, which is located on the surface of hepatocytes, binds specially to Gal and GalNAc residues to internalize and degrade them [46]. Fully sialylated glycans are not recognized by ASGPR, even though the terminal sialic acids will be cleaved off by unspecific sialidases overtime. Once cleaved off, the glycan now bears terminal Gal or GalNAc and can thus bind with ASGPR and be degraded. The presence of sialylated glycan thus prolongs the circulation of glycan in serum (serum half-life).

Wang et. al. [55] found that the presence of a core Fuc (fucose attached to the GalNAc which is linked to the Asn) on N-glycans on the extracellular domain of epidermal growth factor receptor favored binding to the epidermal growth factor. Partridge et. al. [56] show that the presence of a bisecting GlcNAc (β 1,4-linked to the first Man in the N-glycan core) on the same glycans tends to favor the endocytosis of its receptor. Therapeutics antibody can bind their targeted cells with their constant region (Fc) in order to perform an attack aimed at killing the cell called antibody-dependent cellular cytotoxicity (ADCC). ADCC requires the presence of a glycan attached at the Asn²⁹⁷ of a humanized immunoglobulin G1 (IgG1) and Shinwaka et. al. found [57] that the presence of a bisecting GlcNAc and the absence of core Fuc on that glycan

can improve ADCC by up to 100-fold. Glycans can also modify antibody-antigen interactions by steric effects (covering of antigenic sites on the protein surface) or by charge effect if the glycan bears terminal Neu5Ac (sialic acid). For example, lots of O-glycans from mucins can prevent antigenic binding and create immune responses [58].

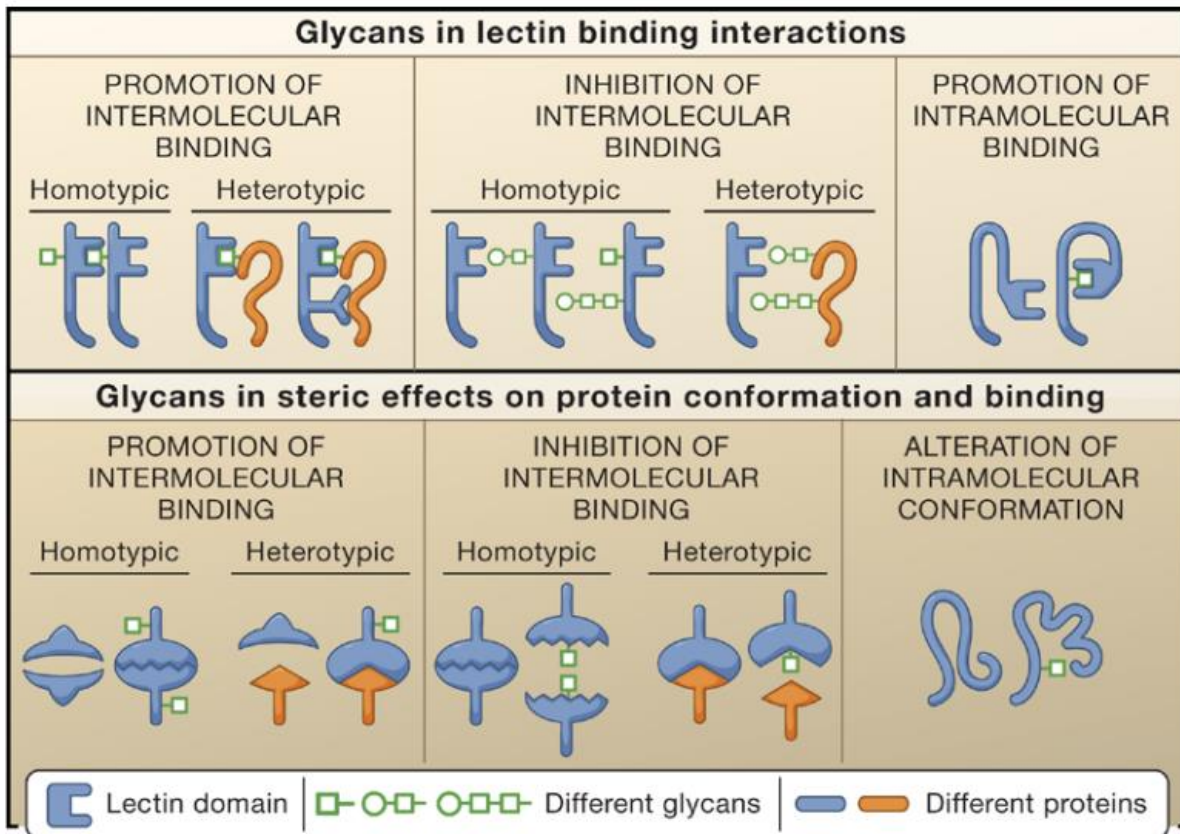


Figure 6 : Influence of the presence of glycans in intermolecular binding and protein conformation by promotion or inhibition of homotypic or heterotypic interactions. From [53].

1.2. Glycoproteins as biomarkers

Given the wide structural complexity of glycans structure and synthesis, and their numerous functions in the human body presented in the previous chapter, it is not surprising that defects in protein glycosylation plays a role in a large array of disorders. While this manuscript does not aim at being exhaustive, common and widespread diseases are first presented, followed by a focus on congenital disorders of glycosylation (CDG). Glycoprotein biomarkers are then presented for CDG defects of N- and O-glycosylation.

1.2.1. Biomarkers of various diseases

Cancer is a major health concern in developed countries, with an estimated 23.6 million new cancer cases and 10 million cancer-related deaths in 2019 [59]. Glycosylation modifications were first described in cancer patients at the end of the 60s [60]. Proteins from cancerous cells were observed to have modified glycosylation compared to regular cells. In some cases, mutations resulting in excessive expression of sialyltransferases result in glycans from

cancerous cells bearing more sialic acids [61, 62]. Increased sialylation protects cancerous cells from apoptosis, favor metastases and increase treatment resistance [63]. Carbohydrate antigen 19-9 is a biomarker for pancreatic, colorectal and gastric cancers, where increased sialylated forms proportion are correlated to low survival chances [64, 65]. Increased sialylation is also related to development of numerous tumors and metastases in lung and brain cancers [66, 67]. In hepatocellular carcinoma, increased fucosylation of alpha-fetoprotein L3 is a biomarker [68], and augmented fucosylation of N-glycans is observed in lung and breast cancers [69]. Decrease in galactosylation of Immunoglobulin G (IgG) was found to happen in prostate cancer, myeloma, stomach adenocarcinoma and gastric cancer [70].

In another fashion, protein glycosylation is involved in Alzheimer's disease (AD), the most common neurodegenerative disease, involving as of 2020 approximately 50 million people worldwide [71]. Protein Tau, who stabilize the microtubules of axons, bear 3 sites of N-glycosylation who are normally empty. Presence of N-glycans at these 3 sites is associated with AD as it makes the protein Tau more susceptible to phosphorylation [72, 73].

While not being a disease, chronic alcohol abuse can lead to alcoholic liver disease, pancreatitis, esophageal cancers and strokes [74]. As patient tend to underestimate their alcohol intake, an accurate biomarker is required to measure alcohol consumption. Transferrin, a glycoprotein of hepatic origin, is observed to have its glycoforms modified by heavy alcohol intake. Carbohydrate deficient transferrins (CDT) are abnormal glycoforms with fewer terminal sialic acid than normal glycoforms which can be detected after two weeks of heavy alcohol intake (>60 g/day). CDTs can also be used for monitoring patient recovery, with CDT levels gradually decreasing during alcohol abstinence (half-life of ~15 days).

1.2.2. Congenital disorders of glycosylation

Congenital disorders of glycosylation (CDG) represent an ensemble of an ever-increasing number of genetic diseases related to proteins in lipids glycosylation. First reported in 1984 by Jaeken et. al. [75], the number of CDG has more than tripled in the last 10 years, with over 150 different CDG discovered as of today, with most being defects in N-glycosylation [7, 76]. CDG are an ultra-rare group of diseases, as its estimated prevalence is of 0.1-0.5/100,000 in Europe [7]. Diagnostic of CDG is challenging due to the sheer number of different CDG often presenting varying symptoms affecting multiple organs. Symptoms of CDG are summarized in [Figure 7](#). Most common symptoms include dysmorphic facial features, abnormal fat distribution, variable coagulation, and endocrine defects.

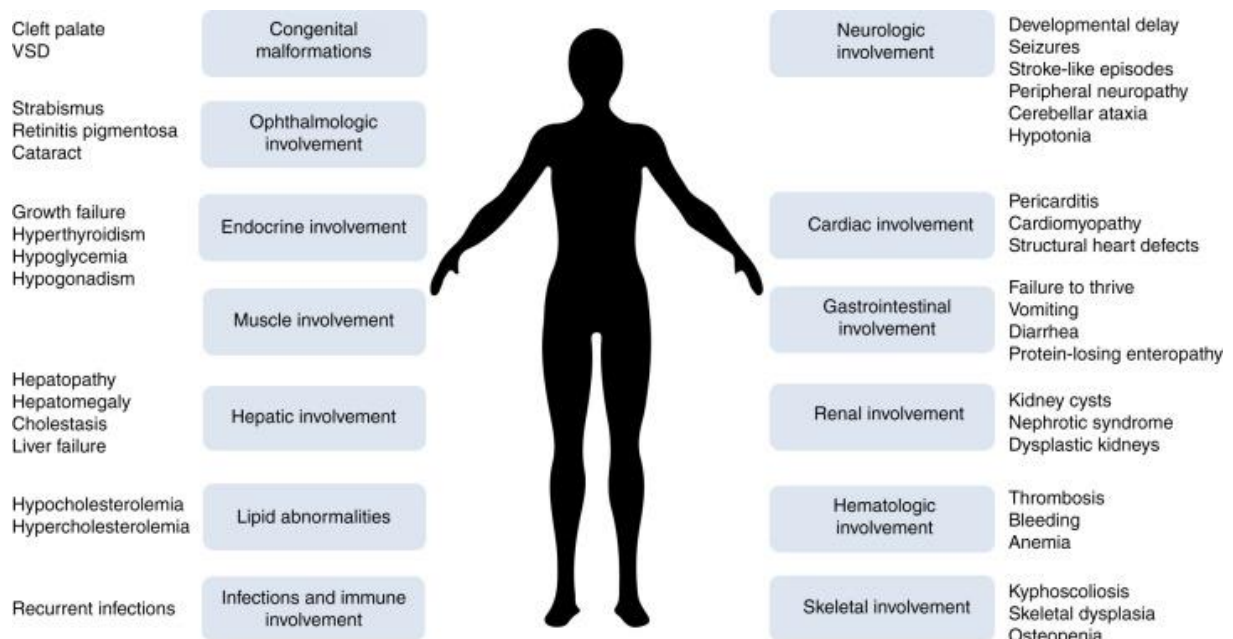


Figure 7 : Organ systems with available therapies involved in disorders of N-glycosylation. From [76].

There are two main types of glycosylation pattern defects, which can be called disorders of N-glycosylation:

- CDG-I (type 1): CDG that are most often related to defects before or during the transfer of the $\text{GlcNAc}_2\text{Man}_9\text{Glc}_3$ precursor to the protein during biosynthesis. They result in glycosylation sites not being fully occupied.
- CDG-II (type 2): CDG that are most often related to defects during the maturation of glycans. They result in glycans being incomplete, with sometimes whole antenna missing.

Limitations for evidence-based therapeutic recommendations include the limited number of patients for individual CDG types, and absence of “disorder-specific” treatments for some symptoms in CDG patients [76]. Some successful treatment strategies in N-linked glycosylation CDG include (for more details, consult [76]) Monosaccharide supplementation, Dietary intervention, Transplantation, Molecular chaperones, Gene therapy.

An early and accurate diagnosis in order to provide adapted therapy (when available) is crucial for CDG. As we have shown in this subchapter, CDG are numerous, with very different symptoms, origins, and treatments. Several glycoproteins are used as biomarkers for the diagnosis of CDG.

1.2.3. Biomarkers of N-glycosylation defects

1.2.3.1. Transferrin

Diagnostic of CDG is routinely performed by isoelectric focusing of serum transferrin, Serum transferrin (Tf or Trf) is the first-line biomarker tested for routine screening of CDG. Tf is an abundant 79 kDa glycoprotein of liver origin found in serum and plasma. It carries two N-glycosylation sites at Asn^{413} and Asn^{611} , which are fully occupied with bi-antennary glycans in

physiological conditions [31]. Those two glycans are typically fully mature, with both glycans bearing two terminal sialic acids, meaning a total of four sialic acids. As seen in Figure 8, this 4-sialo glycoforms represent approximately 80% of all glycoforms, with 3-sialo and 2 sialo representing respectively 4% and 1% [77].

CDG-I (type 1) results in sites of N-glycosylation not being occupied, and the 2-sialo and 0-sialo glycoforms proportions are higher while the proportion of the 4-sialo glycoform is lower. In CDG-II (type 2), N-glycosylation sites are fully occupied, but antenna are incomplete (sometimes a whole antenna is missing). As a result, 4-sialo glycoform proportion becomes lower in CDG-II while 3-sialo and 1-sialo glycoforms proportions increase.

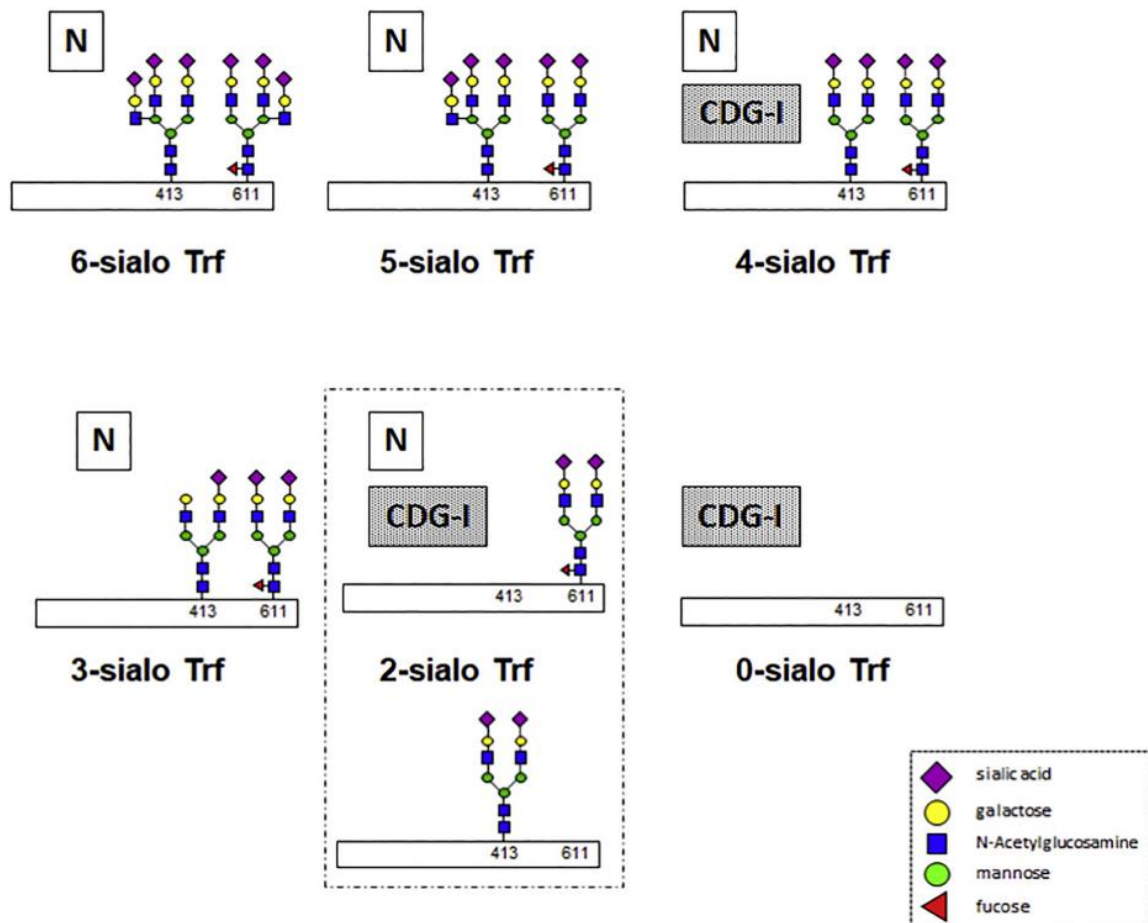


Figure 8 : Glycoforms of serum Transferrin in controls and CDG-I. 4-sialo Trf proportion is notably decreased while 2-sialo and 0-sialo proportion increases. From [6].

1.2.3.2.A1-antitrypsin

Alpha-1-antitrypsin (A1AT) is a protein found in the liver, whose concentration in blood plasma increases in response to inflammation. A1AT has 3 sites of N-glycosylation at Asn46, Asn83 and Asn247 [78]. While it can be also used to differentiate between CDG-I and CDG-II, the presence of one more N-glycosylation site increases the number of possible glycoforms and thus the complexity of analysis [79]. It should be noted that it can still be used as an alternative biomarker for CDG screening, notably in situations when Tf screening is difficult or inconclusive, for example during the first weeks of life when N-glycosylation of Tf is sometimes incomplete [80, 81].

1.2.3.3. Haptoglobin and α 1-acid glycoprotein

Haptoglobin (Hp) is a plasma protein which binds to free hemoglobin to inhibit its oxidative activity. Its β -chain bears 4 N-glycosylation sites. α 1-acid glycoprotein (AGP) is also a plasma protein, whose concentration in blood plasma increases in response to inflammation. AGP bears 5 N-glycosylation sites. While both glycoproteins can be used for routine CDG screening [82, 83], it is more complex to analyze their glycosylation and sialylation state because they have respectively 4 and 5 N-glycosylation sites. In particular, their analysis with charged-based separation methods is not as easy to implement as with Tf: in the case of Hp glycoforms, presence of α -chains makes matters worse, while in the case of AGP glycoforms it is highly acidic isoelectric points pl. Hpt and AGP are still useful, mainly for the screening of CDG-I which can be performed using mass-based separation techniques.

1.2.3.4. Immunoglobulin G

Immunoglobulin G (IgG) represents approximately 75% of serums antibodies in humans. It is a 150 kDa proteins with a glycosylation site at Asn297 on its two heavy chains [70]. Contrary to the previous glycoproteins, IgG is not of hepatic origin, meaning that the concentration and glycosylation of IgG in serum is not as affected by liver or inflammatory diseases commonly associated with CDG. For example, Tf glycosylation patterns are normal in mannosyl-oligosaccharide glucosidase deficiency while IgG glycosylation pattern is altered [84]. It should still be noted that IgG has a very complex and variable glycosylation which makes routine screening with IgG difficult.

1.2.3.5. Total-plasma N-glycans

Clerc et. al. [31] recently presented a review of human plasma N-glycosylation, where glycans from all glycoproteins are enzymatically released from whole plasma. They distinguish 24 main glycoproteins making up 30 mg/mL of the total 70-75 mg/mL of the total plasma protein concentration. Albumin makes up 40 mg/mL of total plasma protein concentration but is not glycosylated, meaning the 24 chosen glycoproteins represent most of the human total plasma N-glycosylation. Figure 9 presents the N-glycans composition of human plasma glycoproteins, with the relative contribution of the 24 main glycans for each glycan. N-glycoproteins is mainly used for second-line elucidation of CDG-II Tf profiles [85]. But it was suggested recently that it could be used as a first-line screening of CDG with unusual N-glycan signatures as a sensitive, robust and semi-quantitative method [86]. Tf only bearing complex glycans can be a limit when testing lots of CDG subtypes, whereas the plasma secreted glycoproteins have broad and different N-glycan profiles: complex, polymannose, hybrid, core fucosylated and/or bisecting glycans...

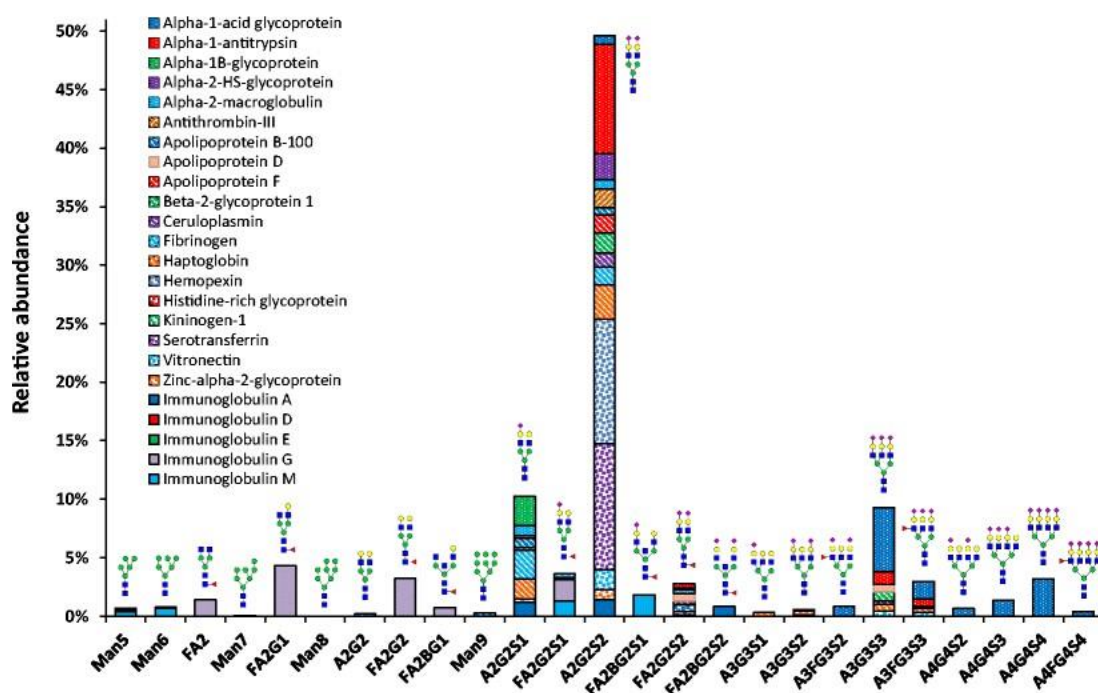


Figure 9 :Relative plasma protein contribution to each specific N-glycan composition. Not all 41 N-glycans found in plasma glycoproteins are shown here. From [31].

Chen et. al. [86] found a total of 41 different N-glycans being consistently detected in normal human plasma and showed that the total plasma N-glycan analysis could be used for the diagnosis of 19 patients with 11 different CDG subtypes, with some patient having been diagnosed with normal Tf glycosylation profiles.

1.2.3.6. Other

Similar to A1AT, Hp and AGP, when Tf patterns are difficult to interpret, other serum N-glycoproteins can be used: thyroxin-binding globulin, anti-thrombin and ceruloplasmin [6].

1.2.4. Biomarkers of O-glycosylation defects

1.2.4.1. Apolipoprotein C-III

Apolipoprotein C-III (apoC-III) is a O-glycosylated serum protein of liver and intestine origin of relatively high abundance and plays a role in lipid metabolism [87]. ApoC-III is O-glycosylated at Thr⁷⁴ and several glycoforms co-exist. Notably, three glycoforms are of particular interest: apoC-III₁, which corresponds to the O-glycan attached to apoC-III bearing one glycan, representing approximately 60 % of all glycoforms, apoC-III₂, representing approximately 40 % and apoC-III₀, representing up to 10 % of all glycoforms [88-90]. As apoC-III is O-glycosylated in the Golgi apparatus, variations in the relative proportions of apoC-III glycoforms can indicate a defect in Golgi apparatus glycan synthesis. Although the specificity of apoC-III for CDG screening is rather low due to acquired conditions like obesity and liver diseases which often imply altered glycoforms patterns [89]. However, as a second-line test, apoC-III can be used for a CDG-II Tf pattern, where an irregular apoC-III glycoform pattern can translate to genes variants affecting the Golgi apparatus homeostasis.

1.2.4.2. Bikunin

Bikunin is a highly glycosylated, serum glycoprotein of liver origin, O-glycosylated at Ser¹⁰ and possessing a GlcA-Gal-GalXyl-O common tetra saccharide linker. Irregular serum Bikunin have been detected in patients with linkeropathies, a rare genetic disease caused by a biosynthesis defect in the tetra saccharide linker [91].

1.2.4.3. α DG

Alpha-dystroglycan is an O-glycosylated membrane glycoprotein, part of the dystroglycan complex, which brings structural integrity in muscle tissues [92]. Defects in enzymes involved in the glycosylation of Alpha-dystroglycan lead to congenital muscular dystrophies, with some variants which can be associated to CDG-I Tf profiles [93 , 94 , 95].

1.3. Analysis of glycoproteins

Given the complexity of protein glycosylation and the numerous different biomarkers existing, lots of analytical techniques are used for the analysis of protein glycosylation. Several strategies exist, each bringing different and complementary information, as shown in [Figure 10](#) below. The first strategy is to analyze the intact glycoprotein and is usually the first kind of analysis performed in a clinical context [96]. It is used to observe the different existing glycoforms, and eventually to characterize them and evaluate their distribution. The second strategy is to analysis glycopeptides i.e., digesting the glycoprotein with a specific endoproteinase, which result in a mix of peptides and glycopeptides [96]. The glycopeptides obtained are carrying individual glycosylation sites, thus identification of site-specific glycosylation properties can be analyzed. This strategy is widely employed but presents several drawbacks: it usually requires purification of glycopeptides, is mostly limited to mass spectrometry techniques and requires advanced software-assisted data analysis [96, 97]. The third strategy is to analyze glycans released from glycoproteins. Glycan analysis enables the advanced characterization of glycan structure (monosaccharide composition and bonds) and their relative abundance [98]. Although high-throughput analysis of glycan can be performed, it typically requires multiple preparation steps, which can be costly and lengthy. The last strategy is to analyze the monosaccharide composition by dismantling glycans into individual monosaccharides by acid hydrolysis, which is not widespread because it does not give information on structure or glycosylation site occupation [99] and due to a lack of universal method for release and analysis [100]. These four strategies require different analytical separation tools in order to characterize macro- and micro-heterogeneity of glycoproteins, resulting in an arsenal of analytical techniques.

In this subchapter, we will focus on only two approaches: intact glycoprotein and glycan analysis. Whenever possible, the techniques used for those approaches will be put in the context of CDG diagnosis, as the two approaches are respectively first-line and second-line methods for the diagnosis of CDG, and provide complementary information [6, 7, 101]. More information on glycopeptides and monosaccharides analysis can be found in the following reviews: [96, 97, 99, 100].

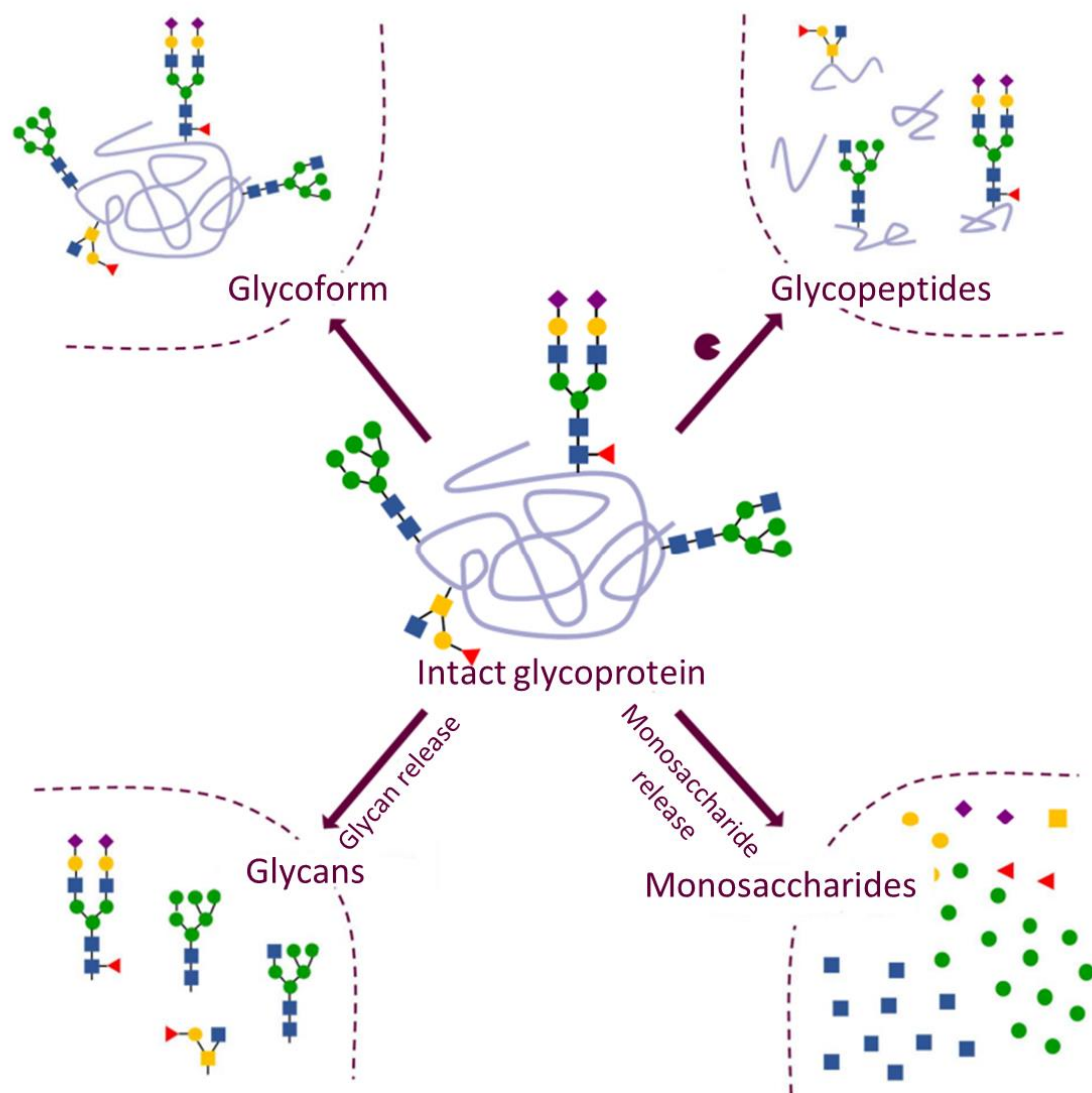


Figure 10 : Different ways of analysing protein glycosylation.

I.3.1. Intact glycoprotein analysis

Analysis of intact glycoprotein can give information on both macro-heterogeneity (glycan sites occupancy) and micro-heterogeneity (glycan structure), especially for sialylated glycans. In this case, discrimination of the differently sialylated glycoforms is possible due to the difference in charge between glycoforms. However, for non-sialylated glycans, if the mass of the protein is too big, the difference in mass between two glycoforms differing by only one monosaccharide is too small and cannot be detected. Difficulties can also arise when trying to analyze glycoproteins with low abundance in complex biological fluids. Liquid chromatography, electrophoresis and mass spectrometer techniques can be used for the analysis of intact glycoproteins. One should remember that even though each techniques has advantages and drawbacks, more than one method is often required for the diagnosis of CDG, meaning some methods work in tandem [6, 7, 96, 101].

1.3.1.1. High-performance liquid chromatography

High-performance liquid chromatography (HPLC) is now extensively used for CDG-I, CDG-II screening and is the reference procedure for Carbohydrate Deficient Trf percentage value (CDT%) in chronic alcohol abuse. Using anion-exchange column and detection at 470 nm, all seven glycoforms of Trf (0-sialo to 6-sialo) can be separated depending on their charge and structure [102]. HPLC analysis are quick (around 20 min), can be semi-automated, require low sample volumes (~100 μ L) and allows quantitative and objective interpretation patterns, contrary to isoelectric focusing and western blot analysis [6]. Although HPLC is suggested to be less resolutive for the detection of Trf protein variants than isoelectric focusing [103, 104], it can be carried out after neuraminidase treatment to check Trf genetic polymorphism.

1.3.1.2. Electrophoretic methods

1.3.1.1.1. Isoelectric focusing

Trf isoelectric focusing (TIEF) is the gold-standard method for CDG screening. Trf glycoforms are separated depending on their charge as prefocused ampholytes in an agarose or polyacrylamide gel generate a pH gradient. They are classically detected after in-gel immunofixation and Coomassie-blue staining [105]. TIEF is a very resolute and accurate technique for separation of Trf glycoforms and requires low sample volume (~10 μ L), but it is time-consuming (~48h), labor-intensive, offers poor reproducibility, is poorly quantitative and is not compatible with anticoagulant that chelates iron [6]. [Figure 11](#) showcases the TIEF analysis of CDG-I and CDG-II patients. As explained in section 1.2.3.1, one can see the proportion of 2-sialo and 0-sialo increases in CDG-I ([Figure 11 A](#)) while 4-sialo proportion decreases. In CDG-II ([Figure 11 B](#)), one can see increase of 3-sialo and 0-sialo glycoforms.

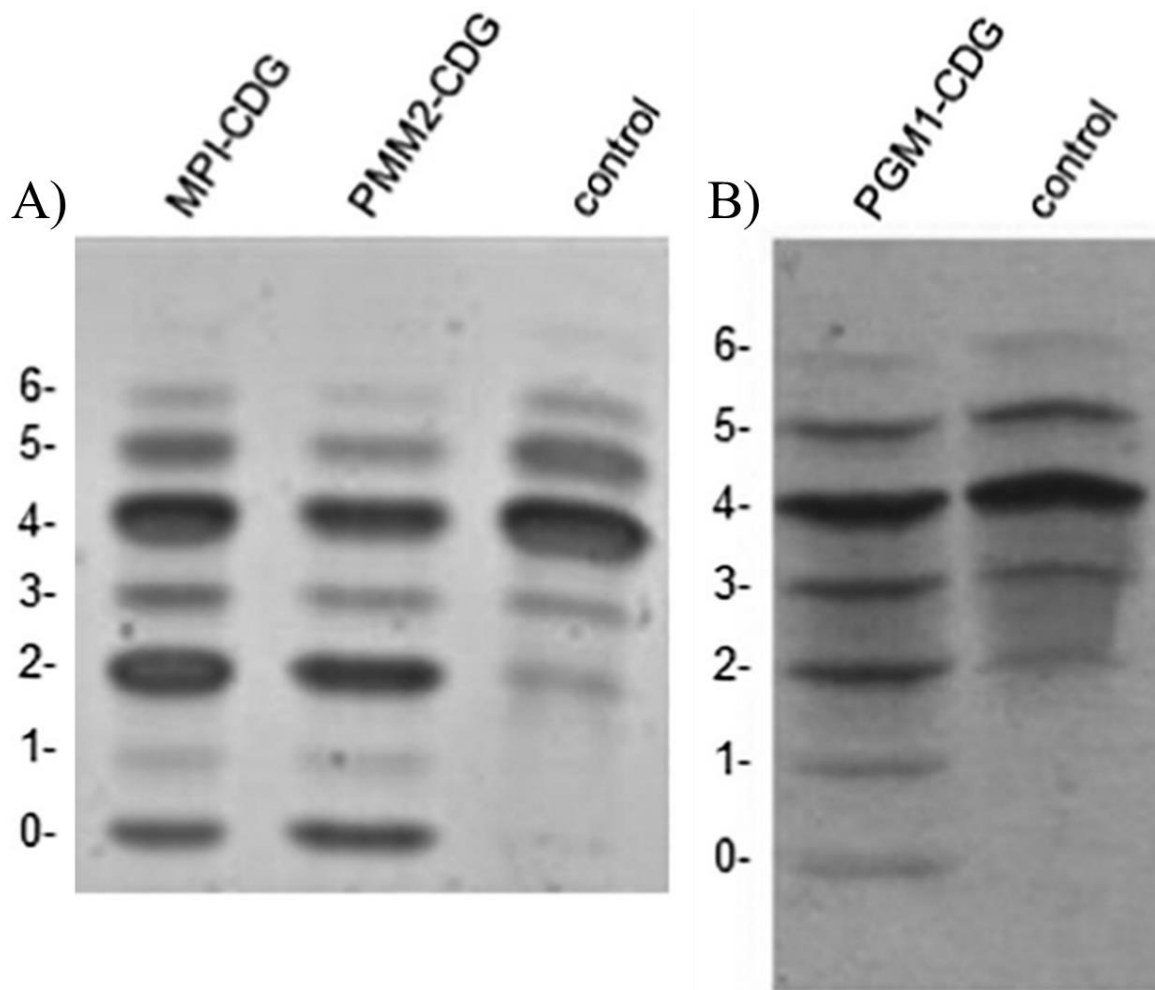


Figure 11 : TIEF analysis for A) CDG-I patients and B) CDG-II patients. Scale represents position of 0- to 6- sialo glycoforms in control samples. Adapted from [6].

I.3.1.1.2. Western blot analysis

Most usual CDG biomarkers can also be separated sensitively by molar weight using classical western blotting after sodium dodecyl sulphate-polyacrylamide gel electrophoresis (SDS-PAGE). Western blot can be relatively standardized and allows parallel separation of up to 30 samples in one run. In the case of CDG-I, because the whole glycan chain is missing (~2.2 kDa), the difference in molar weight between glycosylated and unglycosylated glycoprotein is enough to be detected with SDS-PAGE follow by western blotting [83]. As seen in Figure 12 A), additional lower bands appear in CDG-I patients. For example, two more bands appear in the Trf pattern, corresponding to glycoforms missing 1 and 2 whole glycans respectively. In the case of the majority of CDG-II, since only part of the glycans is missing, the difference in molar weight between glycosylated and unglycosylated glycoprotein is often not observable.

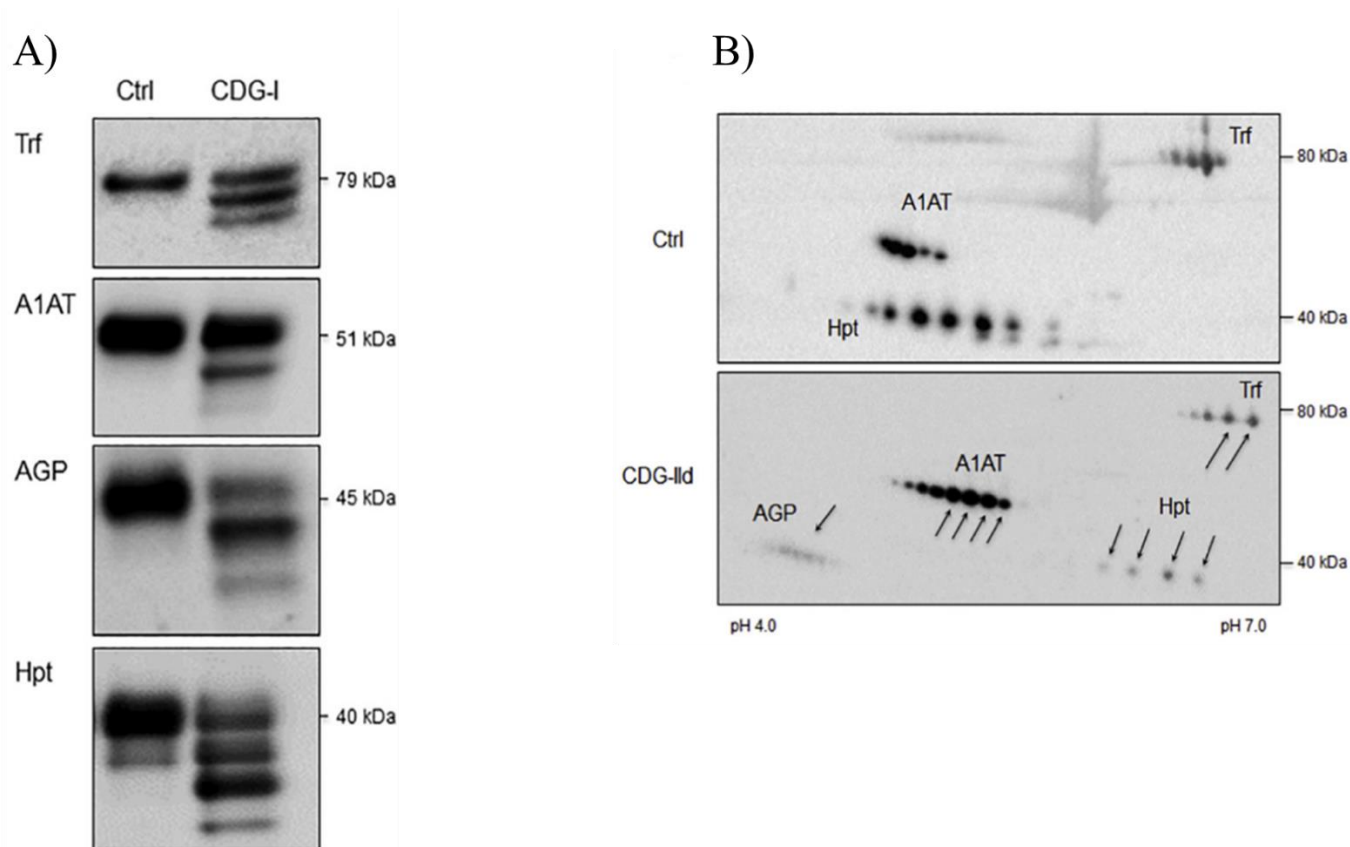


Figure 12: Separation of glycoforms using A) SDS-PAGE and Western Blotting and B) Two-dimensional gel electrophoresis. Adapted from [6].

I.3.1.1.3. Two-dimensional gel electrophoresis

The two above-mentioned techniques, IEF and SDS-PAGE, can be coupled together as a gel-based protein separation method called two-dimensional gel electrophoresis. Although it has been referred to as “old fashioned” [106], it has been extensively applied for CDG screening [107]. Once coupled with Western blotting, simultaneous detection of Trf, A1AT, Hpt and ApoC-III can be performed, as shown in Figure 12 B) for a CDG-II. As one can see, in the CDG-II pattern the bands for each glycoforms are shifted to the left (meaning a loss of Neu5Ac) and to the bottom (meaning a shift of mass). One can also notice that in the case of α 1-acid glycoprotein, which is very acidic, it is only visible in the case of the CDG-II with implies major terminal Neu5Ac losses.

I.3.1.1.4. Capillary zone electrophoresis

In Capillary zone electrophoresis (CZE), analytes are separated depending on their charge, mass, and structure in a capillary of tenth of micrometer dimension (usually fused silica) under a high voltage. Compared to gel-based methods, CZE coupled to UV detection at 200 nm is a fast, accurate and automated techniques which allows for separation and quantification of Trf glycoforms. Similar to HPLC presented previously, CZE separates glycoforms depending on their charge (glycan sialylation) and hydrodynamic radius (structure and mass of glycan). A CZE analysis can be performed in up to 10 min per sample, automated, with good reproducibility and good correlation with TIEF and HPLC for the screening of CDG-I, CDG-II and mixed CDG-I + II [108-111]. As one can see in Figure 13, profiles of Trf in control,

CDG-I and CDG-II are as expected: in control, the glycoform bearing 4 terminal Neu5Ac (4-sialo) is the dominant form. In CDG-I, 2-sialo and 0-sialo form proportion increases (corresponding respectively to one missing N-glycan chain and two missing N-glycan chains) and 4-sialo decreases. In CDG-II, increase of 3- to 0-sialo glycoform show a loss of terminal Neu5Ac.

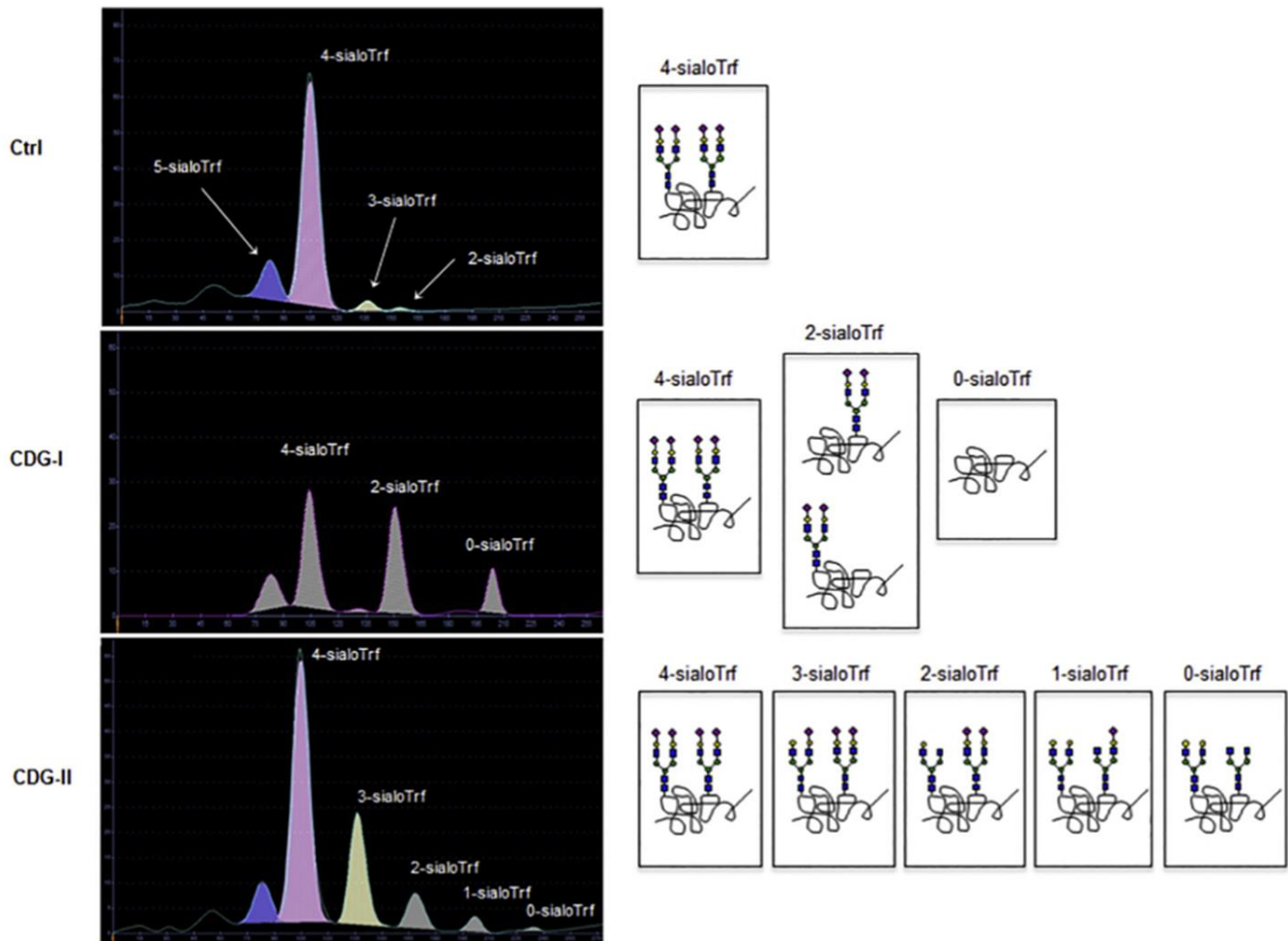


Figure 13 : Capillary zone electrophoresis (CZE) of serum Transferrin in control, CDG-I and CDG-II. From [6].

1.3.1.2. Spectrometric methods

Mass spectrometry methods for the analysis of intact glycoprotein is a powerful tool since it allows determination of glycoprotein mass and observation of different glycoforms. Nevertheless, due to the high microheterogeneity of glycoproteins, mass spectra are often difficult to interpret. Furthermore, glycoproteins tend to be more difficult to ionize than unglycosylated protein because they are highly hydrophilic and their desolvation is less efficient [112]. Two main ionization sources are used for intact glycoprotein mass spectrometry analysis: Matrix-assisted laser desorption/ionization (MALDI) for smaller glycoproteins (up to ~20 kDa) and electrospray ionization (ESI) for larger glycoproteins (up to ~200 kDa) [113].

I.3.1.2.1. Matrix-assisted laser desorption/ionization

Sample containing the glycoprotein is mixed to a matrix of crystallized, aromatic, and UV-absorbing molecules. When dry, the matrix crystal envelops the glycoprotein. Matrix ionization is performed with a laser emitting in UV range, which allows the matrix to transfer a proton to the sample [114-116]. MALDI creates low-charged ions, analyzers with large m/z ratio range are required for satisfying resolution. MALDI coupled with time-of-flight (TOF) mass spectrometry can be used to obtain spectrum with satisfying resolution for small glycoproteins (up to ~40 kDa) with limited number of glycans like RNase B, ovalbumin, α -GPA or ApoC-III [117-119].

In the case of ApoC-III, comparing the ratio of relative areas of peaks corresponding to Apoc-III₁ and Apoc-III₂ glycoforms between control patients and patients with O-glycosylation congenital disorders [119], obesity or sepsis [89] or autosomal recessive cutis laxa type-2 [120] is possible, showcasing the potential of ApoC-III as a biomarker.

MALDI allows the “easy” characterization of glycoproteins, with minimum sample preparation as MALDI can be used with samples with high salt concentrations, compared to other ionization techniques [121]. Nevertheless, isomers cannot be separated with MALDI, and laser power must be highly tuned to prevent loss of Neu5Ac and Fuc [89, 118].

I.3.1.2.2. Electrospray ionization

Electrospray ionization (ESI) is a soft ionization technique to produce gas phase ions. It requires the sample diluted in solution (mM or less in polar volatile solvent) to be introduced into a stainless-steel capillary, which is then put under high voltage, resulting in the dispersion of the sample solution into highly charged electrospray droplets aerosol [122, 123]. Usually, a coaxial flow of N₂ is used around the capillary, helping droplet desolvation.

ESI of large glycoproteins results in multicharged ions in a range of 500-5000 m/z ratio, allowing the use of different analyzers: TOF, Orbitrap or Fourier-transform ion cyclotron resonance mass spectrometry (FTICR) [123].

Compared to MALDI, ESI is a softer ionization method, with excellent resolution and when coupled with capillary electrophoresis or liquid chromatography allows the separation of isomers. The drawback is that ESI requires more complex data treatment with advanced software [123].

I.3.2. Released glycan analysis

The analysis of glycans from glycoproteins is an interesting strategy to investigate the micro-heterogeneity of glycans: saccharides composition, structure and type of glycosidic bonds while completing missing out on any information about sites of glycosylation occupation. In order to obtain free glycans in solution and to be able to detect them, several sample preparation steps are required, which will be detailed in the next subchapter. In the case of CDG, glycan analysis is limited to mass spectrometry methods, but capillary zone electrophoresis seems like a promising method. Both will be detailed in this subchapter [6, 7, 101]

1.3.2.1. Mass spectrometry methods

Matrix-assisted laser desorption/ionization time-of-flight mass spectrometry (MALDI-TOF MS) is the preferred routine MS method for glycan separation in CDG screening [6, 124]. MALDI-TOF MS is a semi-quantitative method, relatively fast, requires low sample volumes and has a high automation potential. It can also be used as a first step for N-glycan profiling to provide an overview of structure diversity [125]. Information on less abundant glycans can nevertheless be lost due to ion suppression as MALDI-TOF-MS does not include a separation step. It is also less suitable for O-glycans which are smaller. For sialylated N-glycans, a supplementary preparation step is needed to protect terminal sialic acid which are otherwise dissociated during analysis.

MALDI-TOF was used for the analysis of serum glycans from 4 patients with various CDG [101]. The study showcased the complementary use of CZE of Transferrin, 2DE of N- and O-glycans, SDS-PAGE Western-blot and MALDI-TOF MS of serum N-glycans for the diagnosis of 4 different CDG. In patient 1, analysis of the MS spectra of serum glycans was enough for direct diagnosis of MGAT2-CDG. In patients 2-4, while providing important information (specially to help decipher Tf CZE patterns), MALDI-MS did not allow direct CDG diagnosis. As MS-based N-glycan profiles are complex and difficult to interpret, its use as a single screening method is limited in routine conditions.

Although a powerful analysis techniques MALDI-TOF MS presents limitations preventing it from being a first line routine technique for CDG screening [126]. Enzymatic release and derivatization of glycans from glycoproteins which is often required for sensitive detection can be long (up to 48h) and can induce high analytical variability. Furthermore, absolute quantification of N-glycan is desired [127] while MS methods often provide only relative quantification, i.e., the MS signal of a N-glycan is expressed as a percentage of the total signal intensity of all detected N-glycans.

In order to solve some of the issues mentioned (mostly method throughput and robustness), Chen et.al. [86] recently proposed a new MS-based method for CDG diagnosis based on the analysis of released glycans. After a 5-min enzymatic release, a 5-min labeling and extraction by HILIC, glycans were analyzed using low injection–electrospray ionization–quadrupole time-of-flight mass spectrometry. The total sample preparation length was less than 60 min, with the MS acquisition requiring only a few minutes, which is one the fastest time-to-result plasma N-glycomics method [126]. This method presents overall promising results, demonstrating high sensitivity and specificity levels which are required for detection of new N-glycan biomarkers of CDG. Still, limitations remain as this method still does not provide absolute quantification. Cost of reagents in this method can also limits its use for routine CDG screening.

Considering these results, CZE appears to be a good alternative technique for the analysis of released glycans in CDG context.

1.3.2.2. Capillary electrophoresis methods

CZE is a powerful and widely used tool for simple samples containing few different glycans, for example for glycan standards or glycans from monoclonal antibodies [8, 9]. For more complex samples, resolution can limit the separation for glycans with the same number of terminal Neu5Ac, the use of gel is then required. UV detection, although being versatile, easy to use and commonly equipped on commercial CE systems, suffers from poor sensitivity compared to LiF, electrochemiluminescence or electrochemical detection [128]. LiF in particular presents more than 1000-fold sensitivity improvement over UV. MS detection can also be used, sometimes in tandem with LiF for information on glycan structure and direct glycan identification.

1.3.2.2.1. Capillary electrophoresis with laser induced fluorescence detection.

Capillary gel electrophoresis (CGE) is a variant of CZE where the buffer solution contains a polymer. This should not be confused with gel electrophoresis techniques presented previously (SDS-PAGE, 2D gel electrophoresis and TIEF) as in this situation there is no sieving on the sugars as they are too small [129]. Gels help minimize analyte diffusion, preventing peak broadening, prevent the absorption of analyte to the walls of the capillary and the good heat dissipation in capillaries allows the use of high voltage in CGE [130]. As other CZE methods, CGE requires derivatization to be detected. Due to its superior sensitivity, LiF detection has become a staple in glycan analysis [131]. 1-aminopyrene-3,6,8-trisulfonic acid (APTS) is the most common used fluorescent dye, due to its three negative charges which help separation and its high fluorescent yield [132]. The whole procedure of sample preparation for the CZE/CGE-LiF analysis of glycans will be covered in chapter I.I.4.

The gel used in commercial kits dedicated to N-glycan analysis from Sciex© “N-CHO Carbohydrate Labelling and Analysis kit” and “Fast Glycan Analysis and Labelling” is composed of a buffer of 25 mM acetate with 0.4% polyethylene oxide (PEO) [133]. Coupled with a Polyvinyl Alcohol (PVA) coated capillary, high-resolution separation of complex oligosaccharide mixes can be performed, as seen in [Figure 14](#) with a mix of ten important synthesized human milk oligosaccharides [134]. One can see that very close structure can be separated, i.e., two isomers like the two first glycans in [Figure 14](#).

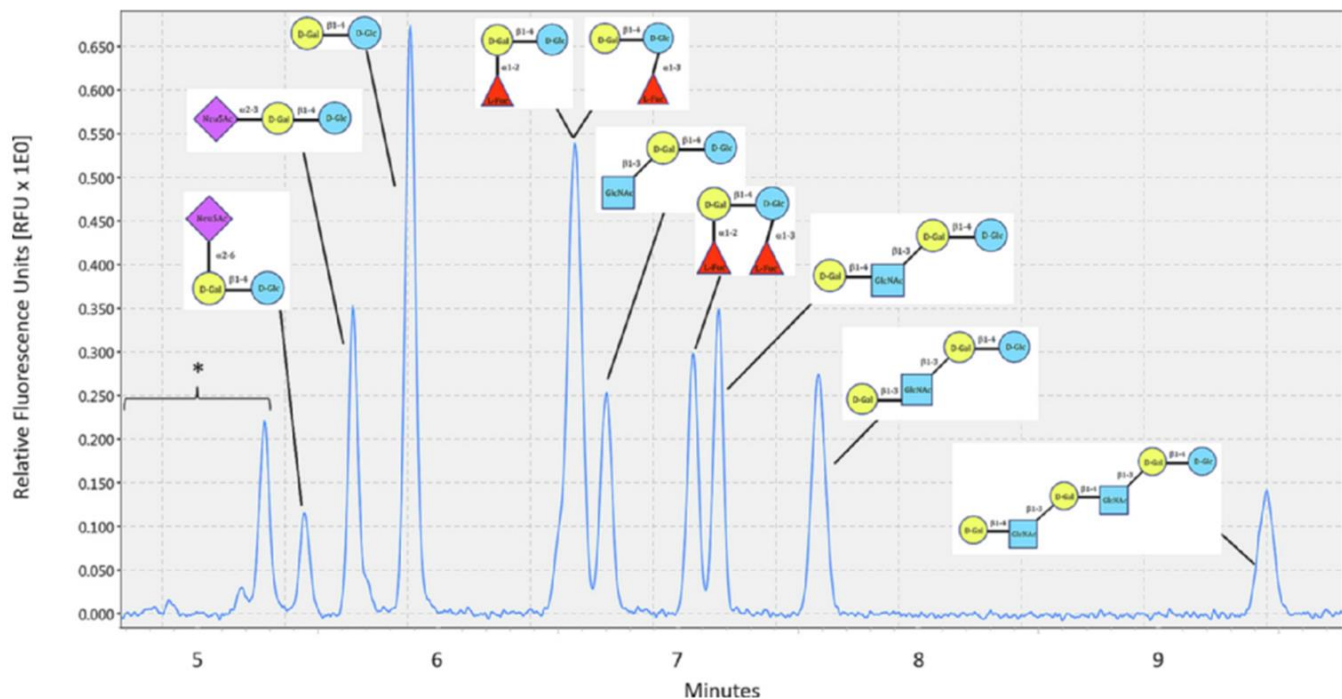


Figure 14 : CGE separation of a mix of synthesized human milk oligosaccharides. From [134].

A study involving 16 independent academic, pharmaceutical and national authorities' laboratories in the USA was performed to showcase the use of this method in N-glycan analysis in the context of the pharmaceutical industry [135]. It showed that this method was suitable for quality control of therapeutic glycoproteins with satisfying inter laboratory reproducibility. This method was also applied to various sample to characterize the glycosylation of monoclonal antibodies [136]. This method has also been used for diagnostic purposes: N-glycans from patients with ovarian cancer [137], in lung diseases [138] or multiple myeloma [139].

The use of the "Fast Glycan Analysis and Labelling" kit from Sciex© has allowed the method of sample preparation for APTS labelling to be completely automatized using a pipetting robot [140]. In the same fashion, multiplexing of several capillary was performed to allow parallel separation of several different samples which provided significant time gain [141, 142]. For the identification of glycans, although it cannot be directly done as with MS techniques, fluorescently tagged glycan standards exist, meaning absolute quantification of N-glycan is possible by CE-LiF [127]. Methods of identification and quantification of glycans in CE-LiF will be covered in I.4.5.

Coupled with LiF detection, CE is a robust, transferrable, automatable, quantitative, resolutive and extremely sensitive method, requires limited amount of sample and can be paralleled for higher throughput [131]. Nevertheless, lengthy required sample treatment is a limitation for high throughput glycan analysis. As CE-LiF is a relatively new staple in glycan analysis, separation methods must still also be improved for LiF detection [131].

I.3.2.2.1.1. Capillary electrophoresis with mass spectrometry detection.

As previously showcased, CZE is a powerful separation method with numerous advantages including high resolution, high reproducibility and ease of use. When coupled with MS detection, the most informative and one of the most sensitive detection techniques [143], capillary electrophoresis with mass spectrometry detection (CE-MS) is obtained. The separation is performed in a classical CZE separation mode, i.e., in a fused silica capillary with applied tension while detection is performed with MS after ionization of the analyte and detection with a time-of-flight mass spectrometer for example. Ionization is mostly performed by ESI in commercial instruments [144]. As always with CZE methods, glycans require derivatization, often with APTS as in CE-LiF [145]. The negative charges added by APTS ensure the glycan can be separated using a neutral capillary, which can be useful when EOF suppression is desired. LiF detection can also be combined with CE-MS for quantification of glycans thanks to the CE dimension while acquiring information on glycan composition thanks to the MS dimension.

Although CE-MS can seem like an ideal separation technique for glycans combining best of both worlds in CE and MS, coupling CE and MS poses technical challenge and requirements:

- In order to be able to ionize the sample, the electrolyte used during CZE separation must be compatible with ESI [144], which limits electrolyte choice to a volatile mix with low ionic strength. This prevents many CZE methods to be used because of non-volatile electrolyte, as well as the use of CGE because gel is not compatible with CE-MS [145]. In practice, standard methods cannot be used and the working electrolyte for CE-MS separation must be optimized in nature and pH.
- Mismatch in working flow rates. In CZE flow rates are usually 1-100 nL/min, while flow rates in MS are ranging from 1-200 μ L/min [143]. One solution is to use a “sheath-liquid”, which is a liquid flown often co-axially to the CZE separation and mixed with the electrolyte at the tip of the capillary [146]. It is used to accelerate the flow rate of the electrolyte, to maintain electrical contact between electrolyte and electrode and to favor ionization. While sheath-liquid is compatible with most electrolytes, it induces analyte dilution and adds “chemical noise” [143]. Alternatives micro- and nano-electrospray systems that are adapted to the range of flow rate used in CZE have been developed, eliminating the need for sheath flow.
- Because the CZE interface is associated with the ESI interface, proper grounding of the electrical system is paramount. CZE capillary outlet and ESI sprayer needle can be grounded using a 40-100 M Ω resistance [143].

CE-MS was used to map N-glycans from human serum glycoproteins [147]. Although separation presents poor resolution, direct identification using MS allowed detection of 77 potential glycan structures in human serum, 31 more than previously.

CE-MS is a technique that shines in terms of sensitivity and direct identification of glycans, while CGE-LiF shines with its great resolution, sensitivity, robustness, quantification and ease of use. In conclusion, CGE-LiF and CE-MS are both very useful for glycan analysis, and they provide complementary information. One requirement for both techniques is enzymatic

release and derivatization of the released glycans, which will be covered in the next subchapter.

1.3.2.3. Chromatographic methods

Chromatographic methods are widely used for the analysis of glycans. As with CE, standards and identification methods are required, and chromatographic methods are great at separating isomers. Furthermore, coupling of liquid chromatography (LC) with electrospray ionization MS detection is easy, making LC and MS very complementary. This manuscript will focus on the two mainly used LC techniques: porous graphitized carbon liquid chromatography (PGC-LC) and hydrophilic interaction liquid chromatography (HILIC).

1.3.2.3.1. Porous graphitized carbon liquid chromatography

In porous graphitized carbon liquid chromatography (PGC-LC), glycans are retained by a graphitized carbon solid phase [148]. Glycans interact with the solid phase based on hydrophobic, polar, and ionic interactions and are eluted usually with a mobile phase containing water, acetonitrile, and a volatile acid, base or buffer. They are separated depending on size, number and bond type (α -2,3 or α -2,6) of terminal sialic acid residue and depending on their antennae disposition. As seen in Figure 15, 3 glycans isomers with the same m/z ratio are separated using PGC-LC. Ionic strength, pH and temperature of the mobile phase play a role in the elution of glycans, notably in sialylated glycans [149]. Mobile phase must then be carefully selected depending on the type of glycans to be observed. With PGC-LC derivatization is not required, minimizing loss of sample resulting from chromophore tagging and following purifications [150].

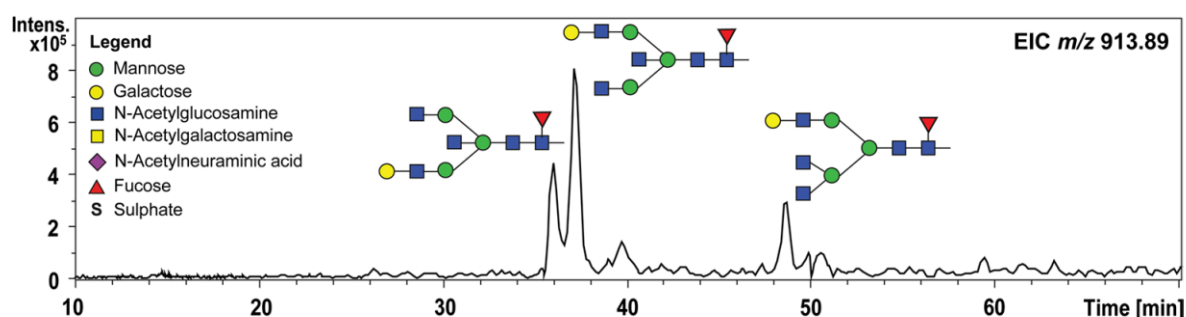


Figure 15: Extracted ion chromatogram of 3 glycans isomers with same m/z ratio separated by PGC-LC with MS detection. From [150].

Contrary to CE (both CZE and CGE), PGC-LC is highly compatible with MS detection and is usually used in tandem with ESI MS. PGC-LC has a high separation power of structural and linkage isomers, molecules with same m/z are separated by the PGC dimension and their content is analyzed by MS [150]. PGC-LC has the highest separation power for sialylated glycans [151], and is also useful for analysis of fucosylated N- and O-glycans and oligomannosidic N-glycans [150].

1.3.2.3.2. Hydrophilic interaction liquid chromatography

Hydrophilic interaction liquid chromatography (HILIC) uses a combination of a hydrophilic stationary phase (amide-derivatized silica is mostly used [152]) and of a hydrophobic, mostly

organic mobile phase (often acetonitrile [153]). Mobile phases are usually compatible with online ESI-MS [154]. Glycans interact with the stationary phase by hydrogen bonding, ionic interactions, and dipole-dipole interactions. They are thus separated depending on their size, charge, and steric properties, resulting in isomer separation [154]. HILIC is the most used chromatographic technique: it provides excellent resolution (isomers separation), good repeatability in elution time and good sensitivity with fluorescence detection.

HILIC with fluorescence detection is a standard method of separation and quantification of N-glycans. Applications of HILIC for glycan separation include analysis of IgG glycosylation in rheumatoid arthritis [155], early perimenopause diagnosis [156], therapeutics antibodies control [157, 158] or separation of sialylated glycans from whole serum separation [159].

Liquid chromatography methods are currently the most used for glycan separation. Techniques exist for both native and labelled glycans, isomeric separation can be performed without losing the possibility of coupling with ESI-MS and separation efficiency and sensitivity can be improved by using UHPLC or nanoLC systems [160]. Relatively long separation times (~1h) and need for relatively high sample volumes can also be partially solved by using UHPLC and nanoLC. PGC-LC is better at separating isomers and has a lower chemical background noise compared to HILIC but is not suited for large scale studies due to robustness issues [125].

I.4. N-glycan analysis workflow for CE-LiF analysis

As seen in the previous chapter, resolute methods for the analysis of glycans cannot be performed on native glycoprotein. First, the glycan must be released from the glycoprotein by enzymatic or chemical means. Then, derivatization is required in order to be able to detect the glycan and/or to protect it. As this subchapter focuses on CE-LiF analysis, most derivatization will not be mentioned. Information on chemical modifications of glycans for fluorescence and MS detection can be found here [161]. After derivatization, purification of the sample is often required to remove excess fluorophore and reagents. This process of glycan sample preparation, or sample treatment can also be adapted into a high-throughput format. After the process is finished, separation by CE, detection by LiF and glycan identification can be performed for identification of glycans from the glycoprotein samples. All these steps are detailed in this subchapter.

I.4.1. Glycan release

Enzymes are the favored way of releasing glycans from the glycoprotein backbone. Chemical methods are less popular because they tend to be time-consuming, employing potentially dangerous reagents and sometimes cause the loss of fragile sugar residues in glycan (mostly sialic acids which are labile) [113, 161]. When available, enzymatic methods are almost always preferred to chemical ones. Both hydrazinolysis and β -elimination, which are used for O-glycan release, are lengthy and mostly not adapted for N-glycans. In the case of O-glycans, due to the variety of glycosidic bonds with the glycoprotein, an enzyme which digests all O-glycans does not exist, but enzymes release specific core 1 O-glycans exist [162]. For other O-glycans, chemical methods such as hydrazinolysis and β -elimination are used but will not

be covered in this manuscript. More information on release of O-glycans can be found here: [98, 162].

1.4.1.1. Enzymatic methods

The most commonly used enzyme for N-glycans release is peptide-N4-(Nacetyl-beta-glucosaminyl) asparagine-amidase (PNGase F) [113]. PNGase F cleaves the amide linkage of the Asn residue linked to the oligosaccharide chain to form Asp and a glycosylamine which is hydrolyzed slowly under physiological conditions to generate free oligosaccharides. Cleavage mechanism is presented in Figure 16. PNGase F is a reliable and versatile enzyme which can cleave all types of N-glycans (complex, high-mannose, hybrid, tetra antennary structures) and does not require harsh reaction condition (optimum working pH of 8.6) [163]. Only the presence of a fucose residue α -1,3-1inked to the first GlcNAc can prevent the release of a N-glycan, which mostly occurs in plant glycoproteins. PNGase F cannot cleave glycans from most native proteins and requires a denaturation step [164], which conveniently is rather simple. Samples containing glycoproteins are reduced using sodium dodecyl sulfate (SDS), iodoacetamide, dithiothreitol and/or mercaptoethanol [165-168].

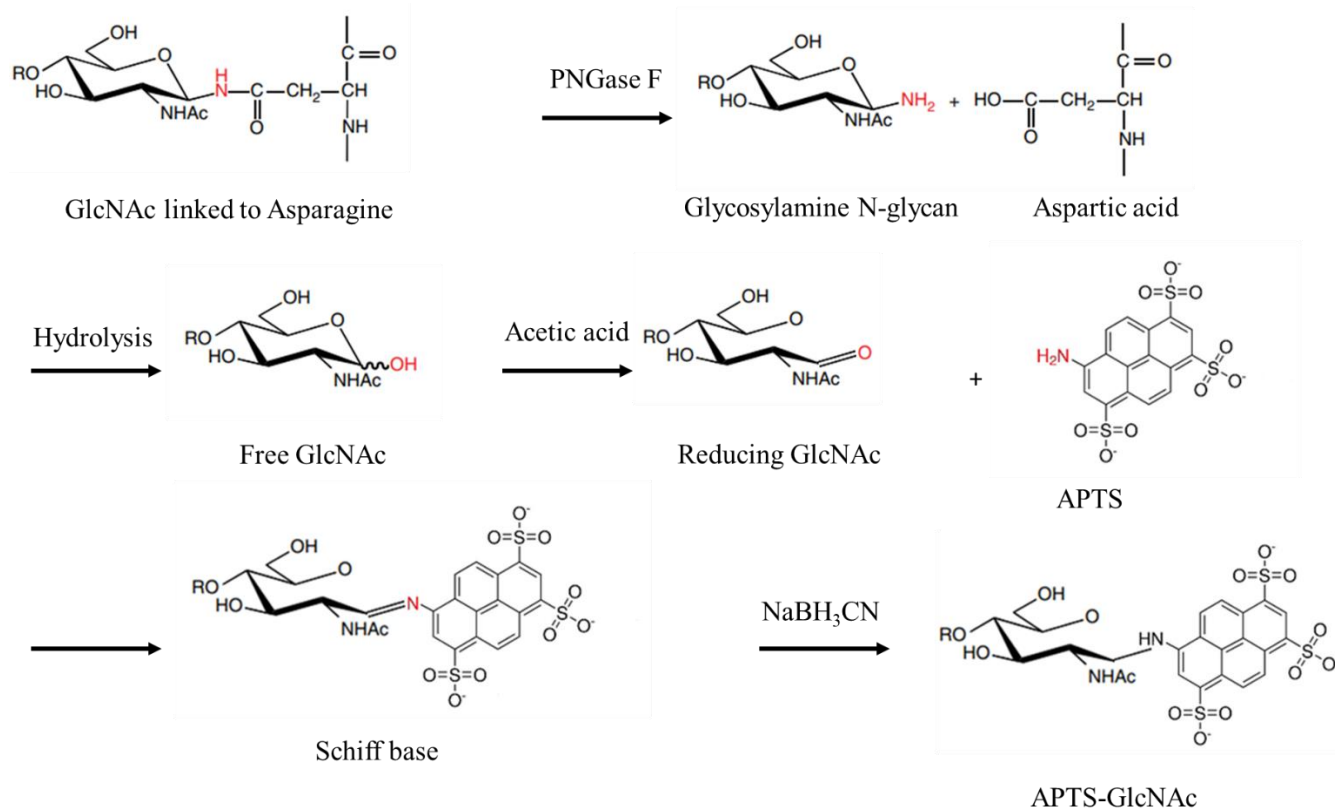


Figure 16: Release and derivatization reaction for APTS-glycans. Release of glycan by PNGase F is followed by reductive amination using acetic acid and NaBH₃CN. Adapted from [169].

Enzymatic release using PNGase F is usually performed in presence of NP-40 [113] at 37°C with overnight incubation [161], but efforts to lower the overall deglycosylation step time led to the study of the influence of temperature in enzymatic digestion with PNGase F of glycoprotein standards [170]. No difference in the amount of release glycans was observed after incubation during 1h at 50°C compared to 37°C overnight. In addition to temperature,

several strategies can be used to accelerate PNGase F glycan release: pressure cycling technology [171, 172], microwave irradiation [173, 174], using immobilized PNGase F in a microreactor [175, 176], immobilized PNGase F on magnetic beads [168] or PNGase F immobilized on graphene oxide reagent [177].

As seen in [Figure 16](#), glycans are released as glycosamine glycans. Glycosamine are stable at pH 8.8 and the hydrolysis reaction to form free glycan is significantly slow [171]. This is useful for direct modification of glycosylamine glycan with amine-reactive fluorescent tags.

If only specific types of glycan are of interest, endoglycosidases exist to cleave specific glycans from native protein (no denaturation is required) [113]. As an example, Endo F1 is an enzyme which cleaves specifically high-mannose or hybrid glycans but not complex glycans while Endo F3 cleaves only bi- and tri-antennary glycans. Overall, a whole array of N-glycosidases and endo-N-acetylglucosaminidases exist for wide range of N-glycan releases.

1.4.1.2. Chemical methods

Even though chemical methods are mostly used for O-glycan release, they can be applied to N-glycans. An improved β -elimination was performed in 1 hour with the addition of hydroxylamine and allowed the release of N-glycans [178]. While notably less expensive than PNGase F release, recovery was not as good as with PNGase F and sialylated glycans were deacylated, hindering separation. Son et. al. [179] presented a method of glycan release using NaClO, which is commonly found in bleach, which released N-glycans in 15 min. While the method is fast and inexpensive, ~20% of glycans are degraded (first GlcNAc is removed) which makes data analysis difficult and requires large amounts of samples, making it unsuitable for use in human.

PNGase F is the preferred way of releasing N-glycans, which then requires fluorophore labeling to be detected by LiF.

1.4.2. Glycan derivatization for laser induced fluorescence detection

APTS is the most used fluorescent dye for CE using LiF detection [131]. Indeed, APTS presents certain advantages in CE:

- APTS-glycan have a fluorescence signal about 40-fold higher than residual APTS [180]. This is due to the combination 488-nm excitation with a carefully selected 520-nm emission filter which suppresses free APTS while selectively detecting APTS-glycan. This in turn limits the intensity of unwanted peaks due to free APTS detection in electropherograms.
- APTS bears 3 negative charges, which allows neutral glycans to migrate in the electric field of CE and thus be separated by charge and hydrodynamic radius [131].
- CE-LiF analysis with APTS-glycan is a robust and reproducible method. It was shown by an inter-institute study, performed between 16 research institutes using the same glycoprotein mixture samples, APTS labeling method and CE-LiF instrumentation [135].
- Excitation at 488 nm is less likely to produce interferences from biological fluids than dye excited at 325 nm [180].

- APTS reductive amination reaction is almost 100% efficient [180]. This ensures no further sample losses occur after enzymatic release.

APTS is added to glycan by reducing amination, which is presented in [Figure 16](#). After enzymatic release the glycan is in solution as a glycosylamine. At this stage, APTS is added in acetic acid, in order to favor hydrolysis and the opening of the ring [181]. The obtained reducing GlcNAc then forms an unstable Schiff base with the APTS, which is then stabilized using sodium cyanoborohydride (NaBH_3CN) as a reducing agent under high temperature (65-80 °C) [161]. The conditions of reductive amination are important, as strong acids and temperature can cause loss of terminal sialic acids, although stronger acids are associated with increased derivatization yield [132, 170]. Interestingly, the optimal conditions were found using an evaporative method rather than with a sealed vial [132]. Assuming that the optimal reagent concentration is reached because of evaporation at some point of the process, APTS labeling of glycan was optimized with the following conditions: released glycans were mixed with APTS in acetic acid and NaBH_3CN solubilized in tetrahydrofuran (THF). The total volume reaction was 15 μL , and incubation was performed at 50°C, first closed vial for 60 min and then the vial lid was opened for evaporative labeling during 60 min. These parameters resulted in the best compromise between labeling efficiency and sialic acid loss. Alternatives also exist for the choice of reducing agent. NaBH_3CN is responsible for the production of the highly toxic and volatile hydrogen cyanide during reductive amination [182]. Non-toxic alternatives include 2-picoline borane [182] and sodium triacetoxymethylborohydride ($\text{NaBH}(\text{OAc})_3$) [183].

Other fluorescent labels used for CE-LiF of carbohydrates include 2-aminobenzoic acid [184, Kinoshita, 2020 #625], 7-amino-4-methylcoumarin [185] and Instant Q [186, 187]. Most analytical techniques, including CE-LiF, require purification of the modified glycans, mostly in order to remove the remaining reagents used in release and derivatization steps which are problematic for the following workflow [161].

I.4.3. Purification

Solid phase extraction (SPE) is the favored mode of purifying glycans samples. Compounds of interest in solution are forced to interact with a solid phase which can retain compounds depending on various physical properties. SPE is sometimes coupled with liquid-liquid extraction, where compounds are transferred to another immiscible liquid phase.

For purification of APTS-glycan, the gold standard method using solid phase reversible immobilization was proposed by Guttman et. al. [132, 170, 175, 188]. Using magnetic beads coated with carboxyl (COOH) groups, they proposed two different types of extraction [170]:

- For the extraction of released glycan right after PNGase F digestion, which is performed at a working pH of 7-8. At this pH, the glycans are released as glycosylamines, which are positively charged while the COOH groups of the beads are negatively charged. Ionic interactions are responsible for the capture of glycans by the magnetic beads, which can be aggregated using a magnet. The reaction solution can then be removed without removing the released glycans. When the beads are eluted

with the aqueous APTS labeling solution in acetic acid, the glycosylamines turn into aldehydes which are no longer positively charged, breaking the ionic interaction with the beads and starting the reaction with the APTS.

- For the extraction of APTS-glycans after labeling. Since APTS bear 3 negative charges, in addition to potential negative charges from sialic acids, APTS-glycans are normally repelled from COOH-beads. In the presence of >80% of acetonitrile (ACN) in water, the ACN acts as a crowding reagent: as the beads are more stable in water due to hydrophilic interactions, the ACN/water mix is not homogenous and water, still containing the APTS-glycans, aggregates on the beads, effectively increasing the local concentration of APTS-glycans in water [170, 189]. Using a magnet to capture the beads, the excess ACN can be removed, and the process can be repeated for several purification steps (usually 4-5 steps are required).

This technique can be performed in any lab as it does not require specific equipment (only a magnet), it is easily integrated in the one-pot glycan sample treatment process and can be automated for high-throughput sample processing [140].

Hydrophilic interaction liquid chromatography can also be used for glycan purification, using aminopropyl- and polyamide-type solid phase. Glycans interact with the stationary phase by hydrogen bonding, ionic interactions, and dipole-dipole interactions, and can first be retained on the solid phase then eluted [190, 191]. For glycan suspended in water-rich conditions, porous graphitized carbon (PGC) sorbents can be used to remove salts and excess reagents [192, 193]. With PGC, sorbents must be carefully chosen depending on the hydrophobicity or hydrophilicity of the fluorescent tag [113, 161]. Solutions exist for the purification of specific glycans, for instance sialylated glycans. As serotonin has a high affinity to sialic acid, serotonin-silica packed column can be used to retain sialylated glycans [194, 195]. Titanium oxide can also be used, although requiring a supplementary preparation step, to enrich sialylated glycans [196].

SPE techniques are powerful and are sometimes coupled to liquid-liquid extraction methods such as non-polar solvent extraction [197] for glycans labelled with hydrophobic reagents. For hydrophilic reagents such as APTS, ion-pair-assisted extraction can be used in tandem with SPE [198]. Free cations are introduced in the sample solution, and free APTS-cation complex are formed and removed using chloroform.

Although necessary, purification processes add to the total length of the already long process, which can take more than 3 days [199]. Efforts to decrease the processing time have been made and high-throughput sample preparation solutions have been presented.

1.4.4. High-throughput sample preparation

Based on the works of the Guttman group [168, 170, 175], the “Fast glycan analysis and Labeling” kit was commercialized by Sciex in 2017. It contains necessary reagents for the five individual steps presented in [Figure 17](#):

- A. After denaturation of the glycoprotein, PNGase F is used for the enzymatic release of the glycans from the protein at 50°C for 1h.

- B. Solution is mixed with magnetic beads and ACN for 87.5% ACN final concentration. After mixing, the tube is placed on a magnetic stand and the supernatant is discarded.
- C. Glycans are eluted from the beads by APTS in 20% acetic acid. Reductive amination is started by the addition of NaBH₃CN in THF. Incubation is performed at 37°C during 2h.
- D. Solution is mixed with magnetic beads and ACN for 87.5% ACN final concentration. After mixing, the tube is placed on a magnetic stand and the excess fluorophore is discarded. This step can be repeated up to 5 times.
- E. The glycans are eluted in water, the beads are aggregated with the magnetic stand and the supernatant is the analyzed by CE (step F).

This process take less than 4 hours, does not require any centrifugation and/or vacuum centrifugation steps and can be automated using a 96-well plate, reducing the process time to ~2h for up to 96 samples [140].

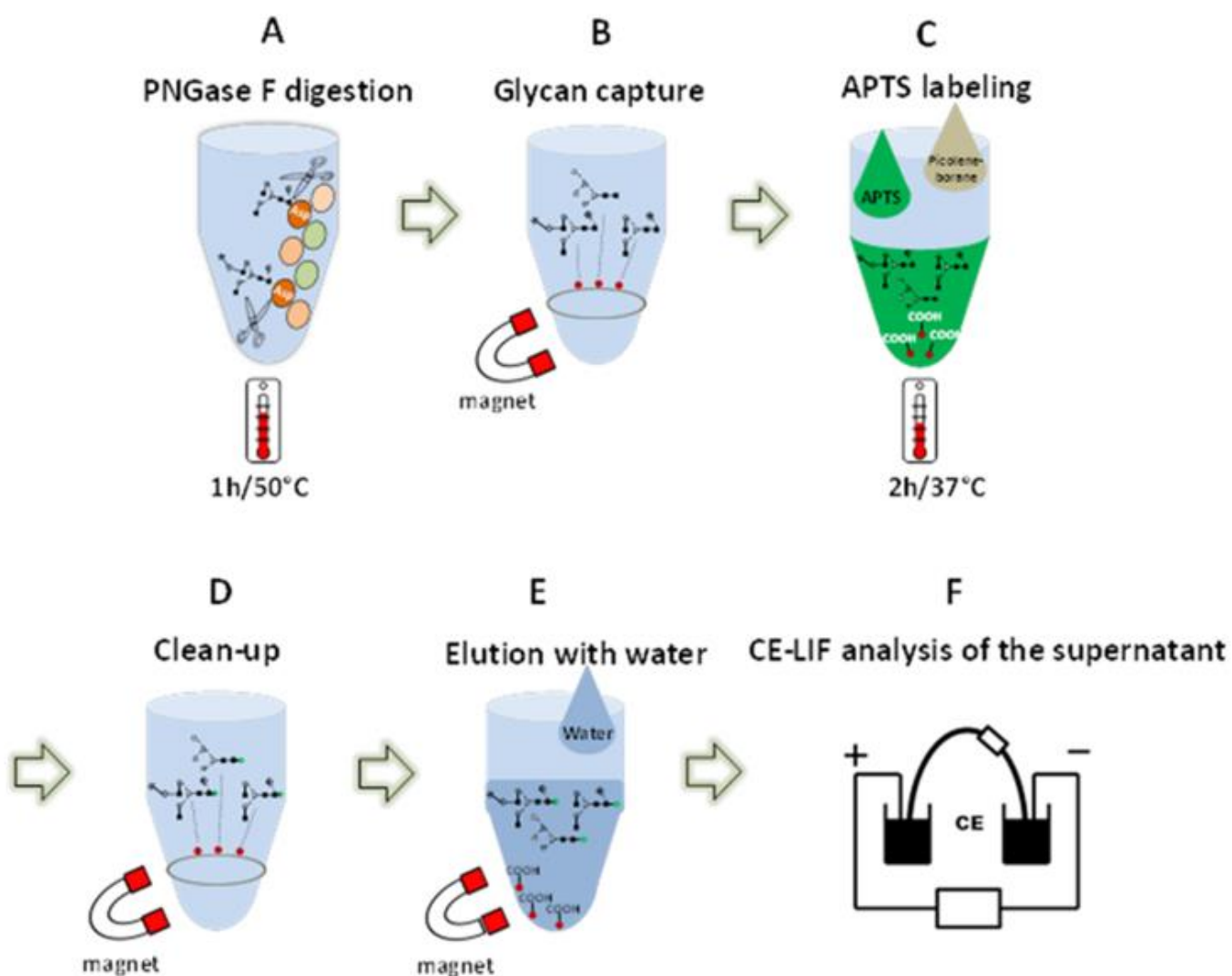


Figure 17: N-glycan release and derivatization process using Sciex kit. From [170].

Aich et.al. presented a high-throughput method for the labeling of glycans from therapeutics antibodies using a 96-well plate [199]. Using only one HILIC-SPE purification step and non-toxic reducing agent, they completed the whole glycan labeling process in 3h. Although faster than the COOH-bead method previously presented, this method is limited to glycoprotein pharmaceutical products (i.e., sample in simple matrix) and is not suitable for complex samples such as plasma or serum.

Furukawa et.al. [200] present a method using hydrazide-functionalized beads for the capture and release of glycans. The whole process for glycan sample treatment (from glycoprotein denaturation to glycan elution) can be performed within 8h for up to 96 samples. This method is then more time consuming than the previous methods presented, but the authors propose a method for the “conversion” of the functionalizing group of glycans, i.e., replacing a fluorophore by another.

The last step remaining after the whole process of glycan sample treatment is performed is to separate the glycans is CE methods.

I.4.5. CE separation and glycan structural identification

The CE separation of glycans is fully detailed in Chapter III.1. CE separation of glycans is usually performed using 50 cm effective length (60 cm total length) neutral coated 50 μm inner diameter capillaries under 30 kV (500 V/cm applied electric field strength) [170]. For rapid separation, 20 cm effective length (30 cm total length) neutral coated 50 μm inner diameter capillaries under 30 kV (1000 V/cm applied electric field strength) can be used [132, 140]. Reverse polarity is used, meaning the anode is at the injection side while the cathode is at the detection side. APTS labeled glycans are negatively charged and migrates towards the cathode while EOF is working against the separation (EOF is towards the cathode). Due to the use of a coated capillary and polymer in the separation buffer, the EOF is suppressed and negligible [129]. Typical CE setup for the analysis of APTS-glycans is showcased in Figure 18.

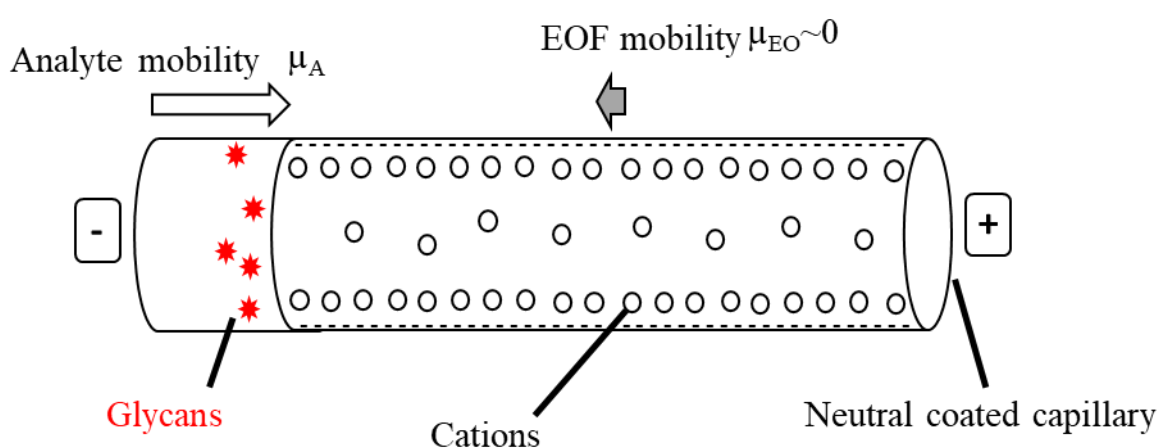


Figure 18: CE setup for the separation of APTS-glycans.

Separation background electrolyte is usually composed of 25 mM of lithium acetate at pH 4.75 with the addition of 0.4 to 1% PEO [129, 133, 140]. Acidic conditions are chosen because

the resolution of glycan separations is best at a pH of 4.75 [133] and because EOF tends to be lower at low pH [201].

Once the separation is performed, the obtained electropherogram must be analyzed and interpreted. As mentioned previously, direct identification of glycans is not possible for techniques such as LC and CE, in opposition to MS. Several techniques have been developed for this purpose, applicable for both CE and LC although CE is our focus in this manuscript.

Maltooligosaccharide ladder (MD ladder) is a mix of polymers of α -1-4-linked glucose, their degree of polymerization (DP) ranging from 1 up to dozens [202]. For each different maltooligosaccharide, a glucose unit (GU) is associated corresponding to its DP. For example, the maltooligosaccharide with a DP of 5 will have a GU of 5 (often written DP5 or GU5). By comparing the electropherogram resulting from a sample of MD ladder to a sample containing glycans under the same conditions, GUs can be associated for each glycan peaks to be identified. Using GU values instead of migration time allows to alleviate all variations that can happen between two different separations: parameter changes, capillary history (new or used capillary) and buffer composition [203]. If we consider a glycan X one wants to identify, its unknown glucose unit GU_X and its measured migration time t_X .

Equation 1 : GU calculation

$$GU_X = G_N + \frac{t_X - t_N}{t_{N+1} - t_N}$$

If we consider t_N and t_{N+1} the migration time of the MD ladder with DP N and N+1 corresponding respectively to the preceding and following the unidentified peak. G_N is the DP of the MD ladder with DP N immediately preceding our glycan X. GU_X is calculated using Equation 1 [203].

Equation 2 : Example of GU calculation for peak 2 of Figure 19.

$$GU_X = 4 + \frac{13,85 - 13,16}{14,24 - 13,16} = 4.63$$

An example is provided in Figure 19. Let us consider the unknown glycan X represented by peak 2. The preceding and following glycans are DP4 and DP5. Equation 2 shows the calculation to obtain GU_X .

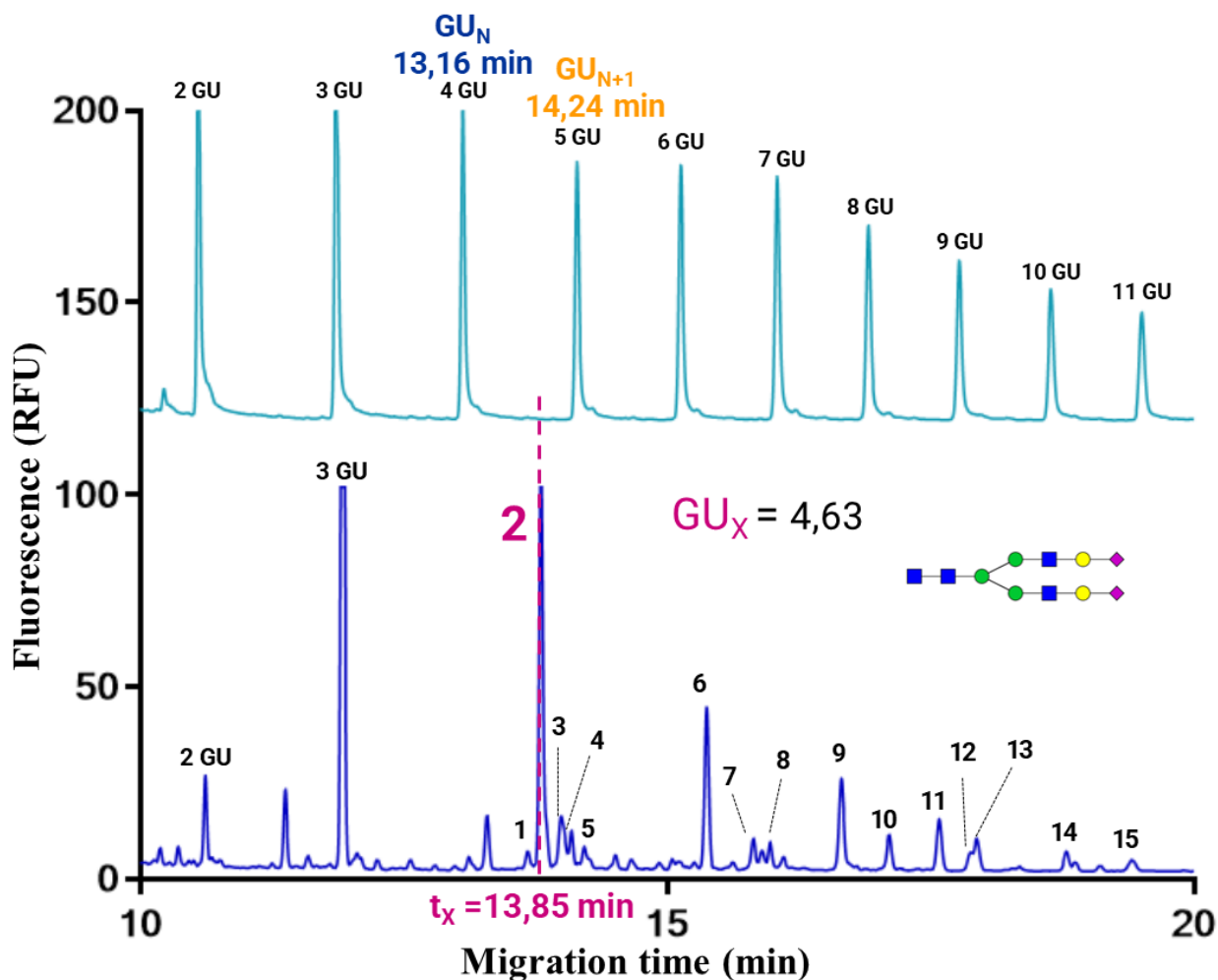


Figure 19 : Example of GU calculation for the unknown glycan represented by peak 2. The top trace represents the migration of a MD ladder sample, and the bottom trace represents the migration of a glycan sample of unknown concentration.

Once the GU values of the peaks to be identified have been calculated, a database can be used to associate the GU with a structure: GlycoBase [204], Glycostore [205] or GlycoSuite DB [206]. In our case the closest structure found in the database corresponds to the bi-antennary, bi-sialylated N-glycan showcased in Figure 19.

As this manual approach to calculating GU can be tedious and time-consuming, Jarvas et. al. [203] developed a software called GUcal which can be used for the automatic calculation of GUs from an electropherogram. Traces for MD ladder and glycan samples are loaded, peaks are automatically detected but can also be added manually. Corresponding migration times are obtained automatically, and for each peak the GU is calculated and a glycan from the software database is proposed.

This GU approach is powerful for the identification of glycans using CE-LiF, but it does present a major drawback: a MD ladder separation is required with each glycan separation for identification, effectively doubling analysis time. While one can use a single MD ladder for

several consecutive separation, separation conditions will vary, and migration time shifts will occur between separations. This is due to variance in wall coverage, i.e., coating issues and adsorbed analyte molecules, alteration of the background electrolyte or impurities [202]. Co-injection of the MD ladder with the sample is not an option, as it is very likely that the MD ladder and sample peaks would overlap.

This approach was then improved by Jarvas et.al. [202] to solve this issue. They found that the migration time of all MD ladder peaks could be reliably predicted based on the measure of migration time for DP2, DP3 and DP15 [202, 207]. By co-injecting the sample with standards of DP2, DP3 and DP15, identification of glycans can be performed accurately and reliably performing only one separation. Conveniently, N-glycans have GU values between 3 and 15, meaning that the DP2, DP3 and DP15 standards will not overlap with the glycans of interest. It should also be noted that DP3 standard can be added during the labelling process to provide information about labelling efficiency, as an internal labelling standard.

Alternatively, a series of exoglycosidases can be used [138]. Exoglycosidases are enzymes that specifically digest single monosaccharides from glycans depending on their linkage and anomericity, i.e., one exoglycosidase can be chosen to selectively digest α 1-3 Fucose and not digest α 1-6 Fucose. By performing an analysis between each exoglycosidases digestion until the pentasaccharide core is obtained, a series of electropherogram can be obtained, and shifts in migration time and peak area can be analysed to deduce the original structures. This can be used when no databases are available, as it requires multiple separation and exoglycosidases digestion for identification, resulting in a lengthy process.

Lectins can also be used for affinity CE [208]. A first normal separation is performed, then a second one is performed with the addition of lectins in the background electrolyte. Depending on the affinity of the lectin to the glycan, complexes will be formed, and migration times will be increased. By comparing the two electropherograms, information can be gathered on the analysed glycans. As previously, series of lectins can be used to facilitate glycan identification [209]. Background electrolyte selection (composition, pH, and concentration) must be carefully tuned for the use of lectins, and they can adsorb to the capillary wall.

1.5. Conclusion

Glycoprotein glycosylation is a complex process: due to enzyme-based glycan synthesis, glycans are highly heterogeneous (macro-and micro-heterogeneity). Each glycoprotein exists under several glycoforms, and numerous glycan structures exist such as: and N-glycan (complex, hybrid, high-mannose) and O-glycan (GalNAc, GlcNAc, Xylose, Gal, Man, Fuc or Glc core). Glycans have various functions in the human body: they help protein fold, limits their aggregation, resistance to thermic denaturation, cellular interactions, antibody-dependent cellular cytotoxicity, prevent antigenic binding and create immune responses. Because of the wide structural complexity of glycans structure and synthesis, and their numerous functions in the human body, glycosylation defects exist under a lot of different forms and are part of plenty diseases, such as CDG. Some abundant glycoproteins can thus be used as biomarkers for the diagnosis of such diseases. Consequently, the analysis of glycoproteins, either the

intact glycoproteins are the released glycans, requires an arsenal of various analytical techniques, such as CE-LiF, which is a resolutive, highly sensitive and robust technique for the analysis of glycans. As glycans are naturally non-fluorescent, a fluorophore (usually APTS) must be attached to the glycan for LiF detection, requiring several preparation steps. First the glycoproteins must be denatured, followed by digestion using PNGase F. Then APTS is attached to the glycan by reductive amination, followed by purification of the excess APTS and reagents by solid-phase extraction using COOH coated magnetic beads. After the CE-LiF separation performed using a background electrolyte containing a polymer for EOF suppression, electropherogram are interpreted and glycans are identified using the GU approach, either by performing a complementary run of MD ladder standard, or by co-injecting a triple standard.

Although efforts have been made to improve both glycan sample treatment and CE-LiF separation of glycans, CE-LiF is not yet ready to be used as a routine analysis technique for the diagnosis of CDG. Glycan sample treatment remains a dangerous process (toxic reagents), requiring a trained worker as it is a manual process and long (4h). CE-LiF separation requires expensive commercial instruments and background electrolytes, and its performance could be improved. In this context, microfluidic solutions could be adapted as an attempt to solve these issues. Microfluidics is a growing field of science with inherent advantages such as reduced sample and reagents consumption, shorter reaction times and better heat exchange [210]. Microfluidics solutions were actually developed for sample treatment of glycan for HPLC separation and/or MS detection [211] but not for CE-LiF to the best of our knowledge. The use of microfluidic droplets, allowing creation and manipulation of discreet droplets considered as micro-reactors inside a microfluidic channel [212] could be a solution for the sample treatment of N-glycans for CE-LiF analysis. In addition, such solutions could be coupled to a droplet-interface microscale electrophoresis and capillary electrophoresis systems, which were the object of a review made during this thesis [15], for on-line separation of the labelled glycans. The next chapter will present the fundamentals of droplet microfluidics, and present solutions both for sample treatment and CE/microscale CE separations using microfluidic droplets.

II. Chapter 2: Droplet microfluidics in analytical chemistry

Microfluidics was born out of miniaturization efforts made for microelectro-mechanical systems (MEMS) in the first place, MEMS being themselves made possible by breakthrough in photolithography for microelectronics. Although we have been able to observe the micrometric scale for a long time (optical microscope invented in the 16th century), acting at a microscopic scale is much more challenging. MEMS were then created to act at the microscopic in the 1980s and a decade of development later, they were diversified and were used for chemical, biological, and biomedical applications. Some of those systems were using fluids under unusual and unexplored conditions, leading to the creation of a whole new field: microfluidics. Microfluidics can be defined as “the study of flows, simple or complex, mono- or multiphase, which are circulating in artificial microsystems” [213]. Although distinction between “macrofluidics” and microfluidics can be made depending on the size of the system, a better distinction can be made by physical effects becoming predominant. Typically, three major phenomena become crucial in microfluidics: highly efficient mass-heat transfer, relative importance of viscous force over inertial forces and significant surface effects [214].

One specific branch of microfluidics focuses on multiphase microfluidic flows: droplet microfluidics. In droplet microfluidics, discrete droplets of micrometric size are manipulated in immiscible multiphase flows in microchannels [214]. Droplets can range from a few μL to sub nanoliter scale and can be seen as microreactors in which isolated chemical reactions can take place with enhanced mixing and heat exchange [214]. Droplet microfluidics is now a significant branch of microfluidics and presents several advantages:

- Miniaturization: droplets can be smaller than a nanoliter, which makes single-cell or molecular analysis possible.
- Compartmentalization: droplets can be seen as independent reactors which can be individually manipulated.
- Parallelization: since droplet creation is most often mono-disperse, large number of reactions can be performed and compared for high-throughput analysis platforms.

In the context of analytical sciences, droplet microfluidics have been used for several techniques: spectroscopy, microscopy, electrochemical detection, mass spectrometry, capillary electrophoresis and sample treatment [11, 12]. This chapter will focus on the use of microfluidic droplets in analytical science, with particular attention to glycan sample treatment and APTS-glycan separation and analysis. First, an introduction to the field of microfluidics will be given, with general considerations and a focus on droplet microfluidics. Then, droplet microfluidics will be highlighted in the context of analytical separation techniques: application of microfluidics droplets will be presented for HPLC, MS and for CE with our review. Finally, microfluidics systems for the sample preparation, enrichment and separation of glycans both with commercial and custom-made instruments will be presented.

II.1. Droplet microfluidics fundamentals

II.1.1. General microfluidic introduction

Although it might not be obvious that physics at micrometric scale is fundamentally different than that of macrometric scale, some phenomenon or objects must be approached

differently. The first consideration is how the equilibrium of forces evolves between macrometric systems (decimetric dimensions) and micrometric ones (micrometer dimensions). One can define the length scale l controlling all dimensions of the system of an object, i.e., when l decreases all dimensions of the system (height, length and width) decrease while maintaining constant aspect ratios. When considering physical quantities, a scaling law can be defined depending on l . For some quantities the scaling law is quite obvious, such as for mass m and volume V where $m \sim V \sim l^3$. The scaling law of some quantities are presented in [Figure 20](#). The general rule using those scaling laws is the following: in miniaturized systems, the quantity which scaling has the lowest exponent will dominate. For example, when comparing the scaling exponent of gravity and capillary forces, one can conclude that gravitational forces are negligible compared to capillary forces in miniaturized systems, while in our macrometric world the opposite is true. This can be illustrated by phenomena happening in nature by looking at water walking: if we consider an animal of characteristic length l , surface forces tend to maintain the animal out of the water while gravity tends to immerse it [213].

Quantity	Scaling law
Intermolecular Van der Waals force	l^{-7}
Density of Van der Waals force between interfaces	l^{-3}
Time	l^0
Capillary force	l^1
Distance	l^1
Flow velocity	l^1
Thermal power transferred by conduction	l^1
Electrostatic force	l^2
Diffusion time	l^2
Volume	l^3
Mass	l^3
Force of gravity	l^3
Magnetic force with an exterior field	l^3
Magnetic force without an exterior field	l^4
Electrical motive power	l^3
Centrifugal force	l^4

Figure 20 : Scaling laws for various physical quantities. From [213].

Some macromolecules such as animal cells can range from 11 to 30 μm . If one considers a microfluidic channel of 100 μm width and 100 μm depth, the size of the cell becomes comparable to the dimension of the channel. Via different strategies in microfluidics, these macromolecules can then be individually manipulated for single-cell analysis [215, 216].

In order to characterize the different equilibrium of forces in fluidic systems, different dimensionless numbers exist for different situations. For a fluid in motion, the Reynolds number represents the ratio of inertial forces to viscous forces:

Equation 3 : Reynolds number. ρ is the density of the fluid, v is the characteristic speed of the fluid, L is the characteristic length of the microfluidic system and η is the viscosity of the fluid.

$$R_e = \frac{\rho v L}{\eta}$$

The Reynolds number is typically used to determine if a flow is turbulent or laminar: for $R_e < 2300$, flow is laminar [217]. In microfluidics, except extreme situations, $R_e < 1$ typically [218] meaning the flow is always laminar. In this situation, a flow in a cylinder-shape microchannel produces a parabolic flow profile: the Hagen-Poiseuille type flow described in Equation 4 and illustrated in Figure 21.

Equation 4 : Hagen-Poiseuille law. The velocity of the fluid v at a distance r from the center of the channel and the flow rate Q depends on the viscosity of the fluid η , the pressure difference $\Delta P = P_{in} - P_{out}$, the radius of the channel R and the length of the channel L .

$$v_z(r) = \frac{1}{4\eta} \frac{\Delta P}{L} (R^2 - r^2)$$

$$Q = \frac{\pi \Delta P R^4}{8\eta L} = \frac{\Delta P}{R_H}$$

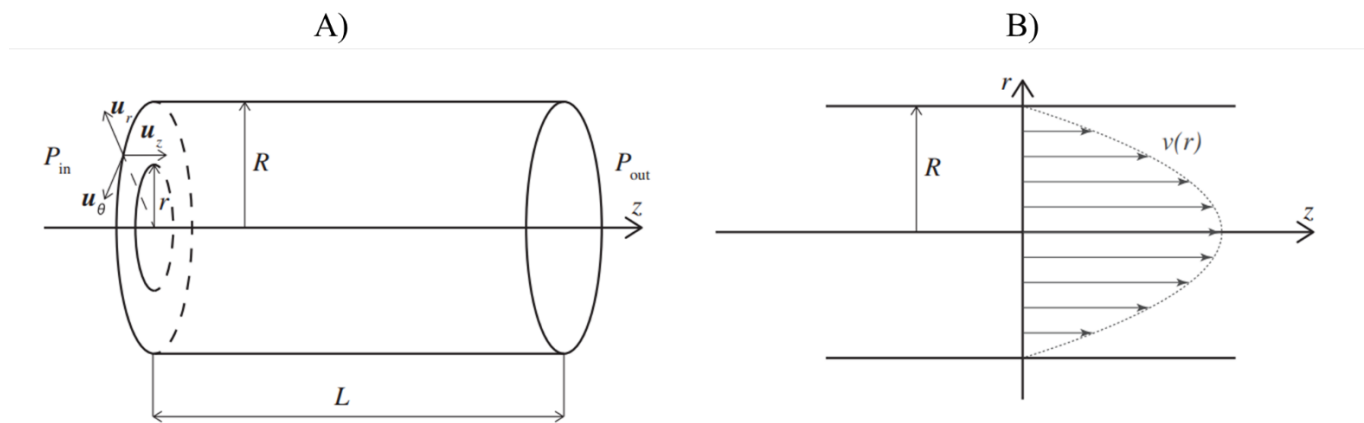


Figure 21 : A) Characteristics of a cylinder-shaped microchannel and B) Hagen-Poiseuille flow profile in such a channel. From [218].

From Equation 4, and in analogy with electrical circuits, one can define the hydrodynamic resistance of a microfluidic system $R_H = \frac{8\eta L}{\pi R^4}$ (Equation 5). In the same fashion that the tension drop ΔV is proportional to the electric current I and depends on the resistance of the circuit R , the pressure drop ΔP is proportional to the flow rate Q and depends on the hydrodynamic resistance (which depends on the dimensions and on the viscosity) R_H . It should be noted

that the expression of R_H depends on the geometry of the system (parabola, triangle, trapezoidal). More information on this can be found here [218].

Equation 5 : Notion of hydrodynamic resistance in comparison with electric resistance

$$\Delta P = Q \times R_H$$

$$\Delta V = I \times R$$

Using this analogy, it is convenient to introduce the equivalent to Kirchoff law to easily predict the total hydrodynamic resistance of complex systems (i.e., systems with varying geometries, several channels in parallel, etc....) [218]:

Equation 6 : Kirchoff law equivalent in microfluidics.

For n hydrodynamic resistance in series.

$$R_{H_{total}} = \sum_{i=1}^n R_{H_i}$$

For n hydrodynamic resistance in parallel.

$$R_{H_{total}} = \left(\sum_{i=1}^n \frac{1}{R_{H_i}} \right)^{-1}$$

Even though working with a laminar flow is very useful in microfluidics as it allows the precise control of fluids, it consequently becomes difficult to mix in microfluidic systems because turbulent regimes are often difficult to reach. In order to evaluate the relative importance of advection and diffusion phenomena during mixing. The Peclet number describes the ratio of hydrodynamic transport forces and the molecular diffusion forces as seen in *Equation 7*:

Equation 7 : Expression of the Peclet number. U is the flow velocity, l the characteristic length of the system and D the diffusion coefficient.

$$P_e = \frac{Ul}{D}$$

Using the scaling laws introduced earlier, one can observe that $P_e \sim l^2$. One could conclude that in micrometric systems, diffusion dominates hydrodynamic transport forces and thus it is useless to agitate fluids because mixing is done thanks to diffusion. In practice because of the usually small values of diffusion coefficients D (typically in the range of $10^{-5} \text{ cm}^2/\text{s}$ for simple liquids [213]), there is no characteristic order of magnitude for the Peclet number. With a channel of dimension $100 \text{ }\mu\text{m}$ and velocities of 1 mm/s , the Peclet number is 100, meaning hydrodynamic transport forces are still dominating mixing. For a channel of dimension $1 \text{ }\mu\text{m}$ and velocities of $10 \text{ }\mu\text{m/s}$, the Peclet number is 10^{-2} , meaning in this case diffusion is dominating mixing. As those two situations are not out of the ordinary in microfluidics, one should conclude that no general conclusions can be made on the equilibrium between diffusion and hydrodynamic transport and should be studied for each system [213]. A common situation in microfluidic is one where $P_e < 1$, meaning the flow is

laminar and no turbulent mixing occurs, while $P_e \gg 1$ meaning diffusive mixing is too slow. Several mixing methods exist in microfluidics and are reviewed in the following articles [219, 220].

In terms of thermal exchanges, microfluidic systems also offer precious advantages compared to macroscopic situations. If one considers a simple system where the fluid subjected to the temperature T_2 and is separated from the ambient air at temperature T_1 by a medium of length L and thermal conductivity K as seen in *Figure 22*, the heat flux going through the medium is written [213]:

Equation 8 : Expression of the heat flux going through a medium of thermal conductivity K , cross section S and length L caused by a difference in temperature $\Delta T = T_2 - T_1$.

$$Q = \frac{KS\Delta T}{L}$$

$$Q \sim KL\Delta T$$

If one supposes that a source of volumetric heat is created: for example, by Joule effect as in capillary electrophoresis or by an exothermic reaction happening in the fluid. One can consider that the heat produced by this source scales as $Q_V \sim l^3$, whereas heat evacuated by conduction scales with l^1 . This means that in microfluidic systems, heat produced by volumetric sources is small compared to heat exchanged with the exterior, which means such systems can easily be thermalized, contrary to macroscopic system. Furthermore, the time constant of thermalization τ associated with such objects scales as $\tau \sim l^2$. This shows that when subjected to a sharp temperature change, microfluidic systems are returning faster to thermal equilibrium.

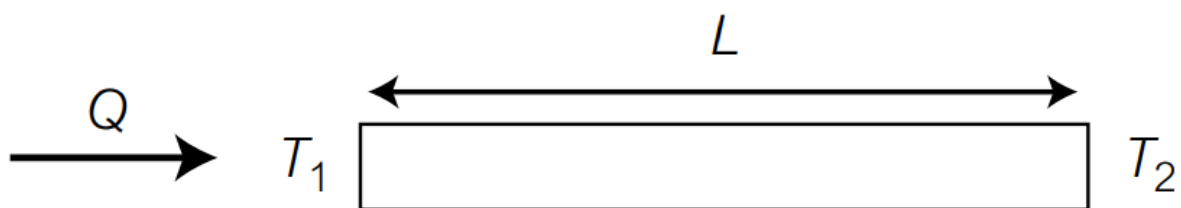


Figure 22 : Simple system for the illustration of the heat flux. From [213].

Another consequence of working at the micrometric scale is the relative importance of surface forces compared to volumic forces. Indeed, the surface to volume ratio $\frac{S}{V} \sim l^{-1}$ meaning that interfaces play a larger role in miniaturized systems [213]. Surface energy at interfaces can be visualized considering that the liquid molecules at the interface have a different “environment” than the molecules in the liquid bulk. Surface tension γ is defined as

the energy W necessary to create an additional surface area ΔA at interfaces and scales with l as seen in *Equation 9*:

Equation 9 : Expression of the surface tension at interfaces.

$$\gamma = \frac{W}{\Delta A} \sim l$$

As surface tension scales with l , in microfluidics this force tends to become dominant and situations where surface tension plays a role are characterized using the Capillary number Ca :

Equation 10 : Capillary number describing the relative importance of viscous and surface tension forces.

$$Ca = \frac{F_{viscous}}{F_{surf.tension}} = \frac{\mu v}{\gamma}$$

Interfaces play a crucial role in droplet microfluidics, where interfaces are created between immiscible fluids and will be detailed in the next subchapter.

As mentioned in the introduction, the development of photolithography for the production of microelectronics was a gateway for microfluidics systems to be created. Now a separate field, microfluidics still uses microfabrication techniques first developed for microelectronics [221] such as photolithography. Microfabrication processes are usually carried out in clean rooms, which are extremely controlled environments (temperature, humidity, traversed by a filtered flux of air) in order to remove any particles which might interfere with microfabrication, dust being the primary concern.

Microfabrication techniques can be divided in two categories depending on the type of material used: hard materials (glass, silicon) and soft materials (elastomers, plastics, paper, hydrogels). Hard materials are a legacy from microelectronics and were the first materials used for microfluidic systems, but nowadays soft materials are mostly used nowadays for several reasons, which are easily understandable by taking the example of polydimethylsiloxane (PDMS), the most used material for microfluidic systems [221]. PDMS is a silicon-based elastomer of formula $(-\text{Si}(\text{CH}_3)_2\text{O}-)$ and has many qualities making it the n°1 material:

- Its elasticity can be modulated to make it more or less stiff, which is useful for several situations. Microfluidic connections are easily connected and tight.
- It is a cheap and disposable material, and fabrication by molding allows the cheap, easy and fast fabrication of numerous amounts of chips which is useful for rapid prototyping or applications where lots of chips are necessary.
- It is transparent, making it possible to perform optical detection or to observe the flow with microscope.
- Native PDMS is hydrophobic but can also be made hydrophilic by oxidation of the surface by plasma or by contact with a strong base meaning it can be used in a wide

range of applications. It is in turn not suited for several solvents, reducing the range of applications.

- It is permeable to gases, meaning it is easier to get rid of air trapped in the system, which is often a burden in microfluidics.

For hard materials, microfabrication techniques are directly taken from microelectronics and in such are well-established and microfluidic channels are often etched either by a chemical attack in liquid phase called wet etching or by ionic species contained in gases or plasmas attacking the substrate called dry etching [213]. In the case of soft materials, the main technique used is molding. The principle of molding is to create a silicon mold using soft photolithography. Briefly, a negative photoresist is spin coated on a silicon wafer and selectively illuminated using a luminous flux and a photolithography mask. By developing it in a solvent, all unexposed photoresist is dissolved in the solvent while the insoluble illuminated zones remain. Once the mold is created, several techniques exist to obtain a negative of the mold in soft materials as seen in *Figure 23*:

- Molding: a mixture of polymer and catalyst is poured onto the mold and heated for reticulation of the polymer. Once reticulated, the solid polymer is peeled off and contains the negative pattern of the mold. This is the technique used for PDMS, and resolution as good as 15 nm can be obtained [221].
- Casting: A heated deformable material is pressed against the mold, cooled and then separated, effectively creating a negative of the mold, with precision of tens of nm [213].
- Injection molding: A heated plastic in liquid state is injected into a mold and cooled down below the glass transition temperature to be solidified. After removal of the mold a negative is obtained.

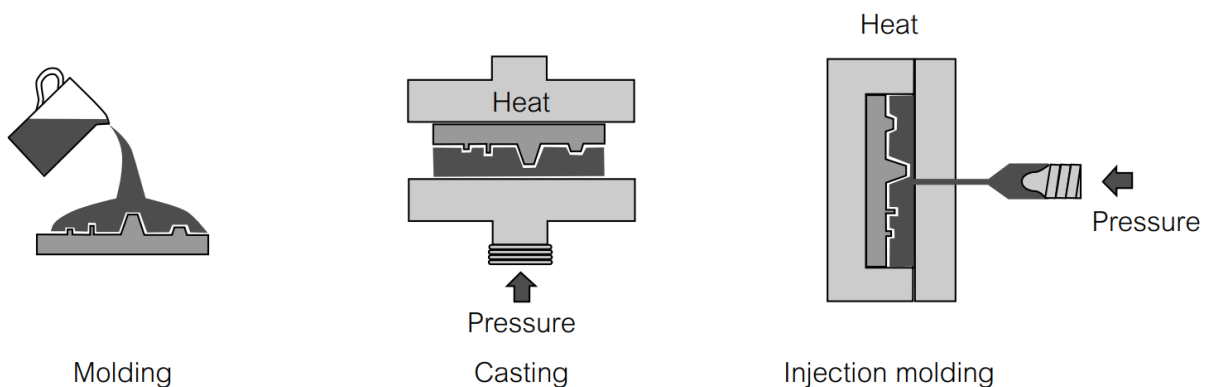


Figure 23 : Different techniques for mold replication: molding, casting and injection molding. From [213].

Other techniques exist where instead of using a mold, the channels are directly engraved. For dimensions larger than 100 μm , computer numeric control micro milling allows the microfluidic channels to be milled directly onto the glass or plastic material. It is a fast, simple technique which does not require clean room facilities and requires low-cost equipment [222]. For higher precision, the material can be directly ablated by precisely focusing a high-

energy laser beam onto it, causing the material to melt or vaporize. One drawback using such techniques is that the obtained surface roughness can be worse than with molding techniques. Finally, 3D printing has become a microfabrication technique of choice due to considerable progress performed in the field. 3D printing is accessible, fast, versatile (use of several materials), low cost, and does not require clean room. Depending on the techniques, features in the range of 100 μm can be obtained [222].

A whole arsenal of microfabrication techniques exists and should be selected depending on the desired application (purpose, material, features). For commercial production of market-ready chips, micro-injection molding is the technique of choice. For proof-of-concept, PDMS casting is usually the go-to technique while micromachining is mostly used for thermoplastics. It should be noted that 3D printing is a very promising technique which should benefit microfluidic a lot in the upcoming years due to its versatility. For more details on the mentioned microfabrication techniques, one can read the following book and article: [213, 222].

II.1.2. Droplet microfluidics

The principle of droplet microfluidics is to isolate discrete volumes of fluids in immiscible multiphase flows such as discrete volume of aqueous solution dispersed in oil. There are two complementary motivations from which droplet microfluidics emerged: to serve as microscale flow reactors in micro total analysis systems (μTAS) and to fabricate droplet-based particles for materials research [214]. In order to manipulate droplets at the micrometric scales, new problems are to be considered arising due to the presence of a deformable interface between the droplet and the carrier fluid.

II.1.2.1. Design considerations

There are a lot of parameters to be considered when designing a droplet microfluidic system. First, the fluids handled must be considered. In the most common case of water droplet carried by oil, it is for example preferable to use hydrophobic materials to limit interactions of droplets with the material. PDMS is usually the go-to material: it is hydrophobic in its native state, meaning water droplets in oil can be easily created, but can also easily be made hydrophilic by plasma treatment for oil droplets in water for example [212]. If the system requires the use of electric fields, glass is usually more adapted. In brief, in addition to constraint such as availability, cost or microfabrication process, the surface properties of the material must be adapted to the fluid of interest. Second, the dynamic parameters of droplet handling must be considered: how fast should the droplets move? How big should they be? How fast should they be created? What operations will they undergo? The chip must be designed for an application including the following considerations: channel geometry, channel aspect ratio and flow rate ratio between dispersed phase and carrier phase affect velocity, formation, length, volume, shape and size of droplets [223]. The viscosity of the carrier phase also affects the size and generation rate of droplets [224], and the surface tension between the two fluids affects the droplets size [225]. In order to decrease surface tension between the two phases, surfactants can also be used. These amphiphilic molecules are mostly found at interfaces, where they will be in the most energetically favorable state

[213]. Not only will the addition of surfactants tend to decrease the size of droplets, it also improves the stability of the droplets interfaces, making it easier to create stable bigger droplets and helping prevent coalescence [212].

II.1.2.2. Droplet creation

The creation of droplets inside a microfluidic system with fine control over droplet shape, size, generation frequency and mono disparity involves several parameters as mentioned above. The first parameter to mention is the relative quantity of the dispersed phase and the carrier phase. The flow rate of both phases will play a role in generation frequency while the flow rate ratio between the two phases will influence the size of the droplets. It is the easiest parameter that can be changed in microfluidic systems since the flow rate of phases is usually controlled by syringe pumps or pressure controllers. The second parameters playing a role is the interfacial tension between the two phases, which can be lowered by adding surfactants as mentioned previously. The last parameter playing a role is the geometry of the channel: the design, shape of the cross-section and size of the channel. This parameter is difficult to modify since it requires a new microfluidic chip which can prove tedious and costly. Droplet generations methods are usually divided in two categories: passive (i.e., relying only on the geometry of the system) and active (using electric, magnetic, centrifugal methods) [212]. In order to illustrate the examples presented in this subchapter, we will consider aqueous droplet dispersed in oil although other suspensions exist.

Passive droplet generation

Passive strategies rely on the geometry of the system to create local deformation of the oil/droplet interface and promote interfacial instabilities. They are usually used to create droplet ranging from nL to fL with polydispersity (standard deviation of the droplet size divided by mean droplet size) as small as 1-3% [226]. In all three main categories of passive creation, oil and aqueous phase are driven separately and meet at a junction where the droplet is created by competition between the pressure due to external flow and viscous shear stress on one hand and capillary pressure resisting deformation on the other.

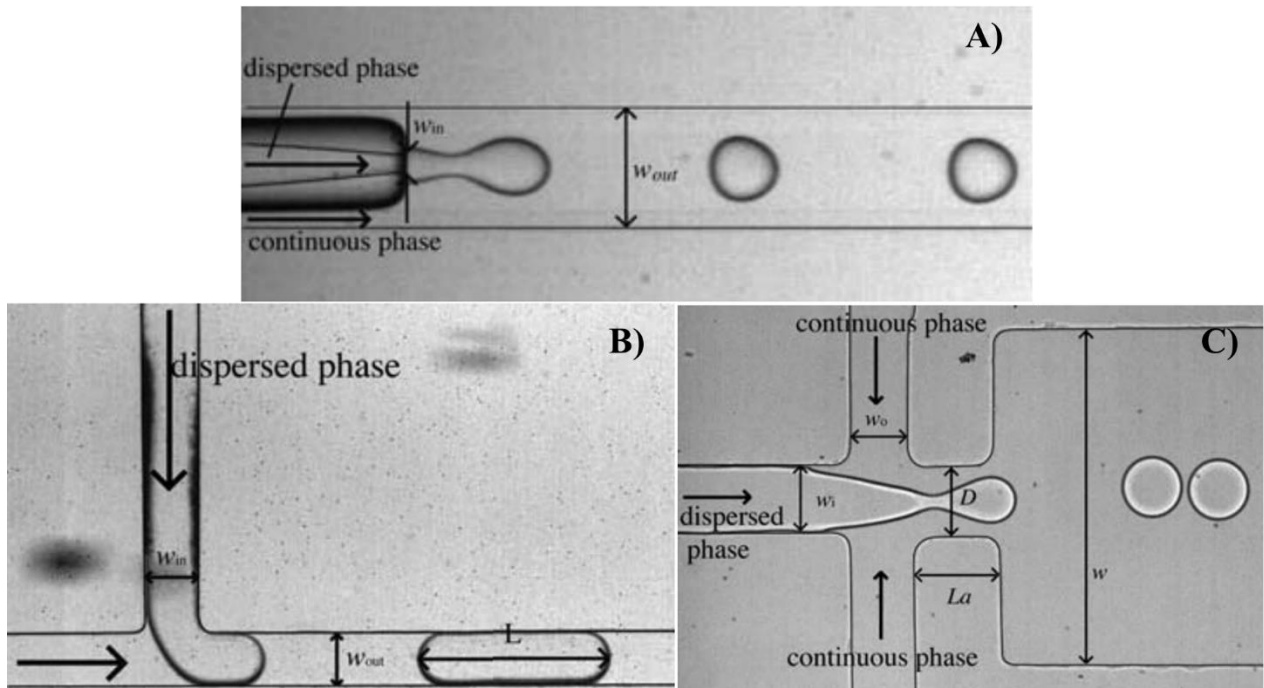


Figure 24 : Passive strategies for the creation of droplets in microfluidic systems: A) Co-flow, B) T-junction and C) Flow focusing. Adapted from [226].

The first passive strategy is to use co-flowing streams of oil and water: in a square rectangle main channel where oil flows, a co-axial cylindrical tube is flowing water parallel to oil. As seen in *Figure 24 A*), the oil “pinches” the aqueous stream, breaking it into droplet: the physical mechanism is related to Rayleigh-Plateau instability and several regimes exist depending on the oil flow rate. The major drawback of this method of droplet generation is that integrating such a cylindrical tube is not trivial with soft lithography and requires advanced microfabrication.

Figure 24 B) presents the T-junction, which is the second strategy used for droplet generation. In these systems the channel containing the dispersed phase is orthogonal to the main channel flowing the continuous phase creating a T shape. When the dispersed phase channel is much smaller than the continuous phase channel ($w_{in} \ll w_{out}$) and the capillary number is high enough, droplets are emitted before they can fill the main channel, similar to co-flowing strategy. But when $w_{in} \approx w_{out}$ and the capillary number is low enough, the droplet grows in the main channel until it completely obstructs it, restricting the continuous phase flow around it. This results in a sharp increase in dynamic pressure upstream of the droplet which results in the pinching of the droplet. The T-junction is the simplest geometry used for droplet generation and requires only trivial soft lithography.

Finally, *Figure 24 C*) presents the third main passive droplet generation strategy: flow focusing. In this strategy, two counter-flowing streams of oil are focused on the aqueous stream and are pinching it to break it into small droplets. In this strategy the geometry plays a larger role as the width of the aperture D , its length L_a and the length of the collector channel w play an important role and four different regimes exist.

More details on the physics of droplet creation and the different regimes for each strategy can be found in the following reviews: [226, 227].

Active droplet generation

The principle of active droplet generation is to modulate the balance of forces acting on the droplet by either introducing an external force or by modifying intrinsic forces. Electrical forces can be applied as an additional force similar to electrospraying: application of an electrical fields to the water phase induces the migration and accumulation of charges at the water/oil interface, helping droplet creation. Electrical forces can also be used to modify intrinsic properties: electrowetting modifies the wettability of the substrate, electrochemical reaction and electrocapillarity can change the interfacial tension and the fluid viscosity can be controlled using electrorheological fluids. Magnetic forces can also be used by placing magnets on the microfluidic system to attract or repel ferrofluids. Other active strategies include using centrifugal forces, modifying the fluid velocity, modifying viscosity, modifying interfacial tension, modifying channel wettability or modifying fluid density. More details on active droplet generation can be found in the following review [227].

Compared to passive strategies, being able to actively generate droplets presents several advantages [227]:

- More flexibility in controlling droplet size and generation frequency, enabling in some cases “on-demand” droplet generation. With passive methods it is almost impossible to vary size and frequency independently.
- Shorter response time, i.e., time required for the system to stabilize the production of droplet. It can be down in the range of ms in active systems while being around seconds or even minutes in passive methods.

The drawback that often comes with active strategies is the requirement of integrating the external force with the microfluidic system. In the case of droplet manipulation using electrical fields, electrodes must be embedded in the microfluidic device, adding microfabrication complexity. For magnetic forces, it is restricted to very specific applications since only ferrofluids or fluids containing magnetic particles can be used.

II.1.2.3. Droplet transport and mixing

Once created, droplets are transported in the microfluidic channels by the carrier fluid. Two situations must be distinguished, as respectively seen in [Figure 25](#) A and B:

- Bubbly flow, in which droplets are smaller than the channel diameter. In this case the droplets are considered to flow at the same velocity as the local velocity of the carrier fluid, meaning droplets close to the center of the channel will flow faster due to the parabolic Poiseuille flow.
- Slug flow where the droplets occupy most of the channel cross section. In this case the flow is strongly modified by capillary effects and by the deformability of the drop interfaces.

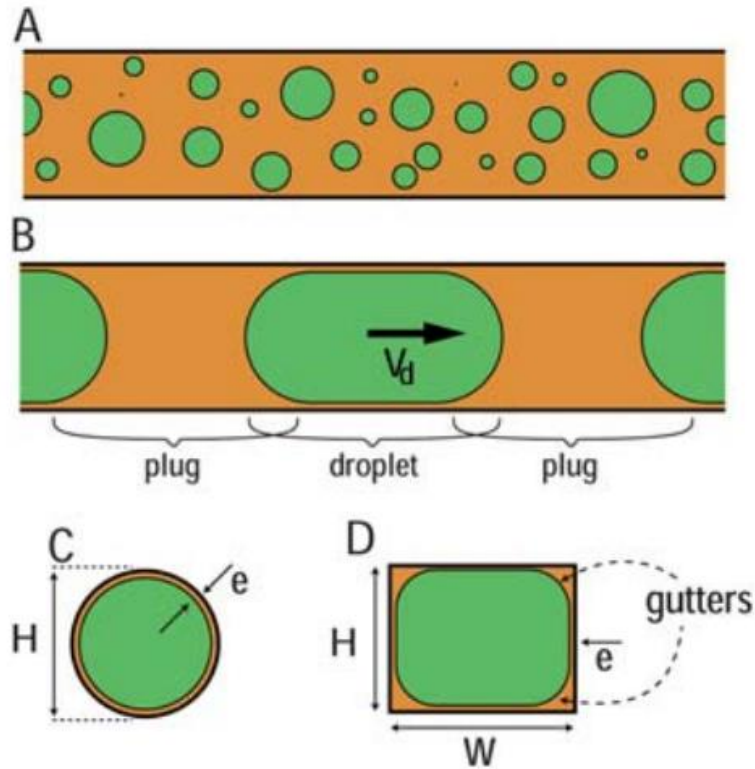


Figure 25 : Transport of droplets inside a microfluidic channel: A) bubbly flow of small droplets, B) slug flow of “plug” droplets, C) thickness of the oil film in a circular channel and D) thickness of the oil film in a rectangular channel with the presence of gutters. From [226].

In the case of slug flow, the hydrodynamic transport is much more complex. If we consider a slug droplet flowing at a velocity V_d from left to right as seen in Figure 25 B), a thin film of the carrier fluid (oil) called lubrication film is deposited between the channel wall and the droplet. In the reference frame of the droplet, the walls are moving in the opposite direction at a speed of $-V_d$ and they pull the carrier fluid by viscous entrainment from right to left, effectively depositing a thin film of oil between the droplet and oil. In competition with this viscous drag, the pressure inside the droplet is greater than the outside pressure due to the Laplace pressure at the interface, pushing against the wall and expelling oil from the deposited films into the bulk of carrier fluid. The thickness of the oil film e in a circular cross-section microfluidic (as seen in Figure 25 C) depends on this competition and therefore on the capillary number of the droplet Ca_d [228]:

Equation 11 : Scaling of the thickness of lubrication films in droplet microfluidics in circular cross-section channels. H is the diameter of the channel. Holds for $Ca_d < 0.01$.

$$\frac{e}{H} \propto Ca_d^{\frac{2}{3}}$$

Experiments [229] and numerical simulations [230, 231] were performed and verified that this scaling can be applied to any microfluidic flow as long as $Ca_d < 0.01$ and indicated that lubrication films have a thickness of 1% to 5% of the channel's half height. The existence of lubrication films in the case of circular cross-sections implies that the droplet must move faster than the average speed of the carrier fluid V_{ext} [226, 229]:

Equation 12 : Scaling of the speed of the droplet V_d depending on the average speed of the carrier fluid V_{ext} and the droplet capillary number Ca_d .

$$\frac{V_d - V_{ext}}{V_d} \propto Ca_d^{\frac{2}{3}}$$

For rectangular cross-section as seen in [Figure 25 D](#), the situation is different since the droplet does not fill entirely the channel and leaves out “gutters” in the corners where the carrier fluid can “freely” flow. The gutter flow is in the direction of the droplet movement and in this case the droplet is slower than the carrier fluid [232, 233]:

$$\frac{V_d - V_{ext}}{V_d} \propto -Ca_d^{-\frac{1}{3}}$$

In both cases, drop transport is affected by the flow field induced by the presence of the immiscible interface. As seen in previously, the flow profile in a cylindric pipe is parabolic and maximal at the center (in the case of a rectangular cross-section the profile is different but presents a similar shape and is also maximal at its center [234]). In the presence of a droplet travelling at a constant velocity V_d smaller than the maximal velocity of the carrier phase, liquid particles going faster than the droplet therefore have to change directions when reaching the interface. In the reference frame of the droplet this means the existence of recirculation zones and stagnation points (points where the fluid velocity is zero) as seen in [Figure 26](#).

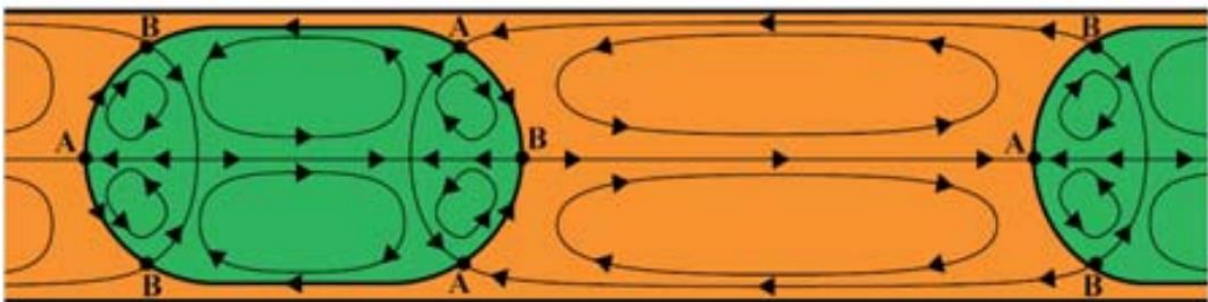


Figure 26 : Recirculation zones and stagnation points resulting from the movement of a droplet in a cylindric channel. From [226].

By applying the same reasoning inside the droplet, the flow field inside the droplet can be seen as a superposition of the Poiseuille flow and of counter-rotating recirculation flows. The fluid inside the droplet does not move uniformly at velocity V_d but its movement can rather be seen as the droplet rolling on the sidewalls in a fashion similar to a treadmill [226]. As mentioned, the situation is a lot more complicated in rectangular channels due to complex dynamics near the gutters, but the idea of recirculation zones and stagnation points is still valid and affects the behaviour of the droplet and notably the mixing inside the droplet.

Indeed, droplet transports enhances mixing inside the droplet compared to single-phase Poiseuille flow due to the recirculation zones creating cross-flow advection in both the dispersed phase and the carrier phase. Although the mixing is more efficient in certain region because the recirculation zones are isolated from each other, introducing a periodic

perturbation in the system enables the possibility of homogeneous mixing. Examples of periodic perturbations include the use of wavy channels [235], periodic laser heating to create Marangoni effect inside the droplet [236] or periodically changing the wall roughness on the path of the droplet [237].

II.1.2.4. Basic operations on droplets

In most droplet microfluidic systems, especially for lab-on-chip applications where several different operations are performed on biological samples (processing, manipulation, analysis...), creating and transporting the droplet is often not enough and actions must be performed on droplets. Frequent operations performed include droplet fusion, droplet fission and droplet sorting. As with droplet generation, strategies either rely on passive or active strategies.

Droplet fusion

Droplet fusion is often necessary in order to perform reactions by fusing droplets with different contents. As mentioned previously, surfactants are usually added to the carrier phase in order to stabilize droplets and prevent undesired droplet coalescence. In the case of droplet fusion, which is basically desired droplet coalescence, the presence of surfactants is then acting against the merging of two droplets. For droplet fusion, the idea is to overcome the stabilizing effect of surfactants in order to break the film of oil separating them. Passive methods aim to control precisely the individual speed of the two droplets to cause them to approach each other. One should note that contact between droplets is not sufficient for coalescence as the film of oil must also be broken. There are two main methods of bringing droplets closer together: the channel geometry can be changed to slow the upstream droplet until the downstream droplet reaches it as seen in [Figure 27 A](#)) or by using droplets of different sizes or different viscosities which flow at different velocities [226]. Once droplets are in contact, they can be fused by a passive method called “decompression merging”: they enter a narrowing channel, causing the droplets to flow at different speed and thus be separated, in the symmetric way of how they were put in contact. This separation causes the interstitial pressure between the drop to decrease, causing the appearance of little pointy structures on the surface of the two droplets. These two “nipples” ([Figure 27 B](#)) are close enough together so that they create a liquid bridge and bring the two droplets together. These nipples are also associated with a local increase in surface area resulting in a decrease in the concentration of surfactants locally which also helps the merging of the droplets [226, 238].

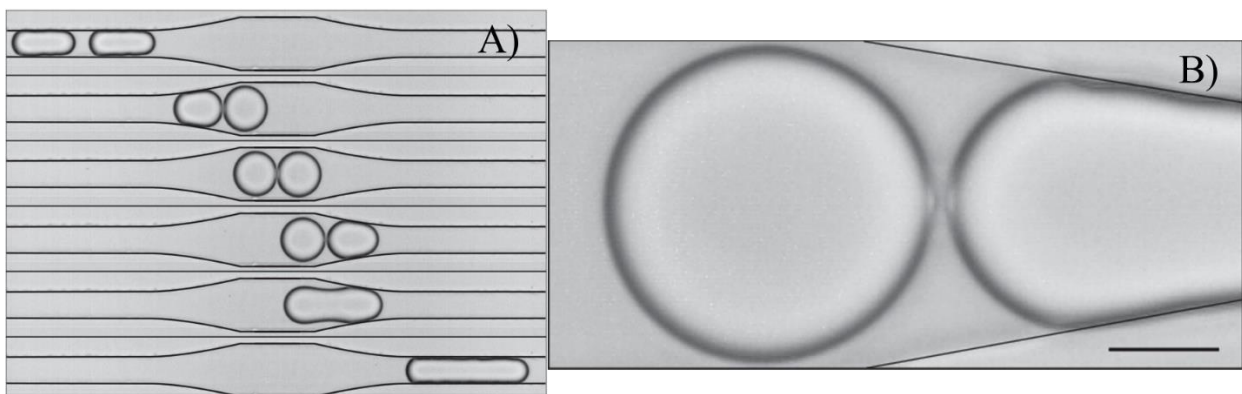


Figure 27 : Passive coalescence of droplets. A) Droplets are first brought closer together then separated using a variation in channel width and B) “Nipples” appearing during separation of the two droplets, inducing droplet fusion. Adapted from [238].

For active coalescence approaches, there are two main approaches. An electric field can be applied to the droplet, inducing dynamic instability of the oil/water interface which facilitates coalescence [239]. The second approaches are based on heating the two adjacent droplets locally with laser heating, resulting in a local depletion of surfactants molecules at the interface but also creates a complex three-dimensional flow in the droplets. These two mechanisms play a role in breaking the thin oil fluid between the two droplets and consequently merging them [240].

Droplet fission

Splitting droplets can be useful for high-throughput generation or to perform group studies [214]. The easiest way to split droplets is to use symmetric Y-shaped junctions as seen in Figure 28 A): when the droplet arrives at the junction, since the hydrodynamic resistance is identical left or right of the droplet, the droplet will split half to the right and half to the left, effectively creating two same-volume droplets. This process can be sequentially repeated to generate large amounts of small droplets [241]. This method based on 2D channels can be upgraded for more complex situations by creating a similar system with a straight θ -shaped channel: instead of splitting left and right, the droplet split into the upper channel and the lower channel [242]. In terms of active approaches, an interesting method uses a narrow surface acoustic waves (SAWs) beam to act as an acoustic knife to deform the droplet interface and cut the droplet in half as seen in Figure 28 B).

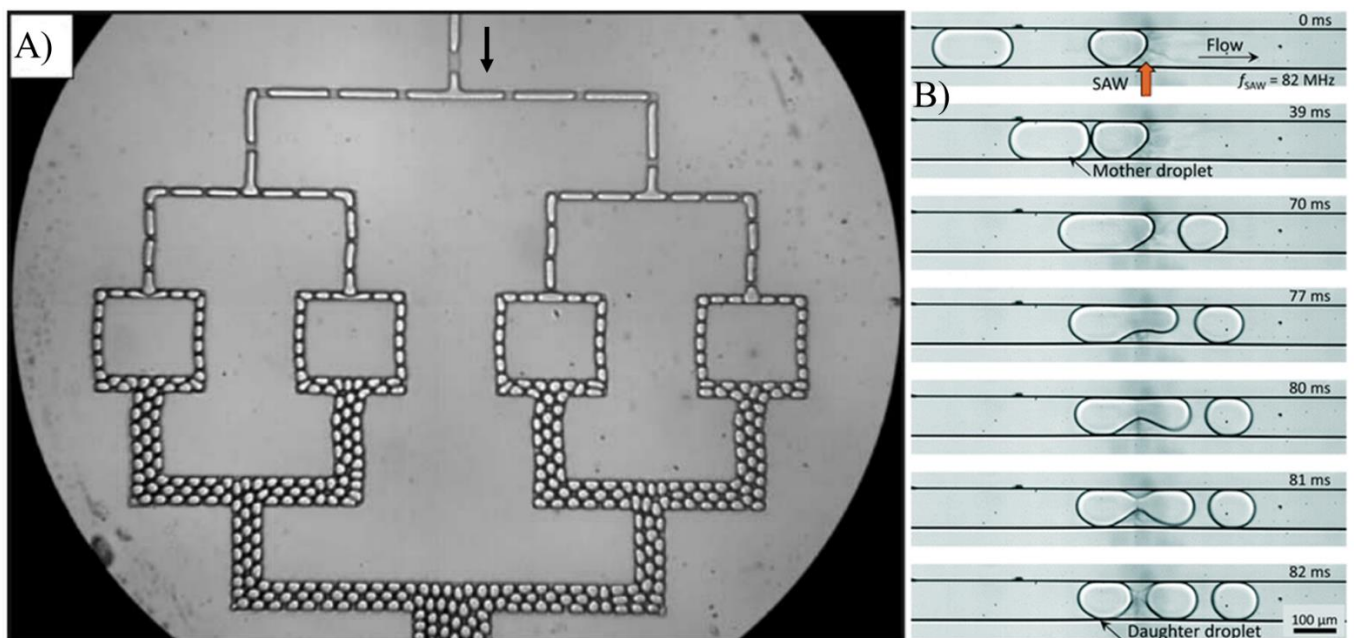


Figure 28 : Strategies for splitting droplets: A) Passive droplet splitting using Y-shaped junction and B) Active droplet splitting using surface acoustic waves. Adapted from [241] and [243] respectively.

Sorting

Implementing operations to manipulate droplets is often necessary in droplet microfluidics systems as was shown previously. The more actions are performed on droplets, the more likely it is that their size can be modified, for example due to accidental coalescence of droplets, leading to lower size monodispersity [244]. In other systems, it is necessary to work with several sizes of droplets, or in the case of single-cell studies, it is necessary to discriminate droplets containing single cells and empty droplets. For all those reasons, sorting droplets is an important function in droplet microfluidics. Droplets can be passively separated depending on their size: two droplets population can be separated using a rectangular channel with dimension between that of the two droplets. As seen in *Figure 29 A*), the bigger droplets occupy most of the channel, leaving the smaller droplets to flow faster and thus eventually reaching the bigger droplets. By placing side channels which are big enough for small droplets but small enough for big droplets, the smaller droplets can be independently collected and separated from the big ones. Passive methods can also be based on gravity or viscosity [214]. As previously, electric forces can be used to actively sort droplets: droplets that would normally go into the left channel are instead pulled into the right channel under dielectrophoretic forces when an electric field is applied as seen in *Figure 29 B*) [245].

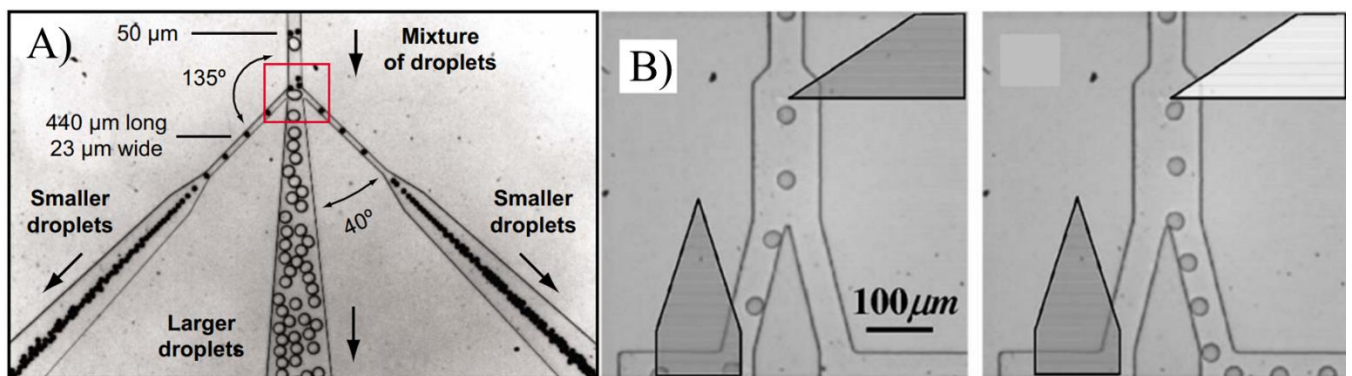


Figure 29: Sorting of microfluidic droplets by passive and active methods: A) Passive sorting of droplets by size using side channels to collect smaller droplets and B) Active sorting of droplets with dielectrophoretic force. Adapted respectively from [244] and [245].

II.2. Microfluidic droplets for separation science

In separation science, the established techniques include HPLC, and CE. MS can be also considered a particular technique of separation based on the mass to charge ratio. As droplet microfluidics gain more and more attraction, it seems logical that those same techniques would benefit from it for the following reasons: reduction of volume used down to femtoliters, high-throughput generation, manipulation and analysis of analytes isolated in droplets, no dilution of the sample, no Taylor dispersion inside the droplet, limited absorption of sample on the channel surface and enhanced mixing and mass transfer inside droplet [12]. Of course, one main difficulty with the separation of aqueous droplets suspended in oil by HPLC, MS or CE is that the oil should be removed from the flow prior to separation to avoid interferences. This subchapter will cover the effort to couple HPLC, MS and CE with microfluidic droplets.

The below content on microfluidic droplets for HPLC and MS is used for a review under preparation.

II.2.1. Microfluidic droplets systems for LC

Following the growing interest in microfluidic systems, efforts to translate established chromatographic methods in a microfluidic chip format were made but ultimately suffered from problems inherent to microfluidics. Indeed, the dispersion of separated bands resulting from molecular diffusion and from the various dead volumes introduced by the channel, detector and collector could degrade the analytical quality of the separation [246]. By collecting fractions of the column effluent in microfluidic droplets, dispersion can be reduced as the droplets are confined in oil during the transportation in the microfluidic channel, and dead volumes can be minimized while preserving the chemical identity of each fraction for further downstream or offline analysis/manipulation [247]. Reverse phase HPLC was first coupled with droplet microfluidics by combining commercially packed nano-LC capillaries with a chip interface. In these systems, the sample is first separated using the nano-LC column and then fractioned into droplets using T-junctions geometries. The droplets can then be deposited on a MALDI stage by contact deposition prior to MALDI-TOF analysis [248]. The proteins in the droplet can be digested on-line by mixing the LC effluent with trypsin before segmentation and mixing in a curved microfluidic channel followed by analysis by MALDI- or ESI-MS [249]. Enzyme inhibitors can be tested by adding the enzyme to the LC effluent containing the inhibitors [250]. The droplets can also be segmented and stored into a capillary for off-line ESI-MS [251].

Another strategy to couple HPLC and microfluidic droplets is to integrate them on the same microchip. This is desirable as it avoids dispersion during compartmentalization [252] and allows to use higher pressure for optimal mobile phase velocity [253]. Indeed, using high pressure is not trivial in “common” microfluidic systems using PDMS which is the go-to material for fast prototyping of microfluidics systems. To tolerate high pressure, alternative materials must be found for droplet microfluidics HPLC systems [246]. The first integrated system was proposed by Kim et. al. [246] and used a two-layer microfluidic chip made of thermoset polyester which was able to withstand up to 8 MPa. As seen in [Figure 30 A](#)), their device was a two-layer chip with the bottom layer consisting of a 1 mm wide channel packed with 5 μm C18 particles for HPLC separation. This bottom channel has one inlet used to introduce the mobile phase and the solution to be analyzed; and one outlet at the end of the C18 packed. This outlet is connected to the inlet of the top layer, on which is a flow-focusing junction to compartmentalize the analytes. An outlet is placed after the T-junction for droplet collection. Comparison of fluorescence measurements performed before and after compartmentalization showed no significant difference, meaning the compartmentalization does not induce significant dispersion. Moreover, the size of droplets can be tuned by selecting the appropriate oil flow rate, meaning that the variation in analyte concentration between two consequent droplets can also be tuned. Nevertheless, the separation performance was rather limited by the “column” quality: 19 and 63 plate numbers for AF 488 and FITC respectively. Since the use of better performing columns requires higher pressure, improvement in separation quality would require using material more resistant to pressure.

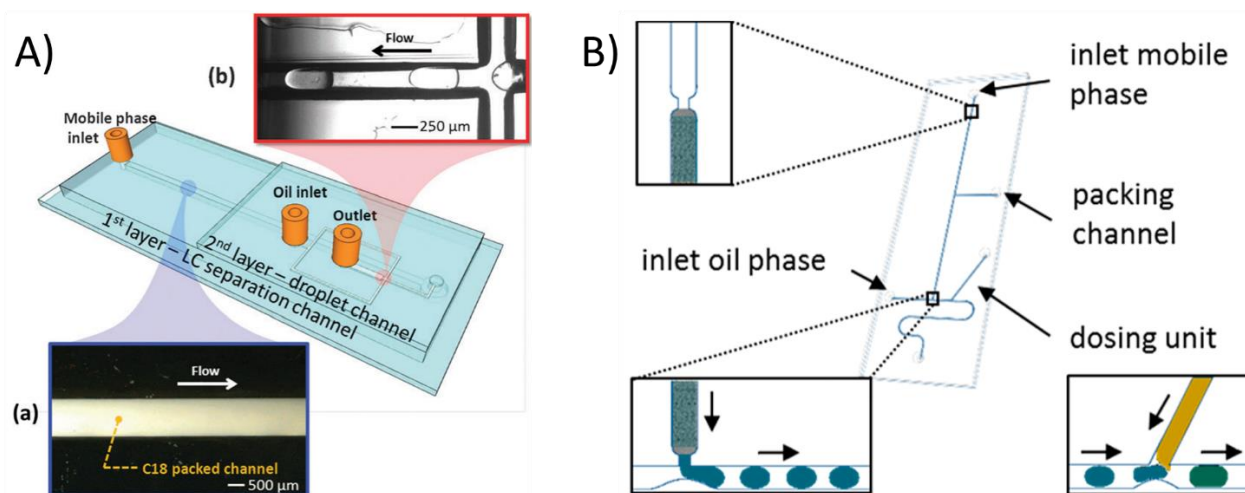


Figure 30: Integrated HPLC microfluidic systems with droplet fractionation: A) Two-layer HPLC device with an HPLC layer and a droplet compartmentalization layer and B) One-layer HPLC device with a dosing unit channel for the addition of reagents to the compartmentalized eluent. From [246] and [252], respectively.

Based on this conclusion, Gerhardt et.al. [252] proposed a different system using soda-lime glass slides, which is a cost-effective method for prototyping over several chip generations but at the cost of uneven and rough channel walls. The authors note that even though the separation performance of this method is not optimal compared to more robust microfabrication methods, well-resolved liquid chromatography separations were still possible. Using soda-lime glass slides, pressures up to 12 MPa can be used. The design of the chip in this case is more straightforward, as the channels are etched in only one layer. As seen in Figure 30 B), the chip is composed of a high-pressure region, where the HPLC separation takes place, and a low-pressure region for eluent compartmentalization and processing. Downstream in the low-pressure region, compartmentalization is performed using a T-junction and a “dosing unit” channel has been added for the addition of reagents to the droplets as an example of downstream processing. For the HPLC part of the system, 1200 plate numbers was obtained for a Coumarin 120 sample, approximately 20 to 50 times better than with the previous system. It should although be noted that the preparation of the HPLC channel is more advanced than previously and requires several steps. As for the encapsulation part, encapsulation does not negatively impact the chromatographic performance. Although in this case it is necessary to perform a hydrophobic surface treatment since the native soda lime glass is hydrophilic which is not suitable for water in oil droplets. To illustrate the usefulness of encapsulation of eluent from HPLC, a downstream addition of a fluorescent quencher was added to the eluent droplets and led to a decrease in signal intensity for the 4 compounds separated. By showing that the signal intensity decreased with increasing quencher concentration, the author highlighted the fast and effective mixing inside the droplets, showcasing that subsequent reactions can be performed inside the eluent droplets. With the right tuning of the “dosing unit” channel flow rate, the addition of reagent does not perturbate the eluent encapsulation, nor droplet creation frequency nor droplet coalescence. Similar strategy was used for normal phase HPLC by carefully selecting a non-polar eluent and a polar continuous phase for eluent

compartmentalization and by switching to a specific flow-focusing geometry to prevent the eluent from wetting the channel walls [253].

Rather than compartmentalizing the eluent after on-chip HPLC separation, the HPLC-droplet coupling strategy can be used the other way around: an individual droplet segmented in a carrier fluid can be directed to the HPLC column and separated. The first attempt to implement such an integrated system for the analysis of single droplets by chip-HPLC/MS was performed by Piendl et.al. [254]. However different challenges were identified compared to post separation compartmentalization, notably penetration of immiscible carrier fluid in the HPLC column and pressure mismatch between the droplet channel operating near atmospheric pressure and the HPLC channel operating at up to hundreds of bars.

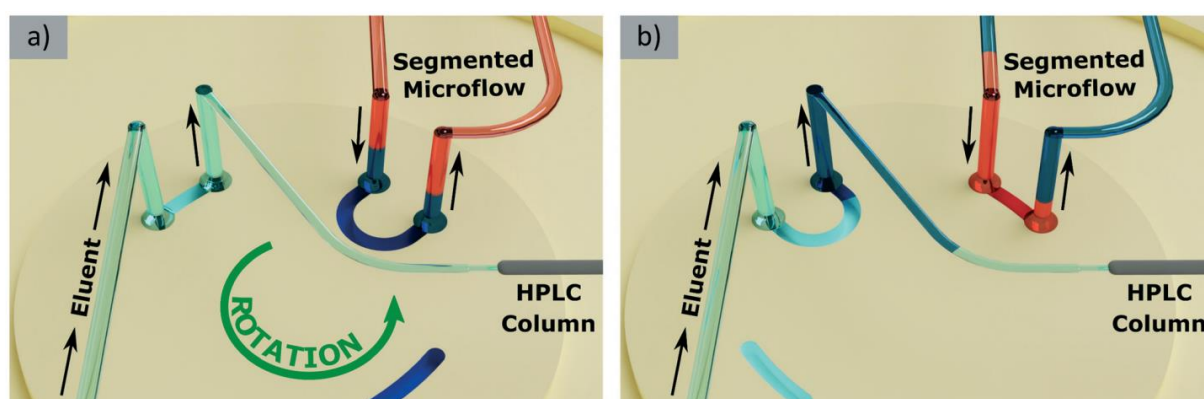


Figure 31 : Schematic of the strategy for injecting segmented microflow in a HPLC column: a) the 10 nL loop is filled with the sample (in blue) and b) after the valve rotates, the sample in the loop is pushed into the HPLC channel by the eluent. From [254].

To solve both these issues, the system they designed uses a rotor-stator interface to desegment the aqueous droplets and transport them to the HPLC channel as seen in Figure 31. The chip design includes a segmented microflow channel to transport droplets and an HPLC channel for separation, and those channels are completely isolated one from the other. Segmented flow is transported to the HPLC channel by a 10 nL loop created in the Polyether ether ketone (PEEK) rotor seal by laser ablation. The difficulty in this system is that the connexion between the chip and the rotor-stator must be perfectly aligned and with no leakage while still being able to rotate. To solve this issue, the chip is composed of 3 different layers. The first layer is etched in a fused silica chip with the segmented flow channel and the HPLC channel connected to a monolithic ESI emitter. The etching is performed with selective laser-induced etching which allows the creation of 3D structures with very high aspect ratio such as the small orthogonal channels used to connect the segmented flow and HPLC channels to the fluidic loops in the rotor-stator and the μ -frit used to retain the particle phase inside the separation channel. For the precise alignment of those orthogonal channels to the first layer, a second glass layer is bonded to the first layer and is composed of a cylindrical recess in the central area of the first layer and is used to connect the PEEK valve. As a proof of concept, they showcased that their system was able to separate enantiomers of warfarin synthesised on-chip in 25 nL segments. 10 nL fractions of the segments were transferred to the HPLC channel.

Table 2 : Summary of some of the different strategies used for coupling HPLC with droplet microfluidics.

Method/strategy	Advantages	Limits	Throughput	Reference
Post HPLC fractioning by a two-layer TPE chip	Droplet size tuneable, compartmentalization does not introduce dispersion	Analytical performances limited by column quality	Up to 50 droplets/s	[246]
Post HPLC fractioning by one layer soda lime chip	Simpler design and fabrication, possibility of adding reagents to the fractions	Analytical performances not optimal due to material	Up to 45 droplets/s	[252]
Normal phase HPLC compartmentalized by a polar continuous phase	Widens the applications to normal phase HPLC	Lower throughput relative to previous systems	Up to 11 droplets/s	[253]
Online HPLC of segmented flow to analyse individual droplets	Analysis of complex and isomeric mixtures in 10 nL droplets	Complex design of the system, limited speed of analysis	ND	[254]

II.2.2. Microfluidic droplets systems for MS

In some cases, the HPLC separation is not necessary prior to MS detection as MS allows separation / identification of target molecules based on their charge / mass after fragmentation. Indeed, coupling microfluidic droplets directly to ESI-MS allows to perform faster analysis without recourse to complex setups. As the Kennedy group showed [255], the coupling of microfluidic droplet to MS can be done by interfacing a sampling capillary containing the segmented flow directly to a modified ESI needle composed of a metal-coated fused silica capillary. This approach is powerful because it removes the step of de-segmenting the flow before analysis as required for droplet-interfaced HPLC or CE. As can be seen in [Figure 32 A](#)), the oil is nebulized but does not form charged droplets, meaning that electrospray stops and starts only when a droplet is exiting the channel. 3072 droplets samples (50 nL each) could be created from eight 384-well plates in parallel ([Figure 32 B](#)) in 12 min and analysed by MS in 26 min. While this high-throughput method is powerful, it is limited to ESI-MS compatible sample matrix. One problem observed was sample carryover, which is amplified at higher analysis rates, due to the transfer of the droplet from the fluorinated ethylene propylene tubing to the fused silica capillary. Even when fluorinating the tubing and capillary surface, the problem with carryover was still observed. To solve this issue to improve their system ([Figure 32 C](#))), the tubing was replaced with Teflon tubing and the ESI needle was replaced by a smaller diameter Teflon tubing inserted directly inside the droplet carrier tubing and sealed with wax to form a zero dead volume union [256]. Carryover was

minimized using this system while the analysis rate was improved to 3.7 droplets/seconds compared to approximately 2 droplets/seconds with the previous system.

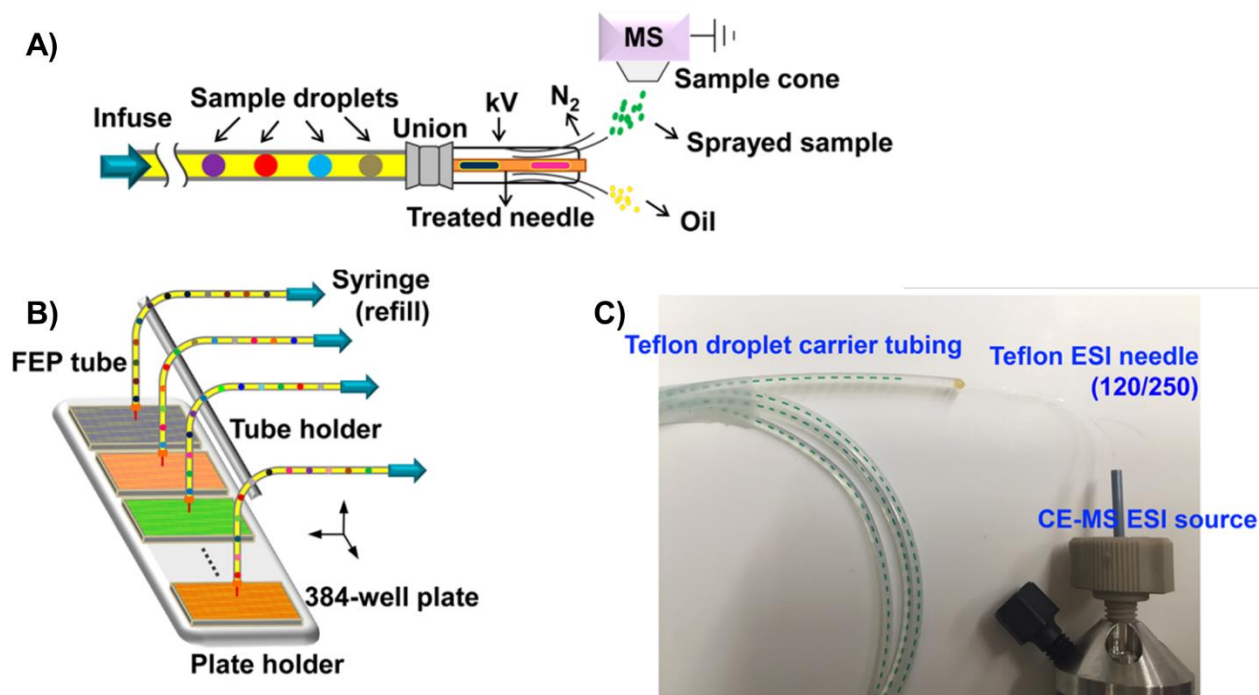


Figure 32 : Working principle of the droplet MS systems from the Kennedy group: A) Introduction of a segmented flow inside a ESI-MS source without removal of the oil phase; B) Strategy for parallel creation of trains of droplets from 384 well plates, and C) Connection of a Teflon tubing transporting the droplets (in green) to the Teflon ESI needle. Adapted from [255, 256].

More recently, they had the idea to combine droplet microfluidics with nanoESI-MS (nESI-MS), which is a low flow variation of ESI-MS presenting improved ionization efficiency and matrix tolerance [257]. nESI-MS is usually limited by low throughput and combining it with a robust and rapid droplet microfluidic sample manipulation was desirable. The goal was to improve the robustness of their high-throughput analysis of cohorts of thousands of biological samples. This system allowed creation and detection of droplet as small as 65 pL at nL/min flowrates for a throughput of up to 10 samples/s and stable over hours of operations. As mentioned previously, HPLC can be coupled to MS in order to analyse fractions of eluent, which can be difficult with classical methods. Using a simple T-junction, Li et.al. [251] collected and segmented eluent from a nanoLC column into droplets and proceeded to perform offline ESI-MS analysis by connecting the capillary containing the collected eluent to an ESI needle like previously presented. This system allows ESI MS analysis of the sample without band broadening of the sample and without mixing of the fractions. Another group also proposed a similar strategy using a flow focusing geometry connect online to an ESI emitter [249]. Similar to previously, the HPLC eluent is mixed with trypsin and buffer matrix before segmentation and mixing using a serpentine channel.

In droplet-interfaced MS, droplet sorting is normally needed to avoid the destroy of the totality of the sample after MALDI or ESI-MS detection. This sorting so far relies mostly on optical detection techniques such as fluorescence activated droplet sorting (FADS) to sort at

high speed and sensitivity droplet based on their fluorescence [258]. Efforts were also made to implement droplet sorting for MS with non-optical approaches. As seen in *Figure 33 A*), it was possible to use MS detection for droplet sorting by splitting droplets in two, analysing the content of the first half by ESI-MS and flowing the other half in a long channel before dielectrophoretic sorting, [258]. A sorting algorithm is used to synchronise the MS detection and the dielectrophoretic sorting of the twin droplets. Another solution for MS detection without destruction of the sample is to spot droplets onto plate, and then have a glass slide for MALDI approach the array of droplets until droplets are attached to the top plate (*Figure 33 B*)). By moving the top plate, the spotted droplets are split in two: the ones on the MALDI glass slide can be dried and matrix can be added for MALDI-MS detection on the droplet content and the other droplets can be conserved for further operations [259]. The author applied this for yeast cells which conveniently remained in the bottom half of the split droplet and could be retrieved or further cultivated.

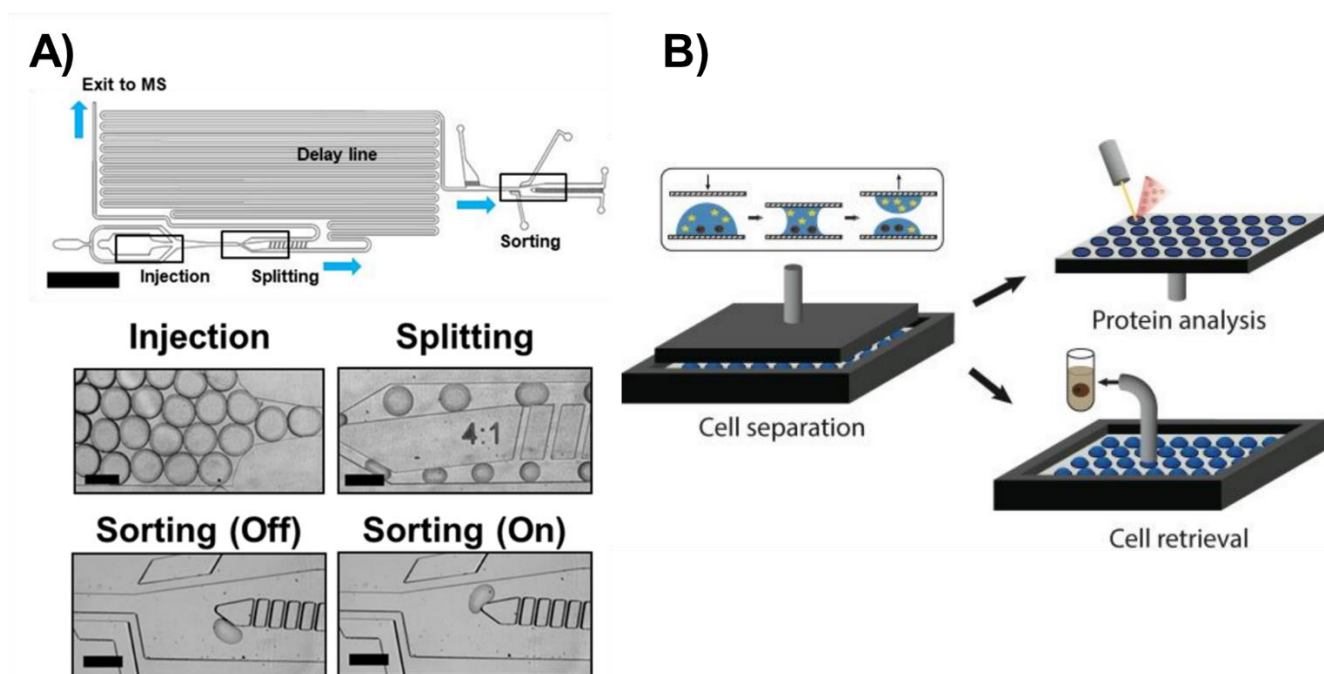


Figure 33: Strategies for droplet MS detection without destruction of the sample: A) Dielectrophoretic droplet sorting coupled to ESI-MS by splitting the droplet and B) Parallel splitting of droplets for MALDI-MS of droplets while keeping the cells inside the droplet viable. From [258] and [259] respectively.

For MALDI-MS, droplets can also be used for sample fractioning after NANO-LC separation [248, 260]. In the system of Pereira et. al., a PDMS interface connects a Nano-LC capillary to a T-junction to fraction the HPLC eluent and mix it with a MALDI matrix. After mixing the content of the droplet using a serpentine channel, the droplets are brought close to a MALDI stage, and the droplet are desegmented using an oleophilic film to absorb the oil. The desegmented droplet can then be deposited on the stage prior to MALDI-MS analysis. Coupling a separation method with MS allows the analysis of more complex samples and segmenting the HPLC eluent allows to analyse sample without any sample dispersion.

Table 3 : Summary of the different strategies (not exhaustive) used for coupling HPLC with droplet microfluidics

Method/strategy	Advantages	Limits	Throughput	Reference
Interfacing a sampling capillary containing the segmented flow to a modified ESI needle.	High throughput, simple, no desegmentation	Matrix compatibility limited, carryover, sample destruction	3.7 samples/s	[255, 256]
Interfacing a sampling capillary containing the segmented flow to a modified nano ESI needle.	Improved ionization and matrix tolerance	Requires treatment of the capillary, sample destruction	10 samples/s	[257]
Coupling HPLC separation to offline MS detection.	No band broadening, 2D separation	Lower throughput, manual manipulation	2 samples/s	[251]
Coupling HPLC separation to online enzymatic digestion followed by ESI-MS.	Online, no band broadening, 2D separation	pH compatibility between digestion buffer and MS buffer	X	[249]
Droplet splitting followed by MS detection for dielectrophoretic sorting of the droplets.	Does not require labelling, sorting applicable for most analytes	Requires complex microfluidic device	0.7 samples/s	[258]
Use of a glass plate to split droplet spotted on a MALDI plate.	High-throughput and parallel single-cell screening tool	No desalting step hinders performances	X	[259]
Segmenting HPLC eluent to spot a MALDI plate	Complex samples can be analysed, no sample dispersion	Time consuming to perform HPLC separation and spot the MALDI plate	X	[248, 260]

II.2.3. Microfluidic droplets systems for CE

Article 1: Droplet-interfacing strategies in microscale electrophoresis for sample treatment, separation and quantification: A review

1 **Droplet-interfacing strategies in microscale electrophoresis for sample treatment,**
2 **separation and quantification: A review**

3

4 **Théo Liénard-Mayor¹, Myriam Taverna^{1,2}, Stéphanie Descroix³ and Thanh Duc Mai^{1*}**

5

6 ¹ *Université Paris-Saclay, CNRS, Institut Galien Paris-Saclay, 92296, Châtenay-Malabry,*
7 *France*

8 ² *Institut Universitaire de France*

9 ³ *Laboratoire Physico Chimie Curie, Institut Curie, PSL Research University, CNRS*
10 *UMR168, 75005 Paris, France*

11

12 **Correspondence:** E-mail: thanh-duc.mai@u-psud.fr;

13

14

15 **Keywords:** droplets; microfluidics; capillary electrophoresis; microchip electrophoresis

16

17 **List of abbreviations:**

18 CE/MCE: capillary electrophoresis / microchip capillary electrophoresis; EOF:

19 Electroosmotic flow; DMF: digital microfluidics; EWOD: Electrowetting on dielectric

20 technology; IL: ionic liquid; QC: quality control; LIF: laser induced fluorescence; SPE: solid

21 phase extraction; PCR-RFLP: PCR-restriction fragment length polymorphism; PDMS:

22 polydimethylsiloxane; PSS: poly(styrene)sulfonate; HTS: high-throughput screening; CGE:

23 capillary gel electrophoresis; PTFE: polytetrafluoroethylene; NGS: next-generation

24 sequencing; MEKC: micellar electrokinetic chromatography; EMMA: mediated

25 microanalysis; PMMA: poly(methyl methacrylate); PEEK: Polyether ether ketone

26 **Abstract**

27 In this study, for the first time we report on a comprehensive overview of different strategies
28 to hyphenate droplet-based sample handling and preparation with electrophoretic separation
29 in different formats (*i.e.* microchip and capillary electrophoresis). Droplet-interfaced
30 electrophoresis is an emerging technique in which micro/nanometric droplets are used as a
31 bridge and carrier of target analytes between sample treatment and electrokinetic separation
32 steps, thus being expected to overcome the challenges of working dimension mismatch and
33 low degree of module integration. This review covers all works on this topic from 2006 (the
34 year of the first communication) up to 2020, with focus being given to three principal
35 interfacing strategies, including droplets in immiscible phases, digital microfluidics with
36 electrowetting-on-dielectric principle and inkjet droplet generation. Different instrumental
37 developments for such purpose, the viewpoints on pros and cons of these designs as well as
38 application demonstrations of droplet-interfaced electrokinetic strategies are discussed.

39

40

41

42

43

44

45

46

47

48

49

50

51 **1. Introduction**

52 Electrokinetic separations in a microchannel (i.e. microchip or capillary) offer several
53 advantages, notably high separation efficiency, low power requirements and limited
54 consumption of sample/chemicals [1-3]. To improve separation resolution, efficiency and
55 detection sensitivity for trace analysis in a complex matrix sample (e.g. biological samples),
56 sample pretreatment is often needed for removal of the sample matrix and target analytes
57 preconcentration prior to their electrokinetic separation and subsequent detection. Readers can
58 refer to various sample treatment techniques as forefront of microscale electrophoresis in
59 different reviews [4-9]. One should note that injection of tiny sample volumes (nL ranges) is
60 normally employed prior to electrokinetic separations in a microchannel whereas much larger
61 volumes (> 10 μ L up to sub mL ranges) are expected when using conventional (batchwise)
62 forefront sample treatment modules. Without an efficient coupling strategy, the majority of
63 the preconcentrated and purified sample volume (in μ L-mL range) at the outlet of the sample
64 treatment module is wasted without being exploited for sensitive and selective determination
65 of the target analytes at the separation step (nL range). To overcome these challenges,
66 different sample pretreatment strategies were developed to couple with microscale
67 electrophoresis, including in-line liquid phase microextraction, on-line electrophoretic
68 preconcentration and sample pretreatment by integrated immobilized enzyme microreactors
69 [10]. In-line solid phase extraction (SPE)-CE with microcartridges using different solid-phase
70 materials such as monolith, sorbent particles and magnetic beads is another well-investigated
71 technique to cope with the problem of working volume incompatibility [11]. Besides the pros
72 and cons for these in-line / on-line techniques that were well discussed in these reviews, they
73 share the same inherent consideration that typically only a limited number of steps (i.e.
74 extraction and / or preconcentration) can be performed within the unique microchannel which
75 is also used for electrophoresis. Furthermore, the sample matrix flow percolating the

76 microchannel during in-capillary extraction and preconcentration may lead to adsorption of
77 unwanted interferences present in the sample matrix to microchannel's walls, resulting in
78 possible degradation of subsequent separation efficiency. If several steps are needed for
79 sample processing (e.g. sample digestion, analyte capture, chemical labelling, purification,
80 preconcentration etc.), these approaches are not relevant anymore. In this case, the sample
81 treatment protocol should be dissociated from the microchannel used for electrophoresis in
82 order to gain operational flexibility and to avoid undesired modification of the capillary /
83 microchip internal surface.

84

85 In another context, droplet microfluidics has witnessed exponential growth over the past
86 decade as a powerful tool for bioanalysis and high-throughput screening purposes [12-15].
87 Droplet microfluidics can be considered, at least to some extent, as the science and
88 technology of generation, manipulation, reaction, analysis and screening of micro to
89 femtoliter microreactors used as discrete functional units (e.g. droplets, particles or bubbles)
90 in micrometric to nanometric channels [14, 15]. In such systems, the liquid is segmented into
91 discrete droplets which are independent of each other, using typically immiscible phases,
92 which in turn prevent cross-contamination between different droplets. Technologies and
93 methods for droplet generation and manipulation can be found in recent reviews [12, 13]
94 whereas many applications exploiting droplet generation, fusion, sorting, splitting and in-
95 droplet solid-phase handling can be gleaned to [14, 15]. Droplet microfluidics is a matching
96 candidate for high-throughput screening and assays such as drug screening, cell sorting,
97 digital PCR as well as biological analysis at single cell or single molecule levels. Following
98 the boom of droplet-based technologies and applications, the use of droplets to empower and
99 facilitate microscale separations has found its increasing interest and significance in recent
100 years. Droplet microfluidics was employed for bridging 2D liquid-phase separations [16, 17],

101 as well as for chemical separation for cellular analysis [18] and biochemical analysis [19].
102 Among all strategies to exploit the power of droplets in separation science, droplet-interfaced
103 microscale electrophoresis is an emerging technique in which micro/nanometric droplets are
104 used as a carrier of target analytes between sample treatment and electrokinetic separation
105 steps. This particular marriage between droplets and microscale electrophoresis is expected to
106 overcome the challenges of working dimension mismatch and low degree of module
107 integration. Limitations encountered in aforementioned batchwise and on-line/in-line sample
108 treatment approaches are expected to be solved with droplet-interfacing strategies. Readers
109 can find some (inexhaustive) applications of droplet microfluidics in microseparation systems
110 elsewhere [20, 21].

111
112 In this review, we report on for the first time a comprehensive overview of different strategies
113 to hyphenate droplet-based sample handling with microchip and capillary electrophoresis.
114 Different instrumental developments for such purpose, the positive features and limitations of
115 these designs, as well as application demonstrations of droplet-interfacing strategies in
116 microscale electrophoresis are discussed. There have been almost 40 research articles on this
117 topic, with several ones released in the last two years, confirming the interest of research
118 community in this emerging and active approach to provide a promising tool to reliably and
119 accurately address the analysis of trace components in complex samples.

120

121 **2. Microscale electrophoresis coupled with droplets in immiscible phases**

122 A summary of all strategies for interfacing droplets to microscale electrophoresis is given in
123 table 1. This overview shows that droplet encapsulation in oil (an immiscible fluid) has been
124 the most frequently practiced (see strategy 1 in table 1), and therefore accounts for the
125 majority of the communicated works on droplet interfacing strategies. This approach employs

126 segmented flow analysis where the sample droplet / plug is carried out by an immiscible fluid
127 to the separation capillary or microchannel, where it is extracted and injected. Isolating
128 samples into droplet present several advantages, notably prevention of axial dispersion during
129 transportation [22], elimination of contamination between samples and evaporation [23],
130 exclusion of valves or other switching mechanism between samples [24] and possibility of
131 internal flow recirculation within a plug for enhanced mixing [24]. One major challenge when
132 using isolation of sample into droplets suspended in oil is that de-segmentation and oil
133 removal are required in order to inject only the aqueous portion of the flow into the separation
134 capillary/microchannel for separation. Indeed, the oil-based carrier fluid is usually non-
135 conductive and may cause instability of the electroosmotic flow (EOF) and plug formation in
136 the separation channel, inducing shortcuts or dielectric device breakdown [25]. Different
137 designs to couple CE/MCE to droplets-in-oil therefore had to come with their distinct
138 instrumental and / or physio-chemical approaches to overcome the challenge of oil intrusion
139 into the separation microchannel. Some typical strategies for oil removal include: i)
140 extraction of aqueous droplets from an oil flow into a methanol stream with an on-chip de-
141 emulsification interface [26], employment of a hydrophilic extraction / separation channel to
142 extract / inject the aqueous fraction [24, 27], oil draining via on-chip micrometric pillars [23],
143 oil soaking with a hydrophobic and oleophilic membrane [28], oil removal via density
144 difference between the CE buffer and the carrier oil [25]. Another strategy which has not been
145 applied yet for CE/MCE but holds a high potential to our opinion is the emulsification/
146 demulsification with microgels (*i.e.* from microgel in oil phase to microgel in medium phase)
147 [29]. At the present state of the art, more efforts have been spent for instrumental conception
148 and optimization for high-throughput sample injection to CE/MCE, using model analytes in
149 many cases. Less attention was given to methodology development for such approaches,
150 which should be expected to come in the next research phase once the instrumental

151 development has been established. Accordingly, the following discussion focuses more on the
152 techno-aspects of the reviewed droplet-interfacing strategies.

153

154 ***2.1. MCE coupled with aqueous droplets in oil***

155 The direction of droplet-interfacing to microscale electrophoresis was first opened by Edgar *et*
156 *al.* in 2006 with the method for integrating droplet generation and MCE [30]. They were the
157 first to report the use of a stable immiscible boundary (also called “virtual wall”) to divide the
158 microfluidic chip into a droplet generation part and a separation part (see Fig. 1 for their
159 setup). In systems using a virtual wall, a stable aqueous/oil interface has to be maintained via
160 optimization of the hydrophobicity of the surfaces, the surface tension, the viscosity of the
161 fluids and / or the channel dimensions [24]. When the sample reaches the interface, the
162 aqueous fraction coalesces with the interface and goes preferably into the hydrophilic channel.
163 Edgar *et al.* reported the use of a simple T-junction to produce droplets that were injected into
164 a straight separation channel. They also found it is possible to inject sample directly into the
165 separation channel by reversibly breaking and sealing the immiscible boundary. Different
166 approaches to stabilize this boundary were investigated using hydrophobic (native
167 polydimethylsiloxane, PDMS) and selectively hydrophilic patterned (poly(styrene)sulfonate,
168 PSS) separation channels. A hydrophobic separation channel with no surface modification
169 required precise regulation of the oil flow to prevent the oil from entering the separation
170 channel. Unsatisfactory repeatability was observed with hydrophobic channels using micro
171 injectors for pressure control and oil handling. Indeed, as oil preferably wets the hydrophobic
172 walls, when it enters the separation channel it will remain wet on the surface, rendering
173 impossible the measurement of EOF. On the other hand, a hydrophilic separation channel,
174 despite a non-trivial selective surface patterning, was found to efficiently prevent the entrance
175 of oil into it. In this case, the oil preferably wets only the hydrophobic walls of the T-junction.

176 The droplet interfacing approach proposed by Edgar *et al.* was applied for the separation of an
177 amino acid mixture segmented into 12 pL droplets as the proof of concept demonstration.
178 While the authors did not mention the achieved throughput, the employed mode of pressure
179 control was found not yet compatible for high throughput. Changing samples with this
180 method would also require several rinsing steps to avoid cross-contamination.

181
182 Following this work, Roman *et al.* presented a system where a shallow channel
183 (electrophoresis channel, 7.5 μm) and a deeper channel (droplet channel, 75 μm) were etched
184 on different glass plates and bonded together [24]. The channels were then aligned in order to
185 overlap, leading to a small stable interface after surface treatment of the droplet channel. The
186 droplet is led into the separation channel due to difference in surface energy and capillary
187 forces. This flow de-segmentation system required two microchip plates to be well aligned. In
188 an effort of simplifying microfabrication, Pei *et al.* later presented a tuned version of this
189 system where the separation channel was placed close to the droplet generation channel (both
190 with 80 μm depth) and these channels intersected via the etching of the glass, creating a small
191 gap (5-10 μm) between them [31]. In order to increase the throughput, three MCE channels
192 were integrated in the same chip. The droplet channel was further treated to become
193 hydrophobic, allowing the creation of an aqueous/oil interface. Wang *et al.* then reported an
194 alternative design with the use of an intermediate hydrophilic and shallow “extraction
195 channel” that connects the hydrophobic droplet channel to the hydrophilic separation channel
196 [22]. Similar to the previous systems, the sample is extracted into the extraction channel due
197 to both difference in surface energy and capillary forces. In this bridge system the whole
198 content of the droplets was injected into the separation channel, whereas in the other ones
199 only a fraction was injected. The droplet-interfaced MCE systems by Roman *et al.* and Wang
200 *et al.* (coupling to microdialysis for the latter) were applied for monitoring concentration

201 changes of derivatized amino acids dissolved in artificial cerebral spinal fluid [22, 24]. The
202 setup by Pei *et al.* was applied for high-throughput screening (HTS) of a GTPase assay, using
203 an array of three electrophoresis channels in the same microchip to achieve a throughput of
204 120 samples in 10 min [31]. One limitation of this system is the instability of the surface
205 coating, which loses effectiveness after 3 to 4 hours of operation. Improvement of the surface
206 treatment is thus needed for longer trials. From our viewpoint, these approaches relying on a
207 stable aqueous/oil interface between the (hydrophobic) droplet generation channel and the
208 (hydrophilic) separation channel are not facile for routine use, especially for users with no /
209 little skill in microfluidics and / or microfabrication. Several parameters have to be carefully
210 optimized to maintain the operational reproducibility, notably long-term hydrophobicity of the
211 total or partial channel's surfaces, as well as the channels' dimensions and intersections.
212 These factors are indeed not trivial to master at the micrometric / nanometric scales, and
213 therefore would not see widespread exploitation by non-expert users in the very near future.

214

215 In a related context, a design was proposed to take advantage of the native properties of glass
216 and PDMS for extraction, without recourse to surface modification [27]. The design was
217 separated in two parts. First, a straight PDMS channel was used to transport the segmented
218 flow from a syringe. This hydrophobic droplet channel was connected via a hydrophilic
219 extraction capillary to a natively hydrophilic MCE glass chip. This strategy was applied for
220 the screening of 140 compounds against protein kinase A. Compared to the 'virtual wall'
221 approach, this method demonstrated a 10-fold improvement of the sample analysis rate and
222 10-fold reduction of the reagent amounts needed for separation. The same system was then
223 improved to allow HTS and used for the identification of sirtuin inhibitors, allowing 1408
224 samples to be analyzed at a frequency of 0.5 Hz in 46 min [32]. For each sample, eight MCE

225 injections were made using the injection cross, generating more than 10 000
226 electropherograms during analysis.

227

228 Rather than extracting the sample droplet from the main oil-based flow, other options focused
229 on removing the oil around the aqueous droplet to inject the sample into the separation
230 channel. Niu *et al.* proposed the use of pillars made of native PDMS in front of a separation
231 microchannel, which were positioned perpendicular to the main flow to remove the oil from
232 the stream [23]. When an aqueous droplet came in contact with the pillars, the surface tension
233 kept the droplet stable and allowed it to flow past the perpendicular pillars without entering it,
234 while the oil was drained through them to a waste reservoir. This method required only simple
235 soft lithography process and relied on channel geometry rather than surface modification to
236 extract the oil passively. It allowed complete injection of a droplet into the separation channel
237 without introduction of any residual oil. For application, the outlet effluent of a peptide
238 mixture from a HPLC-based purification step was segmented into droplets that were
239 subsequently injected into a pillar-interfaced MCE channel. A positive feature of this
240 approach is the possibility to adjust droplet volumes (fL-nL) thanks to the tunable oil flow. Ye
241 *et al.* used this system to fragment the chromatographic effluent of urinary protein digest into
242 353 droplets of 40 nL each, allowing individual HPLC peaks to be fractioned by 4-40 times
243 for subsequent MCE operations [16]. The same group then presented another oil-extraction
244 method using a hydrophobic and oleophilic membrane to soak the oil from the main flow
245 [28]. In this method, a portion of PDMS was removed from the flat PDMS layer at the
246 junction with the separation channel, and a hydrophobic and oleophilic
247 polytetrafluoroethylene (PTFE) membrane was placed instead. When the droplet arrived at
248 the junction, it was injected by capillary forces into the separation channel while the oil was
249 absorbed by the PTFE membrane. While this method does not require surface treatment, the

250 working droplet size (or volume) had to be predefined before experiments, as the geometry of
251 the separation channel and the size of the delivery tubing must be carefully selected for each
252 range of droplet volume. To our opinion, these physical approaches using either on-chip
253 pillars or oil-soaking membrane, thanks to the possibility of prospective massive production,
254 would hold higher potential than the aforementioned chemical treatment alternatives. Users
255 with little expertise in microfabrication could purchase these ready-to-use materials and insert
256 them in front of the electrophoretic module for oil removal and aqueous sample
257 extraction/injection. Before these approaches can be used for routine operation, further
258 instrumental development has to be made to allow facile integration of the pillars or
259 membranes in between the droplet generation and separation parts, as well as their
260 detachment in case of replacement.

261

262 Recently, Ouimet *et al.* presented a method based on the difference of density between the CE
263 buffer and the carrier oil to remove oil from segmented flow [25]. In this system, the
264 separation glass chip was etched at the end of the sampling channel with a gap of 300 μm
265 between the sampling channel and the separation channel. As the segmented flow advanced
266 into the chip, the oil arrived and pooled in the buffer reservoir, whereas formulated sample
267 droplets (~ 30 nL with heavier density than oil) fell at the bottom of the chamber due to a net
268 buoyancy force higher than gravity. The oil came in contact with the separation channel but
269 was prevented from entering due to the native hydrophilicity of glass. When a sample droplet
270 arrived at the outlet of the sample channel, it came in contact with the inlet of the separation
271 channel where it coalesced due to a high voltage continuously applied at the oil removal
272 reservoir. After the samples entered the separation capillary, it migrated to an injection cross
273 where the amount of injection can be controlled by gated injection. This chip was suitable for
274 gel electrophoresis, where the gel matrix was loaded onto the glass chip using vacuum. It was

275 found to sustain up to 630 separations without reconditioning, with a throughput of about 10
276 s/sample). Considerations for this system include dilution of the sample when it goes through
277 the buffer reservoir to the separation capillary and the limited choice of carrier phases for the
278 segmented flow. Note that high-density oils are often preferred in droplets microfluidics for
279 their inert properties and low partitioning of analytes. The low-density oils required for this
280 approach are nevertheless often viscous, rendering them less suitable for droplet
281 microfluidics. We would expect to see more applications of this density-based approach for
282 discrete collection of sample droplets, which can be batchwise transferred to a CE/MCE
283 device for separation. If a high throughput is not required, this sample collection mode can be
284 practiced by any operator thanks to its simple and straightforward protocol.

285

286 Rather than segmenting the aqueous flow in oil and then remove one phase or the other, Quan
287 et al. [33] presented a method where the sample was segmented between two plugs of an
288 immiscible, hydrophobic, conductive ionic liquid (IL). The system was composed of a simple
289 PDMS linear channel interfaced to a silica capillary tube in the way that most of the capillary
290 stayed outside of the PDMS one. One drop of IL, one drop of sample and one drop of buffer
291 were placed on a PDMS slab and connected to the ground. A plug of IL was first
292 electrokinetically injected into the capillary by immersing the tip of the capillary into the IL
293 drop. The operation was then repeated for the sample, and then for the IL. For separation, the
294 capillary tip was immersed in the buffer drop and a high voltage was applied for separation.
295 With this system, the injected sample volume was easily controllable because it depended
296 only on the time and voltage of injection. It requires no de-segmentation of flow, as the carrier
297 fluid was conductive. Nevertheless, surface treatment was required in order to inject IL into
298 the capillary. For application, a model mixture of flavin adenine nucleotides (FAD) and flavin
299 mononucleotides (FMN) was separated using this method, allowing a signal improvement by

300 6.3-folds compared to conventional electrokinetic injection. The authors also showcased the
301 use of this method for the on-line labeling of myoglobin and cytochrome for CE-LIF, with the
302 whole assay involving the sample compartmentalization, labeling and CE analysis completed
303 within 4 min. The widespread use of IL plugs is nevertheless hindered by the fact that this
304 approach can be used only with electrokinetic injection. The more practiced hydrodynamic
305 injection mode has not been investigated with this approach. Furthermore, this method may
306 encounter the same problem with instability of the surface treatment, as already discussed
307 above.

308
309 In a recent study, Serra *et al.* developed an integrated droplet microfluidic device for magnetic
310 particles handling used as solid support for DNA size selection in NGS libraries preparation
311 [34]. In this work, a train of aqueous droplets in fluorinated oil was used to carry out several
312 rounds of sample processing steps, including DNA precipitation on magnetic microparticles,
313 on-bead DNA washing and DNA release to the target matrix (see Fig. 2 for the setup). A high
314 number of steps was made possible thanks to magnetic beads that carried target analytes
315 through a series of droplets without cross-contamination and with high efficiency. Compared
316 to the batchwise procedure for DNA size selection in NGS libraries preparation, this droplet
317 protocol is simpler (thanks to reduction of the number of washing steps), much faster (with
318 on-bead DNA precipitation or in-droplet DNA release in approximately 1 min) and less
319 sample-consuming (using 100 nL droplets in the protocol) while maintaining an excellent
320 quality of purified DNA fragments. The final droplet containing desired DNA fragments was
321 then offline introduced to MCE (BioAnalyzer instrument) via manual droplet collection.
322 Compared to other microchip-based setups for sample handling in droplets prior to MCE, this
323 design exhibited higher flexibility and the possibility to carry out an extended number of
324 sample treatment steps and in particular solid phase extraction. While oil removal was not

325 required for MCE, droplet dilution was the limitation of this setup as it worsened the detection
326 limits and did not allow full integration and automation.

327

328 ***2.2. CE coupled with aqueous droplets in oil***

329 Different approaches to interface water-in-oil droplets to CE have been reported in efforts to
330 seek for a more robust and automatable alternative to the droplet-MCE format. For instance
331 with a practically identical method as already described for droplet-MCE coupling, Niu *et al.*
332 used their oleophilic-PTFE-membrane system for coupling CE with a segmented flow [28].
333 By inserting a capillary into the separation channel in the design previously described, the
334 authors showcased the possibility to use this method for capillary gel electrophoresis (CGE),
335 where a polymer matrix is used to separate large biomolecules by size or mass. By inserting a
336 capillary pre-filled with the sieving matrix into the separation channel, separation of a 50 bp
337 dsDNA standards could be achieved where 14 out of 16 fragments could be unambiguously
338 identified. Note that, as most matrices for CGE are highly viscous, the loading of the buffer
339 into a CE channel required high pressure, which is not fully compatible with droplet-
340 interfaced chip-based systems.

341

342 De La Marre *et al.* proposed an alternative design to remove the oil from the main flow prior
343 to CE operations [35]. In this method, two patterned slabs of PDMS were aligned and bonded
344 together in order to intersect out of plane with a cross geometry. The bottom slab contained a
345 straight 75 μm -wide sample channel, which ended with a punched waste reservoir. The
346 segmented droplets were prepared off-chip and brought into this sample channel by an
347 inserted capillary. The top slab contained a narrower straight separation channel (30 μm
348 wide), with a grounded buffer reservoir punched at its inlet and a silica capillary inserted at
349 the outlet. The top slab's surface (made of hydrophobic PDMS) was selectively modified with

350 a Corona treatment to make it hydrophilic. At the channels cross-section, a stable oil/buffer
351 interface was created. When a droplet arrived at the intersection, it coalesced with the buffer
352 interface and was sucked into the separation channel by surface tension, while the oil was
353 prevented from entering the separation channel. As Corona treatment is quite easy to use, this
354 method offers simplification of the fabrication process, with only two straight channels being
355 used for the chip. This approach allowed injection of almost the whole droplet content into the
356 separation channel, with only some droplet residues (called satellite droplets) observed after
357 the injection. The handling of the segmented flow in this method was performed using a
358 pressure reservoir actuated manually by a thumb, which would be non-optimal and could
359 hinder operation speed. For characterization of the system performance, droplets of 750 pL
360 containing Riboflavin was used allowing temporal resolution of its peak down to 15 s.
361 Basically, this droplet-interfacing setup for CE relied on channel's surface treatment,
362 therefore may find similar challenges to overcome as its counterparts for MCE (see section
363 2.1), before routine use can be envisaged.

364
365 Instead of relying on flow segmentation with oil, Li *et al.* proposed a system where the
366 samples were placed into a nanoliter well array and covered by a non-volatile oil to prevent
367 evaporation [36]. This array was placed on an x-y-z translation stage, and along with vials
368 filled with buffer and various solutions needed for CE separations. The inlet end of a silica
369 capillary was mechanically ground into a tapered tip. The capillary was bent in to a “∩” shape
370 and fixed vertically with the inlet and outlet at the same level. After the capillary was filled
371 with separation buffer, the sample injection occurred spontaneously by plunging the capillary
372 inlet through the cover oil into a sample well, and then removing it quickly. As the surface of
373 the capillary plunged in the sample is uncoated and thus hydrophilic, some sample solution
374 adhered to the capillary sidewall and tip during the capillary withdrawal. The removing speed

375 was well controlled to ensure satisfied injection reproducibility. A pL volume of the sample
376 solution thus remained at the tip of the capillary and was subsequently sucked into the
377 capillary by surface tension, while the oil scraped the sample residual present at the sidewall,
378 limiting cross-contamination between samples (only 0.14 %). The capillary was then placed
379 into the buffer vial connected to electrode for CE separation. For a proof of concept using
380 three amino acids, 25 separations could be implemented in less than 15 min with this system.
381 The system was also used for monitoring the in-droplet derivatisation of amino acids. FITC
382 and three amino acids were added into a 500 nL droplet and separations were carried out
383 every 5 min for 3h. The same group recently used this approach for the detection of multi-
384 gene mutations using PCR-restriction fragment length polymorphism (PCR-RFLP) [37]. A
385 lowest mutation frequency of 0.37% was achieved without cross-contamination between
386 samples. This system has the advantages of being relatively easy to build, requiring no
387 microfabrication. As each droplet is contained within a well, each sample is easily re-
388 accessible via its identified position. The size of injection can be tuned by varying the speed at
389 which the capillary is removed from the sample well [38]. The reloading of the sample wells
390 nevertheless could pose some problem, as it required thorough cleaning of each well, and has
391 to be carried out manually. Variation of sample matrix viscosity should be taken into account,
392 as it may influence the sample quantity to be attached at the tip and sucked into the capillary.
393 This approach hold high potential for widespread use, thanks to its automation feature.
394 Modification of the CE instrument to allow integration of the dedicate sample tray is
395 nevertheless required, which is not yet feasible with existing commercial CE instruments.
396 Utilization of dedicate capillaries is another point to be considered, as the commonly used
397 fused silica capillaries are not adapted to the purpose-made system at the initial state.
398

399 Diverted from de-segmentation of sample flow prior to CE injection, Abdul Keyon *et al.*
400 proposed a method for the compartmentalization of analytes after CE separation, allowing
401 selective processing and detection of target analytes in the fraction of interest which is
402 purified by CE [39]. The droplet-based sample handling is implemented as a downstream of
403 the separation step rather than a forefront operation as in other cases. A micrometric cross
404 was used to create an intersection between four capillaries (see Fig. 3 A and B for their setup).
405 The separation capillary was positioned towards the top whereas at the bottom capillary is
406 located a salt bridge with a Pt electrode connected to the ground to maintain electrical
407 connection during separation. A train of droplets was introduced from the left capillary. The
408 capillary on the right was used for collecting the droplets and postcolumn detection. As the
409 buffer-filled droplets (14 nL each) came in front of the separation capillary outlet and the salt
410 bridge, analytes from the CE separation were electrophoretically transferred into the droplets.
411 By adjusting the frequency at which the droplets were formed, a continuous contact from the
412 separation capillary via droplets to the salt bridge could be maintained to allow a stable
413 separation current. For demonstration, a mixture of two paralytic shellfish toxins was
414 separated by CE and then segmented into droplets where they were oxidized in a post column
415 reaction and detected by fluorescence (see Fig. 3C for a typical electropherogram). The
416 droplets were created at a rate of 1 Hz, with one separation lasting for 10 minutes. When
417 compared to previous precolumn oxidation from the same group [40], the separation was
418 quicker (10 min versus 30 min). Postcolumn derivatization also allowed selective oxidation of
419 only one toxin at a time, avoiding the problem with simultaneous oxidation that complicates
420 product identification encountered with precolumn oxidation. In another strategy for droplet-
421 based detection after CE separation, Mai *et al.* proposed to couple capillary isoelectric
422 focusing (CIEF) to single-step magnetic-beads based immunoassays in a microfluidic droplet
423 for sequential determination of amyloid-beta ($A\beta$) peptide biomarkers for molecular diagnosis

424 of Alzheimer's disease [41]. A β peptides possessing different isoelectric points were
425 compartmentalized into different fractions along a capillary filled with a pH gradient under a
426 high electrical field prior to detection using a droplet-based enzyme-linked immunosorbent
427 assay (ELISA). Using pressure mobilization, these fractions (A β 1–40 in the first (pI = 5.33),
428 A β 2–40 in the second (pI = 5.98) and A β 5–40 in the last one (pI = 6.46)) were then collected
429 and subsequently specifically quantified by the in-drop-ELISA. This platform was composed
430 of a syringe pump and a motorized pipettor arm used for droplet generation, as well as a 384-
431 well plate (for the storage of sample and reagents) placed on a holder that is adjustable in the
432 x-y-z directions. By using oil in the pipetting tubing, the sample and reagents needed for
433 ELISA were first segmented into 200 nL droplets inside the tubing. Four pairs of magnetic
434 tweezers activated by a magnetic coil were placed around the tubing to capture and released
435 antibody-grafted magnetic beads, which were re-suspended in different droplets containing
436 various reagents for the ELISA protocol. Compared to conventional ELISA, this droplet-
437 based alternative offered automation, reduction of working volume and significant diminution
438 of operation time. A throughput of 8 analyses per hour could be achieved with this droplet-
439 based protocol, compared to a duration of 2 hours per analysis required for conventional
440 ELISA. Significant reduction of sample volumes (200 nL / analysis for the droplet protocol
441 vs. 50-100 μ L for conventional ELISA) is advantageous for such type of biomarker detection
442 application as biological sample volumes are often limited. Detection sensitivity with this
443 approach for determination of A β 1-40 and A β 1-42 was still inferior to that obtained with
444 conventional ELISA, and therefore needs to be further improved. Manual transfer between
445 CIEF and droplet-based ELISA protocols is still a point for improvement before full
446 automation and high-throughput is possible.

447

448 An overview of aforementioned approaches revealed that they all generate droplets of a
449 constant-volume (in the pL-nL range), mostly for high throughput sample injection and
450 analysis. Only few studies explored the potential of droplet trains for down-scaling sample
451 treatment protocols. Large room therefore still remains to be exploited in this direction. From
452 our viewpoint, the power and flexibility of droplet microfluidics could be further exploited by
453 employing droplets of different sizes for different sample processing purposes. For example, a
454 large sample droplet can be trapped onto a carrier support and transferred into a much small
455 droplet for preconcentration by solid-phase extraction. In-droplet chemical reactions for
456 fluorescent labeling of target analytes for CE-LIF for instance, or in-droplet enzymatic
457 reactions can be triggered by simple fusion of two separate droplets into a bigger one. The
458 droplet merging or splitting on-demand operations can be implemented simply by modifying
459 the microchannel geometry, oil nature and / or surfactants to be added into droplets for
460 interfacial tension modification [42, 43]. Eventually, sample pre-treatment in a down-leveling
461 droplet sequence in oil would be foreseen as an optimal setup for this oil-based strategy of
462 droplet-interfacing to microscale electrophoresis. For instance, a typical protocol for down-
463 leveling droplet train can start with a large sample (μL range) droplet; then passing through
464 sample processing via solid supports in droplets and/or droplet fusion/splitting; and finally
465 focalizing target analytes into a tiny (nL) droplet for CE injection and separation.

466

467 **3. Microscale electrophoresis coupled to digital microfluidics with electrowetting-on-** 468 **dielectric principle**

469 Another strategy to manipulate droplets in the forefront of CE employed digital microfluidics
470 (DMF) in which the droplets are actuated by Electrowetting On Dielectric (EWOD)
471 technology (see strategy 2 in table 1 for the summary). The EWOD principle is based on
472 electrical potentials to enable manipulation of fluid shape and flow via control of the

473 wettability of liquids on a dielectric solid surface. Indeed, the application of an electric
474 voltage leads to modification of the free energy on the dielectric surface, inducing a change in
475 the wettability on the surface and the contact angle of the droplet. Readers can refer to a
476 fundamental work by Cho et al. for more detailed explanation and demonstration of EWOD
477 principle [44]. The popular scheme of DMF-EWOD allows creation and actuation of
478 individual droplets from a reservoir and their independent manipulation (e.g. transport,
479 division, addition) over a planar electrode array via application of electrical fields. Its
480 principle eliminates the need of complex networks of tubing or microvalves but at the price of
481 more complex microfabrication [45]. While microchannels were typically used to manipulate
482 droplets flowed in an immiscible fluid stream, DMF introduced a distinct paradigm as a basic
483 method for moving droplets on a surface [45-47]. The DMF-EWOD principle was first
484 applied by Abdelgawad *et al.* to develop a digital-to-channel interface for sample processing
485 and MCE separations [48]. This hybrid digital-channel microfluidic device, comprised of an
486 electrode array for sample preparation by digital microfluidics and a network of MCE
487 microchannels (see the side-on design in Fig. 4), was used for on-chip NDA labelling of
488 amino acids and cell lysate as well as for on-chip digestions of singly labelled FITC-insulin.
489 The μL -sized droplet contents were driven into the separation channel electrokinetically for
490 pinched injections with assistance of EOF, followed by separations performed in micellar
491 electrokinetic chromatography (MEKC) mode. The same authors then improved the DMF-
492 MCE side-on design by a multi-layer one, in which droplets are manipulated by DMF in the
493 two-plate format (see the multi-layer design in Fig. 4) [49]. The second DMF-MCE
494 generation, which facilitated sample dispensing from reservoirs, droplet splitting and storage
495 for subsequent analysis, was applied for an on-chip serial dilution experiment as well as
496 multistep enzymatic digestion prior to electrokinetic separations. While DMF platforms were
497 thought to be ideally suited to electrokinetic separations at first sight, these pioneering works

498 on DMF-MCE were then discontinued. The widespread use of DMF-EWOD for droplet-
499 interfaced MCE indeed is still hindered by the typically complicated process of making DMF
500 devices (i.e. the fabrication of microchip-integrated electrodes and coating with layers of
501 dielectric and hydrophobic materials that requires microfabrication and electrical workshop).

502

503 To bring low-cost DMF to microscale electrophoresis, Kaljurand *et al.* exploited the DMF-
504 EWOD phenomenon for transporting sample and buffer droplets in succession under the CE
505 capillary inlet end and allow the capillary to be immersed into the sample/buffer droplet [50].

506 In this portable CE analyzer coupled with a DMF device, the actuation of droplets was
507 achieved via an electrode system prepared from the copper substrate of the common printed
508 circuit coated by food wrap whereas CE separation was performed by applying a high voltage
509 between the (grounded) buffer droplet and CE outlet reservoir (Fig. 5). The system was
510 demonstrated with monitoring of sample concentration kinetics during evaporation of the
511 droplet containing model thiamine, pyridoxine and nicotinamide, using capacitively coupled
512 contactless conductivity detector (C⁴D). A prototype based on this DMF-CE principle was
513 then developed to include solid-liquid extraction of amino acids from sand matrices prior to
514 their determination with CE-C⁴D [51]. Alternatively, the design was rearranged to allow the
515 use of the DMF platform not as a sampler but rather as a collector and transporter of CE
516 fractions after electrokinetic separations [52]. This CE coupled with downstream EWOD
517 actuation of droplets, using air plugs instead of a carrier liquid for encapsulation of the
518 selected fractions, was applied for off-line electrospray ionization mass spectrometry (ESI-
519 MS) characterization of some vitamin standards [52], and MALDI-MS analysis of peptide
520 fractions [53]. In a parallel work, Patel *et al.* developed a system integrating a droplet-based
521 DMF platform with a capillary-based reagent delivery unit and a quantitative CE module for
522 automated quality control (QC) platform for next-generation sequencing (NGS) library

523 characterization [54]. This system consisted of three key modules, including i) fluidic delivery
524 element using fused-silica capillaries connected to an 8-port syringe pump for high-precision
525 fluid metering, ii) DMF unit for sample mixing and fluid routing and iii) CE-LIF separation
526 and detection module. Using this system, double-stranded DNA samples were
527 electrokinetically injected and quantified for quality control prior to NGS with the Illumina
528 Genome Analyzer sequencing platform. This setup allowed detection of double-stranded
529 DNAs in the range of 5–100 pg/ μ L, which is suitable for the commercial sequencing
530 platform, while consuming ten-fold less sample volume than the current Agilent Bio-Analyzer
531 QC technique. This DMF-CE system therefore helps preserve precious samples while
532 providing necessary sensitivity and accuracy for optimal sequencing performance.

533 While these DMF-CE and CE-DMF setups could be of interest to laboratories without access
534 to well-equipped infrastructure (e.g. clean-rooms or lab robots), some electronic skills and
535 facility are still needed to prepare the EWOD boards with etched electrodes for droplet
536 manipulation. The aforementioned challenges encountered with the DMF-CE/MCE coupling
537 would have to be overcome before this droplet-interfacing strategy for microscale
538 electrophoresis could gain more popularity. From this point, 3D printed microfluidics and
539 microelectronics seem to be the matching solution, as they allow microfluidic platforms to be
540 fabricated with fully integrated microelectronics, which are required for electrowetting-on-
541 dielectric (EWOD) phenomena and (on-chip) electrophoresis [55]. Another consideration
542 when using this approach is a relatively large droplet volume generated (typically 2-5 μ L
543 droplets). Downscaling of the working droplet volume will be needed to minimize volume
544 mismatch in the DMF-CE/MCE coupling.

545

546 **4. Microscale electrophoresis coupled with inkjet droplet generator**

547 Among all droplet-interfaced strategies for CE/MCE, inkjet injection could be the one that
548 allows a total compatibility of working volumes (i.e. both in nL ranges) between droplet-
549 based sample handling and electrokinetic separation (see strategy 3 in table 1 for an overview
550 of this approach). This mode is based on inkjet printing principle, which is a type of computer
551 printing to propel droplets of ink onto paper and plastic substrates in order to recreate a digital
552 image. This is the most commonly used type of printers, ranging from small inexpensive
553 consumer machines to expensive professional ones. Inkjet injectors have found their
554 applications not only for office printing technology but also for various industrial fabrication
555 processes [56] thanks to their desirable properties, notably droplet spatial and volume (pL-nL)
556 controllability, high speed, and accurate spotting on the surface of a wide variety of
557 substrates. The coupling of inkjet injection to MCE was first developed by Yasui et al. in
558 2012 for microchannel array electrophoresis analysis of DNA droplets [57]. The inkjet
559 injector in this system (Fig. 6) allowed precise control of the injection volume of DNA
560 samples down to pL-nL ranges and the use of a simple straight microchannel for MCE, which
561 otherwise are not trivial with conventional cross injection method in the cross- or T-shaped
562 microchannels. This droplet-interfaced approach offered some positives features to MCE,
563 including suitability for high density array of microchannels, ability to separate biomolecules
564 by one voltage programming and rapid analysis duration as no sample loading time is needed
565 with the inkjet injection method as in conventional MCE.

566
567 A similar droplet generation concept was then developed for CE setups by Uchiyama *et al.*
568 [58-62]. In their first inkjet-CE design (Fig. 7A), they employed precise control of waveform
569 driving piezoelectric crystal inside the inkjet head to trigger by a drop-on-demand approach
570 stable droplet generation from various solutions. The piezoelectric droplet generator was used
571 for injection of well-defined amounts of sample (179 pL droplets with excellent

572 reproducibility) in capillary electrophoresis, with the droplet size and delivery frequency
573 adjustable via waveform turning. The authors demonstrated its first application with analysis
574 of theobromine, caffeine and theophiline using MEKC [58]. This inkjet-CE setup was then
575 adapted to drop-by-drop introduction process for electrophoretically mediated microanalysis
576 (EMMA), allowing (1) on-line multi-segment injection pattern by alternately ejecting small
577 plugs of sample and reagents, (2) in-capillary incubation for fluorescent labelling reaction
578 with an overlapping region of the plugs for mixing the reactant solutions by electrophoresis
579 and (3) CE-LIF determination of amino acids tagged with a fluorophore (4-fluoro-7-
580 nitrobenzofurazan) [59]. In another application, the system was used to eject a large sample
581 volume onto the inlet end of the capillary and then introduce it into the capillary under gravity
582 and Laplace pressure, allowing quantitative on-line concentration of methylxanthines in
583 bottled green tea via stacking and sweeping in MEKC [60]. The application of the inkjet-CE
584 instrument was then extended for online EMMA-based immunoassays (using ~ 200 pL
585 droplets of fluorescein-labeled anti-human IgG antibody and human IgG), followed by CE
586 separation of the antigen-antibody complex formed in the merged zone in the capillary [61].
587 The method showed a wide linear range of calibration (10–2000 ng.mL⁻¹) with satisfied
588 linearity ($R^2 = 0.9912$). The detection limit (5 ng.mL⁻¹) was substantially lower than those
589 obtained for conventional immunoassays (including CE-based methods). The most recent
590 application of this approach was for CE separation of mammalian cells encapsulated in
591 picometric droplets, in which calibration linearity was obtained by varying the number of
592 droplets (25-400 drops) injected into the capillary for electrokinetic separations [62] (see Fig.
593 7B for a typical electropherogram). Compared to conventional sampling techniques, this
594 inkjet sampling setup allowed precise sample manipulation with spatial and temporal control
595 which is important for sampling at the single cell level. Furthermore, it can realize
596 quantitative analysis of cell by adjusting the cell concentration and the number of droplets,

597 which is otherwise not trivial with the conventional modes. An overview on this inkjet-
598 CE/MCE approach indicated that its applications are still limited despite its power on precise
599 control and generation at high-frequency of CE-volume-matching droplets. Dedicate and
600 complicate electronic and optical instrumentation required for such setup for droplet-capillary
601 alignment and movement would be the reason for the hindering of its replication and
602 widespread use. As modification of commercial CE instruments to include the inkjet module
603 is not favored yet by their manufacturers, only purpose-made CE systems could allow
604 integration of inkjet injectors. To the authors' point of view, this mode could open more doors
605 for utilization / applications only if ready-to-use (off-the-shelf) inkjet injection modules that
606 can be plugged to CE instruments are available.

607

608 **5. Other strategies for droplet introduction to microscale electrophoresis**

609 Besides the main strategies using conventional droplet microfluidics, DMF or inkjet injection,
610 some other approaches were developed for generation and actuation of upstream droplets for
611 CE/MCE. Kaneda *et al.* gave an account of sequential operations of droplet-based reaction
612 process followed by MCE separation realized in a single microfluidic chip with pneumatic
613 handling of liquid [63]. In this system, automated liquid handling (i.e. introduction of liquid
614 samples, generation and merging of 420 pL droplets) was implemented by pressurization (40-
615 100 kPa) through microcapillary vent structures, allowing air to pass and stop liquid flows.
616 The setup was applied for a binding reaction of a single-stranded DNA with a peptide nucleic
617 acid oligomer followed by denaturing electrophoresis to discriminate a single-base
618 substitution. Despite interesting results, no further works using this approach was reported.

619

620 As an alternative to the train of droplets, the SlipChip developed in 2009 by Ismagilov group
621 was adapted to allow parallel and quantitative MCE [64]. This SlipChip, called GelChip,

622 consisted of two poly(methyl methacrylate) (PMMA) plates, *i.e.* a droplet plate containing
623 droplet wells and a separation one on which separation channels were built in parallel. Once
624 the droplet wells were filled with the sample solution, the droplet plate was slid to allow the
625 sample to overlap with the separation channel. Upon contact with the buffer, immediate
626 merging of the sample with the buffer occurred, allowing the total volume of the droplet to be
627 injected into the separation channel. The SlipChip system was applied for rapid separation of
628 DNA ladders, with 30 separations taking place in 120 seconds. The same group also used a
629 modified SlipChip format for isoelectric focusing (IEF) of different proteins (trypsin inhibitor,
630 β -lactoglobulin A, carbonic anhydrase isozyme II, myoglobin, and lectin) [65]. When aligned
631 and clamped together with magnets, the two plates form a zig zag channel where the sample
632 can be loaded and separated by IEF. The chip was then slid to compartmentalize the focalized
633 analytes into 140 wells, allowing the user to collect target droplets for further processing. The
634 SlipChip principle was then coupled with a GelChip for development of a modified platform,
635 which consisted of two plastic plates, the one for droplet wells and the other for separation
636 channels with preloaded/cured gel [66]. The SlipChip-GelChip setup was demonstrated for
637 separations of 30 sub-nL sample droplets containing fluorescent dyes or DNA fragments. The
638 SlipChip design deemed user-friendly, and no flow control was required. Nevertheless the
639 injection volume for a given design cannot be varied, and manual reloading of the chips and
640 plate sliding after separations would hinder full automation of the protocol.

641
642 Opekar *et al.* introduced a syringe-based technique, using a needle of an automated 10 μ L-
643 syringe located directly opposite to the capillary inlet at a defined distance, to produce 125 nL
644 droplets for direct sample injection into the CE capillary via negative pressurization [67]. The
645 setup utilized off-the-shelf microfluidic components (e.g. Hamilton syringe, Supelco
646 connectors, KD Scientific 200 micro-pump) to allow re-fabrication, and was applied for CE-

647 C⁴D separation of inorganic cations. The authors then modified the design with an air-assisted
648 flow-gating interface (FGI), replacing the micro-syringe with a delivery capillary to generate
649 75 nL sample droplets for hydrodynamic injection [68]. This droplet interfacing strategy via
650 FGI was then used for on-line connection of CE with a dialysis unit to allow sample dialysis
651 into an acceptor solution (sub μ L) trapped in a dialysing hollow fibre, prior to CE-C⁴D
652 separations of extracted analytes. This approach was applied for simultaneous determination
653 of the majority minerals in unflavored yoghurts [69], as well as determination of basic amino
654 acids (histidine, lysine and arginine) in a blood serum sample [70]. The most recent approach
655 was communicated by Ngamakarn *et al.*, using a moving drop setup with electrokinetic
656 sample injection for CE [71]. A polyether ether ketone (PEEK) tube functioned as a drop-
657 head tube for solution dropping. For droplet guiding, the system employed a tile path
658 supporter coated with hydrophobic Teflon tape and arranged in a 45° slope compared to the
659 CE capillary position. It can be seen that the large droplet volume (25 μ L) renders this
660 approach less favorable for droplet-interfaced CE due to pronounced working volume
661 mismatch. Note also that these syringe-based, FGI and moving-drop setups, despite their
662 instrumental simplicity to allow facile reproduction and employment, are more adapted to
663 droplet-based injection rather than sample pre-treatment. Design and protocol improvement
664 would be needed before they can be used in a sample processing protocol with extended steps.

665

666 **6. Conclusion remarks and perspectives**

667 Several droplet-interfacing strategies have recently been developed for microscale
668 electrophoresis, allowing the use of tiny working volumes for sample handling and/or high-
669 throughput injection prior to electrokinetic separations of target analytes with CE/MCE.
670 These approaches are gaining more and more interest and both academic and industrial
671 communities have put efforts to develop integrated systems for seamless sample processing

672 and electrophoretic separation with little or no working dimension (volume in particular)
673 incompatibility. Different companies (for instance Inorevia - Innovative Bioassays, Fluigent
674 or Elvesys in France) are exploiting droplet-based operations for sample treatment which can
675 be subsequently connected to separation instruments to our opinion. As existing commercial
676 CE instruments do not allow facile integration of external sample treatment modules, the
677 droplet-interfacing would be promoted at the first time with purpose-made CE instruments.
678 The recent introduction of open-source CE [72] and modular CE [73] may allow flexible
679 instrumentation with a high degree of standardization, which is required to develop automated
680 droplet-CE/MCE systems and further widespread these designs. Of course it is too early at
681 this stage to foresee the utilization of droplet-CE/MCE systems for routine analyses outside
682 the research context, as inherent issues of microscale electrophoresis (notably migration time
683 fluctuation and / or adsorption of unwanted molecules on capillary wall) need to be overcome
684 first. One analytical niche in the future for droplet-CE/MCE systems could be compact, cost-
685 effective and transportable instrumentation allowing both sample processing and
686 electrophoretic separations of target analytes. Towards this direction, fabrication of
687 commercially available prototypes for dedicated uses could be possible by exploiting the
688 commercial microfluidic droplet modules and modular / open-source CE, to our opinion. The
689 droplet-interfacing is also important when working with precious samples of limited volumes
690 (for example cerebrospinal fluids for analysis of neurodegenerative diseases' or brain cancers'
691 biomarkers). Combining CE/MCE with droplet-interfaced sample pretreatment techniques
692 would represent a powerful tool for bioanalytical laboratories for analysis of molecules often
693 present in trace amounts in biological matrices. From these points, the droplet-CE/MCE
694 systems, once they are at a more mature instrumental stage, could see their first applications
695 in biological and clinical domains where the challenges with limited sample volumes and
696 trace amounts of target analytes could be overcome with this droplet interfacing strategy.

697
698 At the present state of the art, droplet-interfacing for CE/MCE is still at its infancy, focusing
699 more on the high-throughput injection / screening aspect, and much less on its potential for
700 down-scaling and automating sample treatment protocols. All instrumental designs presented
701 in this review stop at the utilization of constant-sized droplets. The power of droplet volume
702 variation, droplet fusion and splitting functions is still to be explored. Among all strategies
703 presented in this review, we envision that the coupling of CE with droplet trains flowing in
704 immiscible phases will further emerge and could be transferred to industrial use. Its
705 straightforward and flexible instrumental setups that can be adapted to various types of
706 sample processing and preconcentration (e.g. immune-enrichment on magnetic beads,
707 fluorescent labeling, chemical precipitation, enzymatic reaction etc.) make this droplet-
708 sequence-in-oil approach a particularly important toolset for researchers working in analytical
709 science, especially in the bioanalytical, biomedical, and clinical diagnostic fields.

710

711 **Acknowledgement**

712 The authors are grateful for the financial support by the Agence Nationale de la Recherche
713 (ANR, France) with the grant no. ANR-18-CE29-0005-01.

714 The authors have declared no conflict of interest.

715 **Table 1:** Strategies to interface droplets to microscale electrophoresis

Droplet interfacing strategy	Approach	Setup	Oil removal method	Droplet volume	Application	Remarks (pros / cons)	Reference
Strategy 1: Droplet train in immiscible phases	Parallelized virtual wall and K-shaped interface	MCE-Fluorescence Microscope	Coalescence with immiscible interface	9 nL	GTPase assay	Passive removal, parallel analysis	[31]
	Virtual wall and K-shaped interface	MCE-LIF	Coalescence with immiscible interface	12-17 nL	Separation of fluorescently labeled amino acids	Passive removal, only a fragment of the droplet is injected	[24]
	Segmenting effluent from HPLC for 2 dimension separation	MCE-UV	Pillars to filter the oil	10 nL	Two-dimension separation of a peptide mixture	Passive removal, adjustable droplet volume	[23]
	Sample from a microdialysis probe is segmented and injected into a MCE	MCE-LIF	Extraction bridge	8-10 nL	In vivo chemical monitoring of amino acids	Passive removal, monitoring	[22].
	Open channel with hydrophobic and oleophilic membrane	MCE-LIF	Passive absorption by membrane	4 nL	Separation of 50 bp dsDNA molecular weight standard	Passive removal, suitable with gel CE, high throughput (5 droplet/sec)	[28]
	A PDMS chip is linked to a glass MCE using a hydrophilic capillary	MCE-LIF	Hydrophilic capillary	8 nL	Screening a test library of 140 compounds against using protein kinase A	Passive removal, high-throughput potential	[27]
	A PDMS chip is linked to a glass MCE using a hydrophilic capillary	MCE-LIF	Hydrophilic capillary	8 nL	Screening of 1280 compounds against SIRT5	Passive removal, high-throughput potential	[32]
	Sample are electrokinetically injected into a separation channel while the oil experiences buoyancy and is drained upward	MCE-LIF MGE-LIF	Difference of density between carrier phase and running buffer	5 nL	Separation of protein-protein complexes and enzymatic reactions	Passive removal, some dilution of sample	[25]
	EOF-based	MCE-LIF	-	30 pL	Separation of a mixture	On-chip labeling,	[33]

	compartmentalized sampling/labeling using hydrophobic ionic liquid to segment flow				of flavin adenine nucleotides (FAD) and flavin mononucleotides	electrokinetical injection	
	Integrated droplet microfluidics for magnetic particles handling	MCE-LIF	Manual collection and fusion of outlet droplets via a micro-pipette	100-200 nL	DNA size selection in NGS libraries preparation		[34]
	Array of nano-scaled, oil covered sample wells fixed on a x-y-z translation stage with a fixed capillary	CE-LIF	-	200 pL	Separation of samples made of 3 amino acid	Easy to build, tunable plug volume	[36]
	Selective surface patterning of the channel to create stable interface	CE-LIF	Coalescence with immiscible interface	10 fL	Separation of 3 amino acid	Sample can also be injected directly into the separation channel	[30]
	Out of plane intersecting channels with independent droplet formation	CE-LIF	Surface patterning and geometry	750 nL	Changes in riboflavin concentration	Satellite droplets, manually operated, passive removal	[35]
	Array of nano-scaled, oil covered sample wells fixed on a x-y-z translation stage with a fixed capillary	CE-LIF	-	200 nL	Detection of multi-gene mutations from colorectal cancer samples	Easy to build, tunable plug volume	[37]
	Segmenting effluent from HPLC for 2 dimension separation	CE-UV	Pillars to filter the oil	40 nL	Two dimensional separations of human urinary protein digest	Passive removal, adjustable droplet volume	[16]
	Droplet-based immunoassay with off-line CIEF	CIEF-UV	Manual collection of outlet droplets and dilution prior to CE	200 nL	Detection of amyloid-beta peptide-based biomarkers of Alzheimer's disease	Extended steps of sample processing in a droplet train with back and forth movement. Design flexible for various operations. High throughput CE was not yet	[41]

						possible as droplets need to be collected manually.	
	Effluent from CE are segmented into droplets for post column detection	CE-LIF	-	14 nL	Separation followed by oxidation of paralytic shellfish toxins	-	[39]
Strategy 2: Digital microfluidics with electrowetting-on-dielectric principle	Digital-to-channel interface for MCE (side-on design)	MCE-	-	2.5 μ L	DNA labelling of amino acids and cell lysate; on-chip digestions of singly labelled FITC-Insulin		[48]
	Digital-to-channel interface for MCE (multi-layer design)	MCE-	-	\sim 3 μ L	On-chip serial dilution and multistep enzymatic digestion		[49]
	Digital microfluidic sampler for portable CE	CE-C ⁴ D	-	5-10 μ L	Sample concentration kinetics of thiamine, pyridoxine, nicotinamide		[50]
	Digital microfluidic sampler for portable CE	CE-C ⁴ D	-	3 μ L	Solid-liquid extraction of amino acids from sand matrices		[51]
	Collector and transporter of CE fractions for ESI-MS	CE-MS	-	3 μ L	Characterization of some vitamin standards		[52]
	Collector and transporter of CE fractions for MALDI-MS	CE-MS	-	3 μ L	Analysis of peptide fractions		[53]
	DMF platform with capillary-based reagent delivery unit for quantitative CE	CE-LIF	-	2-3 μ L	Quality control platform for next-generation sequencing (NGS) library characterization		[54]
Strategy 3: Inkjet droplet injector	Droplet injection for microchannel array electrophoresis	MCE-		pL-nL	Electrophoretic analysis of DNA droplets		[57]
	Piezoelectric droplet injector in the inkjet head	CE	-	179 pL	Analysis of theobromine, caffeine and theophiline using MEKC	Droplet size and delivery frequency adjustable via waveform turning	[58]
	Drop-by-drop introduction for	CE-LIF	-	181-183 pL	Determination of amino		[59]

	electrophoretically mediated microanalysis (EMMA)				acids tagged with a fluorophore (4-fluoro-7-nitrobenzofurazan)		
	Quantitative CE by inkjet with on-line concentration	CE-UV	-	(sub)-nL	Quantitative on-line concentration of methylxanthines in bottled green tea		[60]
	Inkjet injection in immunoassays by quantitative on-line EMMA	CE-	-	~ 200 pL	Online EMMA-based immunoassays and CE separation of the antigen-antibody complex		[61]
	CE coupled with inkjet printing system.	CE-	-	~ 200 pL	CE separation of mammalian cells encapsulated in droplets	Calibration linearity via variation of droplet numbers (25-400 drops)	[62]
Other strategies	Single microfluidic chip with pneumatic handling of liquid	MCE-	-	420 pL	Reaction of a ss DNA with a peptide nucleic acid oligomer and denaturing electrophoresis to separate a single-base substitution	Introduction of liquid samples, generation and merging of droplets via pressurization (40-100 kPa), allowing air to pass and stop liquid	[63]
	Syringe-based direct sample injection to CE capillary via negative pressurization	CE-C ⁴ D	-	125 nL	Separation of inorganic cations	Use of off-the-shelf microfluidic components	[67]
	Air-assisted flow-gating interface with a delivery capillary	CE-C ⁴ D	-	75 nL	Separation of inorganic cations	Use of off-the-shelf microfluidic components	[68]
	Dialysis of one sample drop on-line connected with electrophoresis in short capillary	CE-C ⁴ D	-	100 nL	Separation of model inorganic cations (K ⁺ , Ba ²⁺ and Na ⁺) and organic molecules (creatinine, histidine and arginine). Determination	Dialysis in micro-litre sample volumes into submicro-litre volumes of an acceptor solution in a dialysing fibre	[69, 70]

					of basic amino acids (histidine, lysine and arginine) in a blood serum sample. Rapid determination of majority cations in yoghurts.		
	Moving drop setup with electrokinetic injection	CE-C ⁴ D	-	25 µL	Separation of inorganic cations and anions	Pronounced working volume mismatch	[71]
	Slipchip: two patterned plates are moved to generate droplets	MGE-LIF	-	800 pL	Separation of fluorescent dyes, DNA fragments	Suitable for gel CE, easy to use, sample reloading, parallel analysis	[66]
	Collecting segmented sample separated by IEF with a SlipChip	M IEF	-	50 nL	Separation of five standards proteins: trypsin inhibitor, β-lactoglobulin A, carbonic anhydrase isozyme II, myoglobin, and lectin	Easy to use	[65]

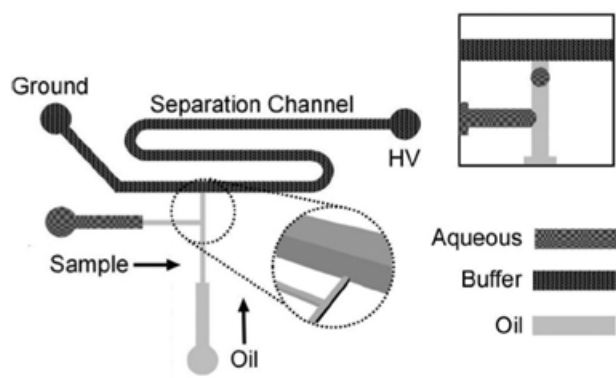
716

717

718 **Figures:**

719

(A)

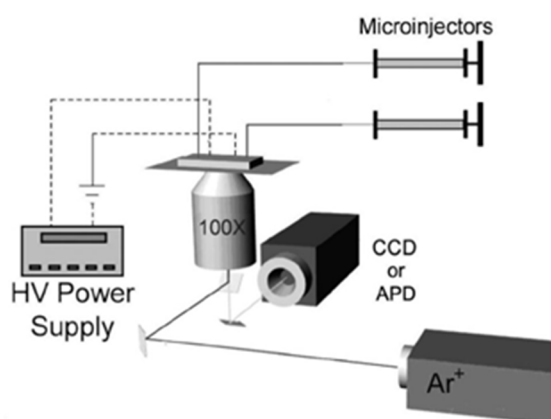


720

721

722

(B)

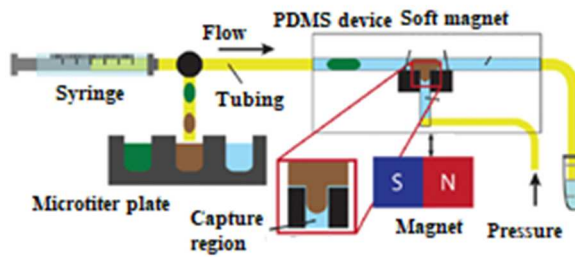


723

724 **Fig. 1:** Schematic showing the first design of droplet-interfaced MCE. (A) The separation
725 channel was $50\ \mu\text{m}$ by $50\ \mu\text{m}$ in cross section; the small T-channel where the sample
726 and oil met had a height of $3\ \mu\text{m}$ and a width of $3\ \mu\text{m}$. The inset highlights the
727 difference in dimension between these two channels. (B) The experiments were
728 performed on an inverted microscope using an Ar^+ laser for exciting fluorescence; a
729 CCD camera was used for wide-field imaging and an avalanche photodiode (APD)
730 for point detection. A set of homebuilt microinjectors and a high-voltage power supply
731 were connected to the microfluidic chip for droplet generation and MCE separation.
732 Reprinted from [30] with permission. Copyright (2006) ACS.

733

(A)



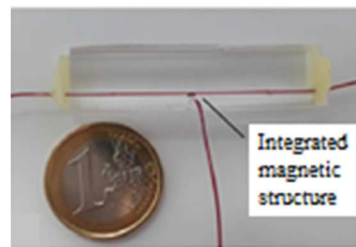
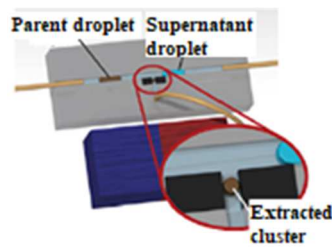
734

735

736

(B)

(C)



737

738 **Fig. 2:** (A) Setup overview of droplet train generator for DNA purification. (B) The particles

739 confined in the parent droplet experience a magnetic force that induces their

740 deflection, extraction and trapping in the capture region (inset). Subsequently, they

741 can be either released in a second flowing droplets or discarded through the

742 secondary channel, according with the desired protocol. (C) Picture of the

743 microfluidic device integrating the micrometric magnetic structures. Red dye is used

744 to underline the channel design. Reprinted from [34] with permission. Copyright

745 (2020) Elsevier

746

747

748

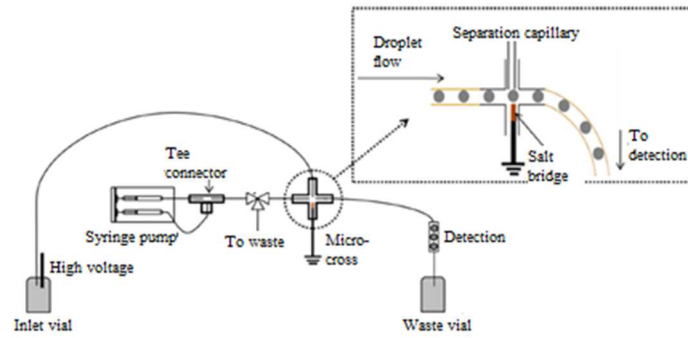
749

750

751

752

(A)



753

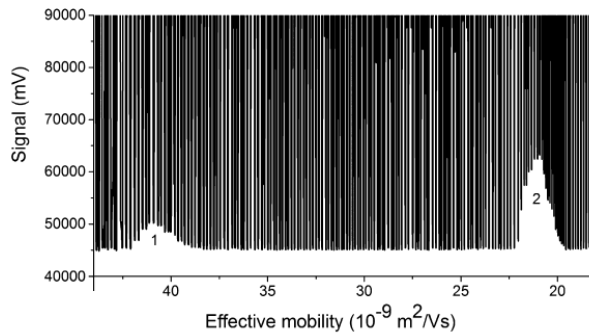
754

755

(B)



(C)



756

757 **Fig. 3:** CE-droplet microfluidics system for post-column detection: (A) schematic outline of
758 the setup used for postcolumn compartmentalization incorporated in a CE instrument.
759 The aqueous phase was segmented by oil in the tee connector (outside CE instrument)
760 and passed the separation capillary outlet to collect the electrophoresed effluent in a
761 compartmentalized manner (within CE instrument). (B) Photograph of the micro cross
762 as the droplet microfluidics interface was positioned in a capillary cassette. Photo
763 label: connection for (1) droplet capillary, (2) separation capillary, (3) detection
764 capillary, and (4) salt bridge electrode. (C) Separation of paralytic shellfish toxins
765 mixture: electropherogram from CZE-droplets microfluidics system demonstrating
766 separation and compartmentalization of electrophoresed analytes into preformed
767 droplets for oxidation. Reprinted from [39] with permission. Copyright (2014) Elsevier.
768

769

(A) Side-on (Previous Work²⁴)		(B) Multi-Layer (New Design)	
Property	Effect	Property	Effect
1. Single-plate droplet actuation configuration	<ul style="list-style-type: none"> ➢ No dispensing from reservoirs or splitting droplets ➢ Large errors caused by pipetting ➢ Evaporation problems 	1. Two-plate droplet actuation configuration	<ul style="list-style-type: none"> ➢ Dispensing from reservoirs and droplet splitting ➢ Pipetting errors made negligible ➢ Evaporation limited
2. PDMS device construction	<ul style="list-style-type: none"> ➢ Easy to fabricate ➢ Undesirable surface properties (i.e., surface adsorption of analytes, solvent incompatibility etc.) 	2. Glass device construction	<ul style="list-style-type: none"> ➢ More difficult to fabricate ➢ Superior material properties (i.e., reduced analyte adsorption, solvent compatible etc.)
3. Shared digital and channel substrate	<ul style="list-style-type: none"> ➢ Limited space for electrodes 	3. Separate digital and channel substrates	<ul style="list-style-type: none"> ➢ Larger space for electrodes

770

771 **Fig. 4:** Comparison of the side-on hybrid microfluidic device configuration and the multilayer

772 hybrid microfluidic device configuration. (A) The side-on configuration comprises a

773 one-plate digital microfluidic device mated to a PDMS microchannel on a common

774 substrate. The design is straightforward to fabricate; however, it suffers from the

775 requirement of dispensing by pipet and material limitations of PDMS. (B) The

776 multilayer device design comprises a DMF array patterned on a top substrate mated

777 to a network of microchannels in a glass substrate below. Although more complex to

778 fabricate, this configuration allows for dispensing droplets from reservoirs and

779 splitting droplets on-chip, and in addition glass is more favorable for microchannel

780 separations. Reprinted from [49] with permission. Copyright (2010) ACS.

781

782

783

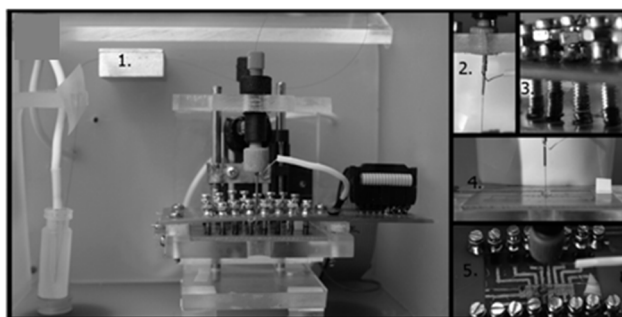
784

785

786

787

(A)

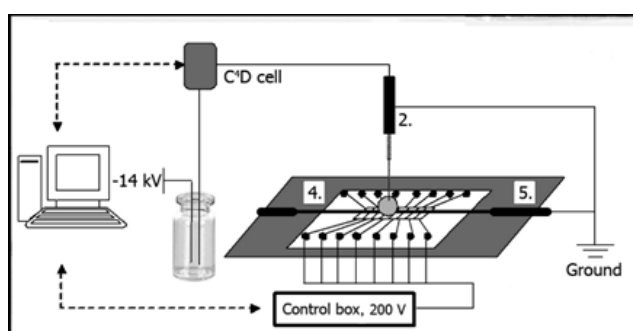


788

789

790

(B)



791

792 **Fig. 5:** *Interfacing the DMF sampler into the portable CE analyzer. (A) Portable CE analyzer*
793 *with DMF sampler. (B) Instrumentation scheme: 1, capacitively coupled contactless*
794 *conductivity detector (C⁴D); 2, grounded piece of syringe needle with the inlet end of*
795 *separation capillary; 3, spring-loaded contact pins; 4, ground electrode during*
796 *droplet actuation; 5, rectangular opening for exposing the electrode array. Reprinted*
797 *from [50] with permission. Copyright (2009) ACS.*

798

799

800

801

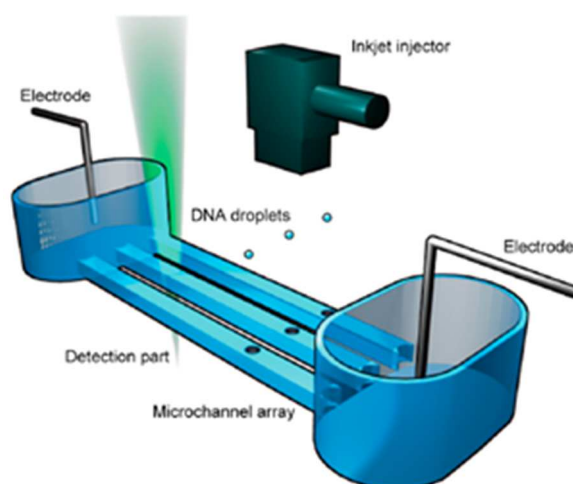
802

803

804

805

(A)



806

807

(B)

(C)

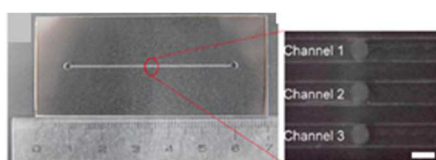
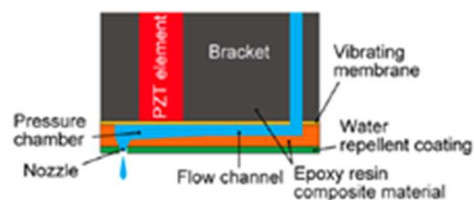


808

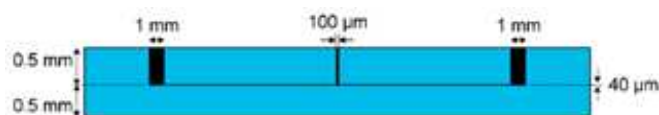
809

(D)

(E)



810

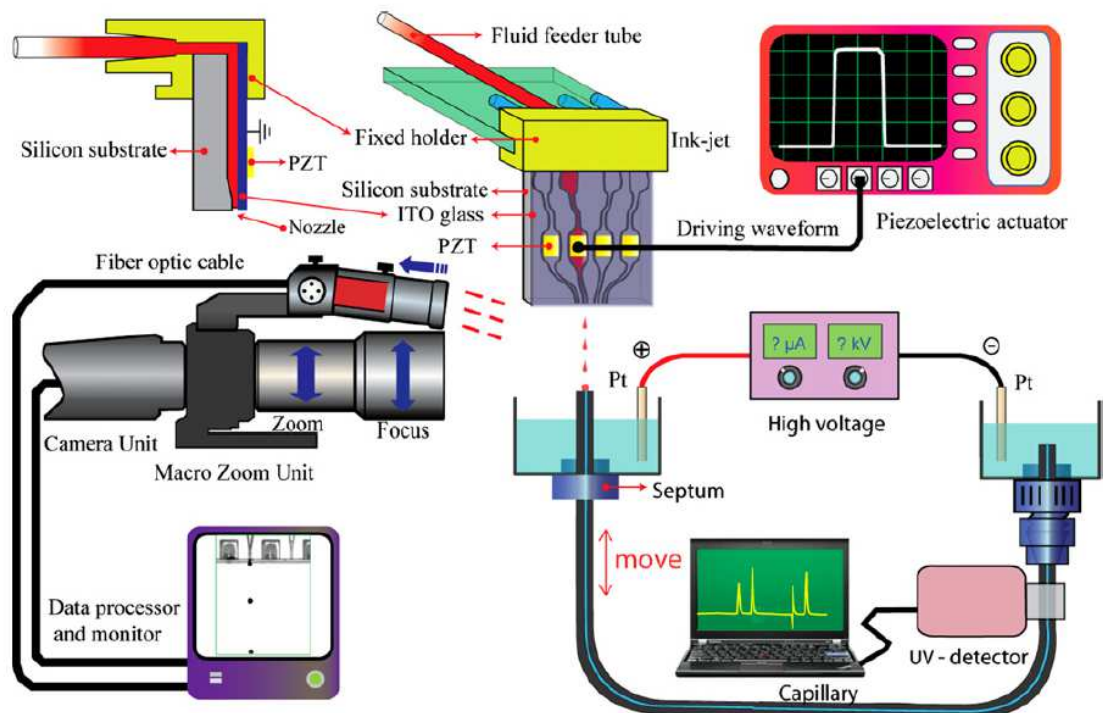


811 **Fig. 6:** (A) Illustration of inkjet injection of DNA droplets for microchannel array
812 electrophoresis. There were two electrodes, a microchannel array, a detection part,
813 and an inkjet injector. (B) Photograph of the PulseInjector with a cartridge. (C)
814 Schematic illustration of the PulseInjector, which is a piezo element-based plastic
815 drop-on-demand type inkjet head. Epoxy resin composite material was used as the
816 structural material; this made it possible to integrate various components, such as a
817 pressure chamber, nozzle with water repellent coating, flow channel, vibrating
818 membrane, bracket, and PZT element into one body, resulting in superior chemical
819 resistance. (D) Photograph of a COC microchip with three microchannels (size: 3 cm
820 \times 7 cm) and magnified image of the injection ports for DNA samples; scale bar, 100
821 μ m. The microchannel width was 100 μ m. (E) Schematic diagram of a cross-sectional
822 view of the COC microchip. The diameters of the reservoirs and injection ports were 1
823 mm and 100 μ m, respectively. The height of the microchannels was 40 μ m.
824 Thicknesses of both the microchannel-patterned and nonpatterned COC substrate
825 were 0.5 mm.. Reprinted from [57] with permission. Copyright (2012) ACS.

826

827

(A)

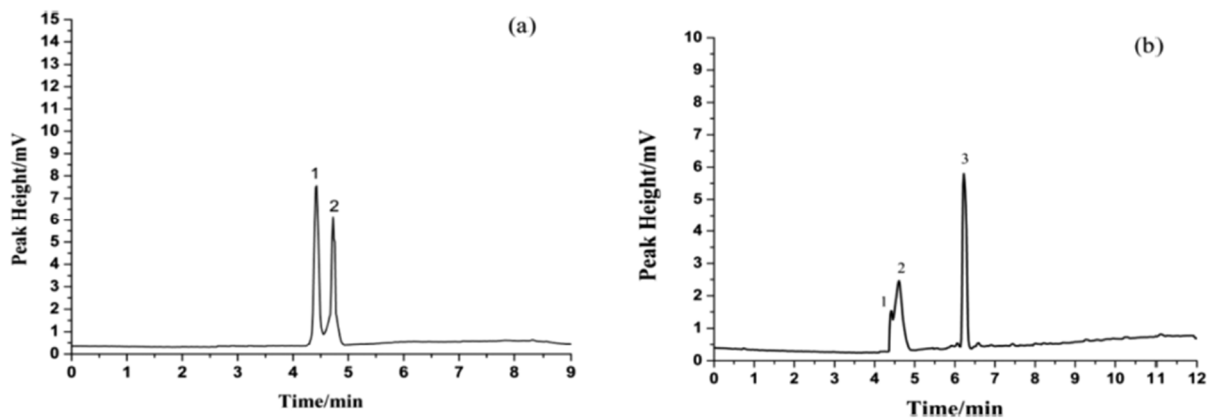


828

829

830

(B)



831

832

833

834

835

836

837

838

839

840

Fig. 7: (A) Schematic illustration of the whole experimental setup. Inkjet printing of droplet generation, high-speed micro-observation system, and capillary electrophoresis system are presented in the figure. Reprinted from [58] with permission. Copyright (2013) Elsevier. (B) Determination of different property of cell by inkjet droplet-interfaced CE: (a) Electropherogram for normal and apoptosis HepG2 cells (Peaks (1) apoptosis cells and (2) normal cells); (b) Electropherogram of a mixture of three kind of cells - (1) Caco-2, (2) HepG2, and (3) HUVEC Cell at the concentration of 1×10^6 cells/mL (200 droplets). Reprinted from [62] with permission. Copyright (2017) ACS.

841 **References:**

- 842 [1] R.K. Harstad, A.C. Johnson, M.M. Weisenberger, M.T. Bowser, Capillary
843 Electrophoresis, *Anal. Chem.*, 88 (2016) 299-319.
- 844 [2] R.L.C. Voeten, I.K. Ventouri, R. Haselberg, G.W. Somsen, Capillary Electrophoresis:
845 Trends and Recent Advances, *Anal. Chem.*, 90 (2018) 1464-1481.
- 846 [3] A. Wuethrich, J.P. Quirino, A decade of microchip electrophoresis for clinical diagnostics
847 - A review of 2008-2017, *Anal. Chim. Acta*, 1045 (2019) 42-66.
- 848 [4] F.A. Hansen, S. Pedersen-Bjergaard, Emerging Extraction Strategies in Analytical
849 Chemistry, *Anal. Chem.*, 92 (2020) 2-15.
- 850 [5] L. Xia, J.N. Yang, R.H. Su, W.J. Zhou, Y.S. Zhang, Y.H. Zhong, S.M. Huang, Y.L. Chen,
851 G.K. Li, Recent Progress in Fast Sample Preparation Techniques, *Anal. Chem.*, 92 (2020)
852 34-48.
- 853 [6] N. Drouin, P. Kuban, S. Rudaz, S. Pedersen-Bjergaard, J. Schappler, Electromembrane
854 extraction: Overview of the last decade, *Trac-Trends Anal. Chem.*, 113 (2019) 357-363.
- 855 [7] P. Kuban, B. Karlberg, Flow/sequential injection sample treatment coupled to capillary
856 electrophoresis. A review, *Anal. Chim. Acta*, 648 (2009) 129-145.
- 857 [8] A. Wuethrich, P.R. Haddad, J.P. Quirino, The electric field - An emerging driver in
858 sample preparation, *Trac-Trends Anal. Chem.*, 80 (2016) 604-611.
- 859 [9] P. Kuban, P. Bocek, Direct coupling of supported liquid membranes to capillary
860 electrophoresis for analysis of complex samples: A tutorial, *Anal. Chim. Acta*, 787
861 (2013) 10-23.
- 862 [10] G. Jarvas, A. Guttman, N. Miekus, T. Baczek, S. Jeong, D.S. Chung, V. Patoprsty, M.
863 Masar, M. Hutta, V. Datinska, F. Foret, Practical sample pretreatment techniques coupled
864 with capillary electrophoresis for real samples in complex matrices, *Trac-Trends Anal.*
865 *Chem.*, 122 (2020).

- 866 [11] L. Pont, R. Pero-Gascon, E. Gimenez, V. Sanz-Nebot, F. Benavente, A critical
867 retrospective and prospective review of designs and materials in in-line solid-phase
868 extraction capillary electrophoresis, *Anal. Chim. Acta*, 1079 (2019) 1-19.
- 869 [12] Z. Dong, Q. Fang, Automated, flexible and versatile manipulation of nanoliter-to-
870 picoliter droplets based on sequential operation droplet array technique, *Trac-Trends*
871 *Anal. Chem.*, 124 (2020) 115812.
- 872 [13] K. Doufène, C. Tourné-Péteilh, P. Etienne, A. Aubert-Pouëssel, *Microfluidic Systems for*
873 *Droplet Generation in Aqueous Continuous Phases: A Focus Review*, *Langmuir*, 35
874 (2019) 12597-12612.
- 875 [14] T.S. Kaminski, O. Scheler, P. Garstecki, Droplet microfluidics for microbiology:
876 techniques, applications and challenges, *Lab Chip*, 16 (2016) 2168-2187.
- 877 [15] M. Serra, D. Ferraro, I. Pereiro, J.-L. Viovy, S. Descroix, The power of solid supports in
878 multiphase and droplet-based microfluidics: towards clinical applications, *Lab Chip*,
879 DOI: 10.1039/C7LC00582B (2017).
- 880 [16] L.Q. Ye, X. Wang, J. Han, F. Gao, L.J. Xu, Z.L. Xiao, P.M. Bai, Q.Q. Wang, B. Zhang,
881 Two dimensional separations of human urinary protein digest using a droplet-interfaced
882 platform, *Anal. Chim. Acta*, 863 (2015) 86-94.
- 883 [17] L. Ranjbar, J.P. Foley, M.C. Breadmore, Multidimensional liquid-phase separations
884 combining both chromatography and electrophoresis - A review, *Anal. Chim. Acta*, 950
885 (2017) 7-31.
- 886 [18] D.T. Chiu, Interfacing droplet microfluidics with chemical separation for cellular
887 analysis, *Anal. Bioanal. Chem.*, 397 (2010) 3179-3183.
- 888 [19] E.Y. Basova, F. Foret, Droplet microfluidics in (bio)chemical analysis, *Analyst*, 140
889 (2015) 22-38.

- 890 [20] Z.L. Xiao, M.L. Niu, B. Zhang, Droplet microfluidics based microseparation systems, *J.*
891 *Sep. Sci.*, 35 (2012) 1284-1293.
- 892 [21] H. Sammerul, Z. Xunli, N. Xize, Droplet-Interfaced Separations as an Emerging Tool for
893 High-Throughput Microchip Electrophoresis, *RMES*, 8 (2019) 845-847.
- 894 [22] M. Wang, G.T. Roman, M.L. Perry, R.T. Kennedy, Microfluidic Chip for High
895 Efficiency Electrophoretic Analysis of Segmented Flow from a Microdialysis Probe and
896 in Vivo Chemical Monitoring, *Anal. Chem.*, 81 (2009) 9072-9078.
- 897 [23] X.Z. Niu, B. Zhang, R.T. Marszalek, O. Ces, J.B. Edel, D.R. Klug, A.J. Demello,
898 Droplet-based compartmentalization of chemically separated components in two-
899 dimensional separations, *Chem. Comm.*, (2009) 6159-6161.
- 900 [24] G.T. Roman, M. Wang, K.N. Shultz, C. Jennings, R.T. Kennedy, Sampling and
901 Electrophoretic Analysis of Segmented Flow Streams Using Virtual Walls in a
902 Microfluidic Device, *Anal. Chem.*, 80 (2008) 8231-8238.
- 903 [25] C.M. Ouimet, C.I. D'Amico, R.T. Kennedy, Droplet sample introduction to microchip
904 gel and zone electrophoresis for rapid analysis of protein-protein complexes and
905 enzymatic reactions, *Anal. Bioanal. Chem.*, 411 (2019) 6155-6163.
- 906 [26] W. Zhang, N. Li, L. Lin, Q. Huang, K. Uchiyama, J.-M. Lin, Concentrating Single Cells
907 in Picoliter Droplets for Phospholipid Profiling on a Microfluidic System, *Small*, 16
908 (2020) 1903402.
- 909 [27] E.D. Guetschow, D.J. Steyer, R.T. Kennedy, Subsecond Electrophoretic Separations
910 from Droplet Samples for Screening of Enzyme Modulators, *Anal. Chem.*, 86 (2014)
911 10373-10379.
- 912 [28] X. Niu, F. Pereira, J.B. Edel, A.J. de Mello, Droplet-Interfaced Microchip and Capillary
913 Electrophoretic Separations, *Anal. Chem.*, 85 (2013) 8654-8660.

- 914 [29] Y. Zheng, Z. Wu, M. Khan, S. Mao, K. Manibalan, N. Li, J.-M. Lin, L. Lin,
915 Multifunctional Regulation of 3D Cell-Laden Microsphere Culture on an Integrated
916 Microfluidic Device, *Anal. Chem.*, 91 (2019) 12283-12289.
- 917 [30] J.S. Edgar, C.P. Pabbati, R.M. Lorenz, M.Y. He, G.S. Fiorini, D.T. Chiu, Capillary
918 electrophoresis separation in the presence of an immiscible boundary for droplet analysis,
919 *Anal. Chem.*, 78 (2006) 6948-6954.
- 920 [31] J. Pei, J. Nie, R.T. Kennedy, Parallel Electrophoretic Analysis of Segmented Samples On
921 Chip for High-Throughput Determination of Enzyme Activities, *Anal. Chem.*, 82 (2010)
922 9261-9267.
- 923 [32] E.D. Guetschow, S. Kumar, D.B. Lombard, R.T. Kennedy, Identification of sirtuin 5
924 inhibitors by ultrafast microchip electrophoresis using nanoliter volume samples, *Anal.*
925 *Bioanal. Chem.*, 408 (2016) 721-731.
- 926 [33] H.H. Quan, M. Li, Y. Huang, J.H. Hahn, A hydrophobic ionic liquid compartmentalized
927 sampling/labeling and its separation techniques in polydimethylsiloxane microchip
928 capillary electrophoresis, *Electrophoresis*, 38 (2017) 372-379.
- 929 [34] M. Serra, T.D. Mai, A.L. Serra, M.C. Nguyen, A. Eisele, L. Perie, J.L. Viovy, D. Ferraro,
930 S. Descroix, Integrated droplet microfluidic device for magnetic particles handling:
931 Application to DNA size selection in NGS libraries preparation, *Sens. Actuators B*, 305
932 (2020).
- 933 [35] M.F. DeLaMarre, S.A. Shippy, Development of a Simplified Microfluidic Injector for
934 Analysis of Droplet Content via Capillary Electrophoresis, *Anal. Chem.*, 86 (2014)
935 10193-10200.
- 936 [36] Q. Li, Y. Zhu, N.Q. Zhang, Q. Fang, Automatic Combination of Microfluidic Nanoliter-
937 Scale Droplet Array with High-Speed Capillary Electrophoresis, *Sci. Rep.*, 6 (2016).

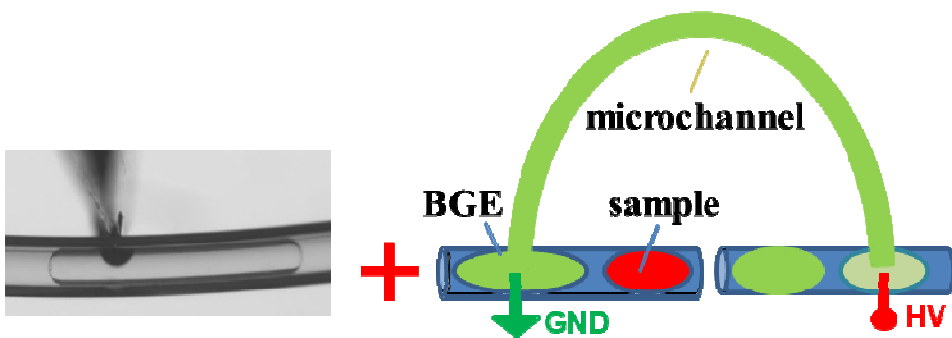
- 938 [37] Y.M. Feng, T.T. Hu, P. Fang, L.L. Zhou, W.M. Li, Q. Fang, J. Fang, Consecutive and
939 automatic detection of multi-gene mutations from colorectal cancer samples by coupling
940 droplet array-based capillary electrophoresis and PCR-RFLP, *Anal. Bioanal. Chem.*,
941 <https://doi.org/10.1007/s00216-020-02567-y> (2020).
- 942 [38] T. Zhang, Q. Fang, W.-B. Du, J.-L. Fu, Microfluidic Picoliter-Scale Translational
943 Spontaneous Sample Introduction for High-Speed Capillary Electrophoresis, *Anal.*
944 *Chem.*, 81 (2009) 3693-3698.
- 945 [39] A.S. Abdul Keyon, R.M. Guijt, C.J. Bolch, M.C. Breadmore, Droplet Microfluidics for
946 Postcolumn Reactions in Capillary Electrophoresis, *Anal. Chem.*, 86 (2014) 11811-
947 11818.
- 948 [40] A.S.A. Keyon, R.M. Guijt, A. Gaspar, A.A. Kazarian, P.N. Nesterenko, C.J. Bolch, M.C.
949 Breadmore, Capillary electrophoresis for the analysis of paralytic shellfish poisoning
950 toxins in shellfish: Comparison of detection methods, *Electrophoresis*, 35 (2014) 1496-
951 1503.
- 952 [41] T.D. Mai, D. Ferraro, N. Aboud, R. Renault, M. Serra, N.T. Tran, J.-L. Viovy, C.
953 Smadja, S. Descroix, M. Taverna, Single-step immunoassays and microfluidic droplet
954 operation: Towards a versatile approach for detection of amyloid- β peptide-based
955 biomarkers of Alzheimer's disease, *Sens. Actuators B*, 255 (2018) 2126-2135.
- 956 [42] D. Ferraro, M. Serra, D. Filippi, L. Zago, E. Guglielmin, M. Pierno, S. Descroix, J.L.
957 Viovy, G. Mistura, Controlling the distance of highly confined droplets in a capillary by
958 interfacial tension for merging on-demand, *Lab Chip*, 19 (2019) 136-146.
- 959 [43] M. Jeyhani, R. Thevakumaran, N. Abbasi, D.K. Hwang, S.S.H. Tsai, Microfluidic
960 Generation of All-Aqueous Double and Triple Emulsions, *Small*, 16 (2020).

- 961 [44] C. Sung Kwon, M. Hyejin, K. Chang-Jin, Creating, transporting, cutting, and merging
962 liquid droplets by electrowetting-based actuation for digital microfluidic circuits, *J*
963 *Microelectromech. Syst.*, 12 (2003) 70-80.
- 964 [45] M.J. Jebrail, M.S. Bartsch, K.D. Patel, Digital microfluidics: a versatile tool for
965 applications in chemistry, biology and medicine, *Lab Chip*, 12 (2012) 2452-2463.
- 966 [46] E. Samiei, M. Tabrizian, M. Hoorfar, A review of digital microfluidics as portable
967 platforms for lab-on a-chip applications, *Lab Chip*, 16 (2016) 2376-2396.
- 968 [47] D.J. Im, B.S. Yoo, M.M. Ahn, D. Moon, I.S. Kang, Digital Electrophoresis of Charged
969 Droplets, *Anal. Chem.*, 85 (2013) 4038-4044.
- 970 [48] M. Abdelgawad, M.W.L. Watson, A.R. Wheeler, Hybrid microfluidics: A digital-to-
971 channel interface for in-line sample processing and chemical separations, *Lab Chip*, 9
972 (2009) 1046-1051.
- 973 [49] M.W.L. Watson, M.J. Jebrail, A.R. Wheeler, Multilayer Hybrid Microfluidics: A Digital-
974 to-Channel Interface for Sample Processing and Separations, *Anal. Chem.*, 82 (2010)
975 6680-6686.
- 976 [50] J. Gorbatoeva, M. Jaanus, M. Kaljurand, Digital Microfluidic Sampler for a Portable
977 Capillary Electropherograph, *Anal. Chem.*, 81 (2009) 8590-8595.
- 978 [51] J. Gorbatoeva, M. Jaanus, M. Vaheer, M. Kaljurand, Digital microfluidics platform for
979 interfacing solid-liquid extraction column with portable capillary electropherograph for
980 analysis of soil amino acids, *Electrophoresis*, 37 (2016) 472-475.
- 981 [52] J. Gorbatoeva, M. Borissova, M. Kaljurand, Electrowetting-on-dielectric actuation of
982 droplets with capillary electrophoretic zones for off-line mass spectrometric analysis, *J.*
983 *Chromatogr. A*, 1234 (2012) 9-15.

- 984 [53] J. Gorbatoeva, M. Borissova, M. Kaljurand, Electrowetting on dielectric actuation of
985 droplets with capillary electrophoretic zones for MALDI mass spectrometric analysis,
986 *Electrophoresis*, 33 (2012) 2682-2688.
- 987 [54] N. Thaitrong, H. Kim, R.F. Renzi, M.S. Bartsch, R.J. Meagher, K.D. Patel, Quality
988 control of next-generation sequencing library through an integrative digital microfluidic
989 platform, *Electrophoresis*, 33 (2012) 3506-3513.
- 990 [55] R.D. Sochol, E. Sweet, C.C. Glick, S.Y. Wu, C. Yang, M. Restaino, L.W. Lin, 3D
991 printed microfluidics and microelectronics, *Microelectron. Eng.*, 189 (2018) 52-68.
- 992 [56] K. Li, J.K. Liu, W.S. Chen, L. Zhang, Controllable printing droplets on demand by
993 piezoelectric inkjet: applications and methods, *Microsyst. Technol.*, 24 (2018) 879-889.
- 994 [57] T. Yasui, Y. Inoue, T. Naito, Y. Okamoto, N. Kaji, M. Tokeshi, Y. Baba, Inkjet Injection
995 of DNA Droplets for Microchannel Array Electrophoresis, *Anal. Chem.*, 84 (2012) 9282-
996 9286.
- 997 [58] F. Chen, Y. Zhang, Y. Nakagawa, H. Zeng, C. Luo, H. Nakajima, K. Uchiyama, J.-M.
998 Lin, A piezoelectric drop-on-demand generator for accurate samples in capillary
999 electrophoresis, *Talanta*, 107 (2013) 111-117.
- 1000 [59] F.M. Chen, Y. Rang, Y. Weng, L.Y. Lin, H.L. Zeng, H. Nakajim, J.M. Lin, K.
1001 Uchiyama, Drop-by-drop chemical reaction and sample introduction for capillary
1002 electrophoresis, *Analyst*, 140 (2015) 3953-3959.
- 1003 [60] Y. Rang, H.L. Zeng, H. Nakajima, S. Kato, K. Uchiyama, Quantitative on-line
1004 concentration for capillary electrophoresis with inkjet sample introduction technique, *J.*
1005 *Sep. Sci.*, 38 (2015) 2722-2728.
- 1006 [61] W. Zhang, S. Mao, J. Yang, H. Zeng, H. Nakajima, S. Kato, K. Uchiyama, The use of an
1007 inkjet injection technique in immunoassays by quantitative on-line electrophoretically
1008 mediated microanalysis, *J. Chromatogr. A*, 1477 (2016) 127-131.

- 1009 [62] W.F. Zhang, N. Li, H.L. Zeng, H. Nakajima, J.M. Lin, K. Uchiyama, Inkjet Printing
1010 Based Separation of Mammalian Cells by Capillary Electrophoresis, *Anal. Chem.*, 89
1011 (2017) 8674-8677.
- 1012 [63] S. Kaneda, K. Ono, T. Fukuba, T. Nojima, T. Yamamoto, T. Fujii, Pneumatic handling of
1013 droplets on-demand on a microfluidic device for seamless processing of reaction and
1014 electrophoretic separation, *Electrophoresis*, 31 (2010) 3719-3726.
- 1015 [64] W. Du, L. Li, K.P. Nichols, R.F. Ismagilov, SlipChip, *Lab Chip*, 9 (2009) 2286-2292.
- 1016 [65] Y. Zhao, F. Pereira, A.J. deMello, H. Morgan, X.Z. Niu, Droplet-based in situ
1017 compartmentalization of chemically separated components after isoelectric focusing in a
1018 Slipchip, *Lab Chip*, 14 (2014) 555-561.
- 1019 [66] S.-u. Hassan, H. Morgan, X. Zhang, X. Niu, Droplet Interfaced Parallel and Quantitative
1020 Microfluidic-Based Separations, *Anal. Chem.*, 87 (2015) 3895-3901.
- 1021 [67] F. Opekar, P. Tůma, Direct sample injection from a syringe needle into a separation
1022 capillary, *Anal. Chim. Acta*, 1042 (2018) 133-140.
- 1023 [68] F. Opekar, P. Tuma, An air-assisted flow-gating interface for capillary electrophoresis,
1024 *Electrophoresis*, 40 (2019) 587-590.
- 1025 [69] F. Opekar, J. Hraníček, P. Tůma, Rapid determination of majority cations in yoghurts
1026 using on-line connection of capillary electrophoresis with mini-dialysis, *Food Chem.*, 308
1027 (2020) 125647.
- 1028 [70] F. Opekar, P. Tůma, Dialysis of one sample drop on-line connected with electrophoresis
1029 in short capillary, *Talanta*, 219 (2020) 121252.
- 1030 [71] K. Ngamakarn, N. Pungwiwat, S. Wangkarn, K. Grudpan, T. Kanyanee, Liquid handling
1031 employing a moving drop for electrokinetic sample introduction system for capillary zone
1032 electrophoresis, *Talanta*, <https://doi.org/10.1016/j.talanta.2020.121118> (2020) 121118.

- 1033 [72] P. Kuban, F. Foret, G. Erny, Open source capillary electrophoresis, *Electrophoresis*, 40
1034 (2019) 65-78.
- 1035 [73] T. Liénard-Mayor, J.S. Furter, M. Taverna, H.V. Pham, P.C. Hauser, T.D. Mai, Modular
1036 instrumentation for capillary electrophoresis with laser induced fluorescence detection
1037 using plug-and-play microfluidic, electrophoretic and optic modules, *Anal. Chim. Acta*,
1038 (2020) in press.
- 1039



Droplet-interfaced Microscale Electrophoresis

Graphical abstract

II.3. Microfluidics for glycan analysis and sample treatment

As was shown in chapter I, the analysis of intact glycans requires preparation step to release the glycan from the glycoprotein, notably denaturation of target glycoproteins, release of glycans via chemical or enzymatical approaches and sometimes labeling of released glycans and / or protection of the terminal sialic acids. Microfluidic systems for the sample preparation and/or separation of glycans have already been proposed as an interesting alternative to the established ones (see chapter I) and are reviewed in this dedicated section.

II.3.1. Non-droplet microfluidic systems for HPLC, MS and MCE analysis of glycans

A commercial system was created by Perkin Elmer for the rapid analysis of N-glycans from recombinant monoclonal antibodies [261]. As seen in *Figure 34 A*), reagents for the denaturation, PNGase F digestion and labeling are pre-loaded onto separate 96-well plates. Glycans samples can be added on the denaturation plate and sequentially transferred to the other plates, all of which can be automated with a pipetting robot. Once the labeling is finished the 96-well plate can be loaded along with the microfluidic chip inside the LabChip GXII Touch© for automatic CE-LiF separation of the glycan samples in ~45 seconds. This method allowed the automatic separation and analysis of the 5 main glycan peaks from IgG with an RSD below 4%. In this case the price to pay for speed was the removal of two “classical” steps of glycan sample treatment: the removal of the cleaved glycoprotein after enzymatic digestion and the removal of the excess labeling reagent after the labeling step. Furthermore, only 5 peaks of IgG could be identified with this method (usually 8 mains peaks are identified) and their relative abundance was quite different than what can be found in the literature [202, 262, 263].

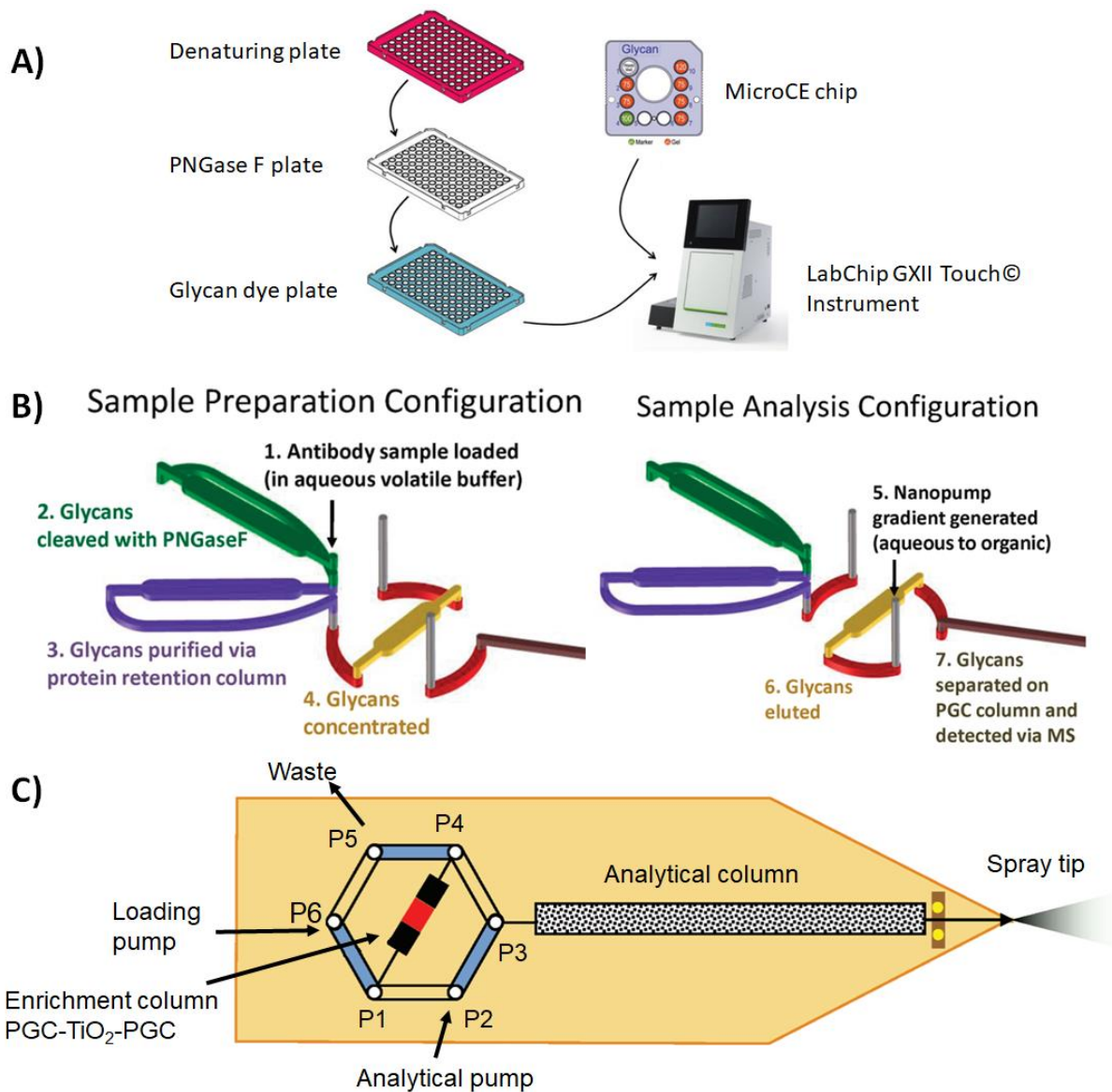


Figure 34: Integrated systems for sample treatment, separation and analysis of glycans: A) Commercial system from Perkin Elmer consisting of preloaded 96-well plates and MicroCE chip from LabChip GXII Touch© instrument, B) 3-layer microfluidic chip for the integrated sample preparation and separation by HPLC/MS and C) Sandwich column chip. Adapted from [261], [264] and [265] respectively.

Another commercial solution is proposed by Agilent: the 1200 series Infinity HPLC/MS© instrument equipped with the ChipCube© interface from Agilent Technologies has become very popular with glycan and intact glycoprotein analysis. A microfluidic chip composed of enrichment and analytical columns, injection channel and electrospray tip is placed in the ChipCube© interface. Glycans from serum [266-268] or milk [269] are usually processed off-chip by PNGase F and solid-phase extraction. More information on this chip can be found in the reference [270]. In an effort to upgrade their system specifically for glycan processing, researchers from Agilent published a 3-layer microfluidic chip for integrated digestion by PNGase F, purification by a C8 bead-packed channel and enrichment on the 1200 series Infinity HPLC/MS© chip [264]. Their idea was to stack three different chips on top of each

other and connect them to a stator-rotor for HPLC manipulations as seen in [Figure 34 B](#)). The glycoprotein sample is first injected into the enzymatic digestion chip (in green), which is reactor chamber packed with PNGase F immobilized on silica beads. After digestion both the released glycans and the deglycosylated protein are brought to the purification layer (in purple), which is a channel packed with 5 μm reverse phase C8 beads to trap the proteins. Finally, the last layer is a commercially available chip which contains 3 elements: an enrichment PGC column/channel (in yellow) to trap the glycans, which can then be eluted in the sample analysis configuration, an HPLC column/channel (in brown) packed with PGC material to separate the glycans and an on-chip nanoESI sprayer for detection of the glycan by MS. For the stacking, alignment and sealing of the 3 layers, an Agilent HPLC ChipCube © was used to sandwich the 3 layers between the top stator and the bottom rotor. This method could be performed in 10 minutes from glycoprotein injection to glycan data, which is a tremendous improvement over the 1-3 days sometimes required for glycan sample preparation prior to MS. The middle layer can also be removed for the analysis of the deglycosylated glycoprotein. Although a very powerful approach, the construction of this 3-layer chip is quite challenging. Generally speaking, it is simpler to construct a chip in a single layer, because it removes the necessity to align them and to make sure the connections are secured. In the case of this system, having it in 3 layer is more suited for method development because it is easier to change one layer than the whole chip. Still, the construction of the digestion channel requires several steps and more than one day of incubation while the process of slurry packing the C8 beads into the purification channel also requires several steps as mentioned in the previous subchapter. Besides the limited lifetime of the chip (about 250 injections), the need to store it at 4°C between experiments and the necessity to work with specific MS instruments render this option to be very cost-efficient. Also, the glycans analyzed with this approach do not have any terminal sialic acid, which usually must be protected during MS detection and thus would require an additional preparation step [271].

Wang et.al. [10] also utilize the same commercial chip from Agilent coupled to the ChipCube based on a design proposed previously [265]. As seen in [Figure 34 C](#)), instead of using a simple PGC column for enrichment as in the previous system, the enrichment column in this case is a of a column made of TiO_2 sandwiched between two PGC columns. The idea in this case is to separate and enrich the negatively charged glycans as TiO_2 has a high affinity for negatively charged molecules. When the sample goes through the sandwich column, all glycans are first retained on the first PGC column. By using a linear gradient $\text{H}_2\text{O}/\text{ACN}$ as mobile phase, the neutral glycans are eluted from the PGC, then go through the TiO_2 column and the second PGC column and finally reach the analytical column. Meanwhile the negatively charged glycans are retained and enriched on the TiO_2 column. By flowing a plug of NH_3 elution buffer, the acidic glycans can then be eluted from the TiO_2 column and retained on the second PGC column, and subsequently transferred to the analytical column by gradient elution. Contrary to the previous system, the whole glycan processing is performed off chip and only the 2-step separation is performed on-chip, although by coupling the previous system to this one, one could imagine that everything could be performed on-line. The specific enrichment of charged glycan allowed the discovery of 20 sulfated and 4 acetylated glycans from IgG. This

approach was used to find glycans biomarkers for rheumatoid arthritis and the authors showcased that this powerful approach could be used to find new glycan biomarkers for auto-immune and infectious diseases.

Instead of stacking layers of chip, Wu et.al. proposed to connect [272] in series the components needed for analysis of glycans by HPLC. For the enzymatic release of the glycans, they use a technology called immobilized enzyme reactor (IMER). IMER consists in modifying the surface of channel by using a polymer scaffold such as poly(glycidyl methacrylate-co-ethylene dimethacrylate) or poly(butyl methacrylate-co-ethylene dimethacrylate) and to graft to it a reactant of interest (in this case PNGase F) [273, 274]. As a solution containing glycoprotein passes through a capillary modified with an IMER, glycoprotein interact with the immobilized enzymes and glycans are cleaved. As seen in *Figure 35*, the glycoprotein samples are first flown inside an (IMER) of PNGase F for 10 min at room temperature in order to digest them. In order to label the released glycans by 6-Aminoquinolyl-N-hydroxysuccinimidyl carbamate (AQC), the released glycans were co-injected at the same flowrate with AQC into a first chip and mixed using a simple curved channel (Chip 1). 10 minutes of reaction time was enough to obtain 90 % labeling efficiently of both neutral and sialylated glycans. As they showed on a previous work [275], it is only necessary to remove the excess deglycosylated glycoprotein to detect AQC-glycans by HPLC with fluorescent detection. For this purpose, the second chip (Chip 2) was added on-line: the deglycosylated glycoproteins will remain on the C18 particles when flushed while the glycans will remain in the liquid due to their strong hydrophilicity. Glycans from RNase B, chicken ovalbumin, transferrin and whole human serum were released and analysed to showcase that all types of glycans (high-mannose, complex and hybrids) are compatible with this method. The whole sample preparation process can be performed in 30 minutes and presents good repeatability, reproducibility and stability while necessitating user intervention only to load the sample and to collect it for offline HPLC. Compared to the previous system, this system is more flexible because it is easier to work on each component (IMER, Chip 1 or Chip 2) and to reconnect them. Of course, one drawback of not stacking the components is that the physical footprint of the system is likely to be bigger.

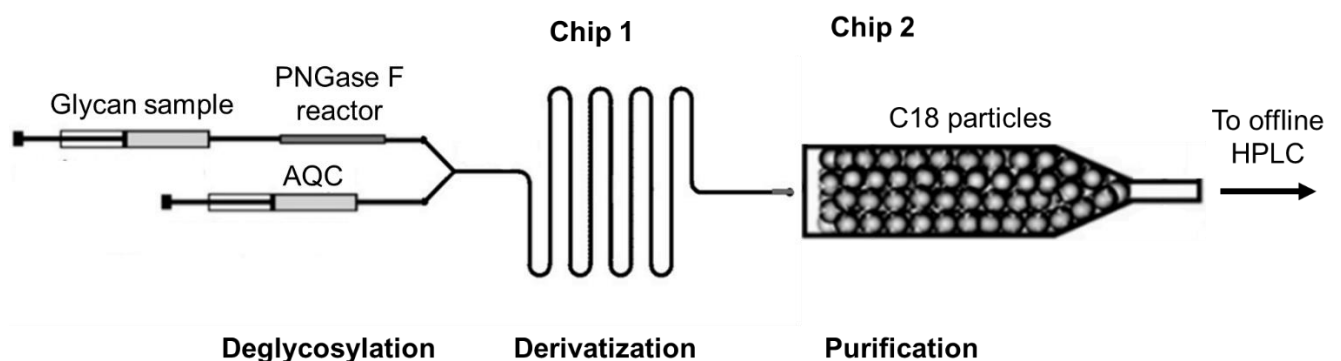


Figure 35 : Online sample preparation for HPLC-FLD analysis of glycans. Adapted from [272].

Yang et.al. [271] presented a microfluidic system based on glycoprotein immobilization for glycan extraction coupled with LC. The system is made of 2 different segments defined by 3 inlets A, B and C as seen in *Figure 36 A*). The first segment A-B is a channel packed with

AminoLink beads, while the second segment A-C is packed with porous graphitized carbons (PGC) grafted on AminoLink beads. The two channels are linked by a constrained channel, which has a decreasing height to prevent AminoLink beads to go inside the separation channel. First, the inlet C is capped, and the glycoprotein sample is injected from B as in [Figure 36 B](#)). During a 2h incubation, the glycoprotein conjugate with the AminoLink beads and are immobilized on them. Once immobilized, the glycoproteins were reduced by NaCNBH_3 in PBS for 2h. An optional step can be performed to protect the sialic acids through an infusion of *p*-toluidine solution followed by a 4h incubation. After a washing, PNGase in solution is infused in the channel followed by a 2h incubation at 37°C. After release, the glycans are enriched at the interface between A-B and A-C by flushing 0.1% formic acid. Then, as in [Figure 36 C](#)), the B port is capped and an eluate consisting of 0.1% of formic acid in 0 to 80% of acetonitrile (the rest being HPLC grade water) is used to separate the released glycans on the PGC beads. After separation the fractions are collected through the port C and analysed offline by MALDI-TOF.

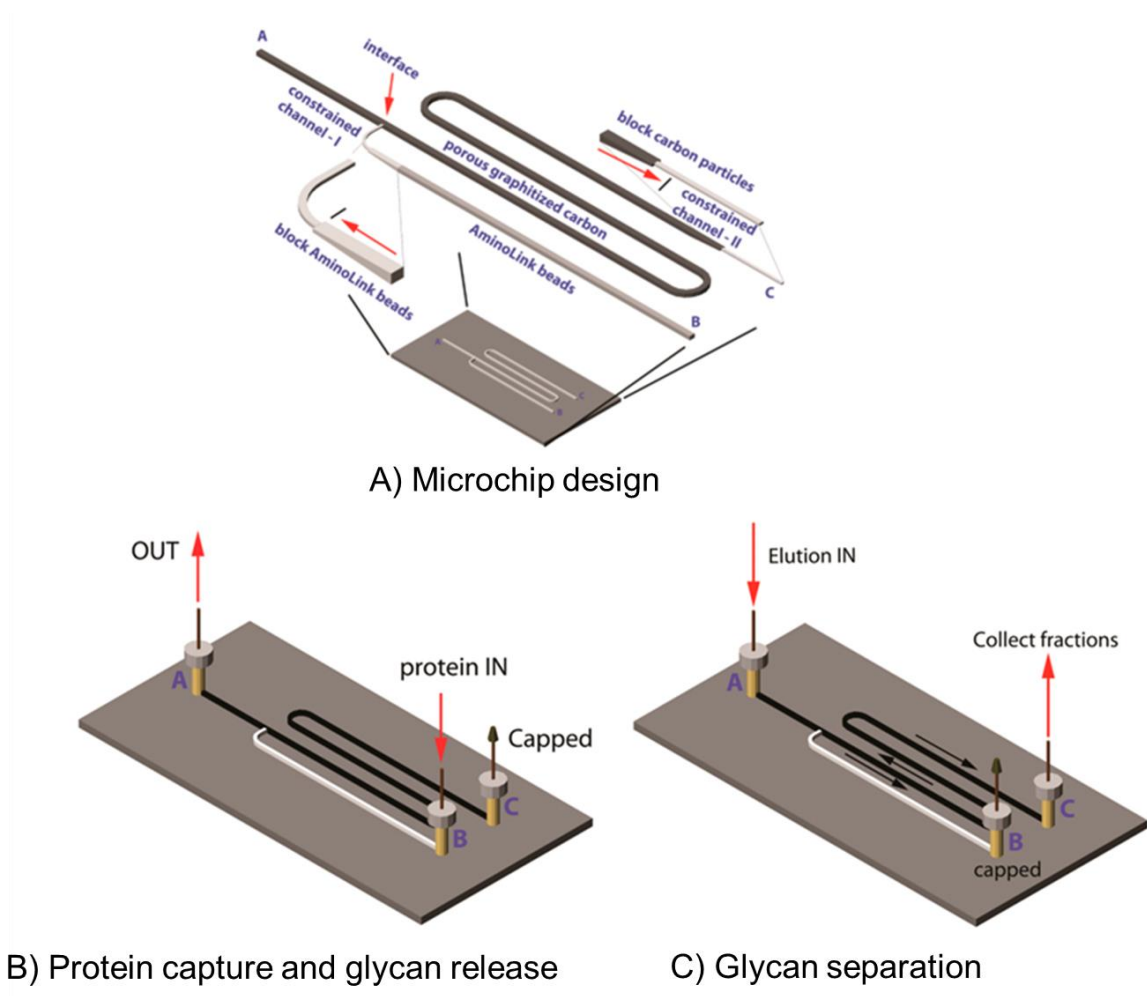


Figure 36 : Preparation and separation of glycan by glycoprotein immobilization: A) design of the chip, B) operation of the chip during glycoprotein capture and glycan release and C) operation of the chip during glycan separation prior to fraction collection. Adapted from [271].

This system was able to identify 148 N-glycan structures inside sample of human serum, although isomers could not be separated and would require further analysis by permethylation of the glycan and tandem MS. The addition of the permethylation step would further increase the total time required for glycan processing which already 8 hours long. This technique is thus powerful but not suited for high-throughput studies.

Table 4 : Summary of the main strategies using microfluidics for glycan processing.

Method/strategy	Advantages	Limits	Throughput	Reference
LabChip GXII Touch Microchip-CE Platform from Perkin Elmer	Automated with a pipetting robot, fast separation	Only 5 peaks IgG are detected instead of 8 usually, relative abundance different, no washing steps	45s for a separation, <4h for processing	[261]
1200 series Infinity HPLC/MS [©] with ChipCube [©] interface from Agilent Technologies	Contains sample enrichment column, HPLC column and MS interface with minimal dead volumes and dispersion	Offline glycan processing	ND	[266-269]
3-layer microfluidic chip for digestion, purification and enrichment on the 1200 series Infinity HPLC/MS [©] chip from Agilent	Ultra-fast, suited for method development	Complex microfabrication and alignment, limited lifetime, only works with specific MS instruments	10 min from sample to data	[264]
Enrichment column composed of TiO ₂ sandwiched between 2 PGC columns	Specific enrichment of negatively charged glycans, discovery of specific glycans	Processing offline	ND	[10]
Processing in series using PNGase F IMER	Robust method, little user intervention, flexible	Offline HPLC, physical footprint of the system bigger	30 min for processing	[272]
Glycoprotein immobilization for glycan extraction coupled with LC	Detection of low abundance glycans	Not suitable for high throughput, no isomer separation	8h from sample to data	[271]

II.3.2. Droplet microfluidic systems for glycan sample treatment analysis: high potential to be exploited

Although some microfluidics solutions have been proposed for the different steps required for glycan analysis for MS, HPLC and microchip CE, there has been no microfluidic system for forefront glycan sample treatment for CE-LIF analysis. The forefront sample treatment prior to the CE-LIF profiling of glycans is of extreme importance and may have a crucial impact on the glycan separation efficiency and reproducibility. Interestingly, while microfluidics-based sample handling was developed for deglycosylation prior to HPLC separation and/or MS detection of released glycans (see chapter above), this miniature approach has never been reported for forefront sample processing for downstream CE-LIF of glycans, to the best of our knowledge. Indeed, glycan sample treatment for CE-LIF requires several steps other than deglycosylation that involve advanced functions (e.g., heating and mixing with organic solvents), which can hardly be down-scaled without any risk of cross contamination between steps. This may be a reason for this delay of development despite the high potential of microfluidics. From our viewpoint, recourse to droplet microfluidics, could be a solution to overcome such challenge. There has been nevertheless no reported work so far on droplet microfluidics for glycan sample treatment and analysis, to the best of our knowledge. As we presented in Chapter II.1.2, several operations can be performed using droplet microfluidics: merging, splitting or sorting for example. One element that was missing from this arsenal of tools was the possibility to purify or extract molecules of interest from complex matrix. Magnetic beads, in a related context, can be used as a controllable carrier to transport target molecules from one droplet to another. In this section, we put our focus on the marriage between microfluidic droplets and magnetic bead manipulations and discuss its potential for glycan sample treatment and analysis.

In macroscopic systems, magnetic beads have become popular as solid phase extraction support as was showcased in Chapter I.IV for the extraction and purification of glycans from complex samples. There are two main reasons for the popularity of suspending magnetic particles as a solid support [276]. First, their surface can be modified with a wide array of surface chemistry, meaning magnetic beads are versatile in terms of aggregation and adsorption. Second, as beads have a micrometric or nanometric size, they have a surface/volume ratio, meaning more groups can be grafted per surface unit and thus an improved capture of analytes.

Due to these features, magnetic beads as solid-state support has gained a central role in bioanalytical methods as numerous methods were adapted in a magnetic bead format and more assays are being adapted [277, 278]. In these methods, magnetic beads coated with specific ligands are suspended in a sample and bind with the molecules of interest. As an example, with glycans, using COOH-coated beads in the presence of ~90% acetonitrile, released glycans will jam on the beads. By placing a magnet near the wall of the tube, magnetic beads can be maintained inside the tube while the supernatant is being pipetted out. In the case of droplet microfluidics, the transfer of magnetic beads between two aqueous droplets suspended in oil was first introduced by Shikidia et.al. [279]. In a very simple system composed of a glass plate covered in silicone oil, one aqueous droplet is separated from

another containing magnetic beads by a glass “gate”. By moving a magnet at the bottom of the glass plate, the beads can be moved from one droplet to the other. This system was limited because it has no flow manipulation, meaning it cannot be used in combination with other droplet microfluidic operations. The manipulation of magnetic beads in a pressure driven flow is more challenging but also more interesting since it can enable the integration of extraction steps in droplet-based protocols. It was first showcased in the same year by two different groups by suspending magnetic beads inside a droplet, then bringing this droplet to a T-junction where the droplet will split in two because the hydrodynamic resistance is equal on both channels [280, 281]. By placing a magnet close to one channel, the beads can be selectively transferred to one droplet which has half the volume of the original one. Although the throughput of such method is good (~tens of droplets per second), the purification rate is limited since only half of the droplet volume is removed. To increase the efficiency of extraction, an asymmetric splitting can be introduced by several methods: difference in hydrodynamic resistance between channels [282, 283], magnetic beads can be transferred to another droplet by electro-coalescence of the two droplets and attraction of the magnetic beads with a magnet followed by asymmetric splitting [284], by using a narrow and asymmetric geometry to cut the droplet in two [285] or by using a symmetric T-junction but adding an additional oil flow to one of the channel to control the flow-rate distributed in each channel and tune the volume ratio of the daughter droplets [286, 287]. With the systems presented so far, re-suspension of the magnetic beads into a subsequent droplet requires merging of 2 droplets and can prove difficult. Indeed, once the droplet with the bead suspension is pushed in the system by the oil, bringing a second droplet in contact for coalescence would require more complex channel designs with integrated valves or synchronization modules [276]. To allow magnetic beads to be resuspended inside droplets, Serra et.al. [276] proposed the use of magnetic “tweezer”, soft ferromagnetic tips terminating in an edge which can be turned on and off. One can place two tweezers facing each other across a capillary with their tip close to the capillary and create a strong magnetic field gradient strong enough to attract paramagnetic beads suspended into droplets flowing inside the capillary. Magnetic beads suspended inside droplets can then be extracted from the droplet when the magnetic field is turned on and resuspended in a subsequent droplet by deactivating the magnetic field.

Because the protocol for processing glycans prior to CE-LIF uses COOH-coated magnetic beads as a cornerstone, such microfluidic systems for sample treatment could very well be adapted for glycans. Indeed, droplet fusion, droplet mixing, sample capture with magnetic bead capture and sample resuspension which are equivalent to adding reagent, mixing reagent, extracting sample and resuspending sample in tube-based protocol can be performed in a microfluidic droplet format as we have showcased in this chapter.

Table 5 : Summary of some typical microfluidic strategies using magnetic beads.

Method/strategy	Advantages	Limits	Glycan compatibility	Reference
Manipulation of magnetic beads in droplets suspended in oil on a glass plate	Very simple system, basis for more advanced systems	Cannot be combined with other microfluidic functions, no resuspension	No	[279]
Use of a T-junction to symmetrical split droplet in two using a magnet	Good throughput (10 samples/s)	Purification rate limited to 50%, no resuspension	No	[280, 281]
Asymmetrical split of a droplet using a magnet	Good throughput, better purification rate	Purification rate still limited, no resuspension	No	[282-287]
Magnetic tweezer technology	Good purification rate, resuspension of beads possible	Limited throughput	Yes	[276, 288, 289, 290, 291]

II.4. Conclusion

In this chapter, Microfluidics was presented as a field of interest in the context of separation science in general, and for glycan sample treatment and analysis in particular. The concrete advantages of microfluidics, and in particular droplet microfluidics include:

- Miniaturization of systems allows for less reagents consumption, which means less expensive products and/or the need for less biological sample.
- Mass and heat exchange in microfluidics are more efficient, even though mixing can then become a problem.
- Confined droplets of samples in oil act as a chemical reactor: droplets are isolated from exterior contact and cross-contaminations are limited.
- Possibility of automation and parallelization are greater than with “traditional” systems.

Translation of standard separation techniques to microfluidic droplet setups was reviewed. They share a common problematic: the oil carrier phase of droplet microfluidics interferes with the separation and/or detection. When separating single droplets with HPLC or CE, it is then crucial to desegment the flow. The separated analytes can also be segmented after the separation for further operations.

In terms of the forefront sample treatment of glycans before separation, microfluidic solution not using the droplet technologies have been proposed both for HPLC and MS. In the case of CE, to the best of our knowledge, no such systems have been proposed. One key element

of the conventional batchwise protocol for the release and labelling of N-glycans for CE-LIF separation is the use of magnetic bead as a solid phase extraction support after the enzymatic release and after the labelling step. The use of magnetic beads and the magnetic tweezer technology for their manipulation in microfluidic droplets is a powerful tool for bioanalytical assays and holds high potential for glycan sample treatment and analysis.

Objective of the thesis

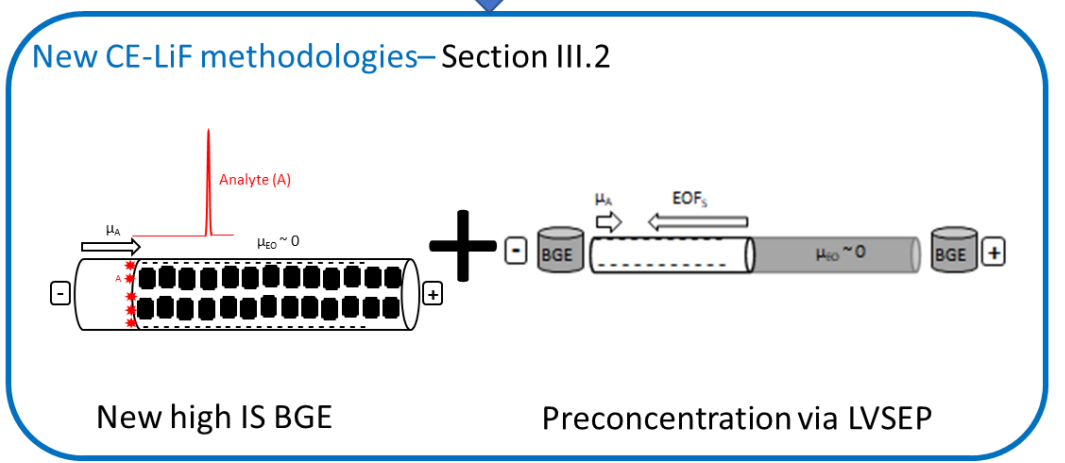
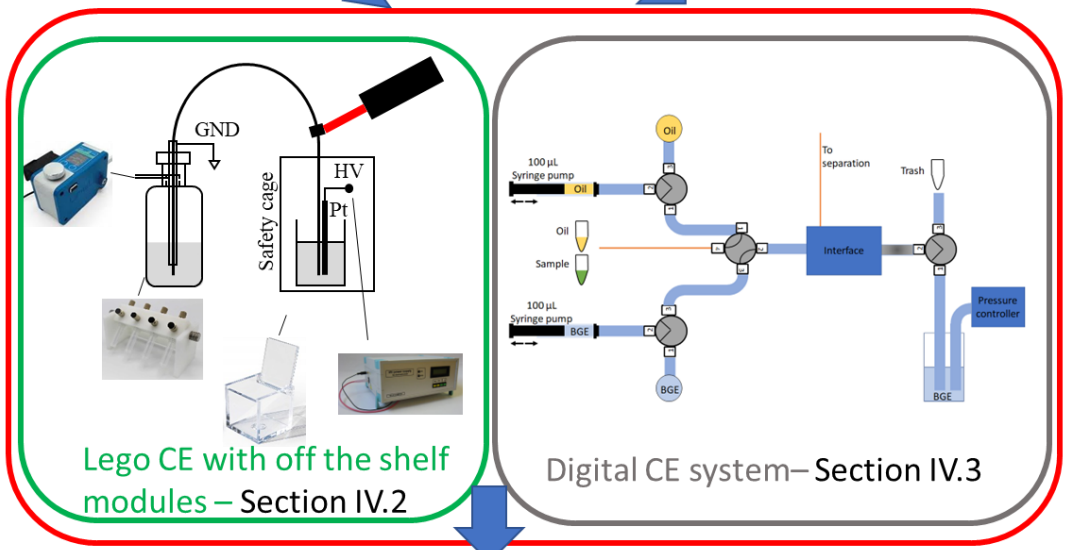
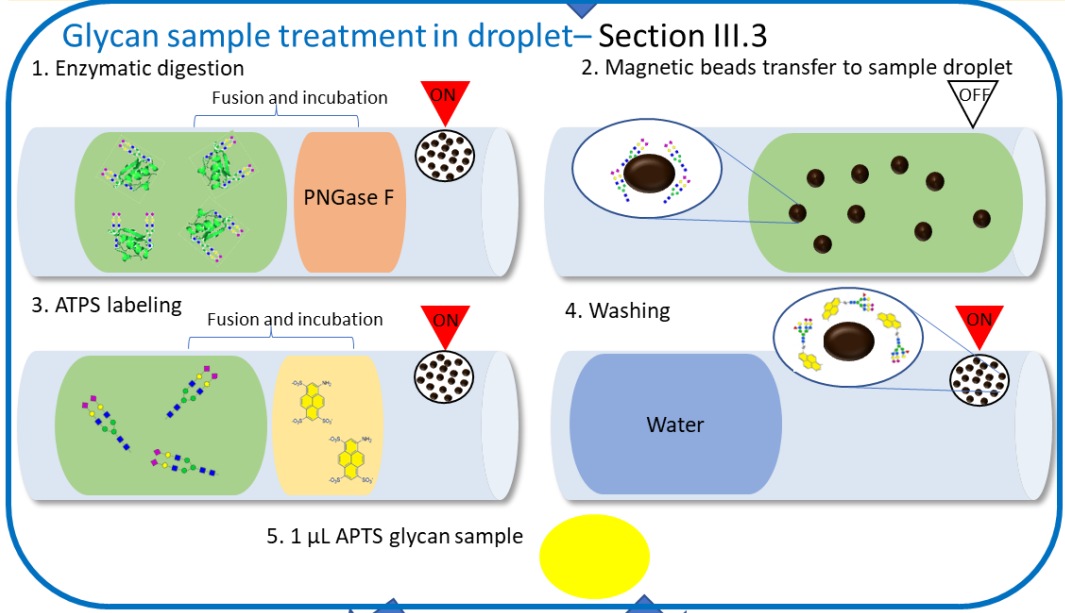
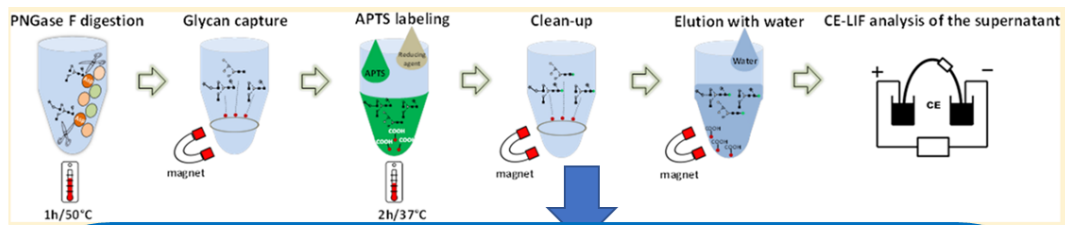


Figure 37 : Schematic representation of the thesis project divided in two parts: methodology and instrumentation.

To the best of our knowledge, droplet microfluidics have never been used for the forefront sample preparation of glycans. This may be due to the fact that extraction and purification steps require specific setups, such as the use of functionalized magnetic beads couples to a magnet for solid phase extraction. Since the cornerstone of the glycan sample treatment protocol is also functionalized magnetic beads, it seems that there is a great potential to couple both techniques in order to translate the protocol into a microfluidic droplet format.

In this regard, the goal of this thesis is to create a unique integrated analytical platform for the consecutive sample treatment of glycans followed by separation and analysis in a CE-LiF system to replace the classical tube protocol. The final goal is to have a μ TAS called Lab in Droplet where all the steps between the manual injection of the plasma or serum sample and the CE-LiF results are automated and in a microfluidic droplet format. Besides automation, the goal is to improve the efficiency of glycan labeling, the throughput, and the sensitivity of CE-LiF without any cross-contamination between samples.

To achieve these steps, experiments were divided into two different categories. First, we focus on the methodology of glycan analysis by CE-LiF, presented in Chapter III. From our point of view, there is two different ways one can improve this methodology: by improving the CE-LiF separation and by improving the forefront sample treatment of glycans. To improve the CE-LiF, we present a new background electrolyte composed of weakly charged, highly concentrated, organic ions. With its high ionic strength, the BGE is capable of suppressing electroosmotic flow during CE separation without having to use neutral capillaries or polymer additives in the BGE. It also provides a stacking effect which increases the sensitivity of detection. In addition, our new BGE is compatible with an electrokinetic preconcentration method based on EOF modulation, still without having to use neutral capillaries or polymer additives. To improve the forefront sample treatment, we chose to implement the protocol into a droplet protocol format using the magnetic tweezer technology. In addition to the inherent advantages of droplet microfluidics, the use of this format presents great synergies with glycan processing. Firstly, both the magnetic tweezer system and the glycan processing protocol rely on functionalized magnetic beads as a cornerstone. Second, because our objective is to create a μ TAS system, coupling the droplet sample treatment with a droplet-based CE system will be easier than coupling it with a regular commercial CE system, at least without diluting the sample. To implement our droplet protocol, we used a custom Magelia machine from the French startup Inorevia.

Second, we focus on the CE-LiF instrumentation for glycans. Two different purpose-made systems are presented: both are inspired from the Lego concept where blocks are assembled to create a construction, but they have different purposes. The first system was built in order to provide an alternative, cost-effective, robust and with a high degree of standardization CE system. It is built using microfluidics, optics and electrophoresis modules that can be bought commercially. It is a good compromise between performance and cost for laboratories wanting to start using CE. The second system is designed to be coupled with our in-droplet glycan protocol. In addition to the previous microfluidic and electrophoresis used in the previous system, a new microfluidic module is added along with a microfluidic chip aimed at

being an interface between the microfluidic system and the separation capillary. A scheme summarizing the thesis project is presented in [Figure 37](#).

Those new approaches are aimed at serving for the analysis of glycans from human serum glycoproteins, in order to screen CDG of a large cohort of sample. From our point of view, our Lab in Droplet μ TAS system is an innovative and promising project for the diagnosis of CDG.

Experimental part

III. Chapter 3: Development of new Methodologies for high performance analysis of glycans with CE-LIF

We showed in Chapter I that glycans are complex structures: they are composed of monosaccharides (7 different in human glycoproteins), linked together with glycosidic bonds between one of the 6 hydroxyl groups of the first sugar and one of the 6 hydroxyl groups of the second sugar and two different configurations of the glycosidic bond exist: α or β . We also showed that glycans have crucial and varied biological and physical functions: protein folding, augment protein solubility, limit protein aggregation, better resistance to thermic denaturation, protect proteins from proteases, interactions with the cell's environment (other cells, antibodies, viruses or bacteria) and in antibodies they help targeting and killing the targeted cell. Given the wide complexity of glycan structure and their functions, we showed that glycans defects are involved in a lot of diseases and thus glycoproteins can often be used as biomarkers: in cancers, Alzheimer's disease, chronic alcohol abuse which leads to diseases (alcoholic liver disease, pancreatitis, esophageal cancers and strokes) and CDG, a group of diseases caused by glycosylation defects. For the analysis of glycans released from glycoproteins, CZE-LIF is a staple technique [6, 131].

Since glycans are not naturally fluorescent, their detection using LIF requires a chemical modification with a fluorophore. We presented in detail in Chapter I.4 the gold standard process for releasing and labeling glycans with APTS using magnetic beads as a cornerstone for solid phase extraction of glycans. This process consists of denaturing the glycoprotein, enzymatically releasing glycans, labeling them and purifying them before eluting them for analysis. We have showcased in Chapter II.3.2 the potential of coupling droplet microfluidics systems manipulating magnetic beads to glycan sample treatment because both systems rely on magnetic beads as a cornerstone. Beads can be captured and transported from one droplet to another, meaning all the operations that are performed during the in-tube glycan labeling could be performed in the droplet microfluidic format.

Even though CE-LiF is a powerful and extremely sensitive detection tool, further improvement of CZE-LiF is desirable to be able to detect glycans from low abundance glycoproteins and low abundance glycans from common glycoproteins such as IgG [10]. From our point of view, there are two ways to improve the method for CE-LiF of glycans:

- Improving the CZE methodology, by re-investigating the optimal BGEs and preconcentration methods usually used for the separation and detection of glycans.
- Enhancing the efficiency of the forefront sample treatment for releasing and labeling glycans by translating it in a droplet microfluidic format.

In this chapter, we first remind the reader about the working principle of CZE, as well as CGE and large volume sample stacking with electroosmotic pump (LVSEP), a preconcentration method to be used to improve the sensitivity of glycan detection. Second, we presented the development of a new CZE-LiF methodology, using an organic BGE with extremely high IS and coupling it with a LVSEP preconcentration method. Finally, we present our translation of the conventional in-tube standard method for the high-throughput, automated forefront treatment of glycans for CE-LiF in a microfluidic droplet format using the magnetic tweezer technology in collaboration with the French startup Inorevia©.

III.1. Introduction to Capillary Electrophoresis

As seen in [Figure 38](#) with a schematic CE setup, typical CE separation involves injecting a sample inside a capillary which is filled with a BGE as a separation medium. Both ends of the capillary are immersed inside a reservoir containing BGE, and when high voltage (typically 20-30 kV of the desired polarity) is applied, charged molecules begin migrating inside the capillary depending on their mass, charge and hydrodynamic radius. In CE, detection is normally performed on-capillary, either by creating a transparent optical window for optical detection (UV, LiF), or by placing electrodes directly on the capillary (via contactless conductivity detection) [292].

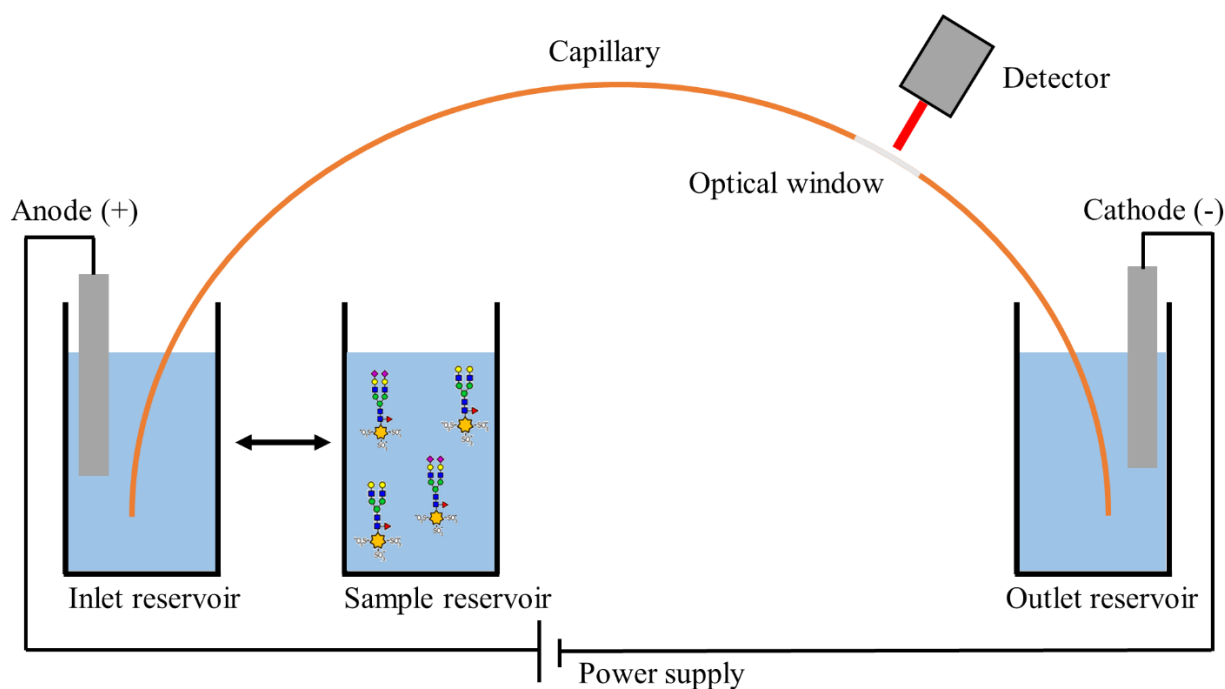


Figure 38 : Typical capillary electrophoresis setup with optical detection.

There are several separation modes available in CE, each with different separation mechanisms: CZE, CGE, Capillary isoelectric focusing, Micellar electrokinetic chromatography, Capillary isotachopheresis or Capillary electrochromatography [293]. For glycans, two variants of CE are mostly used because they are simple and robust methods. CZE where analytes are separated depending on their charge-to-size ratio under a high electrical field and often in the presence of EOF, and CGE where polymers are added in the background electrolyte to suppress the contribution of EOF [129, 294].

III.1.1. Electrophoretic mobility

Under an electric field E ($V \cdot cm^{-1}$) applied to the capillary, a charged species migrates towards the electrode bearing the opposite charge with a velocity v_{ep} ($m \cdot s^{-1}$) that depends on the electrophoretic mobility of the species μ_{ep} ($m^2 \cdot V^{-1} \cdot cm^{-1}$) via the following relation:

$$v_{ep} = \mu_{ep} \cdot E$$

The electrophoretic mobility describes the ability of a charged particle to migrate in a fluid in response to an applied electric field. It depends both on the specific analyte considered and the physicochemical

properties of the electrolyte. In particular, it depends on the charge q (C) of the analyte, its hydrodynamic radius r_h (m) and the viscosity of the fluid η (Pa.s) by the relation:

$$\mu_{ep} = \frac{q}{6\pi r_h \eta}$$

In general, larger molecules have larger hydrodynamic radii, meaning that for two analytes bearing the same charge, the smaller molecule will have a higher mobility. It should also be noted that by convention electrophoretic mobilities are signed quantities: the mobility of cations is positive while for anions it is negative.

III.1.2. Electroosmotic flow

Relating to the surface chemistry of the capillary, the second electromigration mechanism in CZE is the EOF. In a typical CZE separation, a fused silica capillary is typically used, that has ionizable silanol groups (Si-OH) in its inner surface as seen in

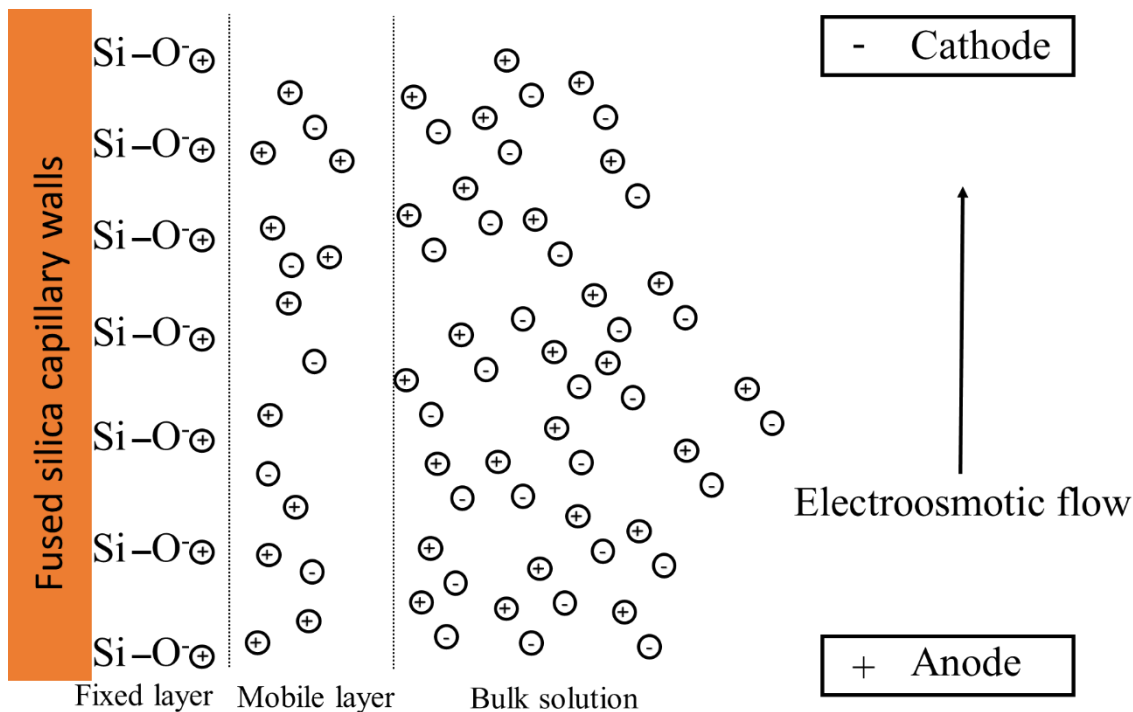


Figure 39. When using a BGE having pH>3, the silanol groups are negatively charged (SiO⁻) [293]. A double layer of hydrating cations then appears at the surface of the capillary: a fixed layer composed of adsorbed positive ions counterbalancing the negative charge at the walls due to the SiO⁻ groups and a charged mobile layer consisting of ions moving under the influence of Coulomb force.

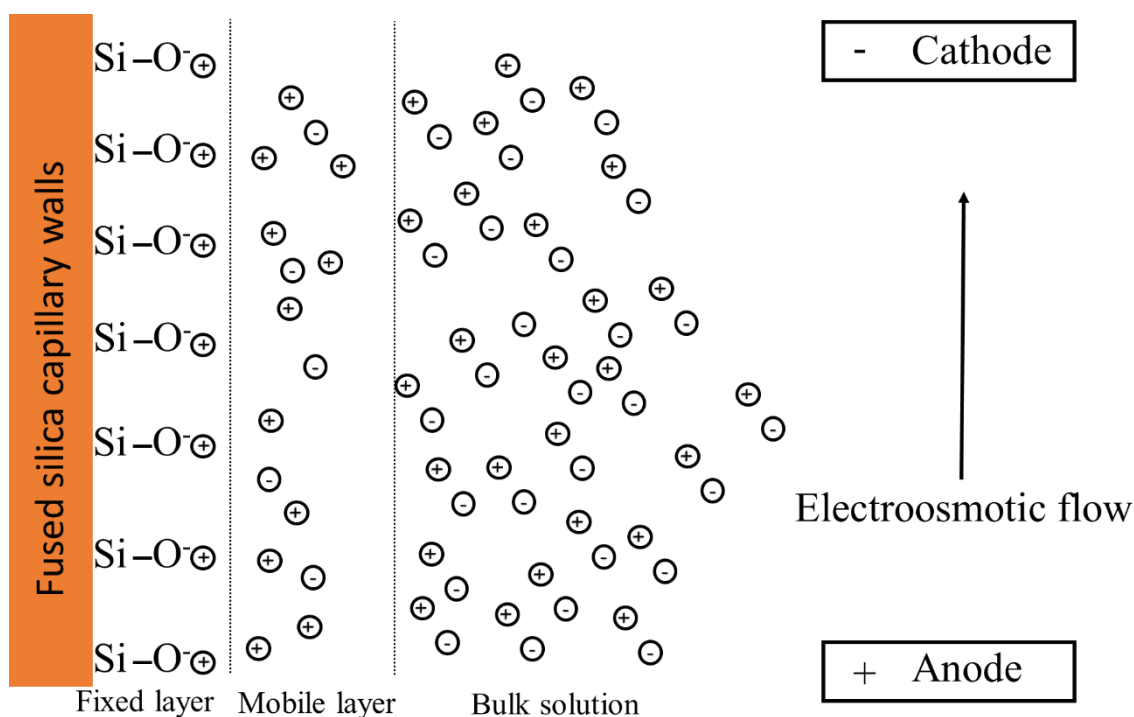


Figure 39 : Electroosmotic flow in a fused silica capillary: positives ions create a fixed layer and a mobile layer.

The double layer has a thickness δ (m) which depends on ϵ_r the relative permittivity of the BGE, ϵ_0 the permittivity of the vacuum ($F.m^{-1}$), R the ideal gas constant ($J.mol^{-1}.K^{-1}$), T the temperature (K), I the ionic strength of the BGE ($mol.L^{-1}$) and F the Faraday constant ($C.mol^{-1}$) by the relation:

$$\delta = \sqrt{\frac{\epsilon_r \epsilon_0 RT}{2IF^2}}$$

This double layer results in a surface potential ζ (V) which depends on the double layer thickness δ , the density of surface charges of the capillary σ ($C.m^{-2}$) by the relation:

$$\zeta = \frac{\delta \sigma}{\epsilon_r \epsilon_0}$$

In the mobile layer, cations are attracted to the negative electrode and create a flow called the electroosmotic flow.

Unlike pressure flows in cylinder capillaries which have a parabolic shape (which is the case notably in HPLC), the EOF has a flat shape in the bulk flow which limits dispersion of the sample during separation and allows CE to provide high separation efficiency. Similar to how the electrophoretic mobility was defined, one can define the electroosmotic velocity v_{eo} ($m.s^{-1}$) and the electroosmotic mobility μ_{eo} ($m^2.V^{-1}.s^{-1}$) as:

$$v_{eo} = \mu_{eo} E = -\frac{\epsilon_r \epsilon_0 \zeta}{\eta} E$$

Electroosmotic flow is a crucial parameter in capillary electrophoresis and depends on several parameters, and notably on the BGE used (pH, viscosity, relative permittivity and ionic strength). Careful selection of the BGE is necessary to tune the EOF depending on the desired application. EOF has a strong dependency on the pH of the BGE: at high pH the silanol groups are mostly deprotonated, leading to high magnitudes of EOF while at lower pH they are mostly protonated resulting in EOF suppression. In some cases where EOF is undesired, one solution which will be detailed later is to use BGE containing polymers to perform a variant of CZE called capillary gel electrophoresis. Another solution is to use surface treatment to neutralize the silanol groups for example with polymer coatings.

Separation of analytes using CZE thus results from the action of electrophoretic and electroosmotic mobilities. The apparent mobility μ_{app} is then defined as their sum, which can be calculated using the measured migration time of the analyte using the following equation:

$$\mu_{app} = \mu_{eo} + \mu_{ep} = \frac{Ll}{Vt_m}$$

Where L is the total length of the capillary (m), l the length from the injection end of the capillary to the detector (m), V the voltage applied to the capillary (V) and t_m the migration time (s) of the analyte. An example in [Figure 40](#) is shown for CZE separation of negative, neutral and positive species under a normal polarity mode where the positive electrode is positioned at the injection side.

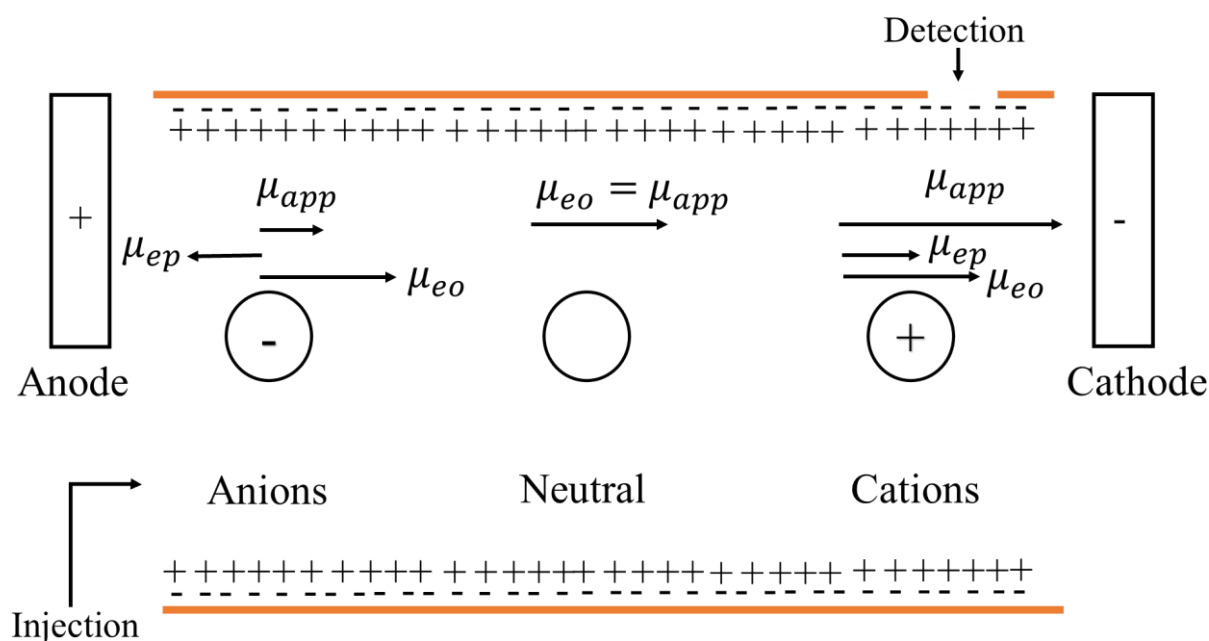


Figure 40: Schematic of the CZE separation of molecules inside a silica capillary. Species are separated depending on their electrophoretic and electroosmotic mobilities.

When using a bare fused silica capillary, EOF migrates from the positive to negative side. For cations, μ_{ep} is also directed towards the negative electrode and thus the apparent mobility of the cations $\mu_{app} > \mu_{eo}$. For neutral analytes, there is no electrophoretic force applied on them thus $\mu_{app} = \mu_{eo}$. Finally for anions, μ_{ep} is directed towards the positive electrode and against the EOF. If $\mu_{ep} < \mu_{eo}$, then

the anions will be dragged by EOF towards the cathode. In $\mu_{ep} > \mu_{eo}$, then the anions will move towards the anode and will not be detected.

III.1.3. Capillary gel electrophoresis of glycans

As mentioned previously, the staple method of separation for glycans is CGE. CGE is a mode of capillary electrophoresis where the BGE used during the separation contains cross-linked or non-cross-linked polymers rendering it a viscous matrix. The gel or polymer network has three main functions in CGE (for more details see [129]): first, they coat the inner walls of the capillary, resulting in a suppressed or lowered EOF $\mu_{eo} \approx 0$ and reducing unwanted sample adsorption to the capillary walls. Second, they have a sieving effect for larger molecules such as proteins and nucleic acids. Lastly, they increase the viscosity of the BGE, decreasing the mobility of analytes.

In the case of glycans, there is no sieving effect since glycans are too small. The use of CGE for glycans is then restricted to EOF suppression and to increase the viscosity, which can be useful to improve resolution [131]. As glycans are neutral or negatively charged molecules at pH 4.75 (due to the acidic sugars, mostly terminal Neu5Ac sialic acids), a separation in positive mode (positive electrode at the injection side) is not desirable if the EOF is negligible since negative glycans would migrate towards the injection end rather than towards detection one and neutral glycans would not really migrate at all. In general, neutral species need to be charged to be separated by CE (except for the particular case of Micellar electrokinetic chromatography, which is not detailed in this context). In our case since the glycan needs to be fluorescently tagged for the LIF detection, it is convenient to kill two birds with one stone by attaching a negatively charged fluorophore to the glycan. This is indeed the case with APTS, which bears 3 negative charges at pH 4.75. CGE under the EOF suppression regime is thus used in negative mode (negative electrode at the injection side) since APTS-glycans will migrate towards the positive electrode. The staple BGE for the separation of glycans in CGE is normally composed of an aqueous solution of Lithium Hydroxide and Acetic Acid at ionic strength 25 mmol.L⁻¹ (LiAc 25 mM) to which is added 0.4 to 1% PEO to create the polymer network [129]. As seen in [Figure 41](#), the first glycan has 3 negative charges while the second has 5 due to terminal sialic acids. Due to the ratio of charge to size, the second glycan will be detected first.

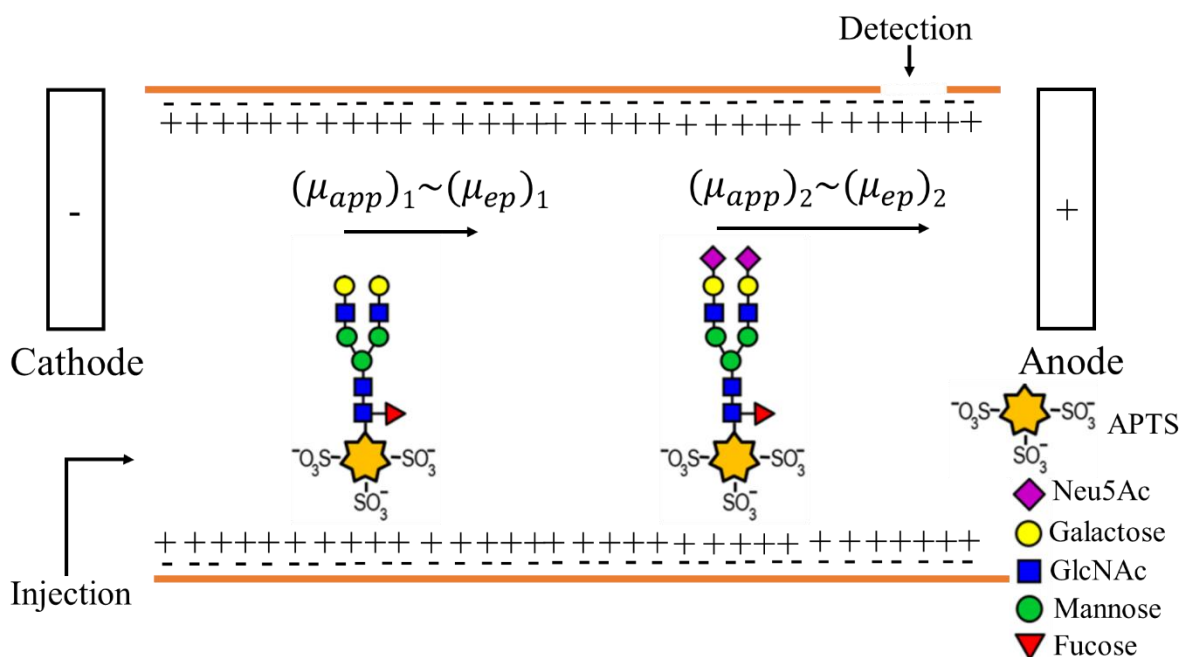


Figure 41 : Separation of glycans with Capillary gel electrophoresis using the negative mode.

III.1.4. Preconcentration of glycans before CZE analysis by large volume sample stacking.

Although CE is an established technique for high-performance separation of glycans, improving the sensitivity of glycan detection is desirable because of the low abundance of some glycoproteins or the low abundance of some glycans for a given protein. Increasing the amount of glycans to be detected after their CE separation is thus desirable and can be achieved using a forefront preconcentration step. While different on-line preconcentration strategies for CE were developed (see [295]), in the context of this thesis we focus on a technique called Large Volume Sample Stacking (LVSS), in particular LVSEP, that has been frequently used to enrich glycans [296-299]. As seen in Figure 42, LVSP consists in injecting a sample volume equivalent to 80-100% of the capillary one, and gradually stacking the anionic sample at the interface between the sample matrix and the BGE while removing the sample matrix gradually thanks to an elevated EOF. First, the capillary is filled with sample in an aqueous matrix (a). When the voltage is applied, the μ_{eo} produced in the sample matrix zone is high sweeping the target anions towards the injection end. At the same time BGE starts filling the capillary, pushing the sample matrix out (b). As BGE fills the capillary, the μ_{eo} produced diminishes while the analytes are stacked at the interface between sample matrix and BGE (c). When most of the sample matrix has been removed (~95%), the electrophoretic mobility of the analyte (μ_{ep}) is now higher than μ_{eo} and thus the stacked analytes start migrating towards the detector for CE separation. Thus, when using LVSEP for negatively charged labelled glycans, the glycans stacking and separation can be performed consecutively under the same voltage without the need to switch the polarity between these two stages [300].

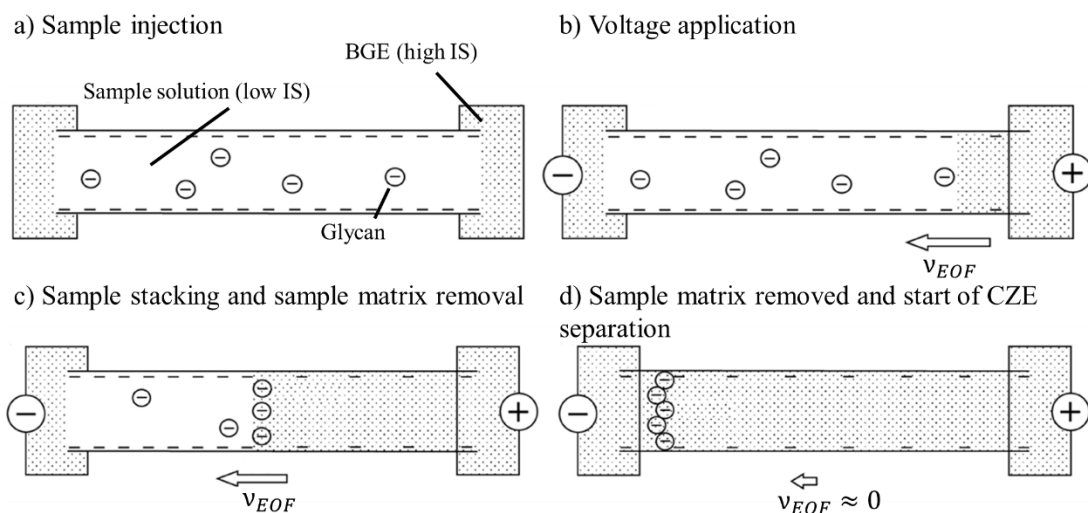


Figure 42 : Principle of LVSEP preconcentration for CZE. Adapted from [300].

LVSEP of glycans normally was achieved by using polyvinyl alcohol (PVA) coatings [297-299] or PDMS coating with an addition of 0.5% hydroxypropylcellulose in the BGE [296] to suppress EOF during the separation step. Unfortunately, the capillary coating is prone to fast deterioration over LVSEP runs [301]. Another alternative for EOF suppression during LVSEP in bare fused silica capillaries is to use very acidic BGEs. In the following subchapter, we present our work on development of a new strategy for high performance CE-LIF of glycans, using new BGE compositions and a new way of LVSEP using a simple bare fused silica capillary.

III.2. Development of a new strategy for high performance CE-LIF of glycans

In order to further improve the performance of CE-LIF of glycans, our goal was thus to find new working BGE conditions meeting the following requirements:

- Improvement of the sensitivity for detection of glycan detection compared to the standard CGE method.
- Simplification of CZE method, i.e., without needing to use capillary coatings or adding polymers into the BGE to suppress the EOF and heavy capillary rinsing steps between separations, i.e., a single rinsing step by flushing the BGE.
- Avoidance of exceeding Joule heating.
- The working condition at pH as close to pH 4.75 as possible to remain in the optimum pH range for glycan separation.

Our novel approach for this purpose relies on new BGE compositions using large weakly charged molecules at extremely high concentrations to increase their ionic strengths (IS) without exceeding the tolerated electric current, which gives the following benefits:

- Decreasing the EOF by reducing the thickness of the double layer δ .
- Increasing the conductivity difference between the sample and the BGE in order to increase stacking of the analyte and thus increase sensitivity.
- Opening the possibility to use LVSEP.

Article 2: High sensitivity capillary electrophoresis with fluorescent detection for glycan mapping.

1 **High sensitivity capillary electrophoresis with fluorescent detection for glycan mapping**

2

3 **Théo Liénard--Mayor¹, Bin Yang¹, Nguyet Thuy Tran¹, Arnaud Bruneel^{2,3}, Andras**

4 **Guttman^{4,5}, Myriam Taverna^{1,6}, Thanh Duc Mai^{1*}**

5

6 *¹ Institut Galien Paris Sud, UMR 8612, Protein and Nanotechnology in Analytical Science*

7 *(PNAS), CNRS, Univ. Paris-Sud, Univ. Paris-Saclay, 5 rue Jean Baptiste Clément, 92290*

8 *Châtenay-Malabry, France*

9 *² Université Paris-Saclay, INSERM UMR1193, Mécanismes cellulaires et moléculaires de*

10 *l'adaptation au stress et cancérogenèse, Châtenay-Malabry, France*

11 *³ AP-HP, Biochimie Métabolique et Cellulaire, Hôpital Bichat-Claude Bernard, Paris, France*

12 *⁴ Translational Glycomics Research Group, Research Institute of Biomolecular and Chemical*
13 *Engineering, University of Pannonia, 10 Egyetem Street, Veszprem 8200, Hungary*

14 *⁵ Horváth Csaba Laboratory of Bioseparation Sciences, Research Centre for Molecular*

15 *Medicine, Faculty of Medicine, University of Debrecen, 98 Nagyerdei Krt, Debrecen*

16 *4032, Hungary*

17 *⁶ Institut Universitaire de France (IUF)*

18

19 * Corresponding author

20 e-mails: thanh-duc.mai@u-psud.fr

21

22 **Keywords:** background electrolyte; capillary electrophoresis; fluorescent detection; large

23 volume sample stacking; N-glycans

24

25 <https://doi.org/10.1016/j.chroma.2021.462593>

26 **Abstract**

27 We present in this study a novel strategy to drastically improve the detection sensitivity and
28 peak capacity for capillary electrophoresis with laser induced fluorescent detection (CE-LIF)
29 of glucose oligomers and released glycans. This is based on a new approach exploiting a
30 polymer-free background electrolyte (BGE) for CE-LIF of glycans. The best performance in
31 terms of sample stacking and suppression of electroosmotic flow (EOF) was found for a BGE
32 composed of triethanolamine / citric acid and triethanolamine / acetic acid at elevated ionic
33 strengths (IS up to 200 mM). Compared to the conventional protocols for CE-LIF of glucose-
34 oligosaccharides and released glycans, our polymer-free strategy offered up to 5-fold
35 improvement of detection sensitivity and visualization of higher degree of polymerization
36 (DP) of glucose oligomers (18 vs 15). To further improve the detection sensitivity, a new
37 electrokinetic preconcentration strategy via large volume sample stacking with electroosmotic
38 modulation without having recourse to neutrally coated capillaries is proposed, offering a 200-
39 fold signal enhancement. This approach is based on variation of the buffer's IS, rather than pH
40 adjustment as in conventional methods, for EOF modulation or quasi-total reduction. This
41 strategy allows selecting with high flexibility the best pH conditions to perform efficient
42 preconcentration and separation. The new approach was demonstrated to be applicable for the
43 analysis of N-linked oligosaccharides released from a model glycoprotein (Human
44 Immunoglobulin G) and applied to map N-glycans from human serum for congenital
45 disorders of glycosylation (CDG) diagnosis.

46

47

48 **1. Introduction**

49 Analysis of glycans released from glycoproteins plays an important role for quality control of
50 therapeutic proteins and diagnostic purposes [1, 2]. Protein glycosylation is by far the most
51 complex common post-translational modification, with more than half of all secretory and
52 cellular proteins being glycosylated [3-5]. An altered glycosidic linkage or one truncated
53 antenna in a glycan may alter the normal functioning and activity of glycoproteins. A
54 variation of glycoform proportion of a given glycoprotein may also have biological
55 consequences or be the result of a pathological state [6]. That is why glycoproteins represent a
56 useful source of biomarkers for various illnesses like cancer and cardiovascular diseases [2].
57 Another typical example is congenital disorders of glycosylation (CDG), a family of
58 multisystem genetic diseases caused by mutations in genes coding for proteins involved in the
59 biosynthesis (CDG-I) or trimming/remodeling (CDG-II) of the oligosaccharide moieties of N-
60 linked glycoconjugates [7]. Thus, CDG-I leaves some N-glycosylation sites unoccupied while
61 CDG-II is associated with subtle structural changes of N-glycans with a whole array of
62 isomers, leading to a great challenge for their separation and identification.

63
64 Until now, analysis of glycans have frequently been carried out with high-performance liquid
65 chromatography with fluorescence detection (HPLC-FLD) [8], matrix-assisted laser
66 desorption/ ionization time-of-flight mass spectrometry (MALDI-TOF-MS) [9, 10], or liquid
67 chromatography connected to electrospray ionization mass spectrometry (LC-ESI-MS) [7].
68 Capillary electrophoresis (CE) coupled with laser induced fluorescent (LIF) detection has
69 become a staple in glycan separation, mostly for N-glycans [11, 12]. Prior to downstream
70 analysis, sample preparation is required, especially when performing sensitive detection is the
71 objective [13]. It stands for both small compounds and large biomolecules. In a standard
72 protocol for glycans, glycans are first released from glycoproteins / peptides, enriched on a

73 solid support (i.e., magnetic beads in most of the cases), then fluorescently labelled with a
74 charged fluorophore (the most frequently used one being 8-aminopyrene-1,3,6-trisulfonic-acid
75 (APTS) [14]) and eventually separated by CE-LIF. Normally, acidic background electrolytes
76 (BGEs) containing different polymer/gel types and concentrations, typically polyethylene
77 oxide (PEO) or polyethylene glycol (PEG), are used [15]. The CE-LIF conditions for glycan
78 analysis have recently been established with the introduction of commercial kits, including
79 polymer-containing buffers [16, 17]. Efforts to use gel-free BGEs for such purpose were also
80 reported in the early 90's [18-20], but were then outnumbered by those that use gels and
81 polymers in recent years.

82

83 So far, reported BGE compositions for CE-LIF of glycans normally employ inorganic and
84 small ions (*e.g.*, phosphate, borate, acetate, sodium, lithium) as well as inorganic acid and
85 base (typically NaOH and HCl) for pH adjustment. From our viewpoint, such BGEs with low
86 UV absorbing features are adapted for UV detection but the significant increase in their ionic
87 strengths, which is required for improving analyte stacking and suppressing further the
88 electroosmotic flow (EOF), is not trivial to achieve due to detrimental increase in electric
89 currents and thus Joule heating. To further increase the detection sensitivity and peak
90 capacity, the challenge is to find a BGE that simultaneously satisfies the criteria of efficient
91 sample stacking (for increased glycans' signals), EOF suppression (for migration of large
92 glycans counter the EOF to the detector) and tolerable current generation. A straightforward,
93 cost-effective and coating-free CE-LIF approach that offers such features for glycan
94 separation is therefore highly desirable. In the diagnostic context, there are still challenges for
95 the detection of glycans used as biomarkers, mostly due to the low abundance of some plasma
96 glycoproteins and unsatisfactory detection sensitivity. This therefore requires continued
97 development to improve the CE-LIF performance towards the screening/diagnosis of

98 aberrant-glycan-related pathologies. Efforts have been focused on glycan sample treatment
99 (fluorescent labeling [21-23]) and glycan enrichment methods based on solid phase extraction
100 [24, 25] or electrokinetic phenomena (notably isotachopheresis and large volume sample
101 stacking) [26-29] prior to CE-LIF.

102
103 In this study, we report a novel strategy to significantly improve the performance of CE-LIF
104 of fluorescently labelled glycans, using polymer-free buffers in conjunction with efficient
105 analyte stacking and EOF suppression in fused silica capillaries. To demonstrate the
106 applicability of our new approach, CE-LIF analyses of N-glycans released from a model
107 glycoprotein (Human Immunoglobulin G) were carried out and the performance in terms of
108 signal sensitivity and peak capacity was compared to currently used methods. The developed
109 approach was applied for mapping of N-glycans released from human serum glycoproteins,
110 serving for CDG screening.

111

112 **2. Experimental**

113 **2.1. Chemicals, reagents and samples**

114 All chemicals for preparation of buffers were of analytical or reagent grade and purchased
115 from Sigma-Aldrich (Lyon, France). Reagents for preparation of glycans (denaturation,
116 digestion, labeling solutions; malto-oligosaccharides (MD ladder), APTS dye, magnetic beads
117 and G3 standard) were taken from the Fast Glycan Analysis and Labeling kit from SCIEX
118 (Villebon sur Yvette, France). Human Immunoglobulin G (IgG), PNGase F and sodium
119 cyanoborohydride (NaBH_3CN) were purchased from Sigma-Aldrich (Lyon, France). Maltose
120 (G2) was obtained from Sigma-Aldrich and Maltohexose (G6) was obtained from Carbosynth
121 Limited (Compton, UK). Beta-alanine (β -Ala), triethanolamine (TEOA), trimellitic acid,
122 acetic acid (AcOH), citric acid (Cit) and lithium hydroxide monohydrate were used for

123 preparation of BGE solutions. Serum samples from CDG individuals and healthy control were
124 kindly provided by Dr. A. Bruneel (Bichat hospital, Paris, France).

125

126 **2.2. Apparatus and Material**

127 Method development was performed with a Beckman Coulter PA800+ and MDQ systems
128 (SCIEX, Brea, CA) coupled with a LIF detector ($\lambda_{\text{excitation}}$: 488 nm, $\lambda_{\text{emission}}$: 520 nm).

129 Instrument control and data acquisition were carried out by using the 32Karat ver 8.0 software
130 (SCIEX). Fused silica capillaries of 50 μm i.d. and 375 μm o.d. from Polymicro (TSP050375,

131 CM Scientific, Silsden, UK) were used for all CE experiments. Deionized water was purified
132 using a Direct-Q3 UV purification system (Millipore, Milford, MA, USA) and the pH values

133 of buffer solutions and samples were measured with a SevenCompact pH meter (Mettler

134 Toledo, Schwerzenbach, Switzerland). Buffer ionic strength (IS) calculations were based on

135 simulations with the computer program PhoeBus (Analis, Suarlée, Belgium). Additional

136 information regarding the simulation by Phoebus program can be found in reference [30]. To

137 maximize the accuracy for a defined buffer's ionic strength, calculation was implemented

138 with correction according to either Debye-Hückel equation (ionic strengths of 1-10 mmol/L),

139 Güntelberg equation (ionic strengths of 10-60 mmol/L) or Davies equation (ionic strengths of

140 60-500 mmol/L). Deionized water was used for the preparation of all solutions.

141

142 **2.3. Methods**

143 *2.3.1. Release and fluorescent labelling of glycoprotein derived-glycans*

144 10 μL of human IgG (10 mg/mL in deionized water) was mixed with 5 μL of the denaturing
145 solution containing 10 μL of D1 solution, 10 μL of D3 solution and 50 μL of D4 solution

146 from the SCIEX kit and incubated at 70°C for 10 min. After denaturation, 12 μL of the

147 digestion solution containing 5 μL of PNGase F in 12 μL of D4 was added and further

148 incubated for 60 minutes at 50°C. The released glycans were then labelled following the
149 protocol described in [22]. Briefly, labelling reagents (3 µL of 40 mM APTS in 20% AcOH, 2
150 µL of 1 M NaBH₃CN) in THF, 4 µL of 20% AcOH and 6 µL of THF) were added into the
151 sample vial and incubated for 60 min at 50°C with closed cap, and then for 60 min at 50°C via
152 evaporative labelling with open cap.

153
154 For the preparation of N-glycans from human serum samples, the magnetic beads delivered in
155 the SCIEX kit were used for sample purification. The tube containing 200 µL of resuspended
156 magnetic beads was placed in a magnetic stand to allow the beads migrating to the magnet,
157 then the storage buffer was removed. This step was performed every time to remove any
158 liquid from the beads. 10 µL of 4-fold diluted serum sample was added onto the beads. 5 µL
159 of denaturing solution was then added, mixed and incubated at room temperature for 7 min
160 with the vial opened. 11 µL of digestion solution from Sciex kit was added to the mixture; and
161 incubated at 60°C for 20 min in an open vial. 200 µL of acetonitrile was then added, mixed
162 and incubated at room temperature for 1 min. The supernatant was removed, and 9 µL of 40
163 mM APTS in 20% acetic acid, 1 µL of NaCNBH₃ and 1 µL of D4 from the SCIEX kit was
164 added, followed by incubation at 60 °C for 20 min in an open vial.

165
166 *2.3.2. Fluorescent labelling of standard oligosaccharides*

167 The preparation of fluorescently labelled MD ladders was performed according to Reider *et*
168 *al.* [22]. Briefly, 2 mg of oligosaccharide ladder was added in a 200 µL PCR tube, followed
169 by addition of 4 µL of 40 mM APTS in 20% AcOH, 4 µL of 20% AcOH and 2 µL of 1M
170 sodium cyanoborohydride (NaBH₃CN) in tetrahydrofuran (THF). The mixture was incubated
171 under mixing at 70°C for 30 min with an open-capped vial. After the reaction, the sample was

172 stocked in 100 μ L deionized water, which was aliquoted and stored at -20°C . Further dilution
173 of this stock solution was carried out before CE-LIF analysis.

174

175 *2.3.3. CE-LIF of APTS-glycans and oligosaccharides*

176 Analyses of the APTS-labeled N-glycans or the malto-oligosaccharide standards were carried
177 out either with various BGEs detailed in Table 1 or using the SCIEX gel buffer system (BGE
178 SCIEX). These separations were done using fused-silica capillaries of 50 μm i.d. with the
179 total length (L_{tot}) of 60 cm, the effective length (L_{eff}) of 50 cm, under a separation voltage of -
180 25 kV applied on the injection (inlet) side . The fused silica capillaries were preconditioned by
181 rinsing with 0.1 M NaOH for 5 min, water for 3 min and the buffer of interest for 10 min prior
182 to use.

183

184 Large-volume sample stacking with EOF modulation was implemented with BGE composed
185 of TEOA / citric acid (IS of 150 mM, pH 4.75). The sample prepared in water was
186 hydrodynamically filled to 100 % of the capillary volume (0.7 psi, 900 sec). A voltage of -
187 25kV was applied on the injection (inlet) side to stack the target oligosaccharides / glycans.
188 The preconcentration step was transitioned into the separation step without user intervention
189 when the current stopped increase and reached a stable value.

190

191 **3. Results and Discussion**

192 **3.1. Polymer-free BGEs for CE-LIF of APTS-labeled malto-oligosaccharides and** 193 **glycans**

194 *3.1.1. Proposed principle*

195 Our proposed approach, illustrated in Fig. 1A, is to push the ionic strengths (IS) of the BGE
196 and concentrations to extremely high levels (IS up to 200 mM, which require concentrations

197 up to a thousand mM) to allow high stacking of APTS-labelled glycans induced by the
198 conductivity differences between the sample and buffer zones [31, 32]. At the same time,
199 these conditions ensure suppression of EOF without recourse to any capillary coating via
200 diminution of the electrical double layer thickness on the internal capillary surface [33, 34],
201 while still maintaining tolerable electric currents. This EOF suppression is desirable to allow
202 the anionic labeled glycans to migrate towards the detector. Whereas this was difficult with
203 buffers containing inorganic ions, we expected it to be realizable with BGEs composed of
204 large weakly charged molecules with low degrees of protonation / ionization. These molecules
205 have indeed been used for preparation of BGEs for CE coupled with contactless conductivity
206 detection. Their concentrations in this case are normally kept low (less than 50 mM in
207 general) in order to minimize the generated background signal [31, 35]. In our study, we
208 targeted much higher buffer concentration ranges (up to a thousand mM) than typically
209 reported. As the electric currents are directly related to the conductivity, which in turns links
210 to the ion density of the BGE (*i.e.*, IS) and ions' electrophoretic mobilities (μ_{ep}), the very-
211 slowly-migrating ions (ideally, μ_{ep} approaching zero) were anticipated to provide much lower
212 currents than the conventional BGE constituents, even at very high IS and concentrations.

213

214 **3.1.2. Performance of the polymer-free BGEs**

215 To follow the logic described above, several BGEs that were designed by simulation using the
216 Phoebus software to meet the aforementioned criteria were selected (Table 1). Four BGE
217 candidates from the simulated ones were experimentally tested, including TEOA/ citric acid,
218 TEOA / acetic acid, β -Ala / acetic acid and β -Ala / trimellitic acid. The EO mobilities
219 obtained with these BGEs, measured using the method developed by Williams et Vigh [36],
220 were $0.47 \times 10^{-5} \text{ cm}^2 \cdot \text{V}^{-1} \cdot \text{s}^{-1}$ for TEOA/ citric acid, $1.28 \times 10^{-5} \text{ cm}^2 \cdot \text{V}^{-1} \cdot \text{s}^{-1}$ for TEOA / acetic
221 acid, $4.82 \times 10^{-5} \text{ cm}^2 \cdot \text{V}^{-1} \cdot \text{s}^{-1}$ for β -Ala / acetic acid and $4,72 \times 10^{-5} \text{ cm}^2 \cdot \text{V}^{-1} \cdot \text{s}^{-1}$ for β -Ala /

222 trimellitic acid buffer, respectively. The EO mobility was reduced by up to 10 folds when
223 using TEOA-based BGEs instead of β -Ala-based ones. Note that the EO mobilities achieved
224 with neutral coatings are normally inferior to $1 \times 10^{-5} \text{ cm}^2 \cdot \text{V}^{-1} \cdot \text{s}^{-1}$ [37, 38]. These BGEs were
225 used for the separation of the APTS-labeled MD ladder, and the performance was evaluated in
226 terms of peak intensity and capacity. The lithium acetate buffer (LiOH/AcOH), a polymer-
227 free BGE employed by many groups for CE-LIF of oligosaccharides [11, 15], was also tested
228 as a reference. The others in the list (e.g., TEOA / gluconic acid, TEOA / sorbic acid, etc.)
229 were not tested due to limited solubilities of the least soluble components in these buffers.
230 Performance comparison for CE-LIF of the APTS-labelled oligosaccharide ladder with the 5
231 investigated BGEs is shown in Fig. 2. As can be seen, peak signals achieved with our 4
232 proposed BGEs (Fig. 2B-E) are all significantly higher than those obtained with LiOH/AcOH
233 buffer (Fig. 2A). Particularly, the peak heights obtained with TEOA/Cit and TEOA/AcOH
234 were up to 5-fold higher than those obtained with LiOH/AcOH BGE. Furthermore, the
235 TEOA-based buffers could suppress EOF more efficiently, allowing detection of longer
236 glucose oligomers, up to 12 and 17 glucose units (DP) for TEOA/AcOH (Fig. 2D) and
237 TEOA/Cit (Fig. 2E), respectively, whereas only 6 DP peaks are found with LiOH/AcOH
238 under the same CE conditions. In the case of 150 mM β -Ala/Trimellitic acid (Fig. 2B) and
239 150 mM β -Ala / AcOH (Fig. 2C), one can see that the signals were also approximately 5-fold
240 higher than those from the reference LiOH/AcOH. The number of observed malto-
241 oligosaccharides was, however, much lower than that for TEOA based buffers. The best
242 performance in terms of peak heights and detected DP number was achieved with
243 TEOA/AcOH and TEOA/Cit buffers. Table 2 further shows that the signal to noise ratios
244 were approximately 10-times higher with TEOA-based buffers compared to the standard
245 LiOH/AcOH one. Satisfactory repeatability for migration times (RSD % < 0.5 %) and peak
246 areas (RSD < 5 %) was achieved for the investigated peaks with these buffers (Table 2). The

247 overall results clearly show the superiority of TEOA/Cit BGE. The improved signals observed
248 with our buffers are probably linked to the prolonged duration (Δt) to maintain the stacking
249 effect. Indeed, good sample stacking in CE is not only dependent on the conductivity
250 difference ($\Delta\sigma$) between the sample and electrolyte zones (similar to optimization of
251 conductivity signals [31]), but also on the duration (Δt) to maintain such difference. With
252 conventional BGE, the initial $\Delta\sigma$ is normally satisfied (*via* high μ_{ep} at low and moderate IS) at
253 the starting moment, however, decreases when the fast-moving ions in the BGE zone
254 penetrate into the sample zone (Kohlrausch regulating function [39, 40]). This stacking effect
255 is on the other hand expected to reach the maximum for extremely concentrated slowly
256 migrating BGE ions (see Fig. 1A), thanks to high $\Delta\sigma$ (*via* very high IS even with low μ_{ep}) and
257 longer Δt (due to retardation of the ion penetration from the BGE into the sample zone).
258 Furthermore, by using an extremely dense zone of large weakly charged ions in the BGE, the
259 diffusion of stacked analytes may be hindered by the clusters or groups of electrolyte
260 molecules [41]. This in turn can help “blocking” the stacked analytes more efficiently at the
261 sample-BGE boundary for further peak height improvement.

262
263 The IS of this BGE was then further increased in order to achieve greater stacking effect, and
264 thus gaining further improvement of peak signals for the APTS-labeled MD ladder (Fig 3).
265 Oligosaccharide peaks obtained with TEOA/Cit BGE at IS of 200 mM were slightly higher
266 (1.3 - 1.5x improvement) compared to those obtained with 150 mM IS. Interestingly, the EOF
267 was slightly higher with the 200 mM BGE with some retardation of the oligosaccharide peaks,
268 which was probably due to some increase in pH. Indeed, when working with very
269 concentrated solutions, their experimentally measured pH values were found slightly shifted
270 from the simulated ones. In the case of TEOA/Cit BGE at IS of 200 mM, the measured pH
271 was 5.05 instead of 4.75 as simulated. This can refer to a similar situation when measuring the

272 pH values of very salty solutions, where the aqueous proton (H^+) concentration is different
273 from its activity, leading to a shift of pH value that reflects the solution H^+ activity.
274 Consequently, fewer malto-oligosaccharide peaks (15 DPs) were observed in that case over 20
275 min. Thus, IS can be selected between 150 or 200 mM depending whether a higher number of
276 detected malto-oligosaccharides is required. The variation of MD ladders' signals at lower IS
277 ranges was also verified for the TEOA / Cit BGE (Fig S1 in the ESI). The signals approached
278 the plateau at IS from 100 mM; and the increase in peaks' signals was less significant between
279 100 - 200 mM. The use of high IS (150 or 200 mM rather than 100 mM or less) is indeed not
280 only for signal improvement, but also for efficient EOF suppression to facilitate the migration
281 of glycans to the detector. IS higher than 200 mM was as well tested but then was not
282 considered for further experiments due to too high currents (more than $65 \mu A$, which can
283 generate pronounced Joule heating for a capillary of $50 \mu m$ i.d.). The TEOA/Cit BGE was
284 also compared with the commercial one (SCIEX polymer containing BGE) for successive
285 separations of oligosaccharides (over 15 runs). Peak heights were almost 4-fold higher for
286 TEOA/Cit 200 mM (Fig. 3B) compared to those obtained with the commercial buffer (Fig.
287 3C). The TEOA/Cit BGE exhibited similar repeatability of migration times ($RSD \% < 0.8 \%$
288 over 15 runs for DP 1, DP 6 and DP 10 oligomers, (table S1 in the supplementary material) as
289 with the commercial buffer. Better peak capacity was achieved for TEOA/Cit polymer-free
290 buffers. This advantageous feature can be explained by several features. First, thanks to the
291 drastic reduction of the zeta potential of the inner capillary surface at very high IS of the
292 buffer, significant EOF suppression could be obtained [33, 34]. Second, the efficiency of
293 alkylamines in BGEs for capillary surface coverage via electrostatic interaction with the
294 ionized silanols of the capillary was higher than that offered by monovalent cations (Na^+ , Li^+ ,
295 K^+ , NH_4^+) in conventional BGEs [42]. Third, when using very high concentrations of BGE
296 constituents (approaching their saturation), it is assumed that the solvation degree of the

297 silanol groups of the capillary was decreased due to competition with other ions in the
298 electrolytes for hydration. The presence of very concentrated ions in our BGEs, thus, could
299 allow coverage and reduction of the capillary surface charge, decreasing its zeta potential,
300 which in turn gives a similar effect as a ‘virtual coating’ for EOF suppression.

301

302 ***3.1.3. Analysis of human serum glycans from CDG individuals: towards diagnostic***
303 ***applications***

304 For CDG screening via N-glycan analysis, the preferred methods include gel electrophoresis,
305 chromatography and mass spectrometry (MALDI-MS and ESI-MS), whereas CE-LIF has not
306 been listed yet as a well-established method for this purpose [7]. In order to showcase the
307 applicability of our new CE-LIF method for the CDG diagnostics, total N-glycans from two
308 serum samples from CDG patients and one from a healthy person (control) were analyzed by
309 CE-LIF (Fig. 4). Trace (A) corresponds to the control serum, featuring different peaks from
310 biantennated N-glycans (peaks a-b-c). Trace (B) shows the serum glycan profile from a
311 B4GALT1-CDG individual with a quasi-total deficit of galactosylated N-glycans, which
312 differs significantly from the control one. Trace (C) corresponds to a MGAT2-CDG case,
313 where one of the N-glycan antennae presents a major GlcNAcylation defect. An extra peak
314 (peak g at ~11.5 min) that is not present in the control sample was found for this CDG
315 subtype. Accordingly, very typical and distinct profiles are obtained for the different CDG
316 subtypes showing that an adequate diagnosis could be possible with N-glycan profiling by
317 CE-LIF. The peak patterns obtained with our polymer-free BGE were similar to those
318 obtained with the commercial buffer (Fig. S2 in the supporting material), demonstrating the
319 applicability of our approach for the analysis of glycans from biofluids. In both CE-LIF
320 profiles (Fig. 4) and MALDI-MS reference ones [43], featured peaks were found for CDG
321 samples whereas they were non-detectable in the healthy control. It is worthy to note that

322 unlike CE-LIF, no separation step was carried out prior to ionization for MALDI-MS. The
323 MS profiles therefore may present some overlaps of glycans having the same mass to charge
324 ratio and / or presenting poor signals for those hardly ionizable.

325

326 **3.2. Large volume sample stacking with EOF modulation in uncoated capillaries**

327 ***3.2.1. Proposed principle***

328 In conventional methods of large volume sample stacking with electroosmotic pumping
329 (LVSEP), which is the most frequently reported approach for electrokinetic preconcentration
330 of glycans, the EOF variation and suppression is established through buffer pH adjustment
331 and the use of neutral capillary coatings [26-29, 37, 44]. Unfortunately, such mode of
332 preconcentration often leads to fast deterioration of the permanent neutral coating layer over
333 runs [37]. Therefore, we took advantage of our new BGE to develop an analyte
334 preconcentration approach without recourse to any capillary coating via large volume sample
335 stacking (LVSS) with EOF modulation (see Fig. 1B). This electrokinetic preconcentration
336 required indeed two completely different EOF magnitudes for sample preconcentration and
337 for the separation of the stacked analytes. High electroosmotic mobility (for example $\mu_{EO} =$
338 $60 \times 10^{-5} \text{ cm}^2/\text{V/s}$ if the sample is prepared in water) was needed to remove the sample matrix
339 from the capillary during the stacking of negatively charged analytes, whereas a much lower
340 one ($\mu_{EO} \sim 0$) was required to ensure the electromigration of enriched glycans to achieve their
341 baseline separation. Here we propose to use variation of the IS of the BGE, rather than the
342 buffer pH (not the pH of the sample matrix) as in conventional approach for modulation and
343 quasi-total reduction of the EOF.

344

345 ***3.2.2. Procedure optimization and performance***

346 The challenging part of this approach was to establish in the same uncoated capillary two
347 distinct EOF ranges that transiently switch from one to another. The very high μ_{EO} (more than
348 $55 \times 10^{-5} \text{ cm}^2 \cdot \text{V}^{-1} \cdot \text{s}^{-1}$) could in principle be obtained by using either water or very diluted
349 BGE as the sample matrix to be filled in the capillary before the preconcentration step. Our
350 preliminary optimizations revealed that oligosaccharides prepared in water exhibited the best
351 EOF-assisted stacking performance. Note that if the sample was prepared in deionized water,
352 the very low ion density in the sample matrix could sometimes provoke drop of the current
353 profile during the large volume sample stacking, leading to failure of this preconcentration
354 step. This challenge was overcome (or at least alleviated) by replacing deionized water with
355 tap water to ensure a sufficient ion density in the sample matrix. Then, to reach a very low
356 EOF (μ_{EO} approaching zero) required for CE-LIF separation, extremely concentrated buffers
357 were needed (see section 3.1). In our first attempts, the BGEs having IS less than 100 mM
358 were unable to create a sharp EOF transition for efficient preconcentration-separation of
359 oligosaccharides. Much higher IS (150 mM or higher) were required to maintain the drastic
360 change of μ_{EO} between the two steps.

361 Finally, the new preconcentration approach was performed with the TEOA/Cit BGE (IS 200
362 mM). Fig. 5 compares the LVSS-CE-LIF and the CE-LIF method without preconcentration
363 for MD ladders. The monitoring of the current profile during the preconcentration (Fig. S3 in
364 the ESI) showed that the low IS sample matrix filled in the capillary (reflected by the current
365 approaching 0 μA at the beginning) was gradually replaced by the high IS zone of the BGE
366 (as the current increased). The LVSS preconcentration apparently transitioned to the CE-LIF
367 separation mode without operator intervention when the matrix was 100 % removed and the
368 BGE completely filled the capillary (i.e., stable current was reached). Based on the peak
369 heights and injected sample concentrations, a detection sensitivity improvement of 200 times
370 was achieved with the inclusion of LVSS. Besides the contribution of preconcentration effect,

371 this signal enhancement also comes from the fact that the high BGE IS required for EOF
372 elimination during electrophoresis can boost at the same time the sample stacking effect (as
373 shown in Fig. 1A). This resulted in further improvement of peak shapes and detection
374 sensitivity. As the EOF was manipulated through IS changes rather than pH, we could select
375 the best pH conditions for the analytes during preconcentration and separation. The peak
376 sharpness was a bit compromised for the late-migrating peaks in the LVSS-CE-LIF mode.
377 Considering that these peaks resulted from the stacking of a sample volume equivalent to 100
378 % of the capillary volume (compared to 1 % in the normal CE -LIF mode), this slight change
379 in peak sharpness and resolutions was considered to be tolerable. It is worthy to note that the
380 different degree of polymerization glucose oligomers behaved differently in terms of
381 enrichment factor and resolution changes after LVSS-CE-LIF (see Fig. S4). The improvement
382 of peak height was more pronounced for the smallest DPs, whereas the peak resolution
383 decreased more for them (except for DP1 and DP2) after LVSS process. This was probably
384 due to the different DP responses to the new BGE compositions and/or preconcentration
385 process, as it was already observed in another approach for preconcentration and CE-LIF of
386 MD ladders [21]. The triplicates of electropherograms and current profiles from LVSS-CE of
387 MD ladders (Fig. S5 in the ESI) demonstrated good repeatability of this process, with
388 calculated RSD values less than 5 % for peak areas and 0.3 % for migration times. The current
389 profile was used to monitor the successful completion and repeatability of the LVSS-CE
390 process.

391

392 **3.2.3. Analysis of N-glycans**

393 To evaluate the performance of the proposed approach with glycoprotein-derived
394 oligosaccharides, the BGE composed of 200 mM TEOA/Cit was used for preconcentration
395 and CE-LIF separation of APTS-labeled N-glycans released from human IgG using PNGase

396 F. Most of human IgG N-glycans are bi-antennary complex type with low sialylation (5-10
397 %), highly core-fucosylated (> 92 %); and a small proportion contains a bisecting GlcNAc (11
398 %) [45]. By referring to the similar peak patterns assigned for human IgG using CE-LIF with
399 the commercial BGE [46, 47], we could assign the corresponding N-glycan structures to the
400 major peaks with our new buffer (Fig. 6A). Other peak identifications could be gleaned from
401 the reference profile provided elsewhere [47]. With the new LVSS-CE-LIF method (Fig. 6B),
402 while the same major peaks were separated with little decrease in resolution, the detection
403 sensitivity was drastically improved (by approximately 160 folds, based on peak height). This
404 in principle would allow more glycans including even minor ones, which are not easily
405 visualized using standard CE-LIF protocol without preconcentration, to be detected. This
406 method can indeed be applied to other negatively charged analytes, with the conditions that
407 their electrophoretic mobilities are smaller than the EO mobility during preconcentration and
408 at the same time higher than the EO mobility during the separation step.

409

410 **4. Conclusion**

411 In this study we demonstrate the successful development of a new approach for LVSS via
412 EOF modulation without recourse to any capillary coating or polymer addition. EOF can be
413 modulated in a wide range and quasi-totally suppressed just by changing the IS of the BGE.
414 New BGE compositions for CE-LIF were accordingly developed and the best constituents of
415 TEOA/Cit were explored to allow signal improvement (5-fold over conventional protocols)
416 and realization of this new LVSS mode (allowing signal enhancement by 200 times). This
417 preconcentration approach does not require any user's intervention for transition to the
418 subsequent separation step of enriched target molecules. The new mode of LVSS-CE is
419 simple and straightforward and can be implemented on any CE instrument. This opens
420 different alternatives of EOF-assisted preconcentration in fused silica capillaries, which were

421 utilized until now mainly for neutrally coated capillaries. These were successfully applied for
422 separation and detection of glycoprotein-derived N- glycans, potentially offering diagnosis
423 options for glycan-related diseases. Further improvement of glycan signals could be possible
424 in the future by combining the new BGEs with multiple-cycles of large volume sample
425 stacking, which is a recently developed electrokinetic preconcentration strategy [37].
426 Development of other modes of EOF-assisted preconcentration using these new BGE
427 compositions, as well as their exploitations for sensitive and selective determination /
428 characterization of biomolecules and nanometric entities with CE-LIF are envisaged.

429

430

431 *Acknowledgements*

432 The authors are grateful for the financial support by the Agence Nationale de la Recherche
433 (ANR, France) with the grant no. ANR-18-CE29-0005-01. Bin Yang gratefully
434 acknowledgements the China scholarship council for funding her Ph.D. scholarship. We
435 thank Dr. Gabor Jarvas (University of Debrecen, Hungary) for his help in glycan profile
436 interpretation

437

438

439

440

441

442

443

444

445

446

447

448

449
450
451
452
453
454
455
456
457
458
459
460
461
462
463
464
465
466
467
468
469
470
471
472
473

References

[1] P. Zhang, S. Woen, T. Wang, B. Liao, S. Zhao, C. Chen, Y. Yang, Z. Song, M.R. Wormald, C. Yu, P.M. Rudd, Challenges of glycosylation analysis and control: an integrated approach to producing optimal and consistent therapeutic drugs, *Drug Discov. Today*, 21 (2016) 740-765.

[2] M.H. Hu, Y. Lan, A. Lu, X.X. Ma, L.J. Zhang, Glycan-based biomarkers for diagnosis of cancers and other diseases: Past, present, and future, in: L. Zhang (Ed.) *Prog. Mol. Biol. Transl. Sci.*, 2019, pp. 1-24.

[3] B. Cylwik, M. Naklicki, L. Chrostek, E. Gruszewska, Congenital disorders of glycosylation. Part I. Defects of protein N-glycosylation, *Acta Biochim. Pol.*, 60 (2013) 151-161.

[4] T. Hennet, J. Cabalzar, Congenital disorders of glycosylation: a concise chart of glycoalyx dysfunction, *Trends Biochem. Sci.*, 40 (2015) 377-384.

[5] A.P. Corfield, M. Berry, Glycan variation and evolution in the eukaryotes, *Trends Biochem. Sci.*, 40 (2015) 351-359.

[6] A. Barroso, E. Gimenez, F. Benavente, J. Barbosa, V. Sanz-Nebot, Classification of congenital disorders of glycosylation based on analysis of transferrin glycopeptides by capillary liquid chromatography-mass spectrometry, *Talanta*, 160 (2016) 614-623.

[7] A. Bruneel, S. Cholet, T. Tran-Maignan, T.D. Mai, F. Fenaille, CDG biochemical screening: where do we stand? , *BBA - General Subjects*, 1864 (2020) 129652.

[8] G.Y. Qing, J.Y. Yan, X.N. He, X.L. Li, X.M. Liang, Recent advances in hydrophilic interaction liquid interaction chromatography materials for glycopeptide enrichment and glycan separation, *TrAC Trends Anal. Chem.*, 124 (2020).

- 474 [9] M.J. Kailemia, G.G. Xu, M. Wong, Q.Y. Li, E. Goonatileke, F. Leon, C.B. Lebrilla,
475 Recent Advances in the Mass Spectrometry Methods for Glycomics and Cancer, *Anal.*
476 *Chem.*, 90 (2018) 208-224.
- 477 [10] A. Banazadeh, L. Veillon, K.M. Wooding, M. Zabet-moghaddam, Y. Mechref, Recent
478 advances in mass spectrometric analysis of glycoproteins, *Electrophoresis*, 38 (2017)
479 162-189.
- 480 [11] G. Lu, C.L. Crihfield, S. Gattu, L.M. Veltri, L.A. Holland, Capillary Electrophoresis
481 Separations of Glycans, *Chem. Rev.*, 118 (2018) 7867-7885.
- 482 [12] V. Mantovani, F. Galeotti, F. Maccari, N. Volpi, Recent advances in capillary
483 electrophoresis separation of monosaccharides, oligosaccharides, and polysaccharides,
484 *Electrophoresis*, 39 (2018) 179-189.
- 485 [13] M. Alexovič, Y. Dotsikas, P. Bober, J. Sabo, Achievements in robotic automation of
486 solvent extraction and related approaches for bioanalysis of pharmaceuticals, *J.*
487 *Chromatogr. B*, 1092 (2018) 402-421.
- 488 [14] R.A. Evangelista, M.S. Liu, F.T.A. Chen, Characterization of 9-aminopyrene-1, 4, 6-
489 trisulfonate derivatized sugars by capillary electrophoresis with laser-induced
490 fluorescence detection, *Anal. Chem.*, 67 (1995) 2239-2245.
- 491 [15] L.R. Ruhaak, G. Zauner, C. Huhn, C. Bruggink, A.M. Deelder, M. Wuhrer, Glycan
492 labeling strategies and their use in identification and quantification, *Anal. Bioanal.*
493 *Chem.*, 397 (2010) 3457-3481.
- 494 [16] Sciex, Fast Glycan Labeling & Analysis: Sensitive CE-LIF Detection with Automated
495 Glycan Identification, [https://sciex.com/events/fast-glycan-webinar-1017-andras-](https://sciex.com/events/fast-glycan-webinar-1017-andras-guttman)
496 [guttman](https://sciex.com/events/fast-glycan-webinar-1017-andras-guttman), (2018).

- 497 [17] Agilent, CE-LIF glycans,
498

- 521 preconcentration by isotachopheresis and stacking, *J. Chromatogr. A*, 1565 (2018) 138-
522 144.
- 523 [27] E. Fukushima, Y. Yagi, S. Yamamoto, Y. Nakatani, K. Kakehi, T. Hayakawa, S. Suzuki,
524 Partial filling affinity capillary electrophoresis using large-volume sample stacking with
525 an electroosmotic flow pump for sensitive profiling of glycoprotein-derived
526 oligosaccharides, *J. Chromatogr. A*, 1246 (2012) 84-89.
- 527 [28] T. Kawai, M. Ueda, Y. Fukushima, K. Sueyoshi, F. Kitagawa, K. Otsuka, Toward 10
528 000-fold sensitivity improvement of oligosaccharides in capillary electrophoresis using
529 large-volume sample stacking with an electroosmotic flow pump combined with field-
530 amplified sample injection, *Electrophoresis*, 34 (2013) 2303-2310.
- 531 [29] T. Kawai, M. Watanabe, K. Sueyoshi, F. Kitagawa, K. Otsuka, Highly sensitive
532 oligosaccharide analysis in capillary electrophoresis using large-volume sample stacking
533 with an electroosmotic flow pump, *J. Chromatogr. A*, 1232 (2012) 52-58.
- 534 [30] Phoebus,
535 http://5.189.177.170/~nalis/site/objects/media/0/0/5/0/9/0050933_media/media1.pdf.
- 536 [31] P. Kuban, P.C. Hauser, Ten years of axial capacitively coupled contactless conductivity
537 detection for CZE - a review, *Electrophoresis*, 30 (2009) 176-188.
- 538 [32] A.J. Zemann, Conductivity detection in capillary electrophoresis, *TrAC Trends Anal.*
539 *Chem.*, 20 (2001) 346-354.
- 540 [33] B.B. VanOrman, G.G. Liversidge, G.L. McIntire, T.M. Olefirowicz, A.G. Ewing, Effects
541 of buffer composition on electroosmotic flow in capillary electrophoresis, *J.*
542 *Microcolumn Separations*, 2 (1990) 176-180.
- 543 [34] J.C. Reijenga, T. Verheggen, J. Martens, F.M. Everaerts, Buffer capacity, ionic strength
544 and heat dissipation in capillary electrophoresis, *J. Chromatogr. A*, 744 (1996) 147-153.

- 545 [35] P. Kubáň, P.C. Hauser, 20th anniversary of axial capacitively coupled contactless
546 conductivity detection in capillary electrophoresis, *TrAC Trends Anal. Chem.*, 102
547 (2018) 311-321.
- 548 [36] B.A. Williams, C. Vigh, Fast, accurate mobility determination method for capillary
549 electrophoresis, *Anal. Chem.*, 68 (1996) 1174-1180.
- 550 [37] C.C. de Lassichere, T.D. Mai, M. Otto, M. Taverna, Online Preconcentration in
551 Capillaries by Multiple Large-Volume Sample Stacking: An Alternative to
552 Immunoassays for Quantification of Amyloid Beta Peptides Biomarkers in
553 Cerebrospinal Fluid, *Anal. Chem.*, 90 (2018) 2555-2563.
- 554 [38] T.D. Mai, F. d'Orlye, A. Varenne, A Comprehensive Study of Silanization and Co-
555 Condensation for Straightforward Single-Step Covalent Neutral Capillary Coating,
556 *Chromatographia*, 78 (2015) 775-783.
- 557 [39] F. Kohlrausch, Ueber Concentrations-Verschiebungen durch Electrolyse im Inneren von
558 Lösungen und Lösungsgemischen, *Ann. Phys. Chem.* , 298 (1897) 209-239.
- 559 [40] V. Hruška, B. Gaš, Kohlrausch regulating function and other conservation laws in
560 electrophoresis, *Electrophoresis*, 28 (2007) 3-14.
- 561 [41] A. Kamgar, A. Bakhtyari, S. Mohsenpour, C. D'Agostino, G.D. Moggridge, M.R.
562 Rahimpour, Mutual diffusion in concentrated liquid solutions: A new model based on
563 cluster theory, *J. Mol. Liq.*, 232 (2017) 516-521.
- 564 [42] D. Corradini, G. Cannarsa, E. Fabbri, C. Corradini, Effects of alkylamines on
565 electroosmotic flow and protein migration behaviour in capillary electrophoresis, *J.*
566 *Chromatogr. A*, 709 (1995) 127-134.
- 567 [43] A. Bruneel, S. Cholet, V. Drouin-Garraud, M.L. Jacquemont, A. Cano, A. Megarbane, C.
568 Ruel, D. Cheillan, T. Dupre, S. Vuillaumier-Barrot, N. Seta, F. Fenaille,
569 Complementarity of electrophoretic, mass spectrometric, and gene sequencing

570 techniques for the diagnosis and characterization of congenital disorders of
571 glycosylation, *Electrophoresis*, 39 (2018) 3123-3132.

572 [44] F. Kitagawa, T. Kawai, K. Otsuka, On-line sample preconcentration by large-volume
573 sample stacking with an electroosmotic flow pump (LVSEP) in microscale
574 electrophoresis, *Anal Sci*, 29 (2013) 1129-1139.

575 [45] J.N. Arnold, M.R. Wormald, R.B. Sim, P.M. Rudd, R.A. Dwek, The Impact of
576 Glycosylation on the Biological Function and Structure of Human Immunoglobulins,
577 *Annu. Rev. Immunol.*, 25 (2007) 21-50.

578 [46] G. Lu, L.A. Holland, Profiling the N-Glycan Composition of IgG with Lectins and
579 Capillary Nanogel Electrophoresis, *Anal. Chem.*, 91 (2019) 1375-1383.

580 [47] A. Guttman, M. Szigeti, A. Lou, M. Gutierrez, Fast Glycan Labeling and Analysis :
581 High-Resolution Separation and Identification in Minutes,
582 [https://www.sciex.com/products/consumables/fast-glycan-analysis-and-labeling-for-the-](https://www.sciex.com/products/consumables/fast-glycan-analysis-and-labeling-for-the-pa-800-plus)
583 [pa-800-plus](https://www.sciex.com/products/consumables/fast-glycan-analysis-and-labeling-for-the-pa-800-plus), (2018).

584

585

586

587

588

589

590

591

592

593

594

595

596

597

598

599

600

601

602

603

604

605 **Table captions:**

606 **Table 1.** List of BGE compositions at ionic strength of 150 mM and pH of 4.75, as simulated
 607 with Phoebus program for a use in a fused silica capillary of 50 μ m i.d. x 65cm length. The
 608 currents were calculated by the Phoebus program for the pre-defined voltage of 30 kV.

BGE compositions	I (μ A) at 30kV	buffer capacity (mmol/l.pH)	Remark
LiOH 25mM + Acetic acid 47 mM (IS 25 mM)	16	28	Reference BGE
TEOA 150 mM + Acetic acid 266 mM (IS 150 mM)	21	155	Expected good quality
TEOA 150 mM + Citric acid 58 mM (IS 150 mM)	31	44	Expected good quality
β -Ala 1052 mM + Trimellitic acid 30 mM (IS 150 mM)	19	185	Expected good quality
β -Ala 861 mM + Acetic acid 127 mM (IS 150 mM)	57	506	High current generation
β -Ala 861 mM + Pyromellitic Acid 19 mM (IS 150 mM)	16	152	Poor solubility of pyromellitic acid
TEOA 150 mM + Sorbic Acid 270 mM (IS 150 mM)	33	158	poor solubility of sorbic acid
TEOA 150 mM + Gluconic acid 160 mM (IS 150 mM)	27	20	poor solubility of gluconic acid
TEOA 150 mM + aspartic acid 166 mM (IS 150 mM)	31	34	poor solubility of aspartic acid
TEOA 150 mM + anisic acid 210 mM (IS 150 mM)	29	100	poor solubility of anisic acid
TEOA 150 mM + furoic acid 210 mM (IS 150 mM)	31	7	poor solubility of furonic acid

609

610

611

612 **Table 2:** Comparison of the salient data obtained with different BGEs for CE-LIF of613 oligosaccharides, using uncoated fused silica capillaries (50 μm I.D., 65 cm total length)

BGE compositions	Number of DP detected over a 20 min run	Signal / noise ratio for specific DP peaks		RSD % for migration time (n = 3)		RSD % for peak area (n = 3)	
		DP1	DP6	DP1	DP6	DP1	DP6
LiOH / AcOH 25 mM	6	64	48	0.92	0.30	1.37	2.46
β -Ala / Trimel 150 mM	6	366	101	0.67	1.42	16.1	27.4
β -Ala / AcOH 150 mM	4	414		0.83		0.46	
TEOA / AcOH 150 mM	12	646	149	0.28	0.42	1.51	0.59
TEOA / Cit 150 mM	17	659	260	0.26	0.21	4.46	1.06

614 * DP: degree of polymerization of glucose oligomers

615

616

617

618

619

620

621

622

623

624

625

626

627

628

629

630 **Figure captions:**

631 Fig. 1. A) Working principle of the novel BGEs for CE-LIF of oligosaccharides. The ionic
632 strengths (IS) of the BGE composed of large weakly charged molecules are increased
633 to extremely high levels to allow high stacking of target analytes and at the same time
634 suppression of EOF without recourse to any capillary coating. Oligosaccharides can be
635 prepared in water or diluted BGE.

636 B) Principle of large volume sample stacking with EOF modulation and suppression in
637 an uncoated fused silica capillary used in this study. This mode allows two completely
638 different EOF magnitudes (via variation of the IS of the BGE) for sample
639 preconcentration and for the separation of the stacked analytes.

640

641 Fig. 2. CE-LIF of oligosaccharides using different BGE compositions at pH 4.75. **A)** LiOH /
642 AcOH IS of 25 mM (LiOH 25mM + AcOH 47 mM); **B)** β -Ala / Trimellitic acid IS of
643 150 mM (β -Ala 1052 mM and Trimellitic acid 30 mM); **C)** β -Ala / AcOH IS of 150
644 mM (β -Ala 861 mM and AcOH 127 mM) ; **D)** TEOA / AcOH IS of 150 mM (TEOA
645 150 mM and AcOH 266 mM); **E)** TEOA / Cit IS of 150 mM (TEOA 150 mM and Cit
646 58 mM). *F* denotes for residual fluorescent peaks. CE conditions: fused silica
647 capillary, 50 μ m i.d., 50/60 cm, hydrodynamic injection at 50 mbar for 10 s, high
648 voltage of -25 kV.

649

650 Fig. 3: CE-LIF of oligosaccharides using TEOA/Cit BGE at IS of **A)** 150 mM; **B)** 200 mM;
651 **C)** Commercial Sciex BGE. *F* denotes for residual fluorescent peaks. CE conditions as
652 in Fig. 2

653

654 Fig. 4 CE-LIF of N-glycans from human serum of healthy control and CDG individuals,
655 using BGE composed of TEOA / Cit 200 mM in an uncoated silica capillary. A)
656 Control patient, B) B4GALT1-CDG patient and C) MGAT2-CDG patient. Other CE
657 conditions as in Fig. 2.

658
659 Fig. 5: CE-LIF with and without large volume sample stacking (LVSS) with EOF modulation
660 of oligosaccharides, using BGE composed of TEOA/Cit at IS of 200 mM. **A)** LVSS-
661 CE-LIF of oligosaccharides 200,000x dilution; **B)** CE-LIF of oligosaccharides 2000x
662 dilution. Other conditions as in Fig. 2.

663
664 Fig. 6: **A)** CE-LIF of N-glycans released from human IgG; **B)** LVSS-CE-LIF of human IgG
665 glycans using TEOA/Cit BGE at IS of 200 mM. Other CE conditions as in Fig. 2.

666
667
668
669
670
671
672
673
674
675
676
677
678
679

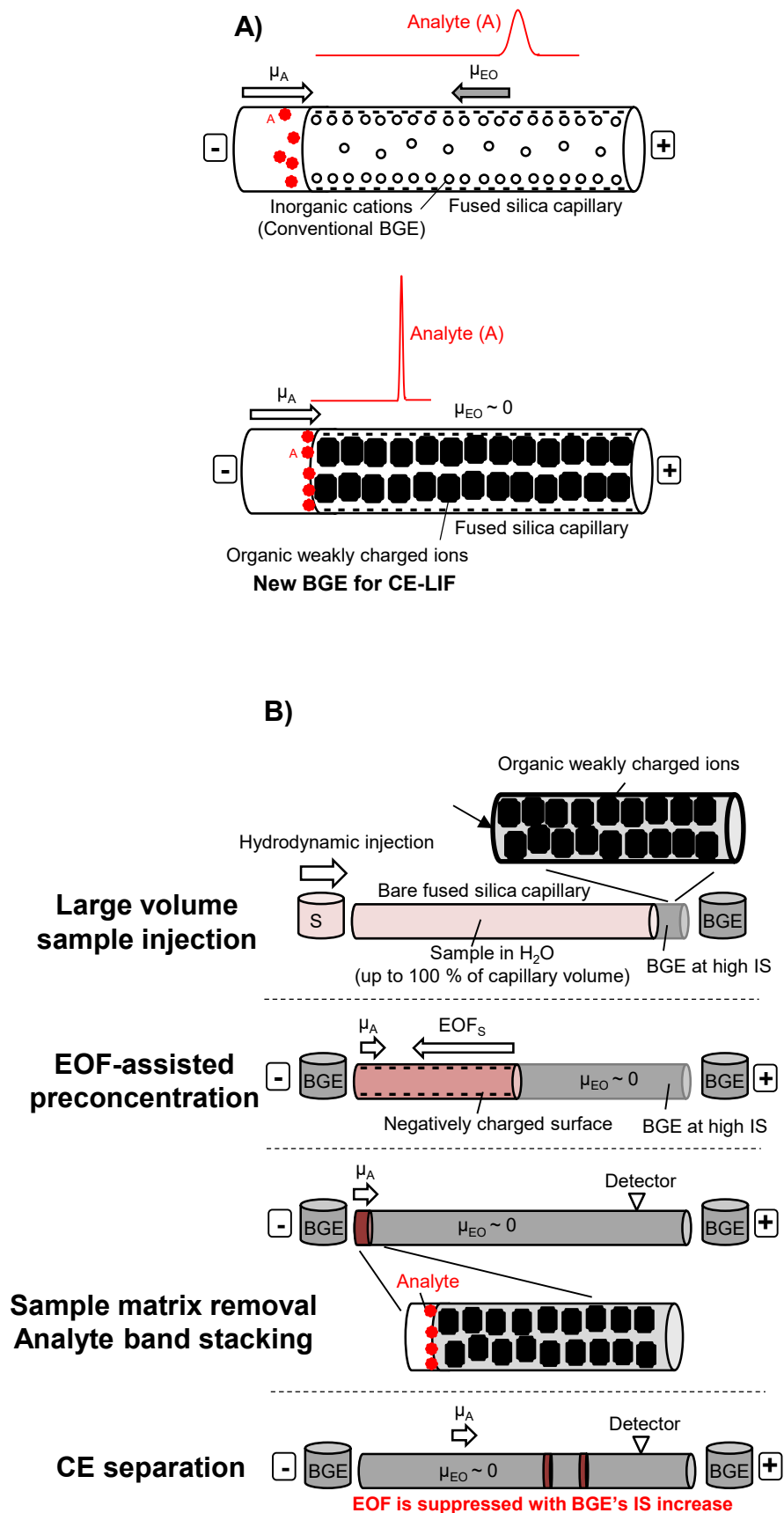


Figure 1

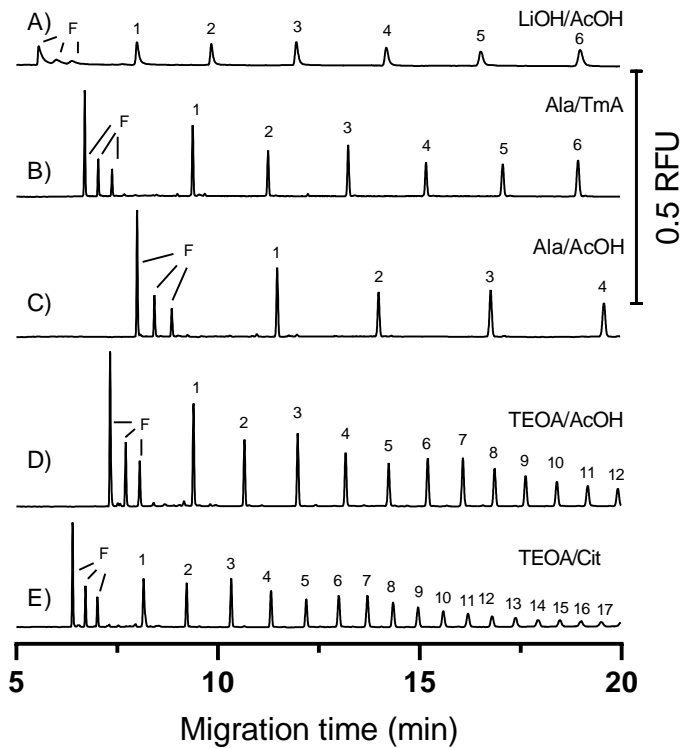


Figure 2

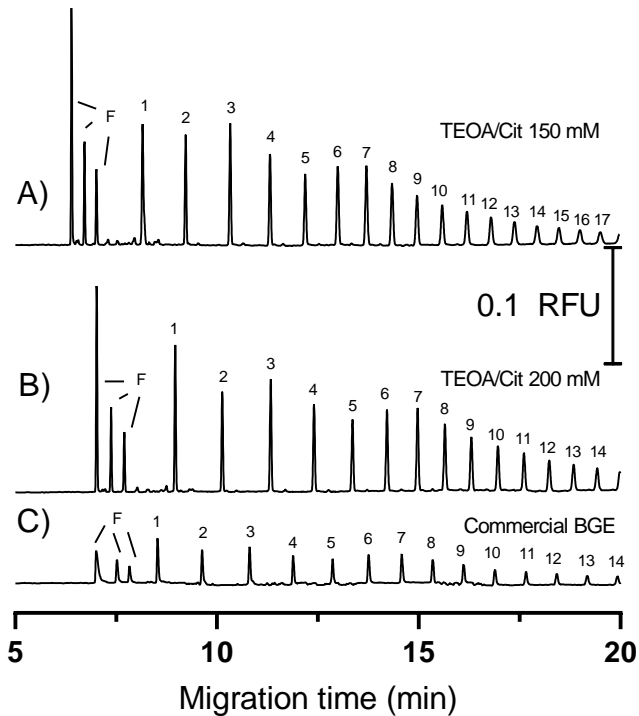


Figure 3

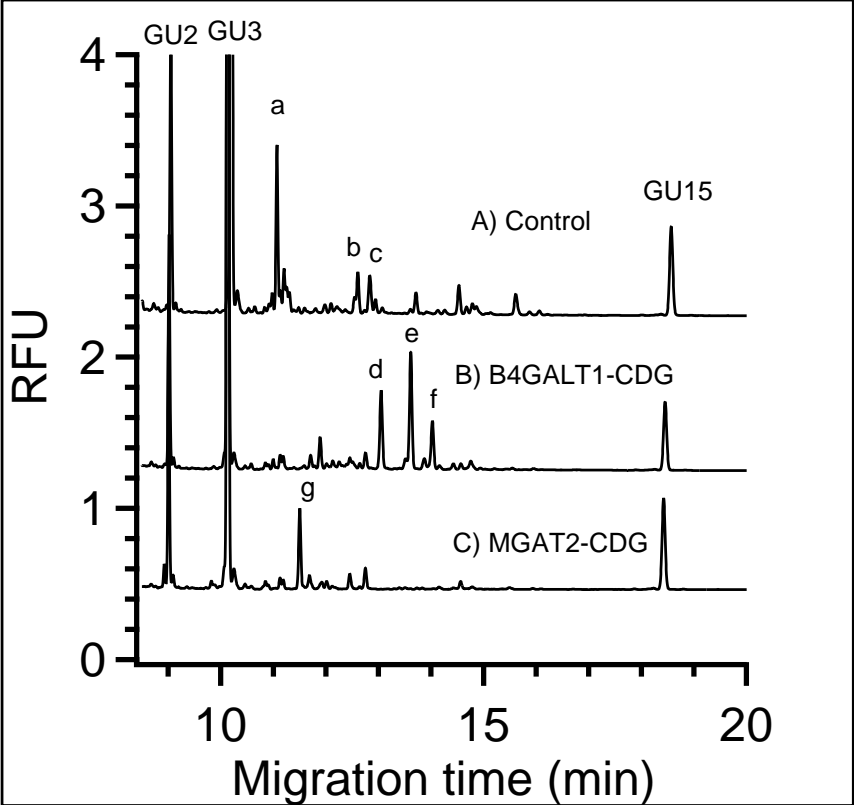


Figure 4

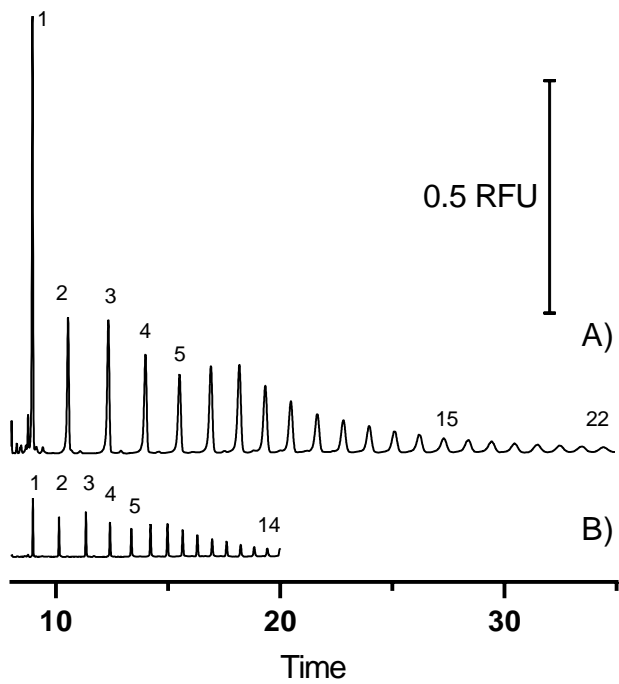


Figure 5

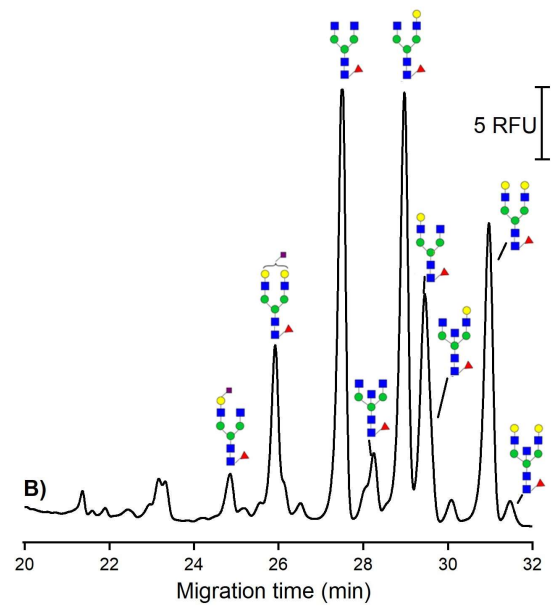
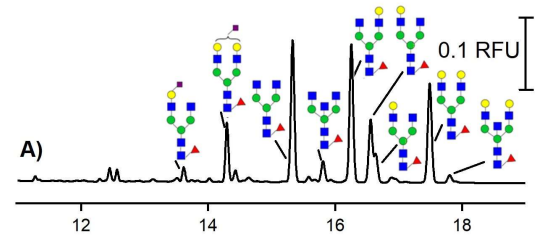


Figure 6

III.3. Development of a new droplet-based sample treatment strategy for CE-LiF of glycans

The second strategy we used in this thesis to improve the performance for CE-LiF of glycans was to implement the forefront sample treatment required in a microfluidic droplet format in order to achieve high throughput, no cross contamination, improved efficiency and automation. So far, the gold standard method used to release and label glycans prior to their CE-LiF separation and detection is performed in 200 μ L PCR tubes and consists of the following steps (normally in manual operations, see [Figure 43](#)):

- A. Glycoproteins (standard or biological samples diluted in deionized water) are denatured and enzymatically released using PNGase F.
- B. Magnetic beads coated with COOH groups are used as for solid phase extraction: when in the presence of \sim 90% ACN, glycans aggregate on the magnetic beads and can be extracted using a magnet.
- C. Extracted glycans are labeled with APTS by reductive amination in the presence of acetic acid and NaBH_3CN in THF.
- D. Glycans are purified with consecutive rinsing steps using magnetic beads.
- E. Purified glycans are eluted in deionized water and analyzed by CE.

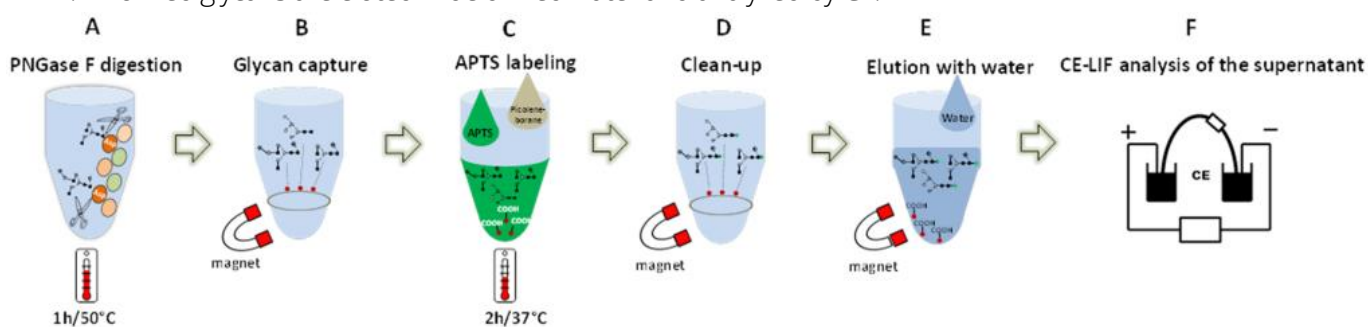


Figure 43 : Steps of the magnetic bead-based protocol for glycan sample treatment prior to CE-LiF. From [170].

Our aim is to develop a lab in droplet platform (see the instrumental development in the next chapter) and the respective method in order to translate the in-tube batchwise protocol into a microdroplet-based one that allows little sample / reagent consumption, full automation and no cross contamination from external environment.

In this development, we still exploited the advantage of magnetic beads for controllable transfer of analytes. To manipulate the magnetic beads, the magnetic tweezer technology was employed. Magnetic tweezers indeed are soft ferromagnetic tips surrounded with electrical coils. The magnetic field can be triggered on and off by activating / deactivating the electric current through the coils. To trap and release magnetic beads from one droplet to another, one can place two tweezers facing each other across a capillary with their tip close to the capillary and create a strong magnetic field gradient strong enough to attract paramagnetic beads suspended into droplets flowing in inert oil inside the capillary [289]. As illustrated in [Figure 44](#) A) a), b) and c), when the trailing edge of a droplet containing magnetic particles approaches the tweezer, the magnetic forces acting on the magnetic beads cluster deforms the droplet. If the magnetic forces overcome the interfacial forces while the viscous drag on the main droplet overcomes both forces ($F_{\text{drag}} > F_{\text{mag}} > F_{\text{cap}}$) then the droplet will split in two: a small droplet representing \sim 1-2% of the total volume containing the magnetic beads which stays at the tweezer, and a big droplet

containing the rest of the volume and being dragged by the oil flow. Since the droplet containing the magnetic bead cluster is immobilized by the magnetic field, the resuspension of the magnetic beads into a new droplet requires a change in the force equilibrium (Figure 44 A d)). Indeed, for the resuspension of the droplet (Figure 44 A e) and f)), the small droplet containing the beads first coalesces with the incoming droplet. If the magnetic tweezers are then deactivated, the beads are suspended inside the new droplet.

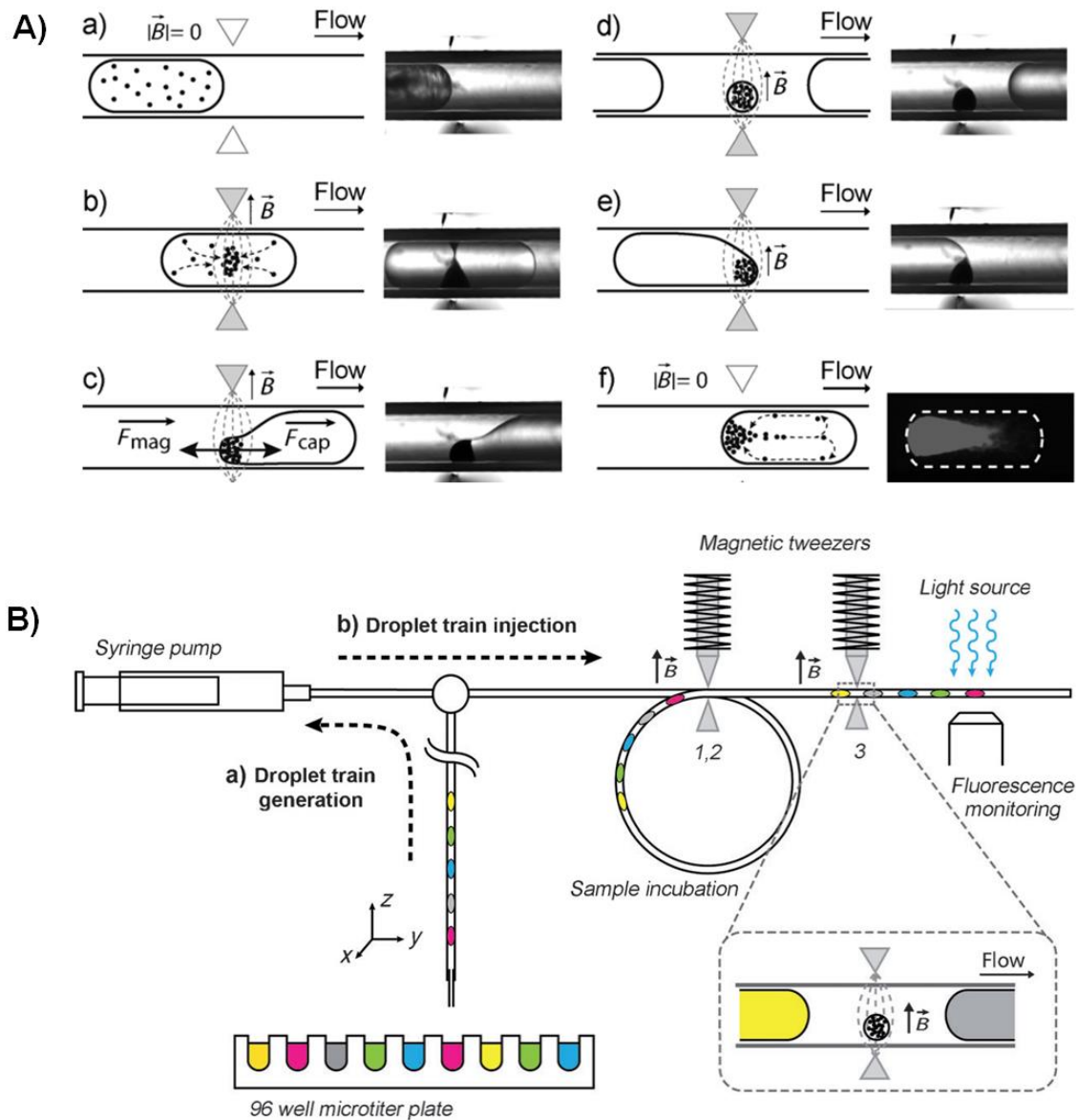


Figure 44: Working principle of the microfluidic platform combining droplets and magnetic tweezers: A) Extraction and resuspension of magnetic beads inside droplets and B) Automatic system for droplet handling composed of a 96 well microtiter plate, a X, Y, Z translation arm and a syringe pump. Adapted from [288].

Because the cornerstone of both the glycan sample preparation method for CE-LiF and the magnetic tweezer microfluidic technology comes from magnetic beads, our strategy for improving the forefront sample treatment of glycans for CE-LiF was to adapt the gold standard protocol performed in 200 μ L PCR tubes in a microfluidic droplets format using the magnetic tweezer technology and magnetic beads. For this purpose, we have collaborated with a French startup (Inorevia, created in 2016®) to exploit the

magnetic tweezer technology and automatic handling of droplets for life science applications. In this collaboration, Inorevia provided us a personalized prototype (called Magelia®) that were constructed according to our specifications needed for glycan sample treatment. Details of the development using the Magelia system is presented in the following article.

Article 3: Lab-in-droplet: From glycan sample treatment toward diagnostic screening of congenital disorders of glycosylation.

1 **Lab-in-droplet: from glycan sample treatment toward diagnostic screening of congenital**
2 **disorders of glycosylation**

3

4 **Théo Liénard--Mayor¹, Camille Bricteux¹, Amel Bendali², Nguyet-Thuy Tran¹, Arnaud**
5 **Bruneel^{3,4}, Myriam Taverna^{1,5}, Thanh Duc Mai^{1*}**

6

7 ¹ *Université Paris-Saclay, CNRS, Institut Galien Paris-Saclay, 92296, Châtenay-Malabry,*
8 *France.*

9 ² *Inorevia, 29 rue du Faubourg St Jacques, 75014 Paris, France*

10 ³ *AP-HP, Biochimie Métabolique et Cellulaire, Hôpital Bichat-Claude Bernard, Paris, France*

11 ⁴ *Université Paris-Saclay, INSERM UMR1193, 92296 Châtenay-Malabry, France*

12 ⁵ *Institut Universitaire de France (IUF)*

13

14 * Corresponding author

15 e-mail: thanh-duc.mai@u-psud.fr

16

17 **Keywords:** microfluidic droplet; capillary electrophoresis; fluorescent detection; N-glycans;

18 Congenital Disorders of Glycosylation

19

20

21

22

23

24

25 <https://doi.org/10.1016/j.aca.2022.340150>

26 **Abstract**

27 We present in this study a new microfluidic droplet platform, named Lab-in-Droplet, for
28 multistep glycoprotein sample treatment. Several operations are required for the sample
29 treatment of a given glycoprotein to profile its N-glycans. In our case, all preparation steps for
30 the analysis of N-glycans from glycoproteins could be realized in an automatic manner and
31 without cross contamination. This could be achieved through several features that are not met
32 in previous droplet setups, notably full automation, droplet sensing and heating. The magnetic
33 tweezer technology was employed to manipulate (capture and release) coated magnetic beads
34 used as analyte cargos over droplets. Droplets ranging from 1 - 10 μ L play the role of
35 confined microreactors, allowing to realize several steps that involve advanced functions such
36 as heating and mixing with organic solvents. A complex sample treatment protocol that has
37 been feasible so far only in batchwise mode can now be converted into a novel microfluidic
38 version. With this Lab-in-Droplet, we can enzymatically release and fluorescently label N-
39 linked oligosaccharides from Human Immuglobulin G and then off-line analyze the labeled
40 glycans by capillary electrophoresis with laser induced fluorescent detection. We
41 demonstrated the superiority of this Lab-in-Droplet over the conventional batchwise protocol,
42 with 10-fold less reagent consumption, 3-fold less time, and 2-fold improvement of glycan
43 labeling yield, without degradation of glycan separation profile obtained by capillary
44 electrophoresis. The platform with the developed droplet protocol was applied successfully
45 for mapping N-linked glycans released from human sera, serving for diagnostic screening of
46 congenital disorders of glycosylation.

47

48

49

50

51 **1. Introduction**

52 Glycosylated proteins represent half the number of all secretory and human cellular proteins.
53 Regular functioning and activity of glycoproteins can be harmed by an altered glycosylation
54 [1, 2]. This latter, which may result in unoccupied glycosylation sites, truncated antennae of
55 glycans, unexpected glycosidic linkages or glycan structures as well as changes in the
56 proportion of glycoforms for a given glycoprotein, can be the consequence of a pathological
57 state [3]. Indeed, several glycoproteins have been considered as potential or validated
58 biomarkers for diverse diseases such as cancer, cardiovascular diseases [4], chronic alcohol
59 abuse [5] or congenital disorders of glycosylation (CDG) [6]. CDG in particular represent a
60 family of more than 150 inherited diseases [6, 7]. Regarding the best known and most
61 frequent CDG affecting the N-linked glycosylation, two main types are considered: CDG-I
62 where some N-glycosylation sites are unoccupied and CDG-II where only subtle structural
63 changes of glycans occur [6]. For the latter where severe pathology must be diagnosed very
64 early on newborns, analysis of released glycans from glycoproteins is of great interest [4, 8].

65
66 Recently, capillary electrophoresis (CE) coupled with laser induced fluorescent (LIF)
67 detection has become an established method for glycan analysis [9, 10], with the introduction
68 of commercial kits [11, 12]. In a standard protocol, released glycans are first fluorescently
69 labeled with 8-aminopyrene-1,3,6 trisulfonic-acid (APTS, a negatively charged fluorophore)
70 and then separated by CE-LIF using acidic background electrolytes (BGEs) containing
71 polyethylene oxide (PEO) or polyethylene glycol (PEG) [13]. To cope with challenges for the
72 detection of low-abundant glycans used as biomarkers, efforts have been made toward glycan
73 enrichment methods based on solid phase extraction [14, 15] or electrokinetic phenomena
74 (notably isotachopheresis and large volume sample stacking preconcentration approaches)
75 [16-19] prior to CE-LIF. To further increase the detection sensitivity for CE-LIF of glycans

76 required for diagnosis of glycan-related diseases, we recently developed new BGE conditions
77 that allow much improvement of peak signals and capacity compared to those provided by
78 commercial kits [20].

79

80 The forefront sample treatment prior to the CE-LIF profiling of glycans is of extreme
81 importance and may have a crucial impact on the glycan separation efficiency and
82 reproducibility. A typical protocol for such purpose includes glycoprotein denaturation,
83 enzymatic deglycosylation with PNGase F (Peptide-N-glycosidase F, to release asparagine-
84 linked oligosaccharides from glycoproteins), residual protein removal, fluorescent labeling of
85 released glycans with APTS [21]), glycan washing and removal of residual fluorophores, and
86 finally elution of labeled glycans for subsequent CE-LIF analysis. The batchwise tube-based
87 approach developed by Guttman *et al.* that employs magnetic beads as the solid support to
88 realize these steps has become now the gold standard method [22-24], with the recent
89 introduction of a commercial kit [11]. This approach that contains different manual in-vial
90 operations and requires relatively high starting concentrations of glycoproteins has been
91 mostly applied for the purpose of drug discovery and development [11]. Based on this
92 method, Perkin-Elmer developed recently a microchip-CE platform that transposes the in-vial
93 operations into a 96-well microtiter-plate-based protocol to release and label N-glycans prior
94 to their separation using microchip electrophoresis [25].

95

96 In a related context, microfluidics with its inherent advantages of reduced sample and reagents
97 consumption, and shorter reaction time has gained much attention for sample processing [26].
98 Interestingly, while microfluidics-based sample handling was developed for deglycosylation
99 prior to HPLC separation and / or MS detection of released glycans [27], this miniature
100 approach has never been reported for forefront sample processing for downstream CE-LIF of

101 glycans, to the best of our knowledge. Indeed, glycan sample treatment for CE-LIF requires
102 several steps other than deglycosylation that involve advanced functions (e.g., heating and
103 mixing with organic solvents), which can hardly be down-scaled without any risk of cross
104 contamination between steps. This may be a reason for this delay of development despite the
105 high potential of microfluidics. From our viewpoint, recourse to droplet microfluidics, an
106 emerging branch of microfluidics that allows creation and manipulation of discrete droplets
107 considered as micro-reactors inside microfluidic channels [28], could be a solution to
108 overcome such challenge. Accordingly, we present in this study a new instrument, named
109 Lab-in-Droplet, and its respective protocol for glycan sample treatment in microfluidic
110 droplets, serving as a forefront for CE-LIF of glycans. New functions that have not been
111 developed in previous droplet systems, including droplet fusion with organic solvents, droplet
112 heating and droplet sensing for automation of the protocol, are explored and exploited for
113 protein denaturation, enzymatic release of N-glycans, residual protein removal, fluorescent
114 glycans labeling, washing and elution to provide an automatic process and avoid cross
115 contamination. The system was applied to the N-glycan mapping of human Immuglobulin G
116 (IgG) and then to total N-glycans released from human serum glycoproteins. We exploited the
117 profiles obtained from both a healthy and a CDG patient after the processing with Lab-in-
118 Droplet to serve for diagnostic screening of CDG.

119

120 **2. Experimental**

121 **2.1. Chemicals, reagents and samples**

122 All chemicals for preparation of buffers were of analytical or reagent grade and purchased
123 from Sigma-Aldrich (Lyon, France). Reagents for preparation of glycans (denaturation,
124 digestion, labeling solutions; malto-oligosaccharides (MD ladder), APTS dye, magnetic beads
125 and G3 standard) were obtained from the Fast Glycan Analysis and Labeling kit from Sciex

126 (Villebon sur Yvette, France). Human Immunoglobulin G, PNGase F and sodium
127 cyanoborohydride were purchased from Sigma-Aldrich (Lyon, France). For the preparation of
128 background electrolyte (BGE) solutions, Triethanolamine (TEOA) and citric acid (Cit) were
129 used. The analyzed serum samples came from the biochemistry department of Bichat Hospital
130 (Assistance Publique - Hôpitaux de Paris, France). This department is officially accredited
131 (French Committee of Accreditation COFRAC -ISO15189 under the number: 8-3490) and is
132 officially recognized as a "Reference Medical Biology Laboratory" (RMBL) in the field of
133 Congenital Disorders of Glycosylation (CDG). All ethical requirements were met to obtain
134 related official agreements. Informed consents were obtained from the adult representative(s)
135 of all tested individuals. Fluorinated oil containing surfactant was obtained from Inorevia
136 (Paris, France).

137

138 **2.2. Apparatus and Material**

139 The CE experiments were performed with a Beckman Coulter PA800+ system (Sciex, Brea,
140 CA) coupled with a LIF detector ($\lambda_{\text{excitation}}$: 488 nm, $\lambda_{\text{emission}}$: 520 nm). 32Karat ver 8.0
141 software (Sciex) was used to carry out the instrument control and the data acquisition.
142 Separations were performed with a fused silica capillary of 50 μm id and 375 μm od from
143 Polymicro (TSP075375, CM Scientific, Silsden, UK), with the total length (L_{tot}) of 60 cm, the
144 effective length (L_{eff}) of 50 cm. Deionized water was produced using a Direct-Q3 UV
145 purification system (Millipore, Milford, MA, USA). The measure of the pH values of buffer
146 solutions and samples were done with a SevenCompact pH meter (Mettler Toledo,
147 Schwerzenbach, Switzerland). Selection of BGE and buffer ionic strength (IS) calculations
148 were based on simulations with the computer program PhoeBus (Analis, Suarlée, Belgium).
149

150 The instrument for droplet handling was developed by Inorevia (Paris, France) according to
151 the criteria and parameters pre-defined by our group (see Fig. S1 in the electronic supporting
152 information (ESI)). It includes a stepper-motor-driven syringe pump with a 250 μL syringe
153 connected to a 3-port selector valve, a magnetic tweezer, two thermal modules and three
154 optical detectors. PTFE tubing is used for all connections. The outlet of the PTFE tubing can
155 be moved into different vials in a vial holder thanks to a robotic arm. Up to 14 vials can be
156 used to load reagents, sample solutions, magnetic beads, oil and for trash reservoir. More
157 details regarding system design can be referred to section 3.1.

158

159 **2.3. Methods**

160 *Fluorescent labelling of standard malto-oligosaccharides (MD ladder) in tube*

161 The protocol for fluorescent labelling of MD ladder was adapted from that by Reider *et al.* [22].
162 Briefly, 50 μL of beads was added in a 200 μL PCR tube. After removing the supernatant, 10
163 μL of MD ladder (0.1 mg/mL in deionized water) and 200 μL of acetonitrile (ACN) were added.
164 After mixing, the supernatant was removed. Then, labelling reagents, including 11 μL of 40
165 mM APTS in 20% AcOH, 1 μL of 1 M NaBH_3CN and 1 μL of NP-40 were added into the
166 sample vial and incubated for 20 min at 60°C with opened cap. ACN 90 % was then added to
167 labelled glycans jammed on magnetic beads while the supernatant containing excess of
168 fluorophore was removed. The elution of glycans captured on magnetic beads was then
169 performed with 20 μL of water.

170

171 *Enzymatic release and fluorescent labelling of glycoprotein-derived-glycans in batch*

172 10 μL of IgG (10 mg/mL in deionized water) was mixed with 5 μL of the denaturing solution
173 containing 10 μL of D1, 10 μL of D3 and 50 μL of D4 from the ‘fast glycan labelling and
174 analysis’ kit from Sciex and incubated at room temperature for 7 min. After denaturation, 12

175 μL of the digestion solution containing 1 μL of PNGase F in 11 μL of D4 was added and further
176 incubated for 20 minutes at 60°C. The obtained solution containing released N-glycans was
177 added to a 200 μL PCR tube containing 50 μL of beads without supernatant. The labelling step
178 was then carried out following the protocol described in [22]. Briefly, labelling reagents (11 μL
179 of 40 mM APTS in 20% AcOH, 1 μL of 1 M NaBH₃CN and 1 μL of NP-40) were added into
180 the sample vial and incubated for 20 min at 60°C with opened cap. ACN 90 % was then added
181 to jam labelled glycans on magnetic beads while the supernatant containing excess of
182 fluorophore was removed. The elution of glycans captured on magnetic beads was then
183 performed with 20 μL of water. This eluent was subsequently analysed with CE-LIF.

184

185 For the preparation of N-glycans from human serum samples, the magnetic beads delivered in
186 the ‘fast glycan labelling and analysis’ kit from Sciex were used for sample purification. The
187 tube containing 200 μL of resuspended magnetic beads was placed in a magnetic stand to allow
188 the beads migrating to the magnet, then the storage buffer was removed. This step was
189 performed every time to remove any liquid from the beads. 10 μL of serum sample (4-fold
190 diluted in water) was added onto the beads. 5 μL of denaturing solution was then added, mixed
191 and incubated at room temperature for 7 min with the vial opened. 11 μL of digestion solution
192 from the ‘fast glycan labelling and analysis’ kit from Sciex was added to the mixture; and
193 incubated at 60°C for 20 min in an open vial. 200 μL of ACN was then added, mixed and
194 incubated at room temperature for 1 min. The supernatant was removed, and 9 μL of 40 mM
195 APTS in 20% acetic acid, 1 μL of NaCNBH₃ et 1 μL of D4 from the ‘fast glycan labelling and
196 analysis’ kit from Sciex was added, followed by incubation at 60 °C for 20 min in an open vial.
197 The subsequent washing and elution steps were then carried out as for the case of IgG.

198

199 *Fluorescent labelling of standard malto-oligosacharrides in droplets*

200 A total of 2.5 μ L of magnetic bead suspension (10 mg/mL) was aspirated in the microfluidic
201 droplet device. The magnetic tweezer was then activated to trap the beads and the supernatant
202 was discarded to the trash tube. The trapped beads were then suspended in a 1 μ L of MD ladder
203 (0.1 mg/mL in deionized water). 7 μ L of ACN was then merged with the droplet containing the
204 beads and the MD ladder. After a 5 min incubation, the supernatant was removed. The beads
205 were then resuspended in a 1 μ L droplet of the labelling solution (40 mM APTS in 20% AcOH
206 / 1 M NaBH₃CN / NP-40 of 9/1/1 v:v ratio). The mixture was incubated for 20 min at 60°C.
207 This droplet was then merged with 9 μ L of ACN to jam labelled MD ladder on beads; and the
208 supernatant droplet containing residual APTS was moved to the trash vial. Elution of captured
209 MD ladder was then performed in 6 μ L of water. This eluent was subsequently analysed with
210 CE-LIF. Further information about the microfluidic device parameters for each step can be
211 found in Table 1.

212

213 *Denaturation, digestion, and fluorescent labelling of glycoprotein derived-glycans in droplets*

214 A total of 2.5 μ L of magnetic bead suspension (10 mg/mL) was aspirated in the microfluidic
215 droplet device. The magnetic tweezer was then activated to trap the beads and the supernatant
216 was discarded to the trash tube. The beads were subsequently suspended in a 2 μ L droplet of
217 standard IgG (10 mg/mL) in PBS, or serum diluted 4 times in water. The droplet containing the
218 beads and the sample was merged with 1 μ L of denaturation solution that contains SDS, DTT
219 and NP-40 at v:v ratio of 1/1/5. After incubation over 7 min, the obtained droplet (3 μ L) was
220 merged with 2.4 μ L of digestion solution containing NP-40 and PNGase F at v:v ratio of 11/4.
221 The 5.4 μ L droplet was incubated during 20 min at 60°C. The beads were then captured by the
222 tweezer and the solution was recovered in a vial. 1 μ L of the recovered solution was then
223 aspirated and the beads were resuspended in it. A droplet of 7 μ L ACN was then merged with
224 this droplet. After incubation over 5 min, the beads were retained at the tweezer and the

225 supernatant was removed. The beads were then resuspended in a 1 μ L droplet of the labelling
226 solution (40 mM APTS in 20% AcOH / 1 M NaBH₃CN / NP-40 of 9/1/1 v:v ratio). The mixture
227 was incubated for 20 min at 60°C. This droplet was then merged with 9 μ L of ACN to jam
228 labelled glycans on beads, and the supernatant droplet containing residual APTS was moved to
229 the trash vial. Elution of captured glycans was then performed in 6 μ L of water. This eluent was
230 subsequently analysed with CE-LIF. Further information about the microfluidic device
231 parameters for each step can be found in Table 1.

232

233 *CE-LIF of APTS-glycans and oligosaccharides*

234 Analyses of APTS-labeled glycans or malto-oligosaccharide standards were carried out with
235 our recently developed BGE composed of TEOA / citric acid (IS of 150 mM, pH 4.75) [20].
236 These separations were done using a fused-silica capillary of 50 μ m id, with L_{tot} of 60 cm and
237 L_{eff} of 50 cm, under a separation voltage of -25 kV. The fused silica capillary was
238 preconditioned by rinsing with water for 5 min, 0.1 M NaOH for 5 min, water for 5 min and
239 the BGE for 30 min prior to first use. Note that no HCl deactivation was needed, because
240 there was no capillary coating in our protocol; and with our new BGE composition at a high
241 ionic strength we could suppress well and reproducibly the surface charge of the capillary.
242 Inter-run rinsing was done with the BGE for 5 min.

243

244 **3. Results and Discussion**

245 **3.1. Design of the microfluidic droplet system**

246 The Lab-in-Droplet system for glycoprotein sample treatment, illustrated in Fig 1, was
247 developed and optimized to bring new features that were not feasible in any previously
248 reported systems using droplets in oil. First, automatic detection and control of droplet
249 position were implemented thanks to an array of optical detectors positioned along the tubing

250 containing oil and droplets. Along the tubing, three optical detectors were installed to detect a
251 change in the optical signal when the meniscus of a droplet passes in front of it, allowing to
252 precisely monitor the position of a given droplet. The first detector was placed before the
253 magnetic tweezer (acting as a magnet), the second between the magnetic tweezer and the first
254 thermal module, and the last after the second thermal module. The magnetic tweezer can be
255 therefore automatically activated (allowing the clustering of magnetic beads inside the tubing)
256 or deactivated (allowing the re-suspension of the beads into droplets inside the tubing) upon
257 passage of the droplet containing magnetic beads that leads to a change in optical signal.
258 Second, a thermostated compartment made of two Peltier plates and integrated with thermal
259 sensors were added in order to allow control of temperatures during the relevant incubation
260 steps of the process. With our design, we don't heat up as a "bulk" the whole system as for
261 droplet PCR, but rather allow more flexibility to move one drop onto a thermal module and
262 the possibility to work with fixed temperatures or with thermal cycling when needed.
263 Temperature ranging from 23 °C up to 92 °C could be established in approximately 1-10
264 seconds, with a precision of +/- 1 °C. Each heating module can be used independently if only
265 one preset temperature is desired. Both can be activated if more precise temperature control is
266 needed. This allows working with microfluidic-droplet-based sample processing at elevated
267 temperatures. Third, the system was designed to allow pre-mixing of magnetic beads in vials
268 before aspirating them into the tubing in order to maintain high homogeneity of beads in
269 droplets. To avoid sedimentation of magnetic beads in the vial, which was the case in previous
270 systems [29-32], the beads were homogenized in the vial by a series of back-and-forth
271 pushing at a flow rate of 2000 $\mu\text{L}/\text{min}$ prior to aspiration of the droplet containing magnetic
272 beads into the tubing. Furthermore, by carefully and accurately tuning the distance between
273 droplets that is monitored with the optical sensors, precise merging of two separate droplets in
274 tubing was made possible. These unprecedented features allow to carry out complex sample

275 processing that has not been possible so far in microfluidic formats. To implement all basic
276 and advanced droplet operations, the system relies on a syringe pump connected to a 3-port
277 selector valve and the droplet handling manifold fixed onto a ‘head’ block that is mounted on
278 a two-dimensional translation robot (Fig 1). Droplet sensing, fusion and heating, as well as
279 capture and release of magnetic beads into droplet were indeed implemented on the ‘head’
280 block. By pulling oil into the syringe with valve in position 1, the syringe can be refilled to
281 ensure sufficient oil quantity to perform fluidic operations. By advancing the piston of the
282 syringe with the valve in position 2, the syringe can be rinsed with fresh oil, allowing the
283 removal of any air bubble or unwanted droplets / beads. Finally, in valve position 3, oil can be
284 dispensed into or aspirated from the manifold for fluidic operations. The instrument is
285 controlled by a computer, and a purpose-made graphical user interface was developed to
286 allow manual intervention, display of the optical signals of the three detectors, setting and
287 monitoring of the temperature of the thermal modules and implementation of automated
288 protocols.

289

290 **3.2. Development of microfluidic droplet protocol for glycoprotein sample treatment**

291 *Microfluidic operation and optimization*

292 The Lab-in-droplet protocol developed for the glycoprotein sample treatment is illustrated in
293 Fig. 2. In the ‘bead capture’ operation (Fig. 2A) required for the steps of glycan capture on
294 magnetic beads, labeling of glycans, washing of labeled glycans and elution of labeled
295 glycans, the magnetic tweezer was activated when a droplet containing magnetic beads passed
296 in front of it in order to cluster the beads. The droplet without magnetic beads was then either
297 recovered or trashed. In the ‘bead resuspension’ operation (Fig. 2B), occurring in different
298 media (APTS solution for glycan labeling, ACN medium for glycans precipitation on beads,
299 or water for elution of glycans), the tweezer is deactivated to allow the target droplet

300 containing the suspension liquid passing through the optical sensor, and resuspend the beads
301 in a synchronized manner. In this ‘bead resuspension’ operation, it is critical that the droplet
302 fully englobes the aggregated beads. One big challenge when automatically handling small
303 droplets (1 μ L) was to monitor and confirm the presence of the target droplet in front of the
304 tweezer prior to release of magnetic beads. The risk of having magnetic beads released in oil
305 outside the target droplet occurred when the viscosity of the liquid inside the droplet varied.
306 This was particularly the case when using ACN medium that has a lower viscosity than water
307 and other aqueous solutions. Optimization and adjustment of the distance between the
308 magnetic tweezer and the arriving droplet prior to releasing magnetic beads from the tweezer
309 was therefore needed. The next operation required for this protocol is the droplet merging
310 (Fig. 2C), which is crucial at almost all steps of the protocol, in order to mix the sample
311 droplet with the denaturation, digestion, or labeling one. Droplet merging is also required to
312 fuse ACN with the glycan-containing droplet to aggregate glycans onto the magnetic beads.
313 To trigger droplet merging, the first droplet was brought to the optical detector 1 (see Fig. 1)
314 for identification, and then delivered to the vicinity of the tubing outlet prior to aspiration of
315 the second droplet. To prevent the unwanted premature fusion during the merging step that
316 would lead to loss of the sample, the small oil volume between the two droplets needs to be
317 carefully tuned. This premature fusion was seen to occur more often when magnetic beads
318 were present in the leading droplet. The between-droplet volume was therefore optimized and
319 the range of 0.5-0.7 μ L was found optimal to avoid such a problem. By pulling the two
320 droplets back into the tubing at a sufficiently high flow rate, the desired merging of two
321 droplets having different viscosities (*e.g.*, the ACN droplet and the sample one containing
322 glycans and magnetic beads) could occur. The droplet merging happens indeed thanks to the
323 intrinsic difference between the speeds of two consecutive droplets having different
324 viscosities and / or interfacial tensions between oil (containing the surfactant) and the droplet

325 in a straight channel [33]. The pulling flowrate must be rigorously tuned to allow successful
326 merging at a desired position along the tubing. A high flow rate of 900 $\mu\text{L}/\text{min}$ was found to
327 successfully trigger droplet fusion without breaking droplets during their movement. The last
328 operation concerns the droplet incubation, in which the target droplet (*e.g.*, the droplet
329 containing glycans and fluorescent labeling agent) is moved back and forth within the thermal
330 modules. This is carried out via a series of aspiration and then dispense of a preset volume of
331 oil to ‘shake’ the droplet in the tubing. During this step, thermal modules can be turned on if
332 needed. To achieve the best mixing efficiency during glycoprotein denaturation, digestion as
333 well as glycan labeling and washing, we put our efforts to optimize the incubation volume,
334 *i.e.*, the displacement volume of oil being aspirated and dispensed, the oil flowrate and the
335 time of incubation. Our results revealed that the incubation (displacement) volume equivalent
336 to that of the droplet allowed the best homogenization of magnetic beads inside the droplet
337 (Fig. S2 in ESI). From the studies on the hydrodynamics of droplet microfluidics [34-36], an
338 increased flow rate would lead to better mixing behavior, thus allowing to shorten the
339 incubation duration. Indeed, in the classical protocol, the labeling step requires an incubation
340 in tube for two hours at 60°C. To shorten this incubation time, several flowrates were
341 therefore tested to achieve the best efficiency of oligosaccharide labeling with APTS, (see Fig.
342 S3 in ESI). The flowrates of 600 $\mu\text{L}/\text{min}$ without the use of thermal modules, and 300 $\mu\text{L}/\text{min}$
343 with the assistance of thermal activation (60°C) were found to be optimal without provoking
344 droplet breaking during this ‘shaking’ incubation. The droplet was often deviated from its
345 starting position after the back-and-forth incubation at high flowrates due to inevitable
346 penetration of dissolved air into the tubing. The droplet could even go out of the visualization
347 zone of the detector D2, resulting in the loss of droplet detection signal and cease of the
348 system. This problem was more pronounced when the droplet heating (up to 90°C) was
349 activated during incubation. To avoid this problem, the starting position of the droplet prior to

350 incubation (for example incubation of released N-glycans with APTS, see Fig. 2D) needs
351 therefore to be optimized and adjusted for each droplet matrix, *i.e.*, moving the initial droplet
352 position upward if the droplet tends to deviate downwards from its starting position, as for the
353 case of droplets containing ACN.

354

355 *Optimization of the glycoprotein treatment protocol*

356 The full protocol for glycoprotein sample treatment, including N-glycoprotein denaturation
357 and digestion, capture of released glycans on magnetic beads, labeling of glycans, washing of
358 labelled glycans and elution of labelled glycans, was developed step by step in droplets and is
359 summarized in Table 1. The glycan capture and labeling steps were optimized first, using
360 oligosaccharide standards that are similar to glycans without the need for forefront
361 denaturation and digestion. To capture and accumulate efficiently all glycans or
362 oligosaccharides onto negatively charged surface of magnetic beads, a solution of 90 % ACN
363 is required in tube-based protocols [23, 37]. This however is a big challenge in droplet
364 microfluidics when a sample droplet (1 μ L) has to be fused with a large plug of ACN (9 μ L)
365 to reach this high ACN ratio. The omnipresence of ACN in the merged droplet provoked
366 clustering of magnetic beads at the bottom of the droplet (see Fig. S2 in the ESI). At the same
367 time the droplet became more fragile due to its size and was prone to breaking. To solve this
368 problem, the amount of ACN to be merged with the droplet sample (1 μ L) was reduced from 9
369 μ L to 7 μ L (*i.e.*, reducing the ACN ratio from 90% to 87.5%); and a flowrate of 600 μ L/min
370 was used for back-and-forth agitation to minimize beads clustering. The capture efficiency
371 and subsequent labeling of oligosaccharides were found unaffected by this ACN ratio
372 reduction thanks to the better mass transfer offered by microfluidics. To remove the excess of
373 fluorophores which is detrimental to subsequent CE-LIF, washing was performed after the
374 labeling step. This indeed involved merging of the droplet containing labeled oligosaccharides

375 and circulating magnetic beads with a large ACN droplet, using the same principle as for the
376 step of glycan capture on beads. It is shown in Fig. 3 the electropherograms of in-droplet-
377 labeled oligosaccharides with different numbers of subsequent washing steps. With no
378 washing, the huge signal of residual fluorophores, observed as the baseline drift over the
379 whole electropherogram, overlapped the peaks of oligosaccharides, which is detrimental for
380 their detection (Fig. 3A). With two washings using two consecutive droplets containing ACN,
381 oligosaccharides were lost and therefore not observed in the electropherogram (Fig. 3C). A
382 compromise was found with one washing droplet only, where residual fluorophore and by
383 products were well removed (reflected by a flat baseline) while the peak zones for
384 oligosaccharides (from 13 min) were not disturbed (Fig. 3B). It is important to note that a
385 tube-based protocol needs at least 5 washing steps to reach an equivalent quality of washed
386 and labeled oligosaccharides achieved with one washing using the Lab-in-Droplet. The
387 droplet protocol development was then extended to N-glycoprotein denaturation and
388 enzymatic digestion, using standard human IgG. In this case, the sample droplet containing
389 IgG was first fused with another one containing a mixture of denaturing and digesting
390 reagents, followed by droplet incubation to release N-glycans from IgG. When adapting the
391 enzyme quantity used for the tube-based method (*i.e.*, commercial PNGase F enzyme
392 accounting for 8.3 % of the digestion solution volume) to the in-droplet IgG digestion, the
393 glycans' signals could hardly be detected with subsequent CE-LIF analysis (see Fig. S4). An
394 increase in PNGase F quantity by 4-folds allowed clear visualisation of all IgG glycans'
395 peaks, confirming successful release of glycans from IgG. Higher enzyme concentrations
396 were also tested but no further improvement of glycans' peak intensity was observed (data not
397 shown). While the translation of tube-based conditions to droplet ones to release glycans from
398 IgG was straightforward thanks to the absence of magnetic beads in these two steps, the
399 challenge resided in the subsequent coupling to the next step of glycan capture on beads. The

400 initial volume of the mother droplet containing released glycans had to be reduced from 5.4
401 μL (see Table 1) to 1 μL prior to fusion of this daughter droplet with a large ACN droplet to
402 reach a final volume of up to 10 μL (*i.e.*, the maximum volume that can be handled by Lab-in-
403 Droplet). This volume reduction was implemented via precise handling of different droplet
404 manipulations, including delivery of the mother droplet (5.4 μL) out of the tubing without
405 ejecting oil and retaining of a daughter droplet (1 μL) at the tubing's extremity.

406

407 *Method validation*

408 Efforts were then made to validate each step in the droplet-based protocol using the optimized
409 parameters for glycoprotein denaturation, digestion, glycan labelling and elution. This is very
410 challenging. Indeed, to obtain results for the validation of each droplet-based step, the steps
411 onwards had to be continued with in-tube batchwise operations, which were unfeasible for
412 some of the considered steps. Accordingly, the outlet micro-droplet to be validated had to be
413 collected after each step, transferred, and diluted in vials to continue the subsequent steps in-
414 tube, prior to the second collection for CE-LIF analysis. All these manual collections and
415 transitions may lead to operational errors and additional variability that should be considered
416 when interpreting the obtained validation data. This could lead to results that could not
417 perfectly reflect the repeatability (for instance) of each step and consequently underestimate
418 largely the validation results. It is shown in Fig. S5A in the ESI the results from triplicates of
419 each step. The variations of CE-LIF signals were better than 22 % for the step of glycoprotein
420 denaturation / digestion, whereas they were better than 15 % for the step of glycan labelling in
421 droplets. Interestingly, the signal variations for the triplicate of the whole protocol in droplets
422 were around 24 %, which are only slightly higher than those obtained with each single step.
423 This demonstrated that the main source of errors could come from the manual intervention for
424 outlet droplet collection and dilution (for subsequent in-tube continuation and / or CE-LIF

425 analysis), and not from the automated in-droplet protocol itself. The relatively elevated RSD
426 values (up to 24 %) deem acceptable, considering that the variations of signals obtained with
427 CE-LIF analysis are the accumulation of errors from several operations, including those from
428 the droplet protocol, electrophoresis analysis, as well as manual in-tube sample collection and
429 dilution. The ratios between the target glycan peak signal and the total one of all principal
430 peaks, obtained with both microfluidic droplet and in-tube batchwise protocols, were
431 compared (Fig. S5B in ESI). No significant variations were observed for all tested peaks
432 regardless of the protocol used, demonstrating equal sample treatment performances for both
433 in-tube and droplet protocols for all glycans. This is very important for non-biased glycan
434 analysis serving for the glycan-defected disease diagnosis purpose. The migration times
435 obtained with CE-LIF of glycans from the droplet protocol showed no significant variations
436 (RSD % < 0.3 %, Fig. S5C in ESI), allowing identification of glycan peaks over runs.

437

438 **3.3. Performance of Lab-in-Droplet**

439 The Lab-in-Droplet with the full optimized protocol was then used to release and
440 fluorescently label N-glycans from human IgG, and the CE-LIF profile of IgG glycans was
441 compared with that obtained with conventional tube-based protocol (Fig. 4). These IgG
442 glycans are known to be mainly bi-antennary complex type with low terminal sialylation (5-
443 10 %), highly core-fucosylated (> 92 %); with a small proportion containing a bisecting
444 GlcNAc (11 %) [38]. Similar glycan profiles for IgG, in terms of peak height ratios between
445 any two peaks among the 8 abundant ones, were achieved (Fig 4). This result indicates that
446 the glycan release and labeling steps in the microfluidic droplet format is equally performant
447 for all glycans, which is of extreme importance for non-biased glycan analysis. By referring to
448 similar peak patterns assigned for human IgG already reported with the commercial tube-
449 based glycan treatment and CE-LIF kits [11, 39], we could assign the corresponding N-glycan

450 structures to the major peaks obtained with our droplet approach. While there was a 5-fold
451 sample dilution induced by our droplet protocol compared to the tube-based method, we
452 observed only a 2-fold decrease in peak height when comparing the glycan profiles obtained
453 from droplet-based and tube-based protocols (Fig. 4A vs B). Note that the profiles are slightly
454 different for Fig. 4A and 4B, especially for the peak height ratio of peaks 3 and 5 in the
455 electropherograms. This slight difference may be due to the two different ways of sample
456 preparation (with and without dilution for Lab-in-droplet and in-tube protocols, respectively)
457 prior to CE analysis.. The amounts of reagents were reduced by up to 10 folds for Lab-in-
458 Droplet. The droplet protocol is also much shorter (1.3 hours) and fully automated, compared
459 to the time required for conventional manual batchwise procedure (2.5 hours). To further
460 highlight the superiority of our approach, the performance of Lab-in-Droplet for glycan
461 sample processing was then compared with those achieved with previous methods for the
462 same purpose (table S1 in the ESI). Among sample treatment methods compatible with CE-
463 LIF of APTS-labelled glycans, our approach offers the shortest duration, full automation, least
464 working sample volumes and no risk of contamination with external environments. Note that
465 for purpose of diagnostics of glycan-defected diseases, the relative ratios of target glycans in
466 comparison to the total signal of major glycan peaks in the same CE-LIF electropherogram
467 attract more attention than absolute quantification of a particular glycan. The Lab-in-Droplet
468 system is therefore perfectly matching this requirement of glycan profile screening, as it offers
469 equal sample treatment performance for all glycans for non-biased glycan analysis.

470

471 For CDG screening via N-glycan analysis, CE-LIF has not been listed yet as a gold method
472 but attracts particular attention and holds great potential thanks to its high performance for
473 glycans separation [6]. In order to showcase the applicability of our Lab-in-Droplet as a
474 forefront for CE-LIF for the CDG diagnostics, total N-glycans from three serum samples,

475 from two CDG-affected individuals and one healthy person (control) were released and
476 labeled with Lab-in-Droplet and analyzed with CE-LIF (Fig. 5). Different peaks from highly
477 probable normal biantennary N-glycans were obtained for the control serum from a healthy
478 person (peaks a, b in trace A). The glycan profiles are different for the CDG individual with a
479 known quasi-total deficiency in galactosylation (B4GALT1-CDG) leading to N-glycans with
480 truncated antennae (Trace B), and for the CDG patient with deficiency in GlcNAcylation of
481 one of the 2 antennae of N-glycans (MGAT2-CDG, trace C). It is worthy to note that only
482 human serum samples with confirmed CDG probability were used in this test in order to
483 provide accurate evaluation on the performance of the new instrumental concept. The peak
484 patterns obtained with our droplet protocol were similar to those obtained with the
485 conventional tube-based method (see [20]), demonstrating the applicability of our Lab-in-
486 Droplet approach for the analysis of glycans from biofluids. Note that the relative fluorescent
487 signal scales for Fig. 4 and Fig. 5 are different because the experiments were done at different
488 periods. Direct comparison of the signal intensities in Fig. 4 and those in Fig. 5 is therefore
489 not considered. Regardless of the sample treatment method used (droplet or batchwise), very
490 typical and distinct profiles were obtained for the CDG patient vs healthy person, indicating a
491 high potential for diagnosis of CDG with N-glycan profiling by CE-LIF. At the present stage
492 of the work using our newly developed BGE for CE-LIF of glycans, prediction of glycan
493 structures for human serum samples (Fig. 5) with high precision is not yet possible with the
494 existing software for this purpose.

495

496 **4. Conclusion**

497 Our novel microfluidic droplet system has been successfully developed for the multiple-step
498 sample treatment of glycoproteins prior to glycan profiling. New approaches in instrumentation
499 and methodology are proposed to this purpose and challenging operations were performed in

500 droplets, using a variety of complex reagents and media. N-glycans from standard human IgG
501 and human serum were successfully released, fluorescently labeled, washed and eluted with this
502 droplet approach for subsequent analysis by CE-LIF. With Lab-in-Droplet, the glycan
503 fingerprints were found similar to those obtained by traditional or macroscopic strategies. At
504 the same time, a signal gain by 2-folds, a reduction of operation time by 2-folds, and a reduction
505 of required reagent amounts by 10-folds could be achieved. Analysis of a large cohort of CDG
506 samples with a more mature version of Lab-in-Droplet under a clinical context will be envisaged
507 in order to validate its potential for the diagnostic purpose. While the inaugural application of
508 Lab-in-Droplet has been made for glycan analysis, this platform could be extended to other
509 biological applications using magnetic beads functionalized with different ligands (e.g.,
510 antibodies for immunocapture or immunoassays in droplets). Thanks to automation and
511 miniaturization that we achieved with droplet microfluidics, higher throughput can now be
512 envisioned.

513

514

515 *Acknowledgements*

516 The authors are grateful for the financial support by the Agence Nationale de la Recherche
517 (ANR, France) with the grant no. ANR-18-CE29-0005-01. We thank Inorevia team, in
518 particular Julien Autebert, David Gosselin and Camille Soucies, for their support for
519 instrument development and method optimization.

520 **Table 1.** Protocol for sample droplet glycans. RT: room temperature

Step	Step in droplet	Droplet size	Optimized parameters
Denaturation	Droplet of beads with mixing	2.5 μ L	
	Capture of the beads by the tweezer	2.5 μ L	
	Trash the supernatant	2.5 μ L	
	Droplet of sample	2.0 μ L	
	Resuspension of the beads in the droplet	2.0 μ L	
	Merging between sample and denaturation solution	3.0 μ L	
	Incubation at RT	3.0 μ L	Droplet speed: 600 μL/min Incubation time: 7 min
Digestion	Merging between sample and digestion solution	5.4 μ L	
	Incubation at 60°C	5.4 μ L	Droplet speed: 600 μL/min Incubation time: 20 min
	Capture of the beads by the tweezer	5.4 μ L	
	Recovery of the sample	5.4 μ L	
Capture of the glycans	Droplet of sample recovered previously	1.0 μ L	
	Resuspension of the beads in the droplet	1.0 μ L	
	Merging between sample and ACN	8.0 μ L	
	Incubation at RT	8.0 μ L	Droplet speed: 600 μL/min Incubation time: 5 min
	Capture of the beads by the tweezer	8.0 μ L	
	Trash the supernatant	8.0 μ L	
Fluorescent labeling	Droplet of labelling solution	1.0 μ L	
	Resuspension of the beads in the droplet	1.0 μ L	
	Incubation at 60°C	1.0 μ L	Droplet speed: 300 μL/min Incubation time: 20 min
Washing	Merging between sample and ACN	8.0 μ L	Fusion flowrate: 800μL/min
	Incubation at RT	8.0 μ L	Droplet speed: 600μL/min Incubation time: 3 min
	Capture of the beads by the tweezer	8.0 μ L	
	Trash the supernatant	8.0 μ L	
Elution	Droplet of H ₂ O	6.0 μ L	
	Resuspension of the beads in the droplet	6.0 μ L	
	Incubation at RT	6.0 μ L	Droplet speed: 500μL/min Incubation time: 3 min
	Capture of the beads by the tweezer	6.0 μ L	
	Recovery of the sample	6.0 μ L	

521

522

523

524

525

526

527

528 **Figure captions :**

529 Fig. 1 Schematic drawing of the Lab-in-Droplet system (a prototype named Magelia®
530 by Inorevia) used in our work, adapted from Magelia® user manual.

531 Fig. 2 Basic operations performed with our Lab-in-Droplet system in order to carry out
532 the glycoprotein sample treatment: A) Bead capture, B) Bead resuspension, C)
533 Droplet fusion and D) droplet incubation

534 Fig. 3 Electropherograms of in-droplet-APTS-labeled oligosaccharides: A) Without
535 washing step, B) With 1 washing step and C) With 2 washing steps. CE-LIF
536 conditions: fused silica capillary, 50 µm i.d., 50/60 cm, hydrodynamic injection
537 at 50 mbar for 10 s, high voltage of -25 kV. BGE: Triethanolamine and citric acid
538 at ionic strength 150 mM and pH 4.75. LIF detection at $\lambda_{\text{excitation}}$ of 488 nm and
539 $\lambda_{\text{emission}}$ of 520 nm.

540 Fig. 4 Electropherograms of APTS-labeled N-glycans released from standard human
541 IgG, using (A) Lab-in-Droplet and B) conventional tube-based protocol. CE
542 conditions as in Fig. 3

543 Fig. 5 Electropherograms of APTS-labeled N-glycans released from human serum
544 samples using Lab-in-Droplet. **A)** Healthy person (control) with peaks a and b
545 from highly probable normal bi-antennated N-glycans; **B)** CDG patient with a
546 known quasi-total deficiency in galactosylation (B4GALT1-CDG) leading to N-
547 glycans with truncated antennae (peaks c, d, e); and **C)** CDG patient with

548 deficiency in GlcNAcylation of one of the 2 antennae of N-glycans (MGAT2-
549 CDG) (peaks f, g). CE conditions as in Fig.3

550

551 **References**

- 552 [1] T. Hennet, J. Cabalzar, Congenital disorders of glycosylation: a concise chart of
553 glycolyx dysfunction, *Trends Biochem. Sci.*, 40 (2015) 377-384.
- 554 [2] A.P. Corfield, M. Berry, Glycan variation and evolution in the eukaryotes, *Trends*
555 *Biochem. Sci.*, 40 (2015) 351-359.
- 556 [3] A. Barroso, E. Gimenez, F. Benavente, J. Barbosa, V. Sanz-Nebot, Classification of
557 congenital disorders of glycosylation based on analysis of transferrin glycopeptides by
558 capillary liquid chromatography-mass spectrometry, *Talanta*, 160 (2016) 614-623.
- 559 [4] M.H. Hu, Y. Lan, A. Lu, X.X. Ma, L.J. Zhang, Glycan-based biomarkers for diagnosis of
560 cancers and other diseases: Past, present, and future, in: L. Zhang (Ed.) *Prog. Mol. Biol.*
561 *Transl. Sci.* 2019, pp. 1-24.
- 562 [5] I. Kohler, M. Augsburger, S. Rudaz, J. Schappler, New insights in carbohydrate-deficient
563 transferrin analysis with capillary electrophoresis–mass spectrometry, *Forensic Sci. Int.*,
564 243 (2014) 14-22.
- 565 [6] A. Bruneel, S. Cholet, T. Tran-Maignan, T.D. Mai, F. Fenaille, CDG biochemical
566 screening: where do we stand? , *BBA - General Subjects*, 1864 (2020) 129652.
- 567 [7] R. Péanne, P.d. Lonlay, F. Foulquier, U. Kornak, D.J. Lefeber, E. Morava, B. Pérez, N.
568 Seta, C. Thiel, E.V. Schaftingen, G. Matthijs, J. Jaeken, Congenital disorders of
569 glycosylation (CDG): Quo vadis?, *European Journal of Medical Genetics*, 61 (2018)
570 643-663.
- 571 [8] P. Zhang, S. Woen, T. Wang, B. Liau, S. Zhao, C. Chen, Y. Yang, Z. Song, M.R.
572 Wormald, C. Yu, P.M. Rudd, Challenges of glycosylation analysis and control: an

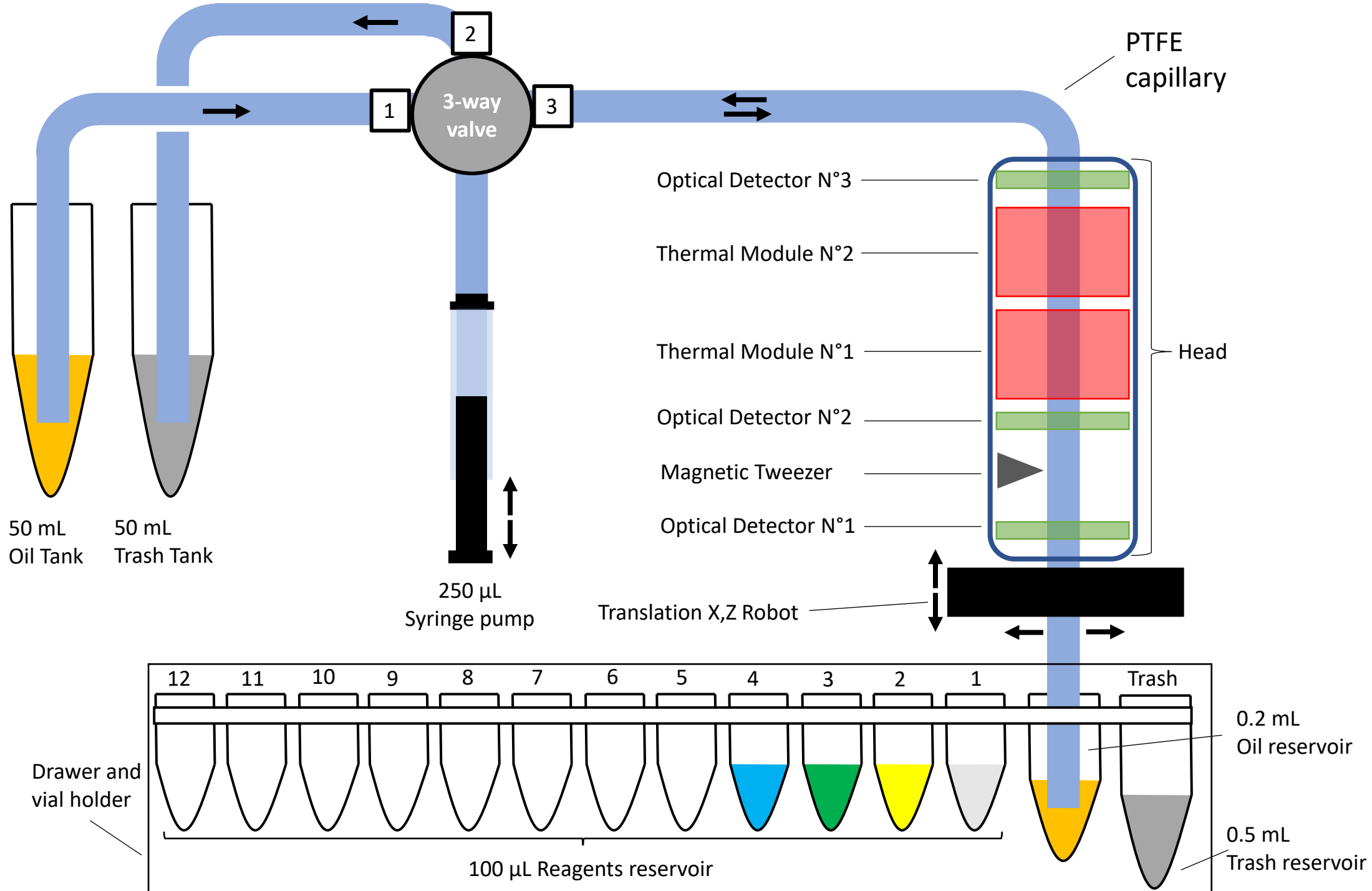
- 573 integrated approach to producing optimal and consistent therapeutic drugs, Drug
574 Discov. Today, 21 (2016) 740-765.
- 575 [9] G. Lu, C.L. Crieffield, S. Gattu, L.M. Veltri, L.A. Holland, Capillary Electrophoresis
576 Separations of Glycans, Chem. Rev., 118 (2018) 7867-7885.
- 577 [10] V. Mantovani, F. Galeotti, F. Maccari, N. Volpi, Recent advances in capillary
578 electrophoresis separation of monosaccharides, oligosaccharides, and polysaccharides,
579 Electrophoresis, 39 (2018) 179-189.
- 580 [11] Sciex, Fast Glycan Labeling and Analysis: High-Resolution Separation, Quantification
581 and ID, [https://sciex.com/content/dam/SCIEX/pdf/tech-notes/all/Fast-Glycan-Labeling-](https://sciex.com/content/dam/SCIEX/pdf/tech-notes/all/Fast-Glycan-Labeling-and-Analysis-High-Resolution-Separation-and-Identification-in-Minutes.pdf)
582 [and-Analysis-High-Resolution-Separation-and-Identification-in-Minutes.pdf](https://sciex.com/content/dam/SCIEX/pdf/tech-notes/all/Fast-Glycan-Labeling-and-Analysis-High-Resolution-Separation-and-Identification-in-Minutes.pdf), (2018).
- 583 [12] Agilent, CE-LIF glycans,
584 [https://www.agilent.com/cs/library/slidepresentation/public/Agilent-](https://www.agilent.com/cs/library/slidepresentation/public/Agilent-Picometrics%20CE-LIF%20solution.pdf)
585 [Picometrics%20CE-LIF%20solution.pdf](https://www.agilent.com/cs/library/slidepresentation/public/Agilent-Picometrics%20CE-LIF%20solution.pdf), (2018).
- 586 [13] L.R. Ruhaak, G. Zauner, C. Huhn, C. Bruggink, A.M. Deelder, M. Wuhrer, Glycan
587 labeling strategies and their use in identification and quantification, Anal. Bioanal.
588 Chem., 397 (2010) 3457-3481.
- 589 [14] S. Yang, H. Zhang, Solid-phase glycan isolation for glycomics analysis, Proteomics Clin.
590 Appl., 6 (2012) 596-608.
- 591 [15] Z. Szabo, A. Guttman, T. Rejtar, B.L. Karger, Improved sample preparation method for
592 glycan analysis of glycoproteins by CE-LIF and CE-MS, Electrophoresis, 31 (2010)
593 1389-1395.
- 594 [16] T. Kawai, N. Ota, A. Imasato, Y. Shirasaki, K. Otsuka, Y. Tanaka, Profiling of N-linked
595 glycans from 100 cells by capillary electrophoresis with large-volume dual
596 preconcentration by isotachopheresis and stacking, J. Chromatogr. A, 1565 (2018) 138-
597 144.

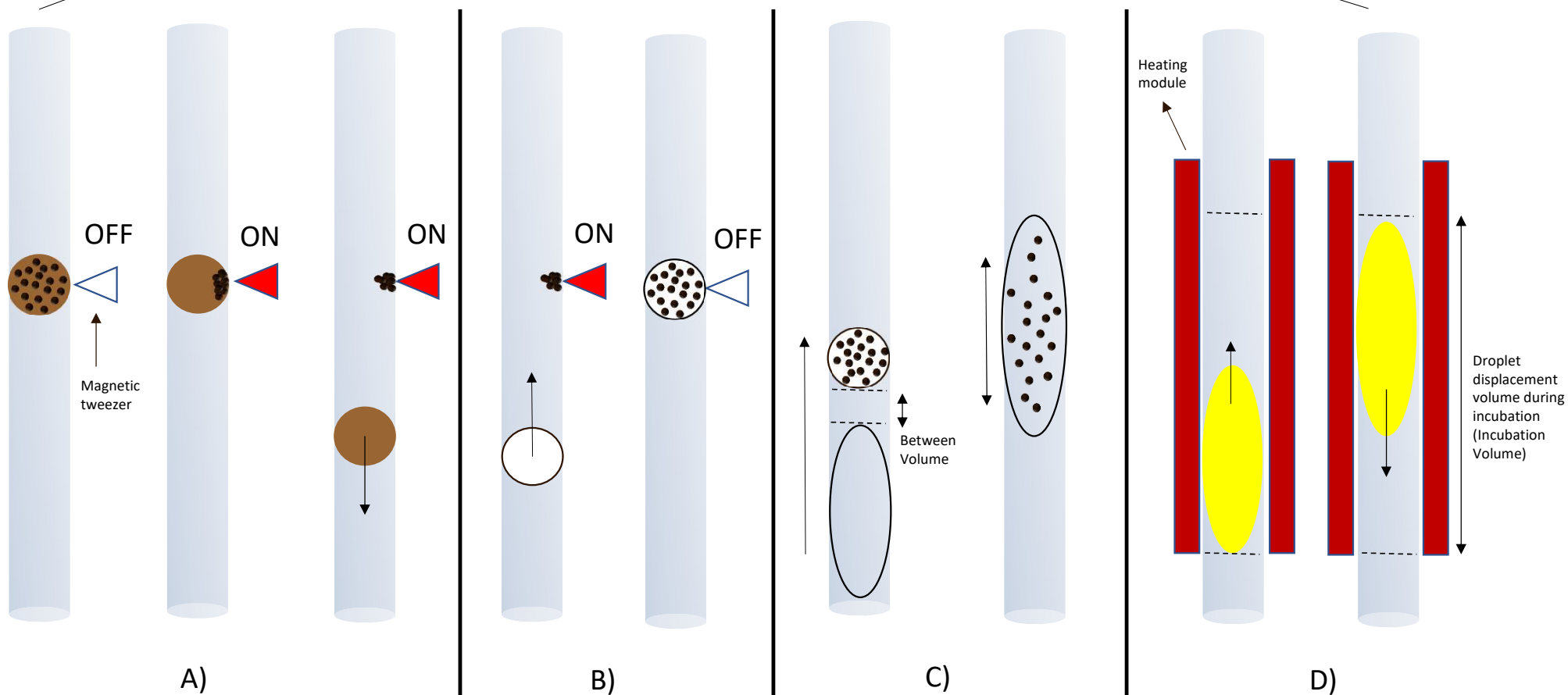
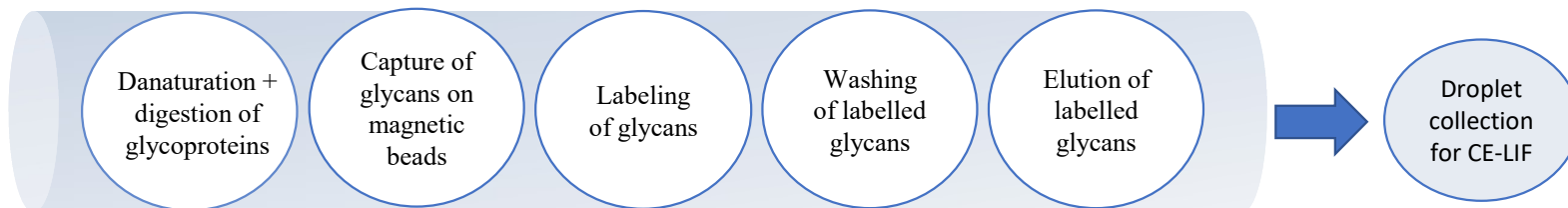
- 598 [17] E. Fukushima, Y. Yagi, S. Yamamoto, Y. Nakatani, K. Kakehi, T. Hayakawa, S. Suzuki,
599 Partial filling affinity capillary electrophoresis using large-volume sample stacking with
600 an electroosmotic flow pump for sensitive profiling of glycoprotein-derived
601 oligosaccharides, *J. Chromatogr. A*, 1246 (2012) 84-89.
- 602 [18] T. Kawai, M. Ueda, Y. Fukushima, K. Sueyoshi, F. Kitagawa, K. Otsuka, Toward 10
603 000-fold sensitivity improvement of oligosaccharides in capillary electrophoresis using
604 large-volume sample stacking with an electroosmotic flow pump combined with field-
605 amplified sample injection, *Electrophoresis*, 34 (2013) 2303-2310.
- 606 [19] T. Kawai, M. Watanabe, K. Sueyoshi, F. Kitagawa, K. Otsuka, Highly sensitive
607 oligosaccharide analysis in capillary electrophoresis using large-volume sample stacking
608 with an electroosmotic flow pump, *J. Chromatogr. A*, 1232 (2012) 52-58.
- 609 [20] T. Liénard--Mayor, B. Yang, N.T. Tran, A. Bruneel, A. Guttman, M. Taverna, T.D. Mai,
610 High sensitivity capillary electrophoresis with fluorescent detection for glycan mapping,
611 *Journal of Chromatography A*, 1657 (2021) 462593.
- 612 [21] R.A. Evangelista, M.S. Liu, F.T.A. Chen, Characterization of 9-Aminopyrene-1,4,6-
613 trisulfonate Derivatized Sugars by Capillary Electrophoresis with Laser-Induced
614 Fluorescence Detection, *Anal. Chem.*, 67 (1995) 2239-2245.
- 615 [22] B. Reider, M. Szigeti, A. Guttman, Evaporative fluorophore labeling of carbohydrates via
616 reductive amination, *Talanta*, 185 (2018) 365-369.
- 617 [23] C. Varadi, C. Lew, A. Guttman, Rapid Magnetic Bead Based Sample Preparation for
618 Automated and High Throughput N-Glycan Analysis of Therapeutic Antibodies, *Anal.*
619 *Chem.*, 86 (2014) 5682-5687.
- 620 [24] G. Jarvas, M. Szigeti, J. Chapman, A. Guttman, Triple-Internal Standard Based Glycan
621 Structural Assignment Method for Capillary Electrophoresis Analysis of Carbohydrates,
622 *Anal. Chem.*, 88 (2016) 11364-11367.

- 623 [25] Perkinelmer, Rapid Analysis of N-Glycans on the LabChip GXII Touch Microchip-CE
624 Platform, [https://resources.perkinelmer.com/lab-](https://resources.perkinelmer.com/lab-solutions/resources/docs/app_rapid_analysis_n-glycans_on_labchip_gxii_touch.pdf)
625 [solutions/resources/docs/app_rapid_analysis_n-glycans_on_labchip_gxii_touch.pdf](https://resources.perkinelmer.com/lab-solutions/resources/docs/app_rapid_analysis_n-glycans_on_labchip_gxii_touch.pdf),
626 (2019).
- 627 [26] E.K. Sackmann, A.L. Fulton, D.J. Beebe, The present and future role of microfluidics in
628 biomedical research, *Nature*, 507 (2014) 181-189.
- 629 [27] U. Aich, J. Lakub, A. Liu, State-of-the-art technologies for rapid and high-throughput
630 sample preparation and analysis of N-glycans from antibodies, *Electrophoresis*, 37
631 (2016) 1468-1488.
- 632 [28] S. Sohrabi, N. Kassir, M. Keshavarz Moraveji, Droplet microfluidics: fundamentals and
633 its advanced applications, *RSC Advances*, 10 (2020) 27560-27574.
- 634 [29] T.D. Mai, D. Ferraro, N. Aboud, R. Renault, M. Serra, N.T. Tran, J.-L. Viovy, C.
635 Smadja, S. Descroix, M. Taverna, Single-step immunoassays and microfluidic droplet
636 operation: Towards a versatile approach for detection of amyloid-beta peptide-based
637 biomarkers of Alzheimer's disease, *Sens. Actuators B*, 255 (2018) 2126-2135.
- 638 [30] M. Serra, T.D. Mai, A.L. Serra, M.C. Nguyen, A. Eisele, L. Perié, J.L. Viovy, D. Ferraro,
639 S. Descroix, Integrated droplet microfluidic device for magnetic particles handling:
640 Application to DNA size selection in NGS libraries preparation, *Sens. Actuators B*, 305
641 (2020) 127346.
- 642 [31] A. Ali-Cherif, S. Begolo, S. Descroix, J.L. Viovy, L. Malaquin, Programmable magnetic
643 tweezers and droplet microfluidic device for high-throughput nanoliter multi-step
644 assays, *Angew. Chem. Int. Ed. Engl.*, 51 (2012) 10765-10769.
- 645 [32] D. Ferraro, J. Champ, B. Teste, M. Serra, L. Malaquin, J.-L. Viovy, P. de Cremoux, S.
646 Descroix, Microfluidic platform combining droplets and magnetic tweezers: application
647 to HER2 expression in cancer diagnosis, *Scientific Reports*, 6 (2016) 25540.

- 648 [33] D. Ferraro, M. Serra, D. Filippi, L. Zago, E. Guglielmin, M. Pierno, S. Descroix, J.L.
649 Viovy, G. Mistura, Controlling the distance of highly confined droplets in a capillary by
650 interfacial tension for merging on-demand, *Lab on a Chip*, 19 (2019) 136-146.
- 651 [34] C.N. Baroud, F. Gallaire, R. Danga, Dynamics of microfluidic droplets, *Lab on a Chip*,
652 10 (2010) 2032-2045.
- 653 [35] A. de Lózar, A.L. Hazel, A. Juel, Scaling Properties of Coating Flows in Rectangular
654 Channels, *Physical Review Letters*, 99 (2007) 234501.
- 655 [36] R.B. Michelle, J.G. Cory, S. Helen, D.T. Joshua, R.F. Ismagilov, Microfluidic Systems
656 for Chemical Kinetics That Rely on Chaotic Mixing in Droplets, *Philosophical*
657 *Transactions: Mathematical, Physical and Engineering Sciences*, 362 (2004) 1087-1104.
- 658 [37] J.B. Marton Szigeti, Douglas Gjerde, Zsolt Keresztessy, Akos Szekrenyes, Andras
659 Guttman,, Rapid N-glycan release from glycoproteins using immobilized PNGase F
660 microcolumns,, *Journal of Chromatography B*,, 1032 (2016) 139-143.
- 661 [38] J.N. Arnold, M.R. Wormald, R.B. Sim, P.M. Rudd, R.A. Dwek, The Impact of
662 Glycosylation on the Biological Function and Structure of Human Immunoglobulins,
663 *Annu. Rev. Immunol.*, 25 (2007) 21-50.
- 664 [39] G. Lu, L.A. Holland, Profiling the N-Glycan Composition of IgG with Lectins and
665 Capillary Nanogel Electrophoresis, *Anal. Chem.*, 91 (2019) 1375-1383.

666





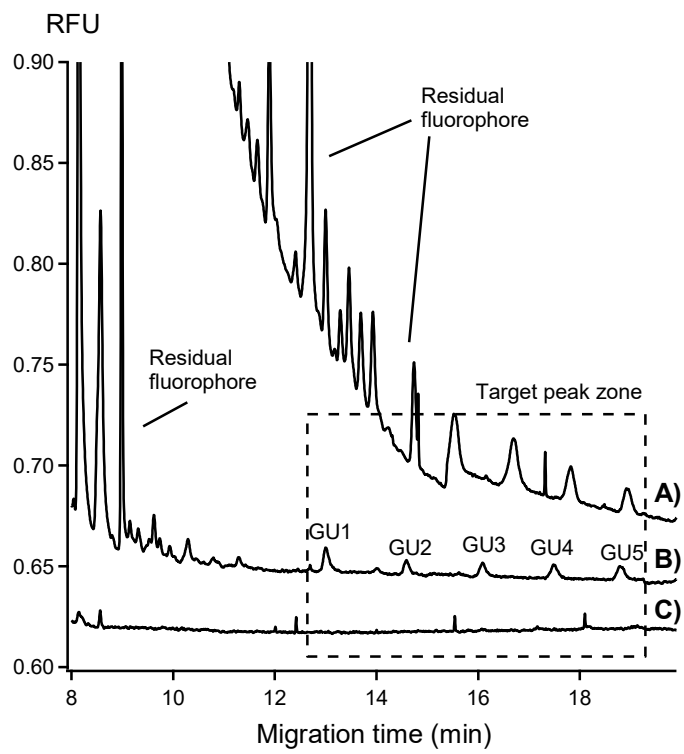


Figure 3

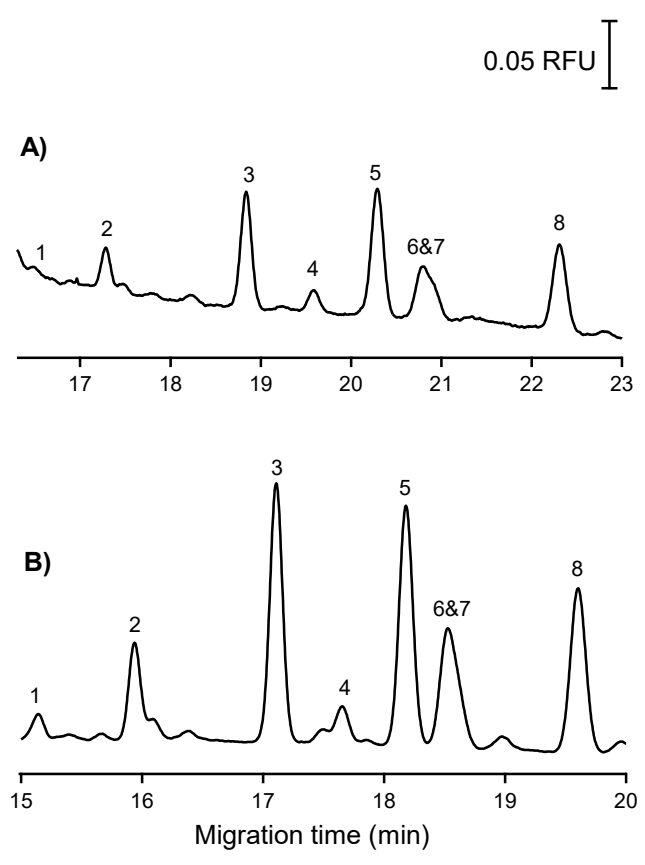


Figure 4

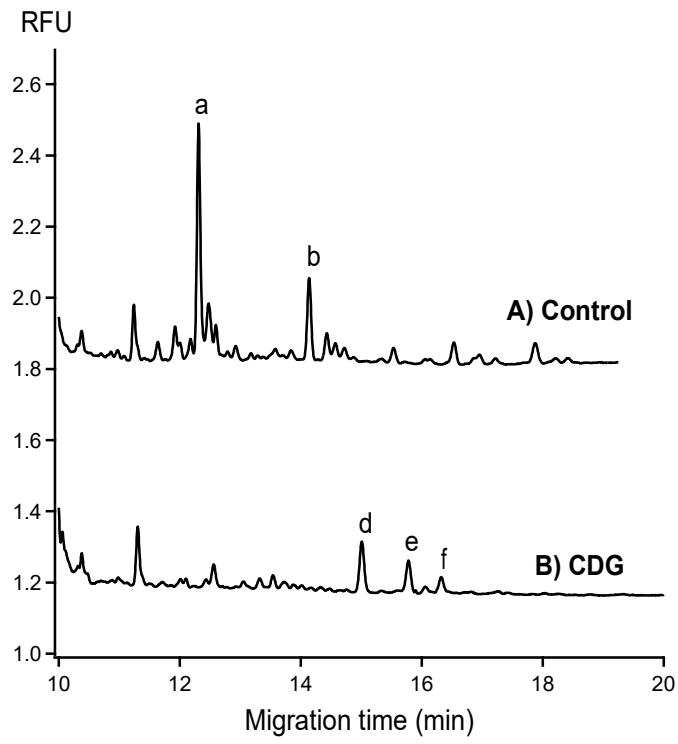


Figure 5

III.4. Conclusion

In this first experimental chapter, we have shown our work aimed at improving performance of CE-LIF of APTS tagged glycans. Our efforts have been focused on two different novel approaches. First, we developed new BGEs that are composed of large weakly charged molecules at extremely high IS which is in contrast with the standard approach of using low ionic strength (IS) BGEs composed of inorganic ions. This approach offers several advantages, notably EOF suppression without gel additives or neutral capillaries, a 4-fold gain in sensitivity, modulable IS depending on the applications and compatibility with a LVSEP method for ~160-fold improved sensitivity.

Our new methodology was applied for the analysis of total serum glycans from patients with two different type II congenital disorders of glycosylation (CDG-II), potentially offering new options for the diagnosis of glycan-related diseases.

Second, we took advantage of the magnetic tweezer technology first developed by the Institut Curie and exploited by the French startup Inorevia® for droplet-based glycan sample treatment. Our approach allows a 10-fold reagents consumption reduction, 3-fold reduced operation time, handling of complex human serum samples, signal gain of 2-fold and automation of the protocol. We used this new method to release, tag and analyse glycans from standard glycoprotein IgG and from CDG-II patients' whole serum glycans. Glycan profiles similar to the ones obtained using the gold standard method in 200 μ L PCR tubes were found, showcasing the possibility of using our Lab in Droplet method for diagnostic purposes.

IV. Chapter 4: Instrumentation for improved detection of glycans

IV.1. Introduction

Open-source mindset and methodology is an emerging science aiming at changing the way of producing things and the way of circulating information. Even though the term “open-source” is often associated with immaterial products such as software, the same concept is applied regarding open-source hardware, such as scientific instruments. The common ground in both cases is that source-files (blueprints, source code, etc....) are publicly available for open-source products. It is difficult to have 100% open-source hardware because it usually happens that at least one non-open-source part needs to be bought. As long as there is no non-disclosure agreement and the intellectual property is respected, such hardware can still be considered open source [14]. From our point of view, open-source hardware is crucial in the context of scientific instruments in academia for two main reasons. Firstly, due to the high cost associated with commercial machines (for example MS, HPLC or CE in our case), it can be difficult for some labs to procure such machines. Open-source plans to build even the simplest instruments (pH meters, colorimeters, etc....) can help the dissemination of science both inside academia and also outreach for non-scientific people. Comprehensive lists of open-source scientific instruments can be found in the following references: [302, 303]. Secondly, open-source hardware tends to be more flexible, more customizable. It means that custom made instruments can more easily be adapted for precise applications, and there is less need to buy different commercial machines for different applications.

In the context of separative techniques previously mentioned, only few open-source HPLC have been reported, with subpar performances due to several technical challenges such as the difficulty to produce reproducible and robust in-house HPLC columns or the need for very steady pumps without pulses. On the other hand, CE is a relatively easy to build instrument with many different reported in-house built instruments [14]. We have already detailed the various advantages of CE as a separation method in Chapter III and have explained why CE is a staple method in glycan analysis. In chapter I, we reviewed the arsenal of analytical techniques necessary for glycosylation analysis in CDG biochemical screening. Given the low prevalence of CDG (circa. 0.1–0.5/100,000 in Europe), and the sheer number of different analytical techniques required for a proper diagnosis, elaborating new open-source CE systems which can be used for CDG screening could be beneficial to equip more laboratories [7].

In this chapter, we will present our efforts to elaborate two standardisable, purpose-made CE instruments, made with the open-source spirit in mind. Both instruments are inspired from the Lego-toy where blocks are assembled to create a construction. In our case, ready to use electrophoretic, optic and microfluidic modules are assembled to create a custom CE-instrument, without the need of having any specific mechanical or electrical skill, nor any special facility. Our first home-made CE instrument is aimed at providing a low-cost alternative to commercial CEs using microfluidic instruments to handle fluids robustly and reproducibly. We also present a custom-made LiF detector serving as an alternative for highly expensive commercial detectors. The second custom-made instrument we present is a purpose-made CE instrument specially designed to separate glycans processed with our Magelia system from 1 μ L sample droplets.

IV.2. Development of the modular CE-LIF instrumentations

A CE system is usually made with three major blocks, including the separation channel with the associated fluid manipulation, the high voltage power supply (HVPS) and the detection together with data acquisition.

For the first part, usually the separation channel is a capillary made of fused silica, most commonly with inner diameters ranging from 25-75 μm . In some cases, such as MCE, the separation channel can be integrated on the chip. For fluid manipulation, in a commercial instrument, recipients are usually small (circa 1 mL) plastics vials, but for an in-house CE system bigger size of vials can be preferred as they are less prone to electrolysis effects which require frequent buffer change [14]. In theory injection does not require supplementary equipment since it can be performed by inserting the capillary in both vials and elevating one vial above the other to create a siphoning effect. However, such injection would not be reproducible because it is prone to human error. Fortunately, manifolds that can be build using conventional machining or 3d printing have been published for various injection methods: pressure injection [304], vacuum injection [305], flow injection [306, 307] or sequential injection [308].

For the second part, HVPS are used to apply to the separation channel the necessary high voltage for separation. Commercial HVPS usually provide ± 30 kV and ± 300 μA . There are usually two different types of HVPS: ready-to use HVPS or HVPS modules. The first one is usually designed to be plug-and-play, easy to use and with some useful features (voltage ramping, polarity switching, automated operation...) [14]. The drawback is that they are usually quite expensive, have a big physical footprint and they are not suitable for portable instruments because they run at 115-220 V AC. The second one is high voltage modules, (DC-DC converters) and require some knowledge of electrical circuit to integrate them into a functional HVPS. They tend to be significantly cheaper and more adapted for portable instruments because they are typically powered by 12 or 24 DC power supplies. One significant drawback with HVPS modules is that they are not originally equipped with the useful features mentioned previously. For example, without polarity switching, not every type of analytes can be analyzed. For a concrete example, if only the positive electrode is available at the injection side (separation in positive mode), then analysis of APTS-glycans which are separated in negative mode (negative electrode at the injection side) cannot be implemented. In terms of electrodes, platinum electrodes are usually found in commercial systems, but in in-house systems stainless steel has been used as a cost-efficient alternative without any known performance issue.

Lastly, a detector in an analytical system is often the most crucial equipment because the quality of detection for a given analyte depends strongly on the sensitivity of the detector. The most popular detector for open-source CE is the Capacitively-Coupled Contactless Conductivity Detectors (C4D). The reason for this is that it is relatively easy and cheap to build a C4D, requiring only mild electronical skills. The drawback is of course that C4D detection in several cases is not sensitive and selective enough (as a bulk detector), and it is mostly adapted for small ions [14]. In terms of optical detectors, both UV detectors and LiF are widely available from various constructors (Sciex, Picometrics, Agilent, Wynsep...). Naturally, commercial detectors are quite expensive, with strong variations of the price depending on the wavelength(s) of interest. Fortunately, more efforts have been focused on development of a wide range of LED, with wide selections of wavelength and with more and more affordable prices, available for in-house built UV and LiF detectors [309, 310]. For data acquisition (DAQ) (i.e., transforming the

measured signal into digital values), researchers often face a dilemma: the easiest but more expensive solution is to buy a commercial DAQ system which is locked to a dedicated software and can also sometimes be equipped for data analysis. The alternative is to build an open-source DAQ system using for example Arduino microcontrollers with acquisition software in the form of Excel script or Python programs. Of course, the latter requires some informatic and electronical skills which not everyone possesses.

Our modular CE-LIF instrumentation was therefore made with considerations to these aforementioned points. Details on development of our modular CE-LIF system are given in the following article.

Article 4: Modular instrumentation for capillary electrophoresis with laser induced fluorescence detection using plug-and-play microfluidic, electrophoretic and optic modules.



HAL
open science

Modular instrumentation for capillary electrophoresis with laser induced fluorescence detection using plug-and-play microfluidic, electrophoretic and optic modules

Théo Liénard–Mayor, Jasmine S. Furter, Myriam Taverna, Hung Viet Pham, Peter C. Hauser, Thanh Duc Mai

► To cite this version:

Théo Liénard–Mayor, Jasmine S. Furter, Myriam Taverna, Hung Viet Pham, Peter C. Hauser, et al.. Modular instrumentation for capillary electrophoresis with laser induced fluorescence detection using plug-and-play microfluidic, electrophoretic and optic modules. *Analytica Chimica Acta*, 2020, 1135, pp.47 - 54. 10.1016/j.aca.2020.08.025 . hal-03492051

HAL Id: hal-03492051

<https://hal.science/hal-03492051>

Submitted on 5 Sep 2022

HAL is a multi-disciplinary open access archive for the deposit and dissemination of scientific research documents, whether they are published or not. The documents may come from teaching and research institutions in France or abroad, or from public or private research centers.

L'archive ouverte pluridisciplinaire **HAL**, est destinée au dépôt et à la diffusion de documents scientifiques de niveau recherche, publiés ou non, émanant des établissements d'enseignement et de recherche français ou étrangers, des laboratoires publics ou privés.



Distributed under a Creative Commons Attribution - NonCommercial | 4.0 International License

1 **Modular instrumentation for capillary electrophoresis with laser induced fluorescence**
2 **detection using plug-and-play microfluidic, electrophoretic and optic modules**

3
4 **Théo Liénard-Mayor¹, Jasmine S. Furter², Myriam Taverna^{1,3}, Hung Viet Pham⁴, Peter**
5 **C. Hauser^{2*}, Thanh Duc Mai^{1*}**

6
7 *¹ Institut Galien Paris Sud, UMR 8612, Protein and Nanotechnology in Analytical Science*
8 *(PNAS), CNRS, Univ. Paris-Sud, Univ. Paris-Saclay, 5 rue Jean Baptiste Clément, 92290*
9 *Châtenay-Malabry, France*

10 *² University of Basel, Department of Chemistry, Klingelbergstrasse 80, 4056 Basel,*
11 *Switzerland*

12 *³ Institut Universitaire de France (IUF)*

13 *⁴ VNU Key Laboratory of Analytical Technology for Environmental Quality and Food Safety*
14 *Control (KLATEFOS), VNU University of Science, Vietnam National University, Hanoi*
15 *(VNU), Nguyen Trai Street 334, Hanoi, Vietnam*

16

17

18 Co-corresponding authors

19 e-mails: thanh-duc.mai@u-psud.fr

20 peter.hauser@unibas.ch

21

22 **Keywords:** Lego instrumentation; capillary electrophoresis; microfluidics; LIF detection;
23 oligosaccharides

24

25

26 **Abstract**

27 This study reports on the development of a novel instrument for capillary electrophoresis (CE)
28 coupled with laser induced fluorescence (LIF) detection that is inspired by the Lego-toy
29 concept. The Lego CE-LIF design is an evolution of purpose-made CE instrumentation,
30 allowing the users to construct their own analytical device with a high degree of
31 standardization (*i.e.* a “standard” setup) without requirement of mechanical and electronic
32 workshop facilities. To allow instrument reproduction outside the original fabrication
33 laboratory, which is not trivial for in-house-built CE systems, the new design is based on
34 unprecedented ‘plugging’ hyphenation of various off-the-shelf parts available for microfluidics,
35 optics and electrophoresis. To render the operation with Lego CE-LIF optimal, we developed
36 a new background electrolyte (BGE), using for the first time extremely high concentrations of
37 zwitterionic and large weakly charged species for much improvement of detection sensitivity.
38 The Lego CE-LIF was demonstrated for separation and detection of oligosaccharides labelled
39 with 8-aminopyrene-1,3,6-trisulfonic acid (APTS). The new gel-free BGE for oligosaccharide
40 analysis also allowed simplification of the conventional CE-LIF protocol used with
41 commercial instruments while keeping satisfactory separation performances. Furthermore, the
42 new BGE is fully compatible with a non-thermostatted Lego CE instrument thanks to low
43 current and therefore low heat generation under application of a high voltage.

44

45

46

47 **1. Introduction**

48 After almost 40 years of development and instrument commercialization, capillary
49 electrophoresis (CE) is now among established analytical techniques and becomes the method
50 of choice for several classes of analytes, notably DNA, glycans, therapeutic proteins, chiral
51 molecules, and inorganic ions [1]. The majority of the works on CE have been carried out
52 using bench-top commercial instruments. While such systems offer robustness with a high
53 degree of automation and standardization, their high prices render them often not accessible to
54 researchers in academia, especially to laboratories with limited budget and modest
55 infrastructure. In this context, in-house built CE instrumentation has appeared as an affordable
56 alternative to satisfy the urgent need for inexpensive and simple analytical devices for
57 versatile applications. Indeed, such purpose-made instruments are not only much less
58 expensive than commercial systems but can also be constructed as portable versions [2-4] or
59 with flexible configurations adapted to different needs [5]. Over 10 years, our groups have
60 demonstrated the use of purpose-made CE devices for various analytical screening
61 applications, notably quality control of antibiotics [6, 7], environmental monitoring [8-10],
62 food control [11, 12], forensics [13] and clinical analyses [14]. With the aim to open further
63 the access to CE instrumentation, Kuban *et al.* have recently presented a review detailing all
64 steps required to construct an open-source CE system [15]. This is indeed part of the action
65 plan of the European network promoting portable, affordable and simple analytical platforms
66 [16]. Nevertheless, a mechanical and electronic workshop, even modestly equipped, is often
67 required for construction of purpose-made and open-source CE systems. Exception can be
68 found only for the simplest CE setup with syphoning injection in which an operator only
69 needs a ready-to-use high voltage (HV) module, one capillary and different small vials to
70 carry out electrophoretic separations. Nevertheless, this mode of injection which is the least
71 reproducible, together with manual capillary flushing with a plastic syringe is not fully

72 appreciated by users due to a high risk of contamination during operation and from the air [6].
73 Construction of more elaborated versions avoiding the syphoning injection normally require
74 some electronic and mechanical skills that are not always available in analytical laboratories
75 with routine operations. This hinders the wider adoption of in-house built CE instrumentation.
76
77 With the goal to drastically improve the CE popularity as a simple and affordable approach to
78 the population, we present herein a Lego CE concept to facilitate technology/ methodology
79 transfer between different laboratories and eliminate the workshop facility requirement. This
80 design is inspired by the Lego toy concept, in which the users with no mechanical and
81 electronic competences can easily assemble a CE system from different commercially
82 available ready-to-use electrophoretic and microfluidic modules. This new CE instrument was
83 coupled with a laser induced fluorescence (LIF) detector that was also constructed with the
84 Lego design, using off-the-shelf optical, electronic and microfluidic parts. The performance of
85 Lego CE-LIF was evaluated in terms of injection reproducibility and detection sensitivity. A
86 demonstration of the Lego CE-LIF system was made with separation and detection of
87 oligosaccharides labelled with 8-aminopyrene-1,3,6-trisulfonic acid (APTS). Such analyses
88 are commonly carried out on commercial bench-top CE instruments using conventional
89 buffers containing inorganic ions that may not be optimal for CE-LIF. To significantly
90 improve the CE-LIF detection performance, a new background electrolyte (BGE) was
91 therefore developed using for the first time zwitterionic and large weakly charged species at
92 very high concentrations to allow excellent stacking of fluorescently labelled
93 oligosaccharides. The new BGE for CE-LIF is inspired from low-conductivity buffers for CE
94 coupled with capacitively coupled contactless conductivity detection (C⁴D) [17, 18] and
95 electrolytes buffered with an isoelectric ampholyte for CE with indirect photometric detection
96 [19]. Comparison was made with a conventional BGE used for this purpose to highlight the

97 advantageous features of our new buffer for CE-LIF. This optimization was inspired by our
98 recent work on reinvestigation of CE-LIF conditions for proteins and peptides analyses [20].
99 Finally, different modes of pressure-assisted electrophoresis was demonstrated with the Lego-
100 CE-LIF instrument, using the new BGE for CE-LIF, for the optimized separations of labelled
101 oligosaccharides.

102

103 **2. Experimental**

104 **2.1. Chemicals and reagents**

105 All chemicals for preparation of buffers were of analytical or reagent grade and purchased
106 from Sigma-Aldrich (Lyon, France). Glucose oligosaccharides (dextran ladder) and
107 fluorescent reagents (APTS and fluorescein isothiocyanate FITC) were bought from Sciex
108 (Villebon sur Yvette, France). β -Alanine, 2-(N-morpholino)ethanesulfonic acid (MES), acetic
109 acid, lithium hydroxide monohydrate, tris(hydroxymethyl)aminomethane (Tris) and 2-
110 (Cyclohexylamino)ethanesulfonic acid (CHES) were used for preparation of background
111 electrolyte (BGE) solutions.

112

113 **2.2. Apparatus and Material**

114 Method development for establishment of new BGEs for CE-LIF was performed with a
115 Beckman Coulter PA800+ system (Sciex Separation, Brea, CA) coupled with a LIF detector
116 ($\lambda_{\text{excitation}}$: 488 nm, $\lambda_{\text{emission}}$: 520 nm). Instrument control was carried out using Karat 8.0
117 software (Sciex Separation). A standalone LED induced fluorescence (LEDIF) detector was
118 purchased from Adelis (Zetalif, Picometrics, Toulouse, France). Data acquisition (for Zetalif
119 or Lego LIF detector) was done with a Mini-corder ER181 data acquisition system (eDAQ
120 Europe, Warszawa, Poland) connected to the USB-port of a personal computer. Polyimide
121 coated fused silica capillaries of 50 μm id and 375 μm od (TSP050375, Polymicro, CM

122 Scientific, Silsden, UK) or UV transparent coated fused silica capillaries of 50 μm id and 375
123 μm od (TSH050375, CM Scientific, Silsden, UK) were used for all CE experiments.

124 Deionized water was purified using a Direct-Q3 UV purification system (Millipore, Milford,
125 MA, USA). pH values of buffer solutions and samples were acquired with a SevenCompact
126 pH meter (Mettler Toledo, Schwerzenbach, Switzerland). Selection of BGE compositions and
127 buffer ionic strength (IS) calculations were based on simulations with the computer program
128 PhoeBus (Analis, Suarlée, Belgium).

129
130 For Lego CE instrumentation, all fluid connections were made with 0.02 in. inner diameter
131 (id) and 1/16 in. outer diameter (od) Teflon tubing from Upchurch Scientific (Oak Harbor,
132 WA, USA). The electrophoresis module was based on a dual polarity high voltage power
133 supply with ± 30 kV maximum output (HVPS for CZE, Villa Labeco, Slovakia). The high
134 voltage safety cage is a regular Perspex box purchased from Amazon. The microfluidic
135 manifold is composed of different modules purchased from Fluigent (Paris, France), including
136 an ElectroWell (or FluiWell 4C) setup and a pressure controller (Flow EZ). Capillary flushing
137 and sample injection were done with a device to generate either vacuum (MZ 2NT,
138 Vacuubrand, Wertheim, Germany) or compressed air (FLPG Plus, Fluigent).

139
140 For modular LIF setup, the current amplifier (DC-100kHz, AMP120), the fiber patch cables
141 (1000 μm , M35L01 and 600 μm , M53L01), an optical breadboard (MBH4545/M), spacers
142 (BA2S7/M), the in-line fiber optic filter mount (FOFMS/M-UV) and cover (FOFM-CV), the
143 488nm notch filter (NF488-15) and the FITC emission filter (MF530-43) were purchased
144 from ThorLabs (Maisons-Laffitte, France). The photosensor module with PMT tube (H10721-
145 210), the fiber adapter (E5776-51) was purchased from Hamamatsu Photonics (Massy,
146 France). A microfluidic manifold Assy 5 port (P-154, Upchurch) was used for optical cell

147 setup. The 488 nm laser module (488L-14A, Integrated Optics) was purchased from Acal Bfi
148 (Evry, France).

149

150 **2.3. Methods**

151 *Preparation and storage of fluorescently labelled oligosaccharides*

152 The preparation of fluorescently labelled glucose oligosaccharides was performed according
153 to the protocol of Reider *et al.* [21]. Briefly, 2 mg of dextran ladder was added in a 200 μ L
154 PCR tube, followed by addition of 4 μ L of 40 mM APTS in 20% acetic acid (AcOH), 4 μ L of
155 20% AcOH, 2 μ L of 1M sodium cyanoborohydride (NaBH₃CN) in tetrahydrofuran (THF).
156 The mixture was incubated at 70°C for 30 mins with open vial cap. After the reaction the
157 samples were diluted in 100 μ L deionized water, aliquoted and stored at -20°C. Further
158 dilution of this stock solution was carried out before CE-LIF analysis.

159

160 *CE-LIF of oligosaccharides*

161 Analyses of APTS-labeled oligosaccharides were carried out with a BGE composed of either
162 858 mM β -Alanine and 822 mM MES (IS = 50 mM, pH 5.04) (BGE 1); 364 mM Beta-
163 Alanine and 538 mM MES (IS =25 mM, pH=4.75) (BGE 2); or 25 mM LiOH and 47 mM
164 acetic acid (IS = 25 mM, pH=4.75) (BGE 3). The optimized BGE (BGE 1) was adopted for
165 the rest of the study. CE separations with the Lego-CE-LIF system were implemented using
166 fused-silica capillaries with ID of 50 μ m, the total length of 45 cm and effective length of 23
167 cm under a separation voltage of -25 kV. The fused silica capillaries were preconditioned with
168 1 M NaOH for 5 min, water for 5 min, 1M HCl for 5 min, water for 5 min, and the BGE 1 for
169 15 min prior to use. Between runs the capillary was rinsed with the BGE for 5 min.

170

171 **3. Results and Discussion**

172 **3.1. System design and performance**

173 **3.1.1. Lego CE**

174 Our Lego concept is essentially an evolution of in-house-made compact CE whose first
175 version was introduced by Hauser *et al.* in 1998 [22] and open-source CE introduced by
176 Kuban *et al.* in 2019 [15]. The Lego CE setup is a balance between costly bench-top
177 commercial CE instruments and low-cost in-house-built devices that are hardly reproduced
178 from one laboratory to another. The logic behind the Lego CE concept is demonstrated in Fig.
179 S1 in the electronic supplementary information (ESI). For construction of in-house-built and
180 open-source CE instruments, people normally have to rely on technical drawings that are
181 either provided by the host laboratories (for the in-house-built ones) or available on-line and
182 free-of-charge (for the open-source ones) to reproduce the electronical, mechanical and
183 fluidic modules. To understand and follow these technical drawings, specific knowledge and
184 skills are normally required, which are unfortunately not always available in the majority of
185 analytical laboratories. These challenges could on the other hand overcome with our Lego CE
186 design with a high degree of standardization, and without recourse to any technical drawings
187 for construction of plug-and-play modules. The Lego CE design we developed here is based
188 on unprecedented hyphenation (specifically for CE instrumentation) of various off-the-shelf
189 parts available for microfluidics and electrophoresis. More concretely, we used a high-
190 accuracy miniature pressure controller setup, a high voltage generator for CE, a device for gas
191 compression or vacuum generation and a fluidic interface dedicated to microfluidic operation
192 to build the CE system. A simplified schematic drawing of the Lego CE system is shown in
193 Fig. 1. Compressed air generated from an air compressor or a gas tank is driven to a stand-
194 alone pressure controller (*i.e.* Flow EZ 1000 mbar, Fluigent) to provide precise pressure for
195 hydrodynamic injection (generally from 30 - 100 mbar) and capillary flushing (1000 mbar).
196 Alternatively, similar operations could be carried out from the opposite side of the capillary,

197 using a vacuum generator and a pressure controller (*i.e.* Flow EZ -800 mbar, Fluigent)
198 providing negative pressures for injection (-30 mbar to -100 mbar) and capillary flushing (-
199 800 mbar). If both negative and positive pressures are desired, a Flow EZ push-pull module
200 can be used for pressure manipulation in the range of -800 mbar to +1000 mbar. This offers
201 setup flexibility to users. Note that any pressure in the range from 0 to 1000 mbar (or from 0
202 to - 800 mbar) can be set and monitored for injection or capillary flushing purposes either
203 with physical knob and a digital screen integrated on the pressure controller or with a
204 computer-linked control program (see Fig. S2). In addition, pressure assistance during
205 electrophoresis, which is not trivial in in-house-made CE instruments, can also applied to
206 accelerate the analysis time or improve the separation resolution, as pressure can be precisely
207 controlled and monitored during application of high voltages (see section below). In in-house
208 made CE instruments [6, 9, 13, 23-27], a desired pressure value can sometimes not be
209 precisely set and monitored. Thus, optimization of hydrodynamic injection in these cases is
210 generally done with injection time variation rather than pressure adjustment. Both
211 optimization modes (time and pressure) are now available in our Lego CE version. Solutions
212 to be injected in the capillary (*i.e.* sample, BGE or other generating solutions) can be easily
213 changed by plugging the corresponding vial to the fluidwell or electrowell interface (Fig. S2A
214 and B in ESI for their setup). In our case with the electrowell (Fig. S2C), a platinum electrode
215 is already integrated in this interface so a ground connection can be made easily without any
216 further module modification. If the fluidwell interface is used instead on the GND side, a steel
217 tubing commonly used for HPLC can be employed for ground connection. In this case the
218 capillary end is centered and extruded from the GND steel electrode so that they are both in
219 contact with the working solution (Fig. 1). For high voltage generation, a commercial module
220 containing a $\pm 30\text{kV}$ Spellman unit with an integrated digital display was employed, allowing
221 control and monitoring of the voltage and current during electrophoresis. The high voltage

222 side was isolated using a Perspex box sold for cosmetic or arrangement purposes that can be
223 purchased online. Alternatively, any cage made from electrically isolating materials (e.g.
224 poly(methyl methacrylate), mica, polyvinyl chloride (PVC)) could be used [28]. The total cost
225 for construction of this Lego CE system from these off-the-shelf components is estimated to
226 be 5000 Euros.

227

228 **3.1.2. Lego LIF**

229 The detection module is one of the most critical parts of the whole CE instrument. Among all
230 detection types commonly employed for CE, fluorescence detection, or laser-induced
231 fluorescence (LIF) detection in particular, is often used to improve significantly the detection
232 sensitivity, especially for determination of biomolecules such as proteins and peptides. The
233 popularity of fluorescence detection in CE however is often hindered (at least partially) by
234 very high purchase costs of commercial LIF or LED-induced-fluorescence (LEDIF) detectors.
235 Efforts to produce purpose-made fluorescence detectors adapted to modest budgets and
236 infrastructure were already communicated [29-31], but normally require electronic and
237 mechanical skills and workshop, with 3D-printing facilities in some cases [29, 31]. For
238 teaching purpose, Thompson *et al.* introduced a low-cost CE-LEDIF device for testing some
239 fluorophore standards [32]. As part of the Lego-CE instrument, we developed a new Lego LIF
240 detector. The Lego-LIF design exploits off-the-shelf components commonly used in
241 microfluidics and optics in order to minimize (or eventually eliminate) the need for workshop
242 and skills that are not always available in laboratories with routine analyses. The schematic
243 design of Lego LIF detector is demonstrated in Fig. 2 whereas a photo of the system can be
244 seen in Fig. S3 in ESI. A miniature LIF module from Integrated Optics, powered with a USB
245 cable from a personal computer, was used for the first time in CE-LIF to provide the
246 excitation wavelength of 488 nm which is most commonly used for fluorescence detection of

247 biomolecules. The incident excitation light was set perpendicular to the optical window of the
248 separation capillary using a black microfluidic interface. This interface plays the role of an
249 optical cell, allowing excellent light alignment. The emission light was collected from an
250 outlet of the interface situated perpendicular to both incident light and the capillary (Fig. 2).
251 The emission light was then passed through an optical band-pass filter (or FITC 530 nm
252 emission filter). A notch filter for 488 nm can be optionally added to block any residual
253 excitation light. The filtered light was then diverted to a photomultiplier tube (photo sensor) to
254 convert incident photons into electric current signals. These were subsequently converted into
255 voltage signals and amplified using a trans-impedance amplifier, prior to analog-to-digital
256 conversion and data acquisition into a computer. All these optical, microfluidic and electronic
257 components are ready-to-use modules and can be plugged together using the adaptors
258 provided by the suppliers. Users can choose different laser / LED types for the light source
259 from various suppliers, depending on the budget available and the target applications. In our
260 particular case where cost-effectiveness and miniaturization are the two most important
261 criteria, a miniature USB-powered high-performing laser module was chosen. The overall cost
262 for such Lego LIF detector was estimated to be 5000 euros, which is much cheaper (less than
263 25 %) than the purchase cost of a commercial fluorescence detector for CE.

264

265 ***3.1.3. Performance evaluation***

266 To evaluate the injection function of the new Lego CE, a series of tests were implemented
267 with injection of a standard FITC solution at different pressures and injection times
268 conventionally used in commercial CE systems. The reproducibility data for peak areas
269 obtained at different injection pressures and times are shown in table 1. Good injection
270 reproducibility was achieved at any injection pressure and time, except for the case of 30
271 mbar over 5 sec. The poorest reproducibility in this condition could be probably due to the too

272 short time for pressure manipulation at relatively low pressure range. The reproducibility for
273 migration time was excellent (RSD % < 0.5 %) under a delivery pressure of 400 mbar,
274 proving again the added value of this system, exhibiting precise pressurization. For evaluation
275 of detection signals, the performance of Lego LIF detector was compared to that of a
276 commercial LEDIF detector, using the same separation capillary and CE conditions.
277 Electropherograms for analysis of FITC at 110 nM that were obtained with both detectors are
278 shown in Fig. 3, whereas comparison data are presented in table 2. Very good linearity (R^2
279 better than 0.997) was acquired, whether the calibrations were made with peak areas or peak
280 heights, proving a very good response of the Lego LIF to the variation of FITC
281 concentrations. The detection sensitivity was approximately 10 times better for the
282 commercial LIF (see table 2). This can be explained by the fact that no focusing lens or
283 special optical setups were employed for the Lego LIF as otherwise required for a costly
284 commercial fluorescence detector. In addition, the photosensor module with PMT tube used
285 for Lego LIF is a miniaturized and inexpensive version, which might perform less well than
286 the one used for the commercial counterpart. In the former one, no electronic filtering was
287 included in the photomultiplier tube or trans-impedance amplifier module, whereas this
288 feature was already integrated in the latter one. This explains the more noisy background for
289 the raw signal of Lego LIF (see Fig. 3A), which was not the case for the commercial detector
290 (no signal difference between Fig. 3C and 3D). The lack of electronic filtering in the Lego
291 LIF was therefore compensated by digital filtering function offered by the data acquisition
292 module, allowing significant reduction of background noise and improvement of detection
293 sensitivity (Fig. 3B). The LOD values presented in table 2 were achieved for the filtered
294 signals.

295

296 **3.2. Separation and detection of fluorescently labelled oligosaccharides with Lego CE-**
297 **LIF**

298 Glucose-oligosaccharides are often used as the ladder reference for analyzing N-glycans
299 released from glycoproteins, serving for quality control of therapeutic glycoproteins and
300 diagnostic purposes [33, 34]. For oligosaccharides and glycans labeling, APTS is the most
301 frequently used fluorescent agent whereas BGEs containing inorganic ions are often used for
302 CE-LIF separation of labelled oligosaccharides and glycans [35, 36]. The electroosmotic flow
303 (EOF) is normally suppressed so that the negatively charged APTS-tagged oligosaccharides
304 (and glycans) can migrate against the EOF to arrive at the LIF detector for detection. All BGE
305 compositions reported so far for CE-LIF analysis in general, and CE-LIF for such purpose in
306 particular contain inorganic ions (*e.g.* phosphate, borate etc.) and / or use inorganic acid and
307 base (typically NaOH and HCl) for pH adjustment. These BGEs with low UV absorbing
308 feature, while being well adapted to UV detection, may not be optimal for LIF detection. We
309 have recently demonstrated that a much-improved performance for CE-LIF detection of
310 proteins and peptides could be achieved with our new BGEs for CE-LIF thanks to a better
311 stacking effect and lower current generation [20]. With a similar rationality, we optimized the
312 BGE composition for CE-LIF of labelled oligosaccharides this time. The principle behind this
313 strategy is illustrated in Fig. 4. By using a very dense zone of zwitterionic and large weakly
314 charged ions in the BGE to block the sample zone, the target analytes will be well stacked in
315 the sample-BGE boundary. While this stacking phenomenon can be observed using
316 conventional BGE containing inorganic ions, this effect is expected to be pushed up to the
317 maximum with our new BGE strategy. The use of extremely high BGE concentrations, while
318 not readily possible with inorganic ions due to high current generation, is now feasible thanks
319 to the very low electrophoretic movement of the large and / or zwitterionic molecules
320 constituting the BGE. Via simulation with the Phoebus program, we compared the properties

321 of different new BGEs for CE-LIF at pH 4.75 that have never been used before for such
322 purpose (table 3). The lithium acetate buffer at the same pH, frequently employed by
323 different groups for CE-LIF of oligosaccharides and glycans [35, 36], was used as a reference
324 for these comparisons. Among these new BGEs, beta-alanine / MES exhibits the best buffer
325 capacity and was expected to provide the best stacking effect due to the highest components'
326 concentrations (364 mM beta alanine et 538 mM MES). Another BGE composed of Naphtyl-
327 1-amine and MES, which is thought to offer equivalent performance to that of beta-
328 alanine/MES, is not considered due to the presence of a carcinogenic agent. Separation
329 performance for CE-LIF of APTS-labelled oligosaccharides was thus compared between
330 LiOH/Acetic acid and beta-alanine/MES BGEs, using first a commercial instrument (Fig. 5A
331 and 5B). At IS of 25 mM, the signals of oligosaccharides obtained with beta-alanine / MES
332 were two times higher than those obtained with LiOH / acetic acid buffer. With equivalent
333 background noises observed, this confirms a much better LIF sensitivity with the new beta-
334 alanine / MES BGE. The electroosmotic flow mobility was found a bit higher for beta-
335 alanine/MES buffers, which explains the longer migration times of oligosaccharide peaks. To
336 further improve the stacking effect, the IS of beta-alanine/MES was doubled and the
337 electropherogram for these conditions is shown in Fig. 5C. Conveniently, with beta-
338 alanine/MES BGE, an increase in IS from 25 to 50 mM only leads to a tolerable increase in
339 the generated current (from 13 to 25 μ A under 30 kV). The beta-alanine/MES BGE (IS 50
340 mM) led to a much higher peak sensitivity (almost 3 times) than the conventional
341 LiOH/Acetic acid buffer for the first 5 peaks. For slower-migrating ones (due to the presence
342 of a higher EOF magnitude with our new BGE), the peaks were more broadened, leading to a
343 less performance in detection sensitivity. Compared to previously communicated CE-LIF
344 conditions for this purpose [35, 36], our new BGE offered higher signals. Noted also that low

345 current generation (leading to low Joule heating) was achieved and no bubble formation was
346 observed when working with our non-thermostatted system.

347
348 The Lego CE-LIF was then used with this buffer for separations of APTS-labelled
349 oligosaccharides. The CE-LIF electropherogram obtained is shown in Fig. 6A. Excellent peak
350 shapes and separation resolutions were achieved for glucose units GU1 till GU6. To
351 compensate for the peak retardation when using beta-alanine/MES BGE, pressure assistance
352 could be applied during electrophoresis, which is not a complication when using the Flow EZ
353 pressure controller. As can be seen in Fig. 6B, the peaks arrived faster to the detector and
354 more glucose units could be visualized under the pressure assistance at 30 mbar. The pressure-
355 assisted electrophoresis can even be finely tuned by using a pressure gradient. By applying a
356 pressure of 30 mbar at 0s and then 20 mbar at 5 min, the fast arrival of the first four peaks
357 could be maintained, whereas separation resolution for the slower ones, which could
358 correspond to the sizes of large N-glycans of glycoproteins, was improved (see Fig. 6C). Note
359 that the unit displayed for LIF signals in Fig. 5 was RFU as the electropherograms were
360 obtained with a LIF detector from Sciex, whereas that in Figs. 3 and 6 was in a mV scale as
361 the signals were converted with an external data acquisition module. With this demonstration,
362 we expect to open a door for various applications exploiting both hydrodynamic and
363 electrokinetic principles with Lego CE-LIF. We also provide here a tool that could be tuned to
364 get it adapted for any kind of prospective glycan analysis. Indeed by playing on voltages and
365 pressures we would achieve the best separation performances whatever the kind of glycans to
366 be analyzed (i.e. N- or O-glycans, small or longer ones or even a mixture of these types).

367

368 **4. Conclusions**

369 We successfully developed a new Lego CE-LIF instrument that can be constructed from off-
370 the-shelf modules. Recourse to mechanical and electronic workshops can therefore be
371 avoided. A high degree of standardization with an affordable construction cost can be
372 achieved with this Lego CE-LIF design. The Lego design would allow the users to setup their
373 own analytical devices at a cost at least 70 % cheaper than the purchase price of a commercial
374 system while keeping a high degree of standardization (*i.e.* a 'standard' setup) and facilitation
375 of technology transfer that are not offered by in-house-made versions. This design was
376 demonstrated for separation of fluorescently labelled oligosaccharides that serve as a
377 reference for glycoprotein-derived glycan analysis. We also successfully developed a new
378 BGE based on large weakly charged and zwitterionic molecules at very high concentrations
379 for such analyses. This new BGE matches well to the Lego CE-LIF operation in terms of low
380 current generation (to avoid Joule heating in a non-thermostatted system), and high stacking
381 effect for improved LIF detection sensitivity. Various applications of Lego CE-LIF are
382 envisaged in different domains in order to increase the popularity of such design as an
383 interesting alternative to in-house-built hardly standardizable CE instrumentation.

384

385 ***Acknowledgements***

386 The authors are grateful for the financial support by the Agence Nationale de la Recherche
387 (ANR, France) with the grant no. ANR-18-CE29-0005-01. The VNU Key Laboratory of
388 Analytical Technology for Environmental Quality and Food Safety Control (KLATEFOS) is
389 also acknowledged for some instrumental support. We thank Dr. Thuy Tran-Maignan and Ms.
390 Bin Yang (Institut Galien Paris Sud) for useful discussions and their help in sample
391 preparation, as well as Mr. Jean-Jacques Vachon (Institut Galien Paris Sud) for his help in
392 instrumental setup.

393 The authors declare no conflict of interest.

394

395 **Table 1.** Salient performance data for the test on injection reproducibility realized with the
396 Lego CE system. Analyte: FITC 1 μ M; delivery pressure: 400 mbar; silica capillary with l_{eff}
397 of 35 cm and L_{tot} of 60 cm

Injection pressure	Injection time	Peak area (mV·s) (mean value)	RSD % (n = 4) Peak area
30 mbar	5 s	0.66	10.8
	10 s	1.06	2.37
	20 s	2.03	3.00
50 mbar	05 s	0.97	1.26
	10 s	1.68	4.08
	20 s	3.10	1.51
100 mbar	5 s	1.70	5.88
	10 s	3.33	1.85
	20 s	6.13	1.49

398

399
400
401
402
403
404
405
406
407
408
409
410
411
412
413
414
415
416
417
418
419
420

421 **Table 2.** Data on comparison on LOD and linearity between 2 LIF detectors.
422 Analyte: FITC 1 μ M. CE conditions : BGE composed of Tris / CHES (IS 20 mM, pH 8.4),
423 silica capillary with l_{eff} of 25 cm and L_{tot} of 45 cm; high voltage of 25 kV with normal
424 polarity; hydrodynamic injection at 50 mbar over 10s.

Detector	Calibration range (nM)	Linearity (R^2) with peak area	Linearity (R^2) with peak height	LOD (nM)
Lego LIF	30-1000	0.999	0.997	14
Commercial LIF (ZetaLIF)	3-1000	0.999	0.999	1.2

425
426
427
428
429
430
431
432
433
434
435
436
437
438
439
440
441
442
443
444
445
446
447
448
449
450
451
452
453
454
455
456

457 **Table 3.** Inorganic-species-free BGE compositions at IS of 25 mM and pH of 4.75, simulated
 458 with Phoebus program

459

BGE compositions	I (μA) at 30kV 50μm 65cm	buffer capacity (mmol/L,pH)	Expected quality	Remark
LiOH 25mM + Acetic acid 47 mM	16	28	Reference	
Acetic acid 47mM + His 26mM	14	30		similar to LiOH / Acetic acid
Pyridine 32mM + MES 538mM	16	71	+	carcinogenic
TRIS 25mM + MES 538mM	11	59	+	
Beta-alanine 364 mM + ANISIC Acid 36mM	13	70	+	
Beta-alanine 364 mM + Sorbic Acid 48mM	14	79	+	
Beta-alanine 358 mM + Phenylphosphonic acid 24mM	7	53	+	
Beta-alanine 364 mM + Furoic Acid 26mM	13	54	+	
Beta-alanine 364 mM + methanesulfonic acid 25mM	17	53	+	
Naphtyl-1-Amine 170mM + MES 538mM	9	105	++	carcinogenic
Beta-alanine 364 mM + MES 538mM	13	109	+++	

460
 461
 462
 463
 464

465 **Figure captions:**

466

467 Fig. 1. Schematic drawing of Lego CE design. GND: Ground electrode.

468

469 Fig. 2. Schematic drawing of Lego LIF design

470

471 Fig. 3. Electropherograms for CE-LIF separation of FITC 1 μ M using A) Lego LIF detector
472 without digital filter; B) Lego LIF detector with digital filter; C) commercial LEDIF
473 detector without digital filter; and D) commercial LEDIF detector with digital filter.
474 CE conditions : BGE composed of Tris / CHES (IS of 20 mM, pH 8.4); silica
475 capillary with L_{eff} of 25 cm and L_{tot} of 45 cm; high voltage of 25 kV with normal
476 polarity; hydrodynamic injection at 50 mbar over 10s.

477

478 Fig. 4. Principle of our new BGE optimization strategy for CE-LIF of labelled
479 oligosaccharides

480

481 Fig. 5. Electropherograms for CE-LIF separations of oligosaccharide ladders carried out
482 with a commercial PA800+ system, using A) conventional LiOH/Acetic acid BGE
483 (IS 25 mM, pH 4.75); B) beta-alanine / MES BGE (IS 25 mM, pH 4.75); and C)
484 beta-alanine / MES BGE (IS 50 mM, pH 5.04). CE conditions: HV -25 kV;
485 capillary of 50 μ m ID with total length of 30 cm and effective length of 20 cm;
486 hydrodynamic injection at 50 mbar over 10s.

487

488 Fig. 6. Electropherograms for CE-LIF separations of oligosaccharide ladders using the
489 Lego CE-LIF instrument. CE conditions: BGE composed of beta-alanine/MES with
490 IS of 50 mM and pH 5.04; HV -25 kV; fused silica capillary with L_{tot} of 45 cm and

491 L_{eff} of 23 cm; hydrodynamic injection at 50 mbar over 10s. A) Without pressure
492 assistance; B) With pressure assistance at 30 mbar from $t = 0\text{s}$; C) With pressure
493 gradient: 30 mbar at $t = 0\text{s}$, then 20 mbar at $t = 5\text{ min}$

494

495

496

497

498

499

500

501

502

503

504

505

506

507

508

509

510

511

512

513

514

515

516 **References**

517 [1] R.L.C. Voeten, I.K. Ventouri, R. Haselberg, G.W. Somsen, Capillary Electrophoresis:
518 Trends and Recent Advances, *Anal. Chem.*, 90 (2018) 1464-1481.

519 [2] M. Zhang, S.C. Phung, P. Smejkal, R.M. Guijt, M.C. Breadmore, Recent trends in
520 capillary and micro-chip electrophoretic instrumentation for field-analysis, *Trends*
521 *Environ. Anal. Chem.*, 18 (2018) 1-10.

522 [3] A.V. Schepdael, Recent Advances in Portable Analytical Electromigration Devices,
523 *Chromatography*, 3 (2016) doi:10.3390/chromatography3010002.

524 [4] A.P. Lewis, A. Cranny, N.R. Harris, N.G. Green, J.A. Wharton, R.J.K. Wood, K.R.
525 Stokes, Review on the development of truly portable and in-situ capillary
526 electrophoresis systems, *Meas. Sci. Technol.*, 24 (2013).

527 [5] P. Paul, C. Sanger-van de Griend, E. Adams, A. Van Schepdael, Recent advances in the
528 capillary electrophoresis analysis of antibiotics with capacitively coupled contactless
529 conductivity detection, *J. Pharm. Biomed. Anal.*, 158 (2018) 405-415.

530 [6] T.A.H. Nguyen, T.N.M. Pham, T.B. Le, D.C. Le, T.T.P. Tran, T.Q.H. Nguyen, T.K.T.
531 Nguyen, P.C. Hauser, T.D. Mai, Cost-effective capillary electrophoresis with
532 contactless conductivity detection for quality control of beta-lactam antibiotics, *J.*
533 *Chromatogr. A*, <https://doi.org/10.1016/j.chroma.2019.07.010> (2019).

534 [7] T.N.M. Pham, T.B. Le, D.D. Le, T.H. Ha, N.S. Nguyen, T.D. Pham, P.C. Hauser, T.A.H.
535 Nguyen, T.D. Mai, Determination of carbapenem antibiotics using a purpose-made
536 capillary electrophoresis instrument with contactless conductivity detection, *J. Pharm.*
537 *Biomed. Anal.*, (2019) 112906.

538 [8] P. Kubáň, H.T.A. Nguyen, M. Macka, P.R. Haddad, P.C. Hauser, New fully portable
539 instrument for the versatile determination of cations and anions by capillary

540 electrophoresis with contactless conductivity detection, *Electroanalysis*, 19 (2007) 2059-
541 2065.

542 [9] M.D. Le, H.A. Duong, M.H. Nguyen, J. Saiz, H.V. Pham, T.D. Mai, Screening
543 determination of pharmaceutical pollutants in different water matrices using dual-
544 channel capillary electrophoresis coupled with contactless conductivity detection,
545 *Talanta*, 160 (2016) 512-520.

546 [10] H.A. Duong, M.D. Le, K.D.M. Nguyen, H. Peter C., H.V. Pham, T.D. Mai, In-house-
547 made capillary electrophoresis instruments coupled with contactless conductivity
548 detection as a simple and inexpensive solution for water analysis: a case study in
549 Vietnam, *Environ. Sci. Process Impacts*, 17 (2015) 1941-1951.

550 [11] T.D. Nguyen, M.H. Nguyen, M.T. Vu, H.A. Duong, H.V. Pham, T.D. Mai, Dual-
551 channeled capillary electrophoresis coupled with contactless conductivity detection for
552 rapid determination of choline and taurine in energy drinks and dietary supplements,
553 *Talanta*, 193 (2018) 168-175.

554 [12] T.H.H. Le, T.Q.H. Nguyen, C.S. Tran, T.T. Vu, T.L. Nguyen, V.H. Cao, T.T. Ta, T.N.M.
555 Pham, T.A.H. Nguyen, T.D. Mai, Screening determination of food additives using
556 capillary electrophoresis coupled with contactless conductivity detection: A case study
557 in Vietnam, *Food Control*, 77 (2017) 281-289.

558 [13] T.A.H. Nguyen, T.N.M. Pham, T.T. Ta, X.T. Nguyen, T.L. Nguyen, T.H.H. Le, I.J.
559 Koenka, J. Saiz, P.C. Hauser, T.D. Mai, Screening determination of four amphetamine-
560 type drugs in street-grade illegal tablets and urine samples by portable capillary
561 electrophoresis with contactless conductivity detection, *Sci. Justice*, 55 (2015) 481-486.

562 [14] A.P. Vu, T.N. Nguyen, T.T. Do, T.H. Doan, T.H. Ha, T.T. Ta, H.L. Nguyen, P.C.
563 Hauser, T.A.H. Nguyen, T.D. Mai, Clinical screening of paraquat in plasma samples
564 using capillary electrophoresis with contactless conductivity detection: Towards rapid

- 565 diagnosis and therapeutic treatment of acute paraquat poisoning in Vietnam, J.
566 Chromatogr. B, 1060 (2017) 111-117.
- 567 [15] P. Kuban, F. Foret, G. Erny, Open source capillary electrophoresis, Electrophoresis, 40
568 (2019) 65-78.
- 569 [16] E.C.i.S.a. Technology, PortASAP - European network for the promotion of portable,
570 affordable and simple analytical platform, <http://portasap.eu/>, (2019).
- 571 [17] T.D. Mai, P.C. Hauser, Contactless Conductivity Detection for Electrophoretic
572 Microseparation Techniques, Chem. Rec., 12 (2012) 106-113.
- 573 [18] P. Kubáň, P.C. Hauser, 20th anniversary of axial capacitively coupled contactless
574 conductivity detection in capillary electrophoresis, TrAC - Trends Anal. Chem., 102
575 (2018) 311-321.
- 576 [19] C. Johns, M. Macka, P.R. Haddad, Indirect photomeric detection of anions in capillary
577 electrophoresis using dyes as probes and electrolytes buffered with an isoelectric
578 ampholyte, Electrophoresis 21 (2000) 1312-1319.
- 579 [20] M. Morani, M. Taverna, T.D. Mai, A fresh look into background electrolyte selection for
580 capillary electrophoresis-laser induced fluorescence of peptides and proteins,
581 Electrophoresis, DOI: 10.1002/elps.201900084 (2019).
- 582 [21] B. Reider, M. Szigeti, A. Guttman, Evaporative fluorophore labeling of carbohydrates via
583 reductive amination, Talanta, 185 (2018) 365-369.
- 584 [22] T. Kappes, P.C. Hauser, Portable capillary electrophoresis instrument with potentiometric
585 detection, Anal. Commun., 35 (1998) 325-329.
- 586 [23] T.D. Mai, M.D. Le, J. Saiz, H.A. Duong, I.J. Koenka, H.V. Pham, P.C. Hauser, Triple-
587 channel portable capillary electrophoresis instrument with individual background
588 electrolytes for the concurrent separations of anionic and cationic species, Anal. Chim.
589 Acta, 911 (2016) 121-128.

- 590 [24] T.T.T. Pham, T.D. Mai, T.D. Nguyen, J. Sáiz, H.V. Pham, P.C. Hauser, Automated dual
591 capillary electrophoresis system with hydrodynamic injection for the concurrent
592 determination of cations and anions and application to the monitoring of biological
593 ammonium removal from contaminated ground water, *Anal. Chim. Acta*, 841 (2014)
594 77-83.
- 595 [25] T.A.H. Nguyen, T.N.M. Pham, T.T. Doan, T.T. Ta, J. Sáiz, T.Q.H. Nguyen, P.C. Hauser,
596 T.D. Mai, Simple semi-automated portable capillary electrophoresis instrument with
597 contactless conductivity detection for the determination of beta-agonists in
598 pharmaceutical and pig-feed samples, *J. Chromatogr. A*, 1360 (2014) 305-311.
- 599 [26] T.D. Mai, T.T.T. Pham, J. Sáiz, P.C. Hauser, Portable Capillary Electrophoresis
600 Instrument with Automated Injector and Contactless Conductivity Detection, *Anal.*
601 *Chem.*, 85 (2013) 2333-2339.
- 602 [27] T.D. Mai, S. Schmid, B. Müller, P.C. Hauser, Capillary electrophoresis with contactless
603 conductivity detection coupled to a sequential injection analysis manifold for extended
604 automated monitoring applications, *Anal. Chim. Acta*, 665 (2010) 1-6.
- 605 [28] T.A.H. Nguyen, V.R. Nguyen, D.D. Le, T.T.B. Nguyen, V.H. Cao, T.K.D. Nguyen, J.
606 Saiz, P.C. Hauser, T.D. Mai, Simultaneous determination of rare earth elements in ore
607 and anti-corrosion coating samples using a portable capillary electrophoresis instrument
608 with contactless conductivity detection, *J. Chromatogr. A*, 1457 (2016) 151-158.
- 609 [29] L.D. Casto, K.B. Do, C.A. Baker, A Miniature 3D Printed LED-Induced Fluorescence
610 Detector for Capillary Electrophoresis and Dual-Detector Taylor Dispersion Analysis,
611 *Anal. Chem.*, 91 (2019) 9451-9457.
- 612 [30] M. Ryvolova, J. Preisler, F. Foret, P.C. Hauser, P. Krasensky, B. Paull, M. Macka,
613 Combined Contactless Conductometric, Photometric, and Fluorimetric Single Point
614 Detector for Capillary Separation Methods, *Anal. Chem.*, 82 (2010) 129-135.

- 615 [31] J. Prikryl, F. Foret, Fluorescence Detector for Capillary Separations Fabricated by 3D
616 Printing, *Anal. Chem.*, 86 (2014) 11951-11956.
- 617 [32] J.E. Thompson, K. Shurrush, G. Anderson, An Inexpensive Device for Capillary
618 Electrophoresis with Fluorescence Detection, *J. Chem. Educ.*, 83 (2006) 1677.
- 619 [33] P. Zhang, S. Woen, T. Wang, B. Liau, S. Zhao, C. Chen, Y. Yang, Z. Song, M.R.
620 Wormald, C. Yu, P.M. Rudd, Challenges of glycosylation analysis and control: an
621 integrated approach to producing optimal and consistent therapeutic drugs, *Drug*
622 *Discov. Today*, 21 (2016) 740-765.
- 623 [34] M. Hu, Y. Lan, A. Lu, X. Ma, L. Zhang, Chapter One - Glycan-based biomarkers for
624 diagnosis of cancers and other diseases: Past, present, and future, in: L. Zhang (Ed.)
625 *Prog. Mol. Biol. Transl. Sci.*, Academic Press 2019, pp. 1-24.
- 626 [35] G. Lu, C.L. Carihfield, S. Gattu, L.M. Veltri, L.A. Holland, Capillary Electrophoresis
627 Separations of Glycans, *Chem. Rev.*, 118 (2018) 7867-7885.
- 628 [36] L.R. Ruhaak, G. Zauner, C. Huhn, C. Bruggink, A.M. Deelder, M. Wuhrer, Glycan
629 labeling strategies and their use in identification and quantification, *Anal. Bioanal.*
630 *Chem.*, 397 (2010) 3457-3481.
- 631

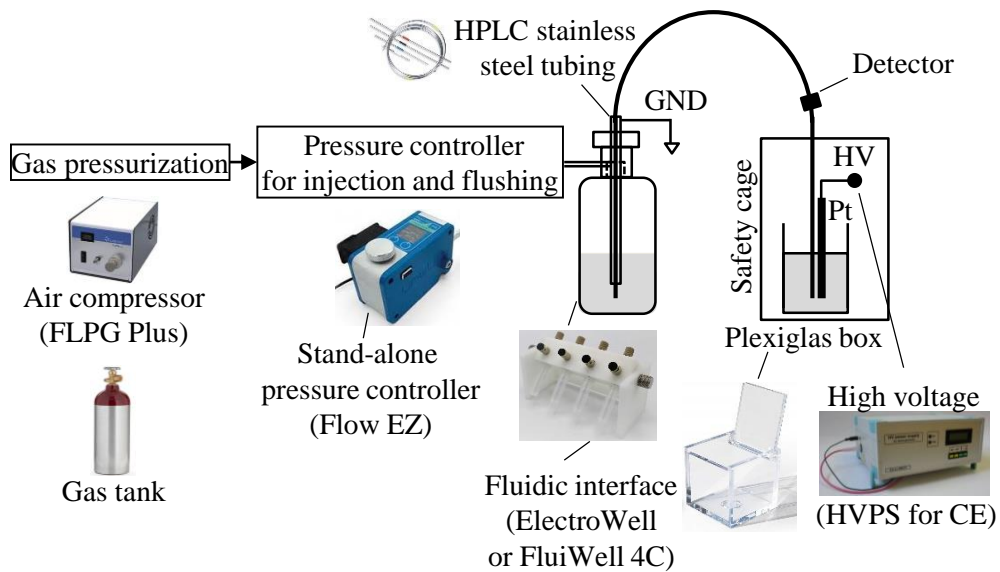


Figure 1

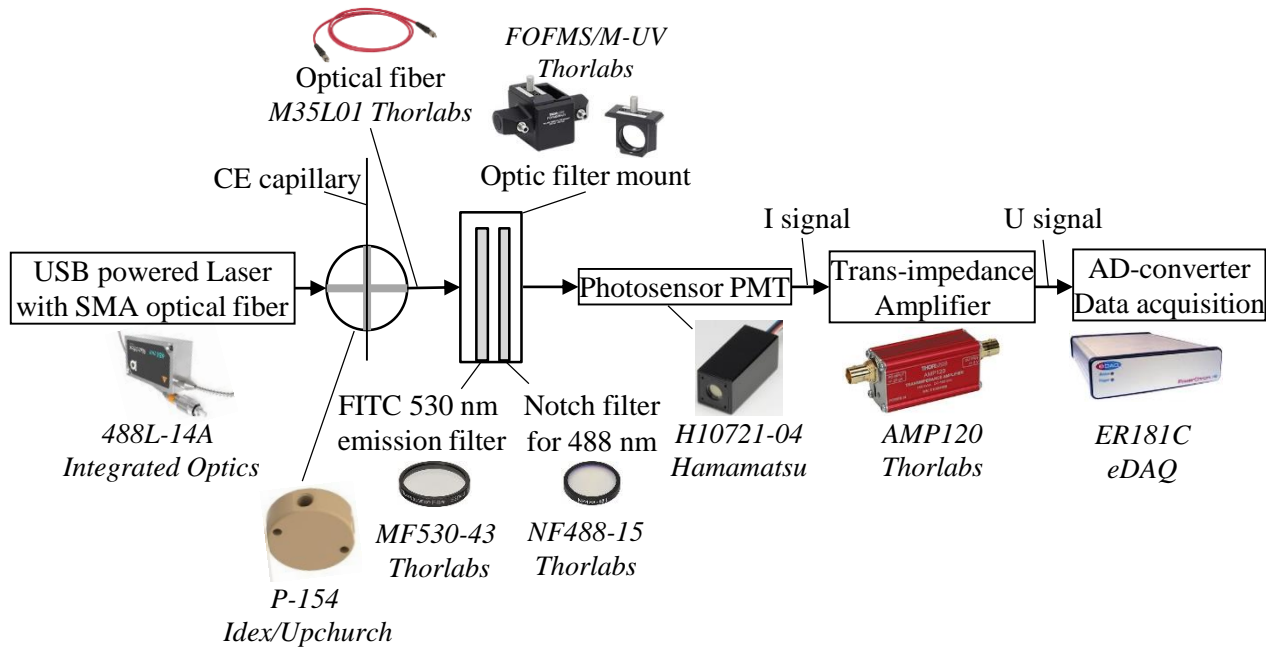


Figure 2

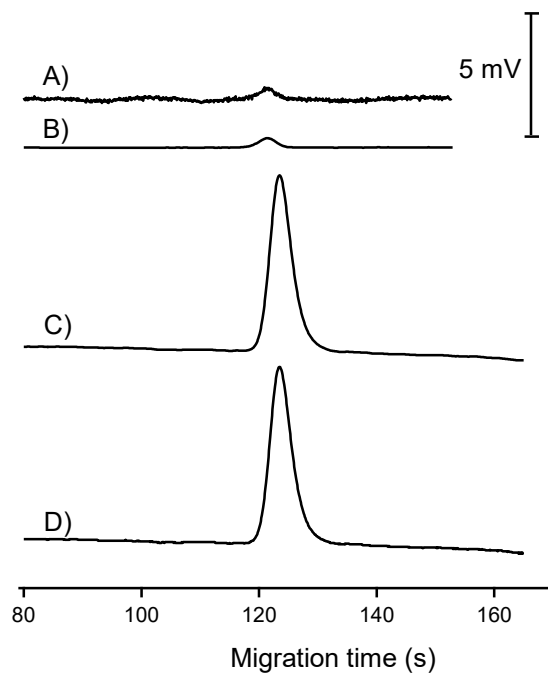


Figure 3

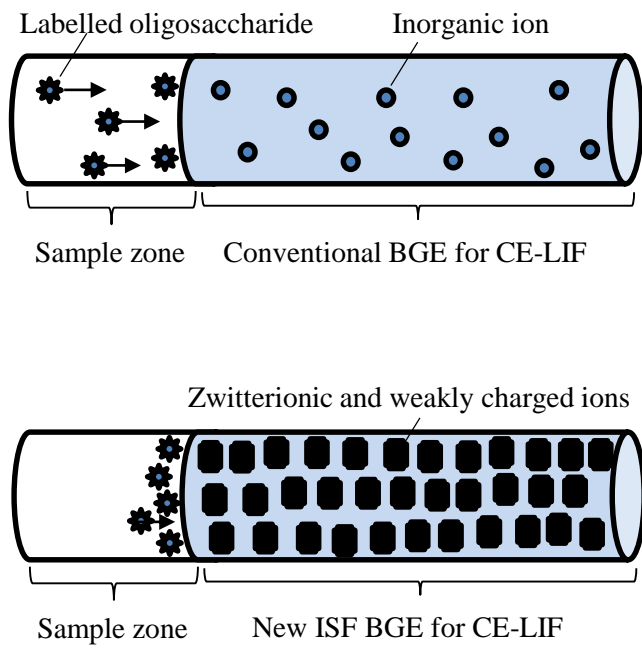


Figure 4

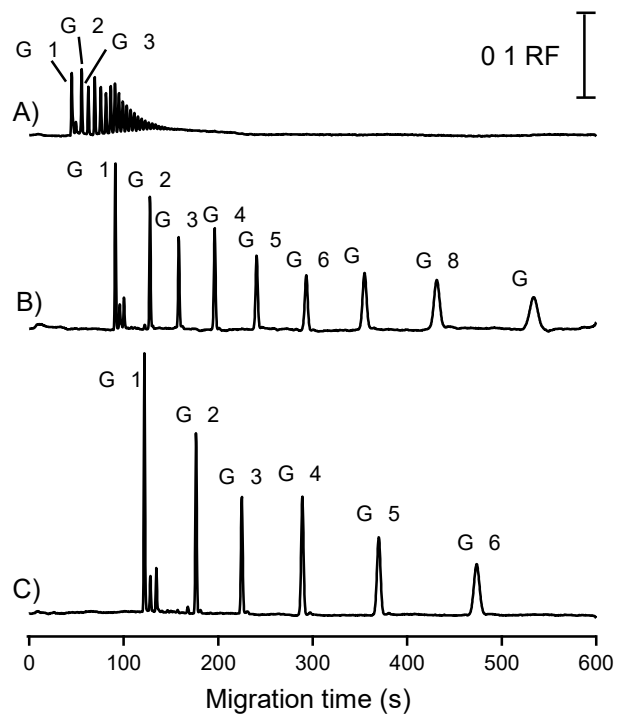


Figure 5

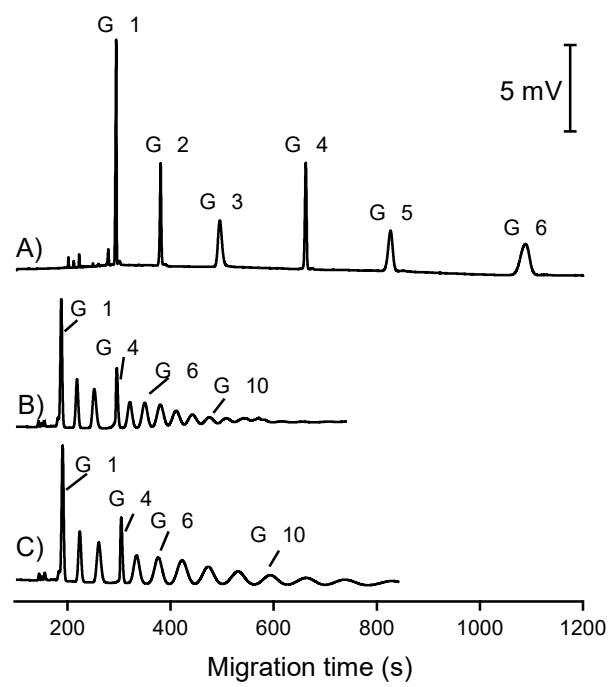
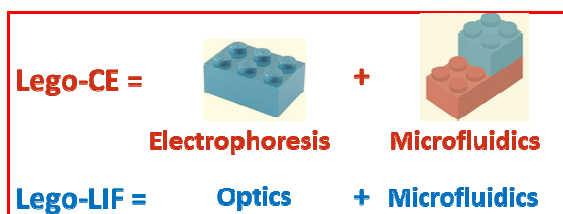


Figure 6

Lego-toy-inspired instrumentation for capillary electrophoresis with laser induced fluorescence detection.

By *Théo Liénard-Mayor, Jasmine S. Furter, Myriam Taverna, Hung Viet Pham, Peter C. Hauser* and Thanh Duc Mai **



IV.3. Development of the Droplet-interfaced CE (digital CE) system

Following our development of a home-made modular CE instrument aimed at providing an alternative solution for costly commercial CE machines, our next goal was then to use the same principle of adding different blocks together (like with LEGO) to create a purpose-made CE instrument customized for our biomarker analysis application. In Chapter III, we showcased our work on adapting the traditional in-tube protocol for the release and fluorescent tagging of glycans from glycoproteins in a droplet format. We were able to downsize the volume of reagents used by approx. 10-fold, the operation time by approx. 3-fold while having a fully automated protocol. At the end of this protocol, we obtain a 1 μ L droplet of sample containing our APTS-glycans which must now be analyzed with CE-LIF. Normally, volumes of samples put in a commercial CE are usually at least 10 μ L, meaning that for small quantities of samples, the sample must be diluted. In our case it would mean to perform a 10-fold dilution leading to a 10-fold concentration loss in the sample. Even though we made progresses and improved the sensitivity of our CE method by 4-5-fold (see Chapter III), our objective is still to be able to have the best sensitivity possible to be able to detect low-abundance glycans. In this context, a solution must be found to prevent this 10-fold dilution step and the 1 μ L droplet must be injected undiluted. For this purpose, we have written a detailed review on electrokinetic separations in a microchannel or microchip capillary electrophoresis (MCE). In our case because the final goal is to have an integrated platform performing both the sample pretreatment and the CE separation with a train of microfluidic droplets. We therefore chose to use the modular CE coupled with droplets in immiscible phase, since we already use droplets in an immiscible phase in our glycan sample treatment system.

Our strategy is thus to collect the 1 μ L droplet of APTS-glycan from the Magelia instrument (see chapter III), and then find a way to introduce it in our purpose-made CE system and inject it into a separation channel without any dilution. Because 1 μ L is relatively large for a microfluidic droplet, we decided on integrating a regular CE silica capillary to a microfluidic interface. The capillary has a sufficiently high inner diameter (50 μ m) so we can bring the droplet in front of it for precise injection. In addition, as the CE capillary is small enough so the difference in hydrodynamic resistance between the main channel and the capillary is significant. Accordingly, when the fluid is pushed through the system, it goes only in the main channel and not in the capillary, eliminating the requirement of valves to open or close the capillary channel. It is crucial to prevent the oil from entering the capillary, which could ruin both the capillary and the separation. Having a classical capillary is also advantageous because it can easily be replaced by a new one, and its length and effective length are easily changeable, which is especially convenient during the elaboration stage.

IV.3.1. Experimental setup

In the same fashion as the Lego CE we presented in Chapter IV.2, the digital CE instrument is composed of several blocks. The sample is stored in a 200 μ L PCR tube and must be carried by oil from the PCR tube in front of the separation capillary. The first and main block is composed of elements from Labsmith (Livermore, USA) and is illustrated in [Figure 45 A](#). On a uPB-05: uProcess breadboard are mounted two 100 μ L syringe pumps (SPS01-080-T116), one containing FC-40 fluorinated oil and the other containing the CE BGE. Two 3-port valves (AV201-T116) are used in combination with the syringes. They are connected to a 1 mL Reservoir (BBRES-T116) and to the central 4-port valve (AV202-T116). The two-port valves have 3 different positions corresponding to different fluidic paths as shown in [Figure 45 B](#). In the first position the syringe is connected to the fluidic reservoir, and by pulling or pushing the

syringe it can be emptied or filled). In the second position the syringe is connected to the 4-port syringe and can be used to push/pull liquid into the interface. The last position corresponds to the “closed” position and no liquid can flow through the valve.

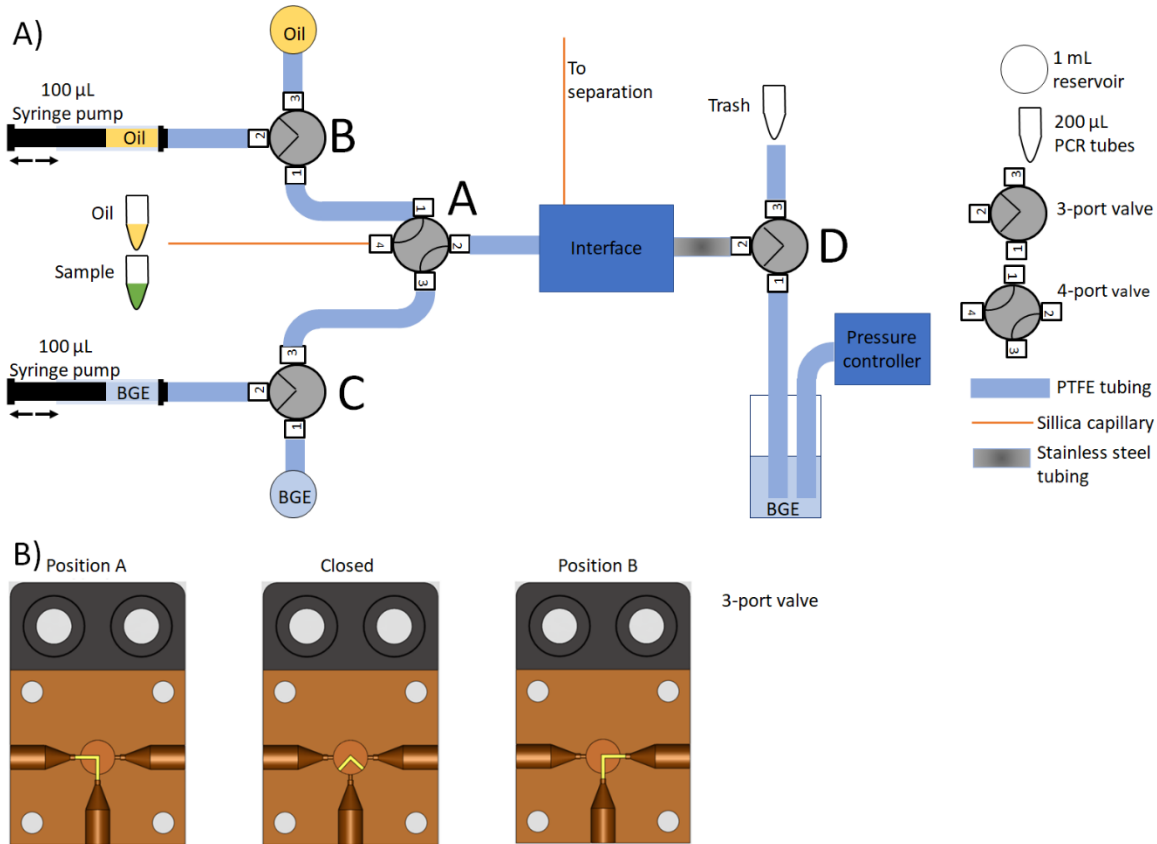


Figure 45 : A) Schematic of our digital CE system mounted on a LabSmith breadboard and B) LabSmith 3-port and 4-port valve positions. The fluidic path is represented in yellow. Adapted from the “AV Series Automated Valve spec sheet” available at: https://labsmith.com/Spec_Sheets/LabSmith_AV_Series_Automated_Valves_Spec_Sheet.pdf

The 4-port valve is the cornerstone of the system because it connects the syringes and allows transportation of the sample, oil and BGE to the interface. The positions of the 4-port valve are illustrated in Figure 45 B) and the number of the ports are shown in Figure 45 A). When ports 2 and 3 of the second 3-port valve are connected, BGE can be sent to the interface. At the same time since ports 1 and 4 of the 4-port valve are connected, the sampling capillary can be placed in the PCR tube containing the sample, and the sample can be pulled towards the syringe pump. When ports 1 and 2 of the first 3-port valve are connected, oil can be sent to the interface. While the syringe-based approach allows delivery of liquid on both back and forth directions, which is required to aspire sample and other solutions from the reservoirs and delivery them to the capillary, it does not allow application of a precise pressure over a pre-defined time (for example 50 mbar over 10 seconds) for hydrodynamic injection of the sample inside the capillary. A microfluidic pressure controller (0 to 1000 mbar, Flow EZ™ model, Fluigent, Paris, France) is thus placed on the other side of the interface which can be used for flushing the capillary with BGE and precise hydrodynamic injection of the sample inside the capillary. A third 3-port valve is connected to the interface and to a trash tube. When ports 1 and 2 of the third 3-port valve are connected, BGE can be pushed from the reservoir towards the separation capillary to rinse it or to inject

the sample. In this situation the 4-port valve is put in closed position to “focus” the liquid inside the capillary. When ports 2 and 3 of the third 3-port valve are connected, the liquid being pushed by the two syringes is being disposed of inside the trash PCR tube. One should note that the tubing connecting the interface to the third 3-port valve is composed of stainless steel and is used as a ground electrode during electrophoretic separation.

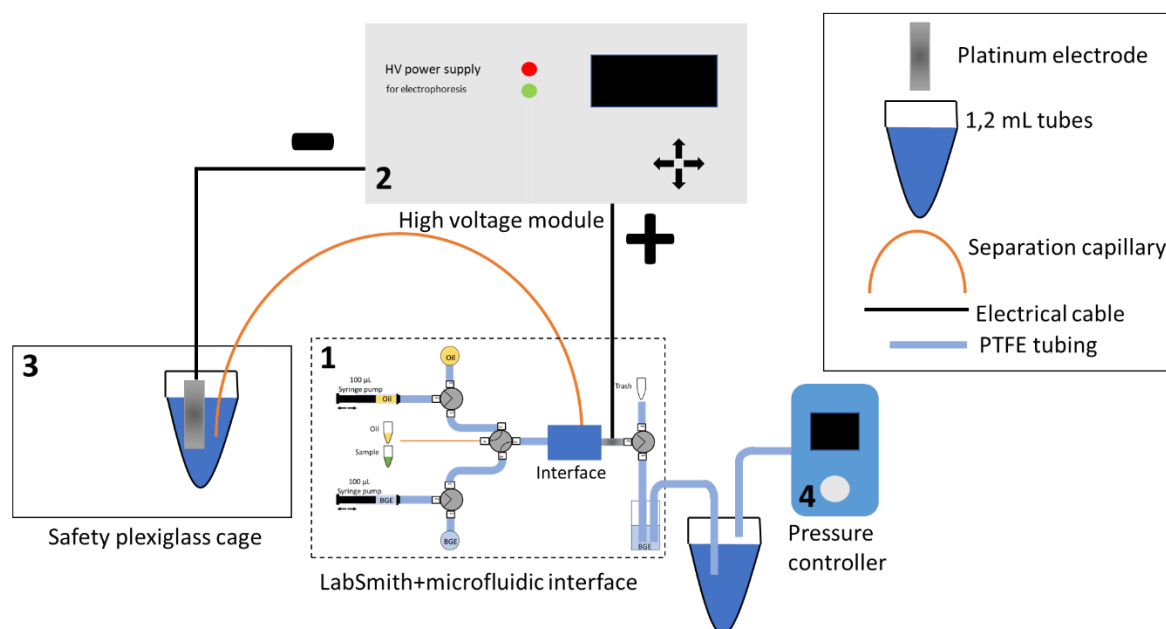


Figure 46: Schematic of the whole system made of 4 different blocks: 1) the main block with the LabSmith valves and syringes connected to the microfluidic interface, 2) the high voltage module for CE, 3) the safety plexiglass cage to protect the user from the high voltage and 4) the pressure controller for precise injection of the sample inside the capillary and for capillary flushing.

This main block is connected to three other blocks, as can be seen in [Figure 46](#). The second block is a high voltage power supply for electrophoresis (Villa Labeco, Spišská Nová Ves, Slovakia) and provides up to ± 30 kV for the separation. Voltage is applied through the stainless-steel tubing (ground electrode) presented in block 1 and to a platinum electrode (HV electrode) which is put in a 1.2 mL Eppendorf tube containing the separation buffer in the safety cage. The separation capillary filled with buffer has one end connected to the microfluidic interface and close to the stainless-steel tubing and the other end inside the Eppendorf tube. To protect the user from potential contact with the high voltage, the Eppendorf tube is placed inside a custom-made safety plexiglass cage (block 3). Holes are drilled into the box so that the capillary and the HV electrode can be placed inside the Eppendorf, and an interrupter is placed such that when opening the lid of the box, the high voltage module turns off and separation can be safely stopped. As already mentioned, the last block is the Fluigent pressure controller unit. It is used to rinse the capillary with the background electrolyte between separation runs and to precisely and repeatably inject the sample inside the capillary.

Generally speaking, one needs to be careful that droplet would not break when traveling inside the microfluidic system. In our case, because the droplets are produced by our Lab-In-Droplet system presented in Chapter III.3, it is not possible to create the droplet in-situ with geometries such as T-junction or flow focusing. The sample is stored first inside a 200 μ L PCR tube and must then be injected

in the LabSmith microfluidic system in order to reach the front of the separation capillary, where the Fluigent pressure controller can then be used for precise injection inside the capillary. In our case this requirement translated into the need for the 1 μL droplet to travel through valves. For droplet microfluidics, it is difficult to find commercial valves that do not break droplets going through them [311]. Two problems arise when flowing a droplet through a valve: i) the fluid displaces when the valve changes position, generating “pulses” which can break droplet and ii) the geometry of the valve can also put some constraint on the droplet, possibly deforming it. The former problem can be caused by the difference channel radius when the droplet reaches the interface between tubing and valve, but also by the geometry inside the valve (for example a straight angle for the 3-port valve in [Figure 45 B](#)). One type of valve that do not cause pulses is the gate valve, where a small part of the valve is moved in order to allow or block the circulation of fluids in the main channel [312]. Rotary valves (a type of gated valves) are available commercially: examples include the Cavro® Centris Pump (Tecan, Männedorf, Switzerland) or uProcess automated valves from Tecan already presented. We tested both valves, and while both did not produce any pulsing while changing position, we found that droplets broke while going through the Cavro valve. Our hypothesis is that the internal diameter of the valve is too big for the droplet, causing an important change in geometry when the droplet is at the interface between tubing and valve. Furthermore, the internal volume of the valve is bigger (2.7 μL) than the size of the droplet (1 μL). In contrast, LabSmith valves have a smaller internal diameter (250 μm) which is the same size as the inner diameter of our tubing, and an internal volume of 130 nL which is much smaller than the Cavro valve. The physical footprint of the Cavro pump is also much bigger than the LabSmith valve where all dimensions are at least twice smaller. In our case the whole LabSmith system and the microfluidic interface for the CE capillary fitted on the 127 mm x 177.8 mm x 6.35 mm uProcess breadboard. We thus chose to use LabSmith gear because it is adapted to the dimension of our droplets and interfaces, and it does not cause breaking of 1 μL droplets passing through the valves. For automation, the valves and syringes can be piloted by the dedicated software uProcess from LabSmith but can also be implemented in general software such as MathLab or LabView where components from different constructors can be piloted together (LabSmith syringes and valves, Fluigent pressure controller, high Voltage source, data acquisition).

IV.3.2. Interface

As we mentioned before, injecting undiluted fractions of 1 μL aqueous sample droplets into a CE capillary comes with technical necessities. In a classical CE instrument, the various solutions required for preconditioning, rinsing and separation are placed in 1-2 mL vials and the tip of the capillary is moved from vials to vials to push a solution inside the capillary. Because they are usually available in much smaller volumes (ten to dozens of μL), samples are placed in smaller (~200 μL) vials, and the system is built such that the tip of the capillary is barely immersed in the sample solution during sample injection. In our case, 1 μL of sample is too few to be injected with commercial CE, even though some special vials exist for injecting from microliters of sample.

During the rinsing of the capillary, the purpose of the interface is to be filled with BGE, so that BGE can be pushed inside the capillary by the pressure controller. The interface must be designed so that at this step, only BGE enters the capillary, and no oil is present in the system so it cannot enter the capillary and ruin its surface. During hydrodynamic injection of the sample inside the capillary, the system is filled with oil in order to transport the 1 μL droplet to move it directly in front of the capillary. The interface

must be tailored so that the droplet can be brought directly in front of the capillary without breaking and without any oil entering it. Finally, during the separation the interface is again filled with BGE. In order for the current to be stable during the separation, it is crucial that the current pathway between the two electrodes is filled with BGE. As a reminder, the first electrode is a metallic tubing connected directly to one side of the interface while the second electrode is put inside a vial containing BGE where the outlet of the capillary is placed.

The first version of the interface is re-used from a previous system developed by our group [313] (see [Figure 47](#)). The interface is composed of a main straight channel that goes one side to the other, and two same-size perpendicular channels. In terms of fabrication, the channels were drilled with a 400 μm metallic thread in a Perspex (Poly(methyl methacrylate)) block (2 cm \times 2 cm \times 3 cm). For the purpose of interfacing the channels to tubing, access holes for 1/4-28 fittings were also drilled. Because of the fabrication method, the channels have a circular cross-section of radius 400 μm , which is approximately the size of the capillaries we use for CE (375 μm outer diameter). This means that using appropriate fitting (1/4-28 1/16" fittings and PEEK capillary tubing sleeves 1/16" OD from IDEX Health & Science, Oak Harbor, USA), the separation capillary can be tightly fitted in one perpendicular channel. The other perpendicular channel was mainly unused, i.e., it was filled with BGE and closed with a PEEK fitting while paying special attention not to leave any air bubbles in the close channel. Some experiments were performed placing a platinum electrode in this channel instead of the stainless-steel tubing presented previously, which was replaced with regular PEEK tubing. PMMA is a plastic polymer and is highly hydrophobic, meaning it is suited for suspending water droplets in oil carrier.

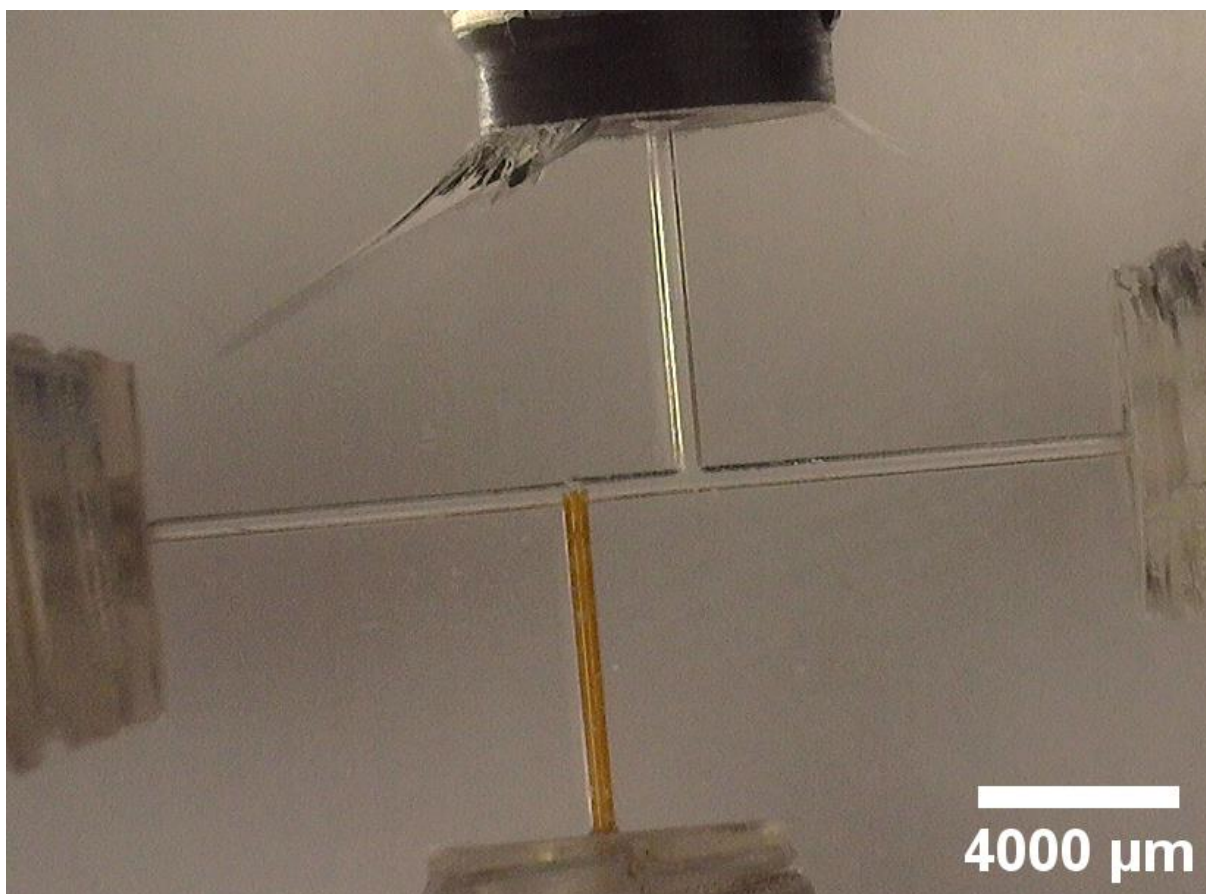


Figure 47 : Digital CE microfluidic interface for the injection of an undiluted 1 μL droplet inside a silica separation capillary. Channels are 400 μm wide.

In the situation of rinsing where all valves are opened and liquid (BGE or oil) is pushed through the system, when the liquid enters the interface via the main channel it is presented with two different fluidics paths with different hydrodynamic resistances: the straight path through the main channel to reach the outlet of the interface and the path through the separation capillary. Of course, at this step it is undesirable that any liquid enters the capillary, especially not oil. As a reminder from Chapter II, the hydrodynamic of a channel is written as: $R_H = \frac{8\eta L}{\pi R^4}$. If we assume that both paths have the same length, then the hydrodynamic resistance ratio between the main channel of radius $R_1 = \frac{400}{2} \mu\text{m}$ and the separation capillary of radius $R_2 = \frac{50}{2} \mu\text{m}$ is written: $\frac{R_{H1}}{R_{H2}} = \left(\frac{R_2}{R_1}\right)^4 = \left(\frac{1}{8}\right)^4 = 2.5 \cdot 10^{-4}$. This means that the hydrodynamic resistance of the capillary channel is 4000-fold higher than that of the main channel, meaning in theory that no oil will enter the capillary while rinsing the interface. In practice, we did not observe any unwanted fluid entering the capillary during rinsing. During capillary rinsing or sample injection, liquid is being pushed in the interface from the right and the 4-way valve is closed, meaning the only fluidic path available is through the capillary.

One issue that happened during electrophoresis is that we started observing air bubbles coming from the metallic tubing (right side of the interface, side of the pressure controller). As the bubble would grow inside the channel, the electrical current would decrease until it reached 0 and the separation would stop. It is known in CE that air can be produced at the electrodes during separation due to electrolysis

of the BGE. It generally does not cause trouble with commercial systems as the air can be released from the vial into air. In other words, the vials in which are placed the electrodes are not hermetically closed, meaning that gas produced during electrophoresis can “float” to the BGE/air interface and not hinder separation. In our case, our microfluidic system is a closed system, and PMMA is not a permeable material, meaning the air cannot escape without exterior intervention. Adding a cooling system to our system to limit Joule heating would require a much more complex design and lengthy development which is not desirable at this stage. The buffer we use is composed of TEOA and citric acid as presented in Chapter III and has a very high ionic strength (200 mM), resulting in a relatively high current during separation (60 μ A for a 60 cm capillary at -25 kV). As we have presented in the previous chapter, the IS of our buffer can be modulated depending on the application. In our case, lowering the IS could be useful to reduce the electrical current produced during electrophoresis. We tried lowering the IS of our buffer down to 50 mM, and also tried using the classical Lithium Acetate 24 mM buffer to see if separation would be hindered. We observed that even though air bubbles grew more slowly with lower IS buffers, it would still end up filling the channel and stopping separation.

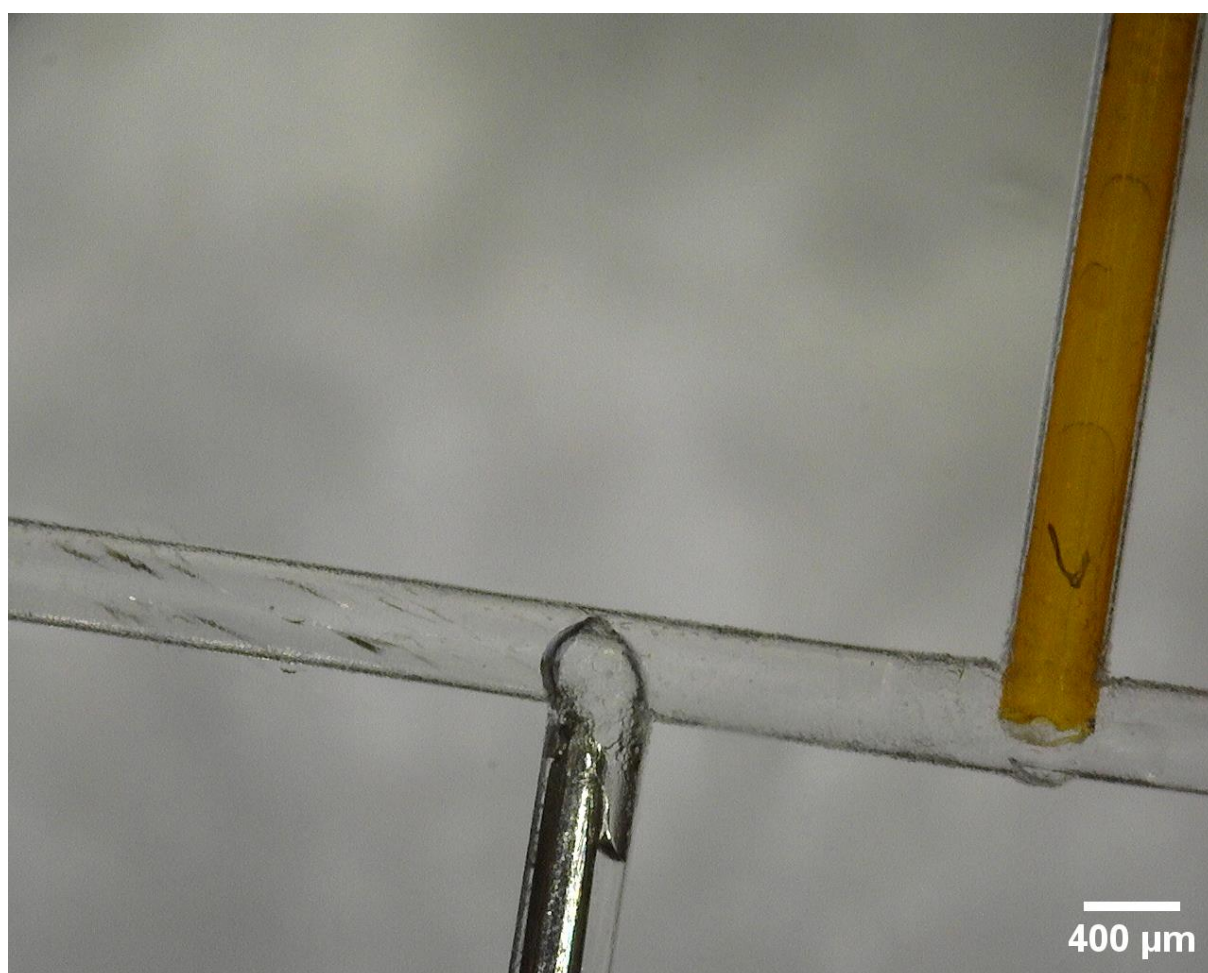


Figure 48 : Gas bubble forming under high voltage at the ground electrode inside the microfluidic interface.

In order to solve this issue, our strategy was to slowly push some BGE in the interface during separation using the BGE syringe. As was explained earlier, because of the difference in hydrodynamic resistance between the PMMA channel and the capillary, liquid pushed from the syringes toward the interface will not enter the capillary and stay in the channel of the interface. By slowly pushing the air building up at

the electrode towards the trash tube, separation can happen without interruption and with a stable current. Although this solution is not ideal, because it requires relatively large volumes of buffer (200-300 μL) per separation, it was the only solution available to us at this moment. In the future, PDMS could be used instead of PMMA since it is permeable to gas and air bubble could be disposed of automatically.

IV.3.3. Results

The automated protocol we developed for our system is described in [Table 6](#). We used the uProcess software from LabSmith to pilot the two syringes and the four valves. The pressure controller was either piloted manually or by the OxyGEN software from Fluigent. Sound warnings are placed in the uProcess code to warn for any manual intervention to be performed. Valve positions and main steps are illustrated in [Figure 49](#).

Table 6 : Fluidic operations for bringing a 1 μL plug of aqueous sample in front of a capillary for CE analysis. For the valve, positions are explained in Fig. 4 below. For the syringes, positive volumes correspond to liquid being pushed by the syringe while negative volumes correspond to liquid being pulled by the syringe.

Step	Valves position	Oil syringe	BGE syringe	Other
Step 1: Initialisation and syringe filling	Valve A 2 Valve B 1 Valve C 3 Valve D 2	Filled to 86 μL 2816.192 $\mu\text{L}/\text{min}$	Filled to 100 μL 2816.192 $\mu\text{L}/\text{min}$	
Step 2: Interface rinsing	Valve A 3 Valve B 3 Valve C 1 Valve D 1		40 μL dispensed 50 $\mu\text{L}/\text{min}$	
Step 3: Capillary rinsing	Valve A 2 Valve B 3 Valve C 1 Valve D 3			Fluigent module setup to 1000 mbar for 120 seconds
Step 4: Filling main channel with oil	Valve A 1 Valve B 3 Valve C 1 Valve D 1	10 μL dispensed 50 $\mu\text{L}/\text{min}$		
Step 5: Sample plug is created and sent between B and C	Valve A 3 Valve B 3 Valve C 1 Valve D 1	In the sample tube -1 μL dispensed 10 $\mu\text{L}/\text{min}$ In the oil tube -12.2 μL dispensed 10 $\mu\text{L}/\text{min}$		Capillary is first placed in the sample tube Then put back in the oil tube
Step 6: Sample plug is moved in front of the capillary	Valve A 1 Valve B 3 Valve C 1 Valve D 1	5.3 μL dispensed 10 $\mu\text{L}/\text{min}$		Script is paused so the user can check if the droplet is in front of the capillary

Step 7: Injection of the sample inside the capillary	Valve A 2 Valve B 3 Valve C 1 Valve D 3			Fluigent module set to 50 mbar for 5 sec
Step 8: Interface rinsing with BGE	Valve A 3 Valve B 1 Valve C 1 Valve D 1		40 μ L dispensed 50 μ L/min	After dispensing, the BGE syringe is filled
Step 9: Start of the separation	Valve A 3 Valve B 1 Valve C 1 Valve D 1			-25 kV high voltage is applied
Step 10: Gas removal during separation	Valve A 3 Valve B 1 Valve C 1 Valve D 1		80 μ L dispensed 10 μ L/min	Cycle of dispensing BGE followed by filling the syringe is repeated 3 times

Step 1 consists in initialising the system: when the Labsmith is first powered on, it is important to make sure the valves are not stuck and will move during the script. To make sure of that, they are first moved around and then put in position for the syringes to be filled. It should be noted that the oil syringe is not fully filled (syringes have 100 μ L capacity) because it will be used to pull liquid, which cannot be done if the syringe is full. Steps 2 and 3 consist in filling the interface in BGE in order to bring fresh buffer inside the system and then rinsing the capillary. Conveniently, as we have shown in Chapter III, inter-run capillary rinsing is performed only with BGE rinsing, meaning no other liquid must be introduced inside the system (HCl or NaOH for example). Step 4 consists in preparing the interface for the arrival of the sample droplet. It is then crucial to make sure that the tubing linking the 4-way valve to the interface and the interface itself are filled with oil, but since no oil will be pushed inside the capillary, as was the case during the previous step, lower amount of oil can be used (10 μ L are enough versus 40 μ L for BGE rinsing). Steps 5 and 6, where the sample is introduced inside the system and brought in front of the capillary, require precise tuning of the volumes dispensed because if the droplet is not exactly in front of the capillary oil will be pushed inside the system instead of sample. These steps require manual intervention to put the capillary inside the oil sample, and then put it back in the oil tube. 1 μ L of sample is pulled by the syringe, and then moved between valves A and B. After changing valve, A from position 3 to 1, the sample is pushed towards the interface and stopped in front of the capillary. In order to be as precise as possible, the volumes to be dispensed were approximated by measuring the length of capillary (to estimate their volume), by using the valve inner volume. A series of trial and error was then performed until the script was robust for sample injection. During step 7, valve A is closed (position 2) and the pressure controller is used for precise injection (50 mbar during 5s). The interface is then flushed with BGE to remove the oil for separation during step 8, which is identical to step 2. Separation can then be started at -25 kV during step 9, while step 10 runs during separation to make sure the gas produced during electrophoresis does not hinder the separation.

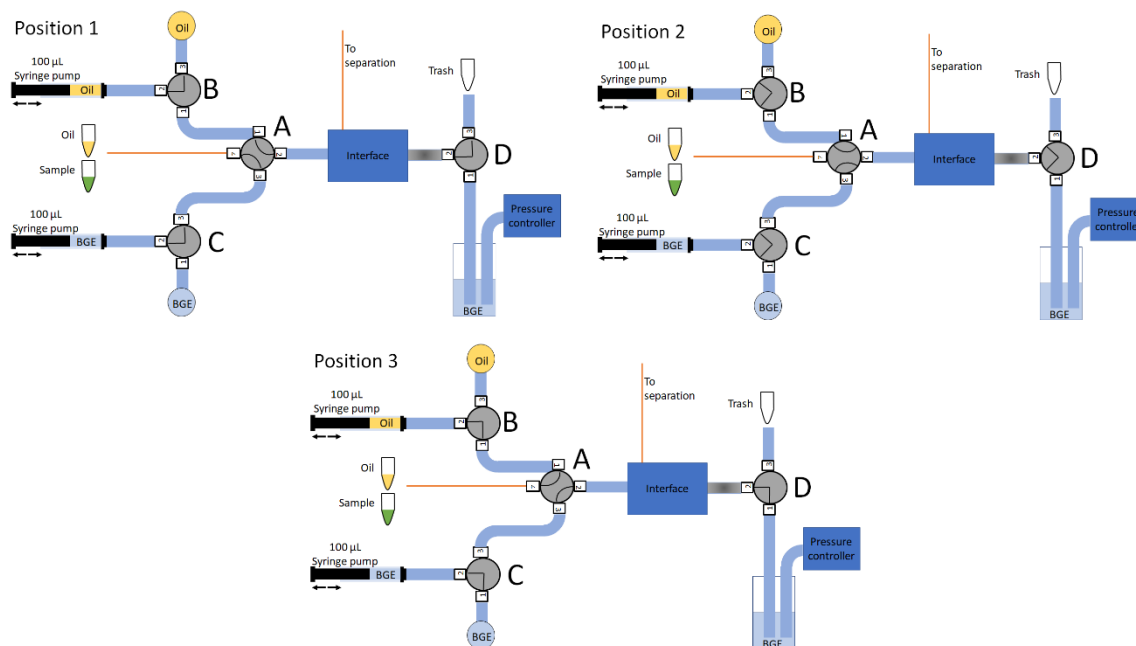


Figure 49 : Valve positions 1, 2 and 3.

First, the injection and its repeatability were tested. Three consecutive runs were performed where 1 µL droplet samples containing FITC were brought in front of the capillary, injection was performed at 50 mbar for 5 sec and separation was performed using 200 mbar pressure (without any voltage). Results

are

shown

in

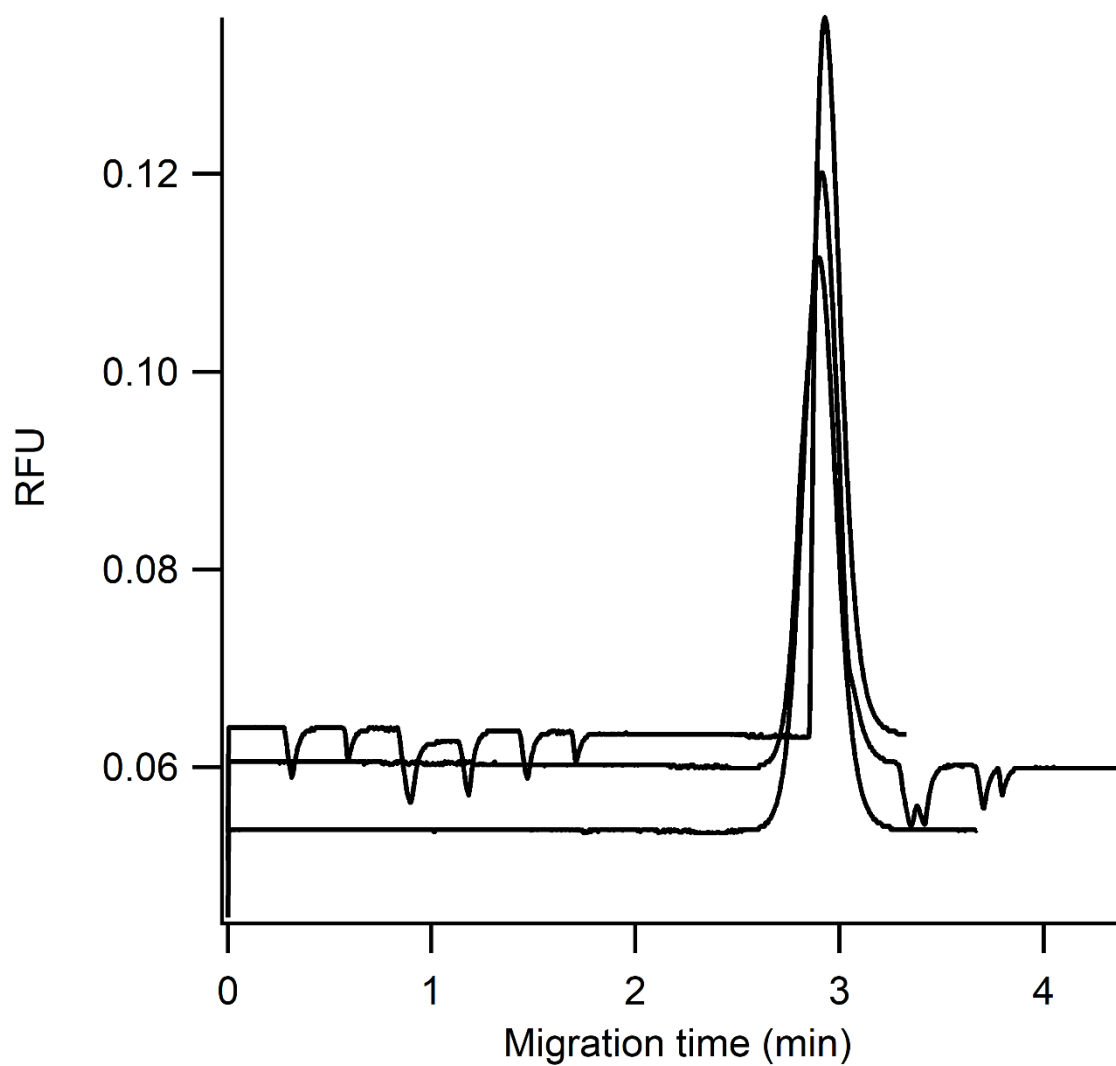


Figure 50 and Table 7.

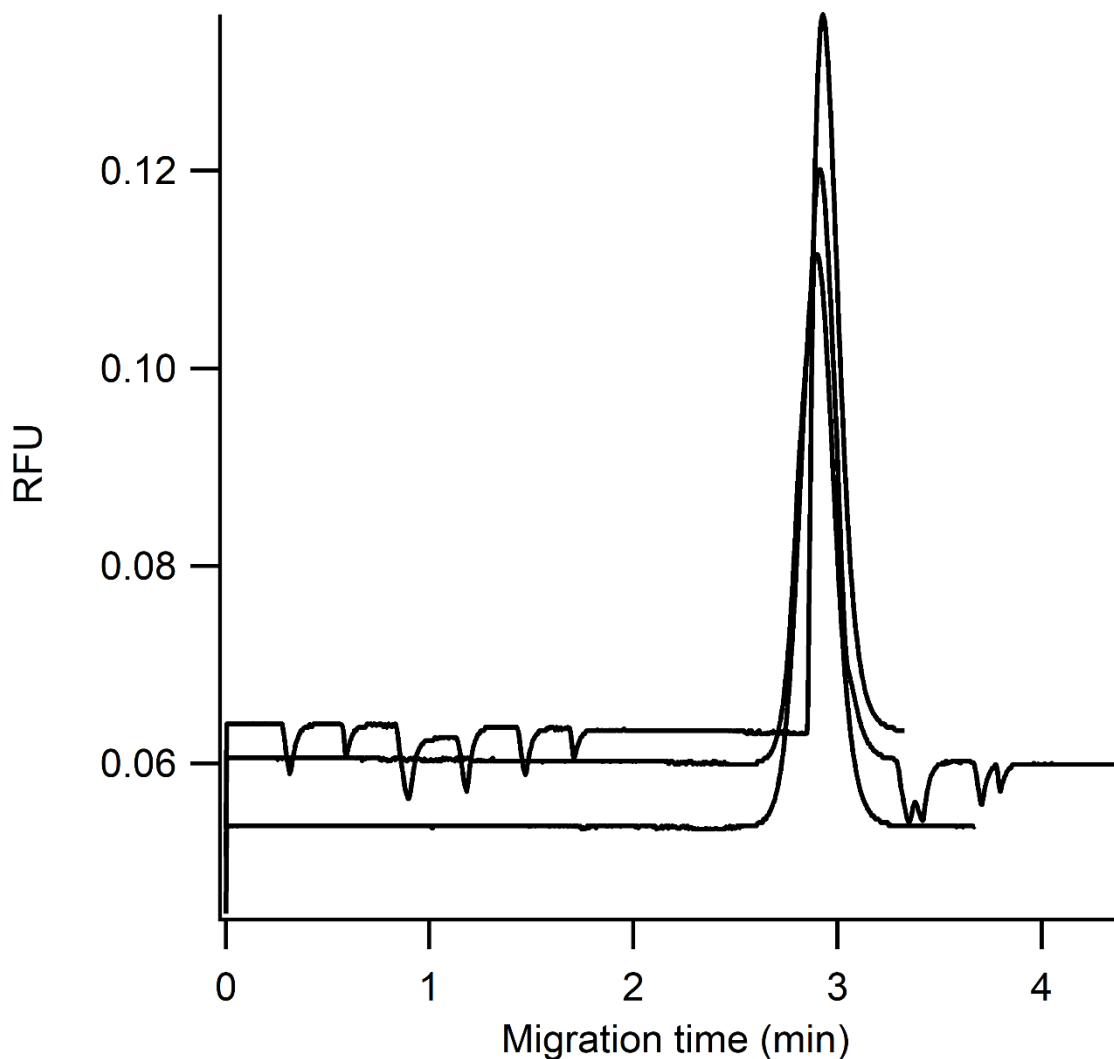


Figure 50 : Repeatability of injection of fractions of 1 μL plugs using our micro-CE system. Operational conditions: 200 mbar pressure, 60 cm capillary/50 cm effective length.

As seen by the superposition of the three runs, the injection of sample inside the capillary is good and reproducible regarding the migration time. Regarding the peak height and peak area, results could indicate that the volume of sample delivered varies between runs. Although it might be necessary to improve it later, we decided that at this step in elaborating the system it was good enough. It should be noted that the “negative” peaks observed in the first trace are most likely due to a defect of our detector and seem to appear randomly during separation.

Table 7 : Statistics for the injection of a FITC sample using our micro-CE system from Figure 50.

	Migration time	Peak height	Peak area
Mean value	2.912	0.062	0.011
Relative standard deviation (%)	0.573	13.714	4.542

After having checked that the injection was reproducible enough, we tried performing CE separations using our digital-CE system. Sample of MD ladder were used, and triplicate separation were performed, as seen in [Figure 51](#).

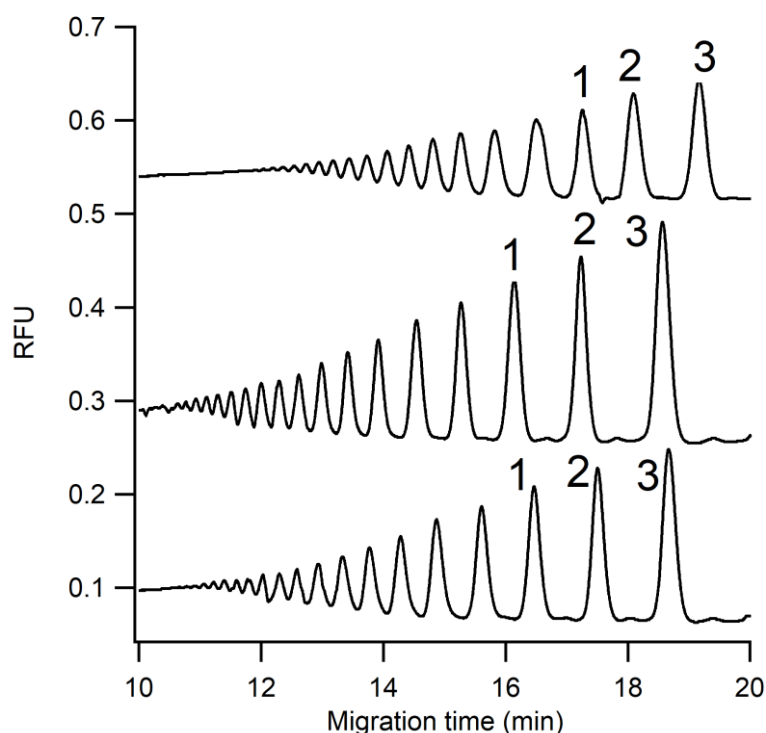


Figure 51 : Triplicate separation of MD ladder using our micro-CE system. Separation condition: -25 kV voltage, 60 cm capillary/50 cm effective length, buffer TEOA acetic acid 150 mM pH 4.75.

As can be seen from statistical results in [Table 8](#), the migration time reproducibility is quite satisfactory (below 5%) while the peak height and peak areas seem to vary between runs.

Table 8 : Normalized standard deviation of the three last peaks of MD ladder samples from Figure 51.

	Migration time	Peak height	Peak area
Stdev for peak 1 (%)	3.48	28.34	27.65
Stdev for peak 2 (%)	2.49	27.10	18.75
Stdev for peak 3 (%)	1.65	29.46	31.15

IV.3.4. Future perspectives

We have designed and ordered new interfaces from ChipShop (Jena, Germany) to be tested. It is made from a microscopic slide sized PMMA chip (7.55*2.55*0.15 cm) and channel are milled. It is a simple single channel chip with 3 entry ports as seen in [Figure 52 A](#)). The idea is that the orange port is considered as an inlet, and the others are outlet. The capillary will be placed at the yellow outlet while the stainless-steel tubing will be connected to the grey port. The channel is 500 μm deep and starts 500 μm wide ([Figure 52 B](#)). After the yellow port, the channel expands until is 1 mm wide at the grey port. The reasoning is that the channel must be narrow enough so the droplet is confined by the walls so it can be easily manipulated through the system. After the droplet has passed the interface, it is not

necessary that the droplet is confined and so the width can be increased to lower the hydrodynamic resistance so that the difference in hydrodynamic resistance between the capillary channel and the outlet channel is even more accentuated than before. Because we will have to use pressure during separation to remove gas bubbles from the stainless-steel channel, decreasing the hydrodynamic resistance should prove useful. It should be noted that due to the microfabrication method, in this case the channels are squared-shape instead of round-shaped as was the case previously.

Another alternative would be to use a gas permeable material such as PDMS in order to be able to remove the gas forming at the electrode. As we have mentioned in chapter II, PDMS has lot of advantages for prototyping and producing chips with similar designs as the one in [Figure 52](#) would not be overly difficult nor costly. However, consideration should be given when using PDMS under very high voltages. Other thermoplastics should therefore be considered as well.

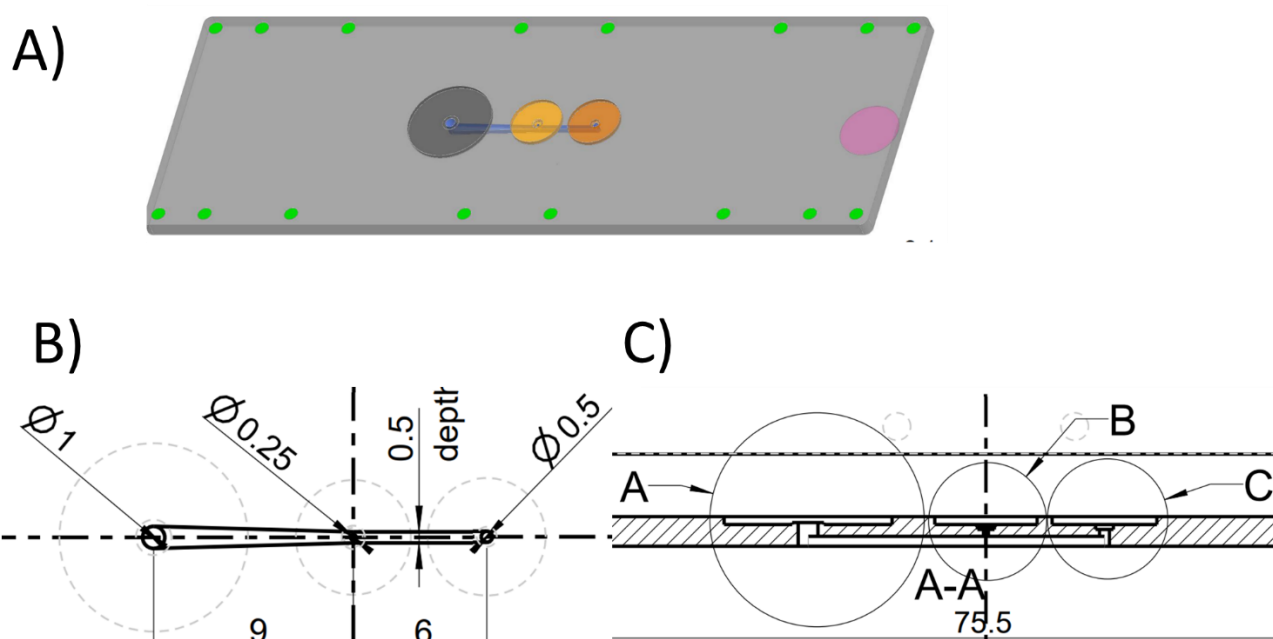


Figure 52 : Schematic of the interface from ChipShop to be tested: A), Schematic of the actual size of the chip, with the 3 entry ports being highlighted in dark grey, yellow and orange, B) Top-view of the chip and C) Side-view of the chip. Dimensions are shown in mm.

IV.4. Conclusion

In this chapter, we focused on the instrumentation part of this project. We reported two different systems designed for different purposes. Blocks were purchased from various suppliers and assembled to create customized CE systems which are an alternative to expensive and commercial CE systems.

The first system we presented is composed of microfluidics, optics and electrophoresis components and was designed to be a robust, cost-effective, and highly standardizable. The system does not require any mechanical workshop, nor any specific skills to be constructed and its overall cost is at least 70% lower than a commercial system. Separation reproducibility was very satisfactory ($RSD\% < 0.5\%$) while detector linearity was also very good ($R^2 > 0.997$). Detector sensitivity was circa 10-fold lower than that of a commercial detector, meaning that a compromise between cost and sensitivity must be made. APTS-

labelled oligosaccharides were successfully separated using a new BGE, which was actually the first results from our work on improving the CE method for APTS-glycans.

The second system we presented is mostly an upgrade of the first system but was designed for a specific purpose: being able to inject undiluted 1 μ L sample droplet for CE separation. Because it is necessary to carry the droplet in oil to prevent sample dilution or diffusion, the design of the system has to be adapted. Some parts of the first system were re-used while a microfluidic interface with a new microfluidic LabSmith system for fluid handling were added. Our preliminary results show that the automatic injection of the sample inside the capillary is robust and reproducible. Triplicates of MD ladder were also separated with our system, Further experiments are required, including using a new custom-made microfluidic interface for the separation. The system, once developed, can be used in the future to separate glycans from patient samples treated with the Magelia system.

Conclusion and perspectives

In this thesis we have laid the first bricks for our project of building a Lab in Droplet platform for the integrated sample treatment and analysis of glycans by CE-LiF.

In Chapter III.2, we presented our new CE-LiF methodology for glycans, based on a high ionic strength BGE coupled with a LVSEP preconcentration technique. A 5-fold increase in sensitivity was achieved, up to 200-fold using a LVSEP preconcentration method, using neither neutral capillaries nor polymer additives. While we are satisfied with the performance of our method, we noticed a slight decrease in resolution in the electropherogram of glycans from IgG using LVSEP. It was not something that we observed in previous experiments [301] and could be explained by the sample matrix not being completely removed from the capillary and the remaining APTS hindering the separation. This lower resolution can prevent the low-abundance glycan from being detected/differentiated from other glycans while we performed LVSEP in the first place to detect low-abundance glycan. One solution to increasing resolution of glycans could be to add some polymer to the BGE to increase the viscosity of the BGE. But it was our initial choice to avoid its use to facilitate the coupling to digital CE. As a matter of fact, it is probably one of the reasons why the commercial solution to CE-LiF of glycan recommends the use of a gel BGE. Another solution could be to improve the removal of APTS prior to separation which could be done using our droplet protocol and improving the washing steps.

In Chapter III.3, we presented our solution to translate the classical in-tube protocol for N-glycans sample preparation prior to CE-LiF in a droplet microfluidic format. Based on the Magelia instrument developed by Inorevia, we managed to denature the glycoprotein, enzymatically digest with PNGase F to release glycans, tag glycans with APTS and purify them from human serum glycoproteins. We managed to reduce reagents consumption by 10-fold, operation time by 3-fold, obtain a 2-fold signal gain and automate the protocol while working with complex human samples. Still, several aspects of this system could be improved. The first obvious shortcoming of our system that we highlighted in Article 3 was the 5-fold dilution of our sample induced after digestion. Indeed, our system can only handle droplets ranging from 1-10 μL and we had to fuse a 5.7 μL droplet with ACN so that the final proportion of ACN was 87.5%. While in theory the range 1-10 μL could be extended, providing the calibration of the machine is changed, it would probably result in less reproducible operations and would overall be a bad solution. One solution would be to perform this capture step in one of the reagents reservoirs. The original 5.7 μL droplet, containing the magnetic beads, the released glycans and residual unglycosylated proteins along with denaturation and digestion reagents, can first be recovered in the reservoir. The volume of ACN required for a droplet containing 87.5% ACN is 39.9 μL . In order to add it to the reservoir, three consecutive 10 μL of ACN can be created in the capillary and then delivered to the reservoir, followed by a fourth droplet of 9.9 μL . For the mixing, series of small aspirations and deliveries can be performed, just like it is done to resuspend magnetic beads that have aggregated to the bottom of the vials. While making sure the magnetic tweezer is ON, one can then aspirate the mix, bring the droplet in front of the capillary so the beads can be

attracted to the magnet, and discard the droplet. It can be done 10 μL at a time, or a 45.6 droplet could be created. In this case the size of the droplet does not cause any problem to the system (if the program piloting allows it) because no complex operations are performed: the droplet is only aspired and then discarded. The droplet is also within range of both the syringe capacity (100 μL) and the size of the reservoir (100 μL).

Another aspect that could be easily improved is the throughput of the system. Granted, we managed to lower the operation time from more than 4 hours to 1.3 hours. But 1.3 hours to process one sample is clearly not high-throughput. The advantage of this kind of system is that they are relatively easy to parallelize. Indeed, Inorevia is in the early phase of commercializing an upgraded version of Magelia which possess 8 parallel capillaries. While parallelization might not be crucial for CDG since they are rare genetic diseases, the fact we managed to implement a protocol involving magnetic beads and organic solvents in a microfluidic droplet format could open up the possibility of translating many similar applications which could benefit from parallelization and higher throughput.

In Chapter IV.2, we showcased our modular CE system designed as an alternative to expensive commercial systems. Even though this system was robust and produced reproducible separations, one major drawback was the performance of the homemade laser, which sensitivity was 10-fold less than the commercial laser it was compared to. Of course, a compromise between performance and cost must be found, especially in a limited resource environment. It is difficult to build a low-cost LiF because laser sources are extremely costly at the 488 nm wavelength. Building our own laser source could be possible but would probably require specific equipment and skills. As an alternative for other applications, C4D detections systems are versatile and usable for many applications, even though its sensitivity is not as good as LiF sensitivity. Nevertheless, open-source C4D detectors can easily be found and constructed as we have mentioned in IV.1. Overall, the modular CE system is a nice alternative which can be easily customized for lots of applications involving CE.

In Chapter IV.3, we presented the first work for our digital CE system, designed to inject fragments of an undiluted 1 μL droplet processed by Magelia containing APTS-glycans. We already discussed to some extent the perspectives of this system in section IV.3.4. Assuming we have finished experiments with this CE system and its performances are satisfactory, another perspective that we can discuss would be how we could couple this system with the Magelia system since our goal is to have an integrated system. Right now, manual operations still happen during the digital CE method. The first reason is that the capillary that transports the sample to the separation capillary has to be moved from a PCR vial containing oil to a PCR vial containing the sample. Although the oil and sample would not mix when put in the same vial, the oil would be at the bottom and injection of the sample would still require manual adjustment. One solution would be to use mineral oil, which is lighter than water. This would be useful for two reasons: the PCR vial containing the sample would be less subject to evaporation because of the oil layer covering it and the sample would always be at the bottom of the vial, meaning if the capillary is properly fixed no manual intervention would be required. The second reason why manual intervention are required is because the software used for

the Labsmith system is not the same as the one used for the Fluigent pressure controller. In the future, both systems should be controlled using the LabView software, which could even control the high voltage tension, meaning the only manual intervention would be to start the script or replace the sample.

In general, we have presented both accessible and versatile systems for the analysis of glycans with the modular CE and specific and dedicated systems with Magelia and digital CE. This means that solution exists both for hospitals specialized in CDG and for smaller laboratories who are interested in glycan analysis or CDG diagnosis. One thing to note in this thesis is that when we analysed human serum samples, we have always shown electropherogram of total N-glycan from serum. As we have discussed in Chapter 1.2.3, while providing useful information, the analysis of total N-glycan can sometimes not be enough, and one could need information on the glycosylation of a specific protein. Indeed, it is more likely that this kind of N-glycan mapping shows preferentially the glycans peaks from the most abundant glycoproteins in the serum (IgG, Transferrin).

And because of the versatility of magnetic beads, it would actually be possible to use magnetic beads grafted with an antibody specific for a given glycoprotein and perform an extraction in a similar fashion as the glycan extraction we perform in our protocol. We actually wanted to implement this to study the glycosylation of Transferrin, but we opted not to because of time limitation. Protein depletion can also be desired, and some commercial kits exist to deplete albumin and immunoglobulins from plasma samples. In a similar fashion, magnetic beads can be functionalised with antibodies specific for albumin and immunoglobulins and could be implemented in our Magelia protocol.

References

- [1] B. Cylwik, M. Naklicki, L. Chrostek, E. Gruszewska, Congenital disorders of glycosylation. Part I. Defects of protein N-glycosylation, *Acta Biochimica Polonica*, 60 (2013) 151-161.
- [2] T. Hennet, J. Cabalzar, Congenital disorders of glycosylation: a concise chart of glycolyx dysfunction, *Trends in Biochemical Sciences*, 40 (2015) 377-384.
- [3] A.P. Corfield, M. Berry, Glycan variation and evolution in the eukaryotes, *Trends in Biochemical Sciences*, 40 (2015) 351-359.
- [4] M.H. Hu, Y. Lan, A. Lu, X.X. Ma, L.J. Zhang, Glycan-based biomarkers for diagnosis of cancers and other diseases: Past, present, and future, in: L. Zhang (Ed.) *Prog. Mol. Biol. Transl. Sci.* 2019, pp. 1-24.
- [5] I. Kohler, M. Augsburg, S. Rudaz, J. Schappler, New insights in carbohydrate-deficient transferrin analysis with capillary electrophoresis–mass spectrometry, *Forensic Science International*, 243 (2014) 14-22.
- [6] A. Bruneel, S. Cholet, T. Tran-Maignan, T.D. Mai, F. Fenaille, CDG biochemical screening: where do we stand? , *BBA - General Subjects*, 1864 (2020) 129652.
- [7] R. Péanne, P. de Lonlay, F. Foulquier, U. Kornak, D.J. Lefeber, E. Morava, B. Pérez, N. Seta, C. Thiel, E. Van Schaftingen, G. Matthijs, J. Jaeken, Congenital disorders of glycosylation (CDG): Quo vadis?, *European Journal of Medical Genetics*, 61 (2018) 643-663.
- [8] H.-t. Feng, M. Su, F.N. Rifai, P. Li, S.F.Y. Li, Parallel analysis and orthogonal identification of N-glycans with different capillary electrophoresis mechanisms, *Analytica Chimica Acta*, 953 (2017) 79-86.
- [9] Y. Mechref, J. Muzikar, M.V. Novotny, Comprehensive assessment of N-glycans derived from a murine monoclonal antibody: A case for multimethodological approach, *ELECTROPHORESIS*, 26 (2005) 2034-2046.
- [10] J.-R. Wang, W.-N. Gao, R. Grimm, S. Jiang, Y. Liang, H. Ye, Z.-G. Li, L.-F. Yau, H. Huang, J. Liu, A method to identify trace sulfated IgG N-glycans as biomarkers for rheumatoid arthritis, *Nature communications*, 8 (2017) 1-14.
- [11] Z. Xiao, M. Niu, B. Zhang, Droplet microfluidics based microseparation systems, *Journal of separation science*, 35 (2012) 1284-1293.
- [12] Y. Zhu, Q. Fang, Analytical detection techniques for droplet microfluidics—A review, *Analytica chimica acta*, 787 (2013) 24-35.
- [13] M. Serra, D. Ferraro, I. Pereiro, J.-L. Viovy, S. Descroix, The power of solid supports in multiphase and droplet-based microfluidics: towards clinical applications, *Lab Chip*, DOI: 10.1039/C7LC00582B (2017).
- [14] P. Kuban, F. Foret, G. Erny, Open source capillary electrophoresis, *Electrophoresis*, 40 (2019) 65-78.
- [15] T. Liénard--Mayor, M. Taverna, S. Descroix, T.D. Mai, Droplet-interfacing strategies in microscale electrophoresis for sample treatment, separation and quantification: A review, *Analytica Chimica Acta*, 1143 (2021) 281-297.

- [16] J.B. Lowe, J.D. Marth, A Genetic Approach to Mammalian Glycan Function, *Annual Review of Biochemistry*, 72 (2003) 643-691.
- [17] D. Voet, J.G. Voet, *Biochimie, De Boeck Supérieur* 2016.
- [18] G. Opdenakker, P.M. Rudd, C.P. Ponting, R.A. Dwek, Concepts and principles of glycobiology, *The FASEB journal*, 7 (1993) 1330-1337.
- [19] C.H. Shao, Z.K. Feng, J.D. Westbrook, E. Peisach, J. Berrisford, Y. Ikegawa, G. Kurisu, S. Velankar, S.K. Burley, J.Y. Young, Modernized uniform representation of carbohydrate molecules in the Protein Data Bank, *Glycobiology*, 31 (2021) 1204-1218.
- [20] D.B. Werz, R. Ranzinger, S. Herget, A. Adibekian, C.W. von der Lieth, P.H. Seeberger, Exploring the structural diversity of mammalian carbohydrates ("Glycospace") by statistical databank analysis, *Acs Chemical Biology*, 2 (2007) 685-691.
- [21] S.N.f. Glycans, *Symbol Nomenclature for Glycans (SNFG)*, 2019.
- [22] J. Hofmann, K. Pagel, *Glycan Analysis by Ion Mobility–Mass Spectrometry*, *Angewandte Chemie International Edition*, 56 (2017) 8342-8349.
- [23] K. F. Aoki-Kinoshita, *Glycan Nomenclature and Summary of Glycan-related Resources*, *Glycoforum*, 22 (2019).
- [24] R.A. Dwek, Obituary: Alan Williams 1945–1992, *Glycobiology*, 2 (1992) 505-506.
- [25] A.D. McNaught, *Nomenclature of Carbohydrates*, (1996).
- [26] R. Ranzinger, M. Frank, C.-W. von der Lieth, S. Herget, Glycome-DB.org: A portal for querying across the digital world of carbohydrate sequences, *Glycobiology*, 19 (2009) 1563-1567.
- [27] M. Matsubara, K.F. Aoki-Kinoshita, N.P. Aoki, I. Yamada, H. Narimatsu, WURCS 2.0 Update To Encapsulate Ambiguous Carbohydrate Structures, *Journal of Chemical Information and Modeling*, 57 (2017) 632-637.
- [28] D.J. Harvey, A.H. Merry, L. Royle, M. P. Campbell, R.A. Dwek, P.M. Rudd, Proposal for a standard system for drawing structural diagrams of N- and O-linked carbohydrates and related compounds, *PROTEOMICS*, 9 (2009) 3796-3801.
- [29] D.J. Harvey, A.H. Merry, L. Royle, M.P. Campbell, P.M. Rudd, Symbol nomenclature for representing glycan structures: Extension to cover different carbohydrate types, *PROTEOMICS*, 11 (2011) 4291-4295.
- [30] C.R. Varki A, Esko JD, Stanley P, Hart GW, Aebi M, Darvill AG, Kinoshita T, Packer NH, Prestegard JH, Schnaar RL, Seeberger PH, *Essentials of Glycobiology* [Internet]. 3rd ed., 2015-2017.
- [31] F. Clerc, K.R. Reiding, B.C. Jansen, G.S.M. Kammeijer, A. Bondt, M. Wuhler, Human plasma protein N-glycosylation, *Glycoconjugate Journal*, 33 (2016) 309-343.
- [32] P. Burda, M. Aebi, The dolichol pathway of N-linked glycosylation, *Biochimica et Biophysica Acta (BBA) - General Subjects*, 1426 (1999) 239-257.
- [33] J. Helenius, D.T.W. Ng, C.L. Marolda, P. Walter, M.A. Valvano, M. Aebi, Translocation of lipid-linked oligosaccharides across the ER membrane requires Rft1 protein, *Nature*, 415 (2002) 447-450.

- [34] M. Aebi, N-linked protein glycosylation in the ER, *Biochimica et Biophysica Acta (BBA) - Molecular Cell Research*, 1833 (2013) 2430-2437.
- [35] U. Schubert, L.C. Antón, J. Gibbs, C.C. Norbury, J.W. Yewdell, J.R. Bennink, Rapid degradation of a large fraction of newly synthesized proteins by proteasomes, *Nature*, 404 (2000) 770-774.
- [36] T. Szul, E. Sztul, COPII and COPI Traffic at the ER-Golgi Interface, *Physiology*, 26 (2011) 348-364.
- [37] P. Stanley, H. Schachter, N. Taniguchi, N-Glycans, in: A. Varki, R.D. Cummings, J.D. Esko, H.H. Freeze, P. Stanley, C.R. Bertozzi, G.W. Hart, M.E. Etzler (Eds.) *Essentials of Glycobiology*, Cold Spring Harbor Laboratory Press
- Copyright © 2009, The Consortium of Glycobiology Editors, La Jolla, California., Cold Spring Harbor (NY), 2009.
- [38] A.V. Nairn, K. Aoki, M. dela Rosa, M. Porterfield, J.-M. Lim, M. Kulik, J.M. Pierce, L. Wells, S. Dalton, M. Tiemeyer, K.W. Moremen, Regulation of Glycan Structures in Murine Embryonic Stem Cells: COMBINED TRANSCRIPT PROFILING OF GLYCAN-RELATED GENES AND GLYCAN STRUCTURAL ANALYSIS ^{*}, *Journal of Biological Chemistry*, 287 (2012) 37835-37856.
- [39] S. Wopereis, D.J. Lefeber, E.v. Morava, R.A. Wevers, Mechanisms in Protein O-Glycan Biosynthesis and Clinical and Molecular Aspects of Protein O-Glycan Biosynthesis Defects: A Review, *Clinical Chemistry*, 52 (2006) 574-600.
- [40] P.V.d. Steen, P.M. Rudd, R.A. Dwek, G. Opdenakker, Concepts and Principles of O-Linked Glycosylation, *Critical Reviews in Biochemistry and Molecular Biology*, 33 (1998) 151-208.
- [41] K.G. Ten Hagen, T.A. Fritz, L.A. Tabak, All in the family: the UDP-GalNAc:polypeptide N-acetylgalactosaminyltransferases, *Glycobiology*, 13 (2003) 1R-16R.
- [42] N. Mitra, N. Sharon, A. Surolia, Role of N-Linked Glycan in the Unfolding Pathway of Erythrina corallodendron Lectin, *Biochemistry*, 42 (2003) 12208-12216.
- [43] N. Mitra, S. Sinha, T.N.C. Ramya, A. Surolia, *N*-linked oligosaccharides as outfitters for glycoprotein folding, form and function, *Trends in Biochemical Sciences*, 31 (2006) 156-163.
- [44] A. Helenius, How N-linked oligosaccharides affect glycoprotein folding in the endoplasmic reticulum, *Molecular Biology of the Cell*, 5 (1994) 253-265.
- [45] J.M. Herrmann, P. Malkus, R. Schekman, Out of the ER—outfitters, escorts and guides, *Trends in Cell Biology*, 9 (1999) 5-7.
- [46] M. Berger, M. Kaup, V. Blanchard, Protein Glycosylation and Its Impact on Biotechnology, in: W.S. Hu, A.-P. Zeng (Eds.) *Genomics and Systems Biology of Mammalian Cell Culture*, Springer Berlin Heidelberg, Berlin, Heidelberg, 2012, pp. 165-185.
- [47] D. Shental-Bechor, Y. Levy, Folding of glycoproteins: toward understanding the biophysics of the glycosylation code, *Current Opinion in Structural Biology*, 19 (2009) 524-533.

- [48] P.M. Rudd, A.H. Merry, M.R. Wormald, R.A. Dwek, Glycosylation and prion protein, *Current Opinion in Structural Biology*, 12 (2002) 578-586.
- [49] C. Wang, M. Eufemi, C. Turano, A. Giartosio, Influence of the Carbohydrate Moiety on the Stability of Glycoproteins, *Biochemistry*, 35 (1996) 7299-7307.
- [50] R.J. Solá, K. Griebenow, Effects of glycosylation on the stability of protein pharmaceuticals, *Journal of Pharmaceutical Sciences*, 98 (2009) 1223-1245.
- [51] H.A. van Veen, M.E.J. Geerts, P.H.C. van Berkel, J.H. Nuijens, The role of N-linked glycosylation in the protection of human and bovine lactoferrin against tryptic proteolysis, *European Journal of Biochemistry*, 271 (2004) 678-684.
- [52] E. Saxon, C.R. Bertozzi, Chemical and Biological Strategies for Engineering Cell Surface Glycosylation, *Annual Review of Cell and Developmental Biology*, 17 (2001) 1-23.
- [53] K. Ohtsubo, J.D. Marth, Glycosylation in Cellular Mechanisms of Health and Disease, *Cell*, 126 (2006) 855-867.
- [54] W.R. Alley, B.F. Mann, M.V. Novotny, High-sensitivity Analytical Approaches for the Structural Characterization of Glycoproteins, *Chemical Reviews*, 113 (2013) 2668-2732.
- [55] X. Wang, J. Gu, H. Ihara, E. Miyoshi, K. Honke, N. Taniguchi, Core Fucosylation Regulates Epidermal Growth Factor Receptor-mediated Intracellular Signaling *, *Journal of Biological Chemistry*, 281 (2006) 2572-2577.
- [56] E.A. Partridge, C.L. Roy, G.M.D. Guglielmo, J. Pawling, P. Cheung, M. Granovsky, I.R. Nabi, J.L. Wrana, J.W. Dennis, Regulation of Cytokine Receptors by Golgi N-Glycan Processing and Endocytosis, *Science*, 306 (2004) 120-124.
- [57] T. Shinkawa, K. Nakamura, N. Yamane, E. Shoji-Hosaka, Y. Kanda, M. Sakurada, K. Uchida, H. Anazawa, M. Satoh, M. Yamasaki, N. Hanai, K. Shitara, The Absence of Fucose but Not the Presence of Galactose or Bisecting *N*-Acetylglucosamine of Human IgG1 Complex-type Oligosaccharides Shows the Critical Role of Enhancing Antibody-dependent Cellular Cytotoxicity *, *Journal of Biological Chemistry*, 278 (2003) 3466-3473.
- [58] G. Walsh, R. Jefferis, Post-translational modifications in the context of therapeutic proteins, *Nature Biotechnology*, 24 (2006) 1241-1252.
- [59] C. Global Burden of Disease Cancer, J.M. Kocarnik, K. Compton, F.E. Dean, W. Fu, B.L. Gaw, J.D. Harvey, H.J. Henrikson, D. Lu, A. Pennini, R. Xu, E. Ababneh, M. Abbasi-Kangevari, H. Abbastabar, S.M. Abd-El Salam, A. Abdoli, A. Abedi, H. Abidi, H. Abolhassani, I.A. Adedeji, Q.E.S. Adnani, S.M. Advani, M.S. Afzal, M. Aghaali, B.O. Ahinkorah, S. Ahmad, T. Ahmad, A. Ahmadi, S. Ahmadi, T. Ahmed Rashid, Y. Ahmed Salih, G.T. Akalu, A. Aklilu, T. Akram, C.J. Akunna, H. Al Hamad, F. Alahdab, Z. Al-Aly, S. Ali, Y. Alimohamadi, V. Alipour, S.M. Aljunid, M. Alkhayyat, A. Almasi-Hashiani, N.A. Almasri, S.A.A. Al-Maweri, S. Almustanyir, N. Alonso, N. Alvis-Guzman, H. Amu, E.W. Anbesu, R. Ancuceanu, F. Ansari, A. Ansari-Moghaddam, M.H. Antwi, D. Anvari, A.E. Anyasodor, M. Aqeel, J. Arabloo, M. Arab-Zozani, O. Aremu, H. Ariffin, T. Aripov, M. Arshad, A. Artaman, J. Arulappan, Z. Asemi, M. Asghari Jafarabadi, T. Ashraf, P.

Atorkey, A. Aujayeb, M. Ausloos, A.F. Awedew, B.P. Ayala Quintanilla, T. Ayenew, M.A. Azab, S. Azadnajafabad, A. Azari Jafari, G. Azarian, A.Y. Azzam, A.D. Badiye, S. Bahadory, A.A. Baig, J.L. Baker, S. Balakrishnan, M. Banach, T.W. Bärnighausen, F. Barone-Adesi, F. Barra, A. Barrow, M. Behzadifar, U.I. Belgaumi, W.M.M. Bezabhe, Y.M. Bezabih, D.S. Bhagat, A.S. Bhagavathula, N. Bhardwaj, P. Bhardwaj, S. Bhaskar, K. Bhattacharyya, V.S. Bhojaraja, S. Bibi, A. Bijani, A. Biondi, C. Bisignano, T. Bjørge, A. Bleyer, O. Blyuss, O.A. Bolarinwa, S.R. Bolla, D. Braithwaite, A. Brar, H. Brenner, M.T. Bustamante-Teixeira, N.S. Butt, Z.A. Butt, F.L. Caetano Dos Santos, Y. Cao, G. Carreras, F. Catalá-López, F. Cembranel, E. Cerin, A. Cernigliaro, R.C. Chakinala, S.K. Chattu, V.K. Chattu, P. Chaturvedi, O. Chimed-Ochir, D.Y. Cho, D.J. Christopher, D.-T. Chu, M.T. Chung, J. Conde, S. Cortés, P.A. Cortesi, V.M. Costa, A.R. Cunha, O. Dadras, A.B. Dagnev, S.M.A. Dahlawi, X. Dai, L. Dandona, R. Dandona, A.M. Darwesh, J. das Neves, F.P. De la Hoz, A.B. Demis, E. Denova-Gutiérrez, D. Dhamnetiya, M.L. Dhimal, M. Dhimal, M. Dianatinasab, D. Diaz, S. Djalalinia, H.P. Do, S. Doaei, F. Dorostkar, F.W. Dos Santos Figueiredo, T.R. Driscoll, H. Ebrahimi, S. Eftekhazadeh, M. El Tantawi, H. El-Abid, I. Elbarazi, H.R. Elhabashy, M. Elhadi, S.I. El-Jaafary, B. Eshrati, S. Eskandarieh, F. Esmailzadeh, A. Etemadi, S. Ezzikouri, M. Faisaluddin, E.J.A. Faraon, J. Fares, F. Farzadfar, A.H. Feroze, S. Ferrero, L. Ferro Desideri, I. Filip, F. Fischer, J.L. Fisher, M. Foroutan, T. Fukumoto, P.A. Gaal, M.M. Gad, M.A. Gadanya, S. Gallus, M. Gaspar Fonseca, A. Getachew Obsa, M. Ghafourifard, A. Ghashghaee, N. Ghith, M. Gholamalizadeh, S.A. Gilani, T.G. Ginindza, A.T.T. Gizaw, J.C. Glasbey, M. Golechha, P. Goleij, R.S. Gomez, S.V. Gopalani, G. Gorini, H. Goudarzi, G. Grosso, M.I.M. Gubari, M.R. Guerra, A. Guha, D.S. Gunasekera, B. Gupta, V.B. Gupta, V.K. Gupta, R.A. Gutiérrez, N. Hafezi-Nejad, M.R. Haider, A. Haj-Mirzaian, R. Halwani, R.R. Hamadeh, S. Hameed, S. Hamidi, A. Hanif, S. Haque, N.I. Harlianto, J.M. Haro, A.I. Hasaballah, S. Hassanipour, R.J. Hay, S.I. Hay, K. Hayat, G. Heidari, M. Heidari, B.Y. Herrera-Serna, C. Herteliu, K. Hezam, R. Holla, M.M. Hossain, M.B.H. Hossain, M.-S. Hosseini, M. Hosseini, M. Hosseinzadeh, M. Hostiuc, S. Hostiuc, M. Househ, M. Hsairi, J. Huang, F.N. Hugo, R. Hussain, N.R. Hussein, B.-F. Hwang, I. Iavicoli, S.E. Ibitoye, F. Ida, K.S. Ikuta, O.S. Ilesanmi, I.M. Ilic, M.D. Ilic, L.M. Irham, J.Y. Islam, R.M. Islam, S.M.S. Islam, N.E. Ismail, G. Isola, M. Iwagami, L. Jacob, V. Jain, M.B. Jakovljevic, T. Javaheri, S. Jayaram, S.B. Jazayeri, R.P. Jha, J.B. Jonas, T. Joo, N. Joseph, F. Joukar, M. Jürisson, A. Kabir, D. Kahrizi, L.R. Kalankesh, R. Kalhor, F. Kaliyadan, Y. Kalkonde, A. Kamath, N. Kameran Al-Salihi, H. Kandel, N. Kapoor, A. Karch, A.S. Kasa, S.V. Katikireddi, J.H. Kauppila, T. Kavetsky, S.A. Kebede, P. Keshavarz, M. Keykhaei, Y.S. Khader, R. Khalilov, G. Khan, M. Khan, M.N. Khan, M.A.B. Khan, Y.-H. Khang, A.M. Khater, M. Khayamzadeh, G.R. Kim, Y.J. Kim, A. Kisa, S. Kisa, K. Kissimova-Skarbek, J.A. Kopec, R. Koteleswaran, P.A. Koul, S.L. Koulmane Laxminarayana, A. Koyanagi, B. Kucuk Bicer, N. Kugbey, G.A. Kumar, N. Kumar, N. Kumar, O.P. Kurmi, T. Kutluk, C. La Vecchia, F.H. Lami, I. Landires, P. Lauriola, S.-W. Lee, S.W.H. Lee, W.-C. Lee, Y.H. Lee, J. Leigh, E. Leong, J. Li, M.-C. Li, X. Liu, J.A. Loureiro, R. Lunevicius, M. Magdy Abd El Razek, A. Majeed, A. Makki, S. Male, A.A. Malik, M.A. Mansournia, S. Martini, S.Z. Masoumi, P.

Mathur, M. McKee, R. Mehrotra, W. Mendoza, R.G. Menezes, E.W. Mengesha, M.K. Mesregah, T. Mestrovic, J. Miao Jonasson, B. Miazgowski, T. Miazgowski, I.M. Michalek, T.R. Miller, H. Mirzaei, H.R. Mirzaei, S. Misra, P. Mithra, M. Moghadaszadeh, K.A. Mohammad, Y. Mohammad, M. Mohammadi, S.M. Mohammadi, A. Mohammadian-Hafshejani, S. Mohammed, N. Moka, A.H. Mokdad, M. Molokhia, L. Monasta, M.A. Moni, M.A. Moosavi, Y. Moradi, P. Moraga, J. Morgado-da-Costa, S.D. Morrison, A. Mosapour, S. Mubarik, L. Mwanri, A.J. Nagarajan, S.P. Nagaraju, C. Nagata, M.D. Naimzada, V. Nangia, A.A. Naqvi, S. Narasimha Swamy, R. Ndejjo, S.O. Nduaguba, I. Negoi, S.M. Negru, S. Neupane Kandel, C.T. Nguyen, H.L.T. Nguyen, R.K. Niazi, C.A. Nnaji, N.M. Noor, V. Nuñez-Samudio, C.I. Nzoputam, B. Oancea, C. Ochir, O.O. Odukoya, F.A. Ogbo, A.T. Olagunju, B.O. Olakunde, E. Omar, A. Omar Bali, A.E.E. Omonisi, S. Ong, O.E. Onwujekwe, H. Orru, D.V. Ortega-Altamirano, N. Otstavnov, S.S. Otstavnov, M.O. Owolabi, M. P A, J.R. Padubidri, K. Pakshir, A. Pana, D. Panagiotakos, S. Panda-Jonas, S. Pardhan, E.-C. Park, E.-K. Park, F. Pashazadeh Kan, H.K. Patel, J.R. Patel, S. Pati, S.M. Pattanshetty, U. Paudel, D.M. Pereira, R.B. Pereira, A. Perianayagam, J.D. Pillay, S. Pirouzpanah, F. Pishgar, I. Podder, M.J. Postma, H. Pourjafar, A. Prashant, L. Preotescu, M. Rabiee, N. Rabiee, A. Radfar, R.A. Radhakrishnan, V. Radhakrishnan, A. Rafiee, F. Rahim, S. Rahimzadeh, M. Rahman, M.A. Rahman, A.M. Rahmani, N. Rajai, A. Rajesh, I. Rakovac, P. Ram, K. Ramezanzadeh, K. Ranabhat, P. Ranasinghe, C.R. Rao, S.J. Rao, R. Rawassizadeh, M.S. Razeghinia, A.M.N. Renzaho, N. Rezaei, N. Rezaei, A. Rezapour, T.J. Roberts, J.A.B. Rodriguez, P. Rohloff, M. Romoli, L. Ronfani, G. Roshandel, G.M. Rwegerera, M. S, S. Sabour, B. Saddik, U. Saeed, A. Sahebkar, H. Sahoo, S. Salehi, M.R. Salem, H. Salimzadeh, M. Samaei, A.M. Samy, J. Sanabria, S. Sankararaman, M.M. Santric-Milicevic, Y. Sardiwalla, A. Sarveazad, B. Sathian, M. Sawhney, M. Saylan, I.J.C. Schneider, M. Sekerija, A. Seylani, O. Shafaat, Z. Shaghaghi, M.A. Shaikh, E. Shamsoddin, M. Shannawaz, R. Sharma, A. Sheikh, S. Sheikhbahaei, A. Shetty, J.K. Shetty, P.H. Shetty, K. Shibuya, R. Shirkoohi, K.M. Shivakumar, V. Shivarov, S. Siabani, S.K. Siddappa Malleshappa, D.A.S. Silva, J.A. Singh, Y. Sintayehu, V.Y. Skryabin, A.A. Skryabina, M.J. Soeberg, A. Sofi-Mahmudi, H. Sotoudeh, P. Steiropoulos, K. Straif, R. Subedi, M.a.B. Sufiyan, I. Sultan, S. Sultana, D. Sur, V. Szerencsés, M. Szócska, R. Tabarés-Seisdedos, T. Tabuchi, H. Tadbiri, A. Taherkhani, K. Takahashi, I.M. Talaat, K.-K. Tan, V.Y. Tat, B.A.A. Tedla, Y.G. Tefera, A. Tehrani-Banihashemi, M.-H. Temsah, F.H. Tesfay, G.A. Tessema, R. Thapar, A. Thavamani, V. Thoguluva Chandrasekar, N. Thomas, H.R. Tohidinik, M. Touvier, M.R. Tovani-Palone, E. Traini, B.X. Tran, K.B. Tran, M.T.N. Tran, J.P. Tripathy, B.S. Tusa, I. Ullah, S. Ullah, K.K. Umapathi, B. Unnikrishnan, E. Upadhyay, M. Vacante, M. Vaezi, S. Valadan Tahbaz, D.Z. Velazquez, M. Veroux, F.S. Violante, V. Vlassov, B. Vo, V. Volovici, G.T. Vu, Y. Waheed, R.G. Wamai, P. Ward, Y.F. Wen, R. Westerman, A.S. Winkler, L. Yadav, S.H. Yahyazadeh Jabbari, L. Yang, S. Yaya, T.S.Y. Yazie, Y. Yeshaw, N. Yonemoto, M.Z. Younis, Z. Yousefi, C. Yu, D. Yuce, I. Yunusa, V. Zadnik, F. Zare, M.S. Zastrozhin, A. Zastrozhina, J. Zhang, C. Zhong, L. Zhou, C. Zhu, A. Ziapour, I.R. Zimmermann, C. Fitzmaurice, C.J.L. Murray, L.M. Force, Cancer

- Incidence, Mortality, Years of Life Lost, Years Lived With Disability, and Disability-Adjusted Life Years for 29 Cancer Groups From 2010 to 2019: A Systematic Analysis for the Global Burden of Disease Study 2019, *JAMA Oncol*, 8 (2022) 420-444.
- [60] S.I. Hakomori, W.T. Murakami, Glycolipids of hamster fibroblasts and derived malignant-transformed cell lines, *Proc Natl Acad Sci U S A*, 59 (1968) 254-261.
- [61] C. Büll, T.J. Boltje, M. Wassink, A.M.A. de Graaf, F.L. van Delft, M.H. den Brok, G.J. Adema, Targeting Aberrant Sialylation in Cancer Cells Using a Fluorinated Sialic Acid Analog Impairs Adhesion, Migration, and In Vivo Tumor Growth, *Molecular Cancer Therapeutics*, 12 (2013) 1935-1946.
- [62] S. Zhang, H. Shu, K. Luo, X. Kang, Y. Zhang, H. Lu, Y. Liu, N-linked glycan changes of serum haptoglobin β chain in liver disease patients, *Molecular BioSystems*, 7 (2011) 1621-1628.
- [63] G. Yogeewaran, P.L. Salk, Metastatic Potential Is Positively Correlated with Cell Surface Sialylation of Cultured Murine Tumor Cell Lines, *Science*, 212 (1981) 1514-1516.
- [64] S.E. Baldus, T.K. Zirbes, S.P. Mönig, S. Engel, E. Monaca, K. Rafiqpoor, F.G. Hanisch, C. Hanski, J. Thiele, H. Pichlmaier, H.P. Dienes, Histopathological Subtypes and Prognosis of Gastric Cancer Are Correlated with the Expression of Mucin-Associated Sialylated Antigens: Sialosyl-Lewis^a, Sialosyl-Lewis^x and Sialosyl-Tn, *Tumor Biology*, 19 (1998) 445-453.
- [65] K.S. Goonetilleke, A.K. Siriwardena, Systematic review of carbohydrate antigen (CA 19-9) as a biochemical marker in the diagnosis of pancreatic cancer, *European Journal of Surgical Oncology (EJSO)*, 33 (2007) 266-270.
- [66] H. Shigematsu, L. Lin, T. Takahashi, M. Nomura, M. Suzuki, I.I. Wistuba, K.M. Fong, H. Lee, S. Toyooka, N. Shimizu, T. Fujisawa, Z. Feng, J.A. Roth, J. Herz, J.D. Minna, A.F. Gazdar, Clinical and Biological Features Associated With Epidermal Growth Factor Receptor Gene Mutations in Lung Cancers, *JNCI: Journal of the National Cancer Institute*, 97 (2005) 339-346.
- [67] F. Tanaka, Y. Otake, T. Nakagawa, Y. Kawano, R. Miyahara, M. Li, K. Yanagihara, K. Inui, H. Oyanagi, T. Yamada, J. Nakayama, I. Fujimoto, K. Ikenaka, H. Wada, Prognostic Significance of Polysialic Acid Expression in Resected Non-Small Cell Lung Cancer1, *Cancer Research*, 61 (2001) 1666-1670.
- [68] S.R. Stowell, T. Ju, R.D. Cummings, Protein Glycosylation in Cancer, *Annual Review of Pathology: Mechanisms of Disease*, 10 (2015) 473-510.
- [69] T.M. Block, M.A. Comunale, M. Lowman, L.F. Steel, P.R. Romano, C. Fimmel, B.C. Tennant, W.T. London, A.A. Evans, B.S. Blumberg, R.A. Dwek, T.S. Mattu, A.S. Mehta, Use of targeted glycoproteomics to identify serum glycoproteins that correlate with liver cancer in woodchucks and humans, *Proceedings of the National Academy of Sciences*, 102 (2005) 779-784.
- [70] B.A. Cobb, The history of IgG glycosylation and where we are now, *Glycobiology*, 30 (2020) 202-213.

- [71] Z. Breijyeh, R. Karaman, Comprehensive Review on Alzheimer's Disease: Causes and Treatment, *Molecules*, 25 (2020) 5789.
- [72] Y. Sato, Y. Naito, I. Grundke-Iqbal, K. Iqbal, T. Endo, Analysis of N-glycans of pathological tau: possible occurrence of aberrant processing of tau in Alzheimer's disease, *FEBS Letters*, 496 (2001) 152-160.
- [73] F. Liu, T. Zaidi, K. Iqbal, I. Grundke-Iqbal, R.K. Merkle, C.-X. Gong, Role of glycosylation in hyperphosphorylation of tau in Alzheimer's disease, *FEBS Letters*, 512 (2002) 101-106.
- [74] T. Suzuki, A. Eguchi, R. Shigefuku, S. Nagao, M. Morikawa, K. Sugimoto, M. Iwasa, Y. Takei, Accuracy of carbohydrate-deficient transferrin as a biomarker of chronic alcohol abuse during treatment for alcoholism, *Hepatology Research*, 52 (2022) 120-127.
- [75] J. Jaeken, H.G. van Eijk, C. van der Heul, L. Corbeel, R. Eeckels, E. Eggermont, Sialic acid-deficient serum and cerebrospinal fluid transferrin in a newly recognized genetic syndrome, *Clinica Chimica Acta*, 144 (1984) 245-247.
- [76] J. Verheijen, S. Tahata, T. Kozicz, P. Witters, E. Morava, Therapeutic approaches in Congenital Disorders of Glycosylation (CDG) involving N-linked glycosylation: an update, *Genetics in Medicine*, 22 (2020) 268-279.
- [77] J.P. Bergström, A. Helander, Influence of alcohol use, ethnicity, age, gender, BMI and smoking on the serum transferrin glycoform pattern: Implications for use of carbohydrate-deficient transferrin (CDT) as alcohol biomarker, *Clinica Chimica Acta*, 388 (2008) 59-67.
- [78] T. Mega, E. Lujan, A. Yoshida, Studies on the oligosaccharide chains of human alpha 1-protease inhibitor. II. Structure of oligosaccharides, *Journal of Biological Chemistry*, 255 (1980) 4057-4061.
- [79] K. Mills, P.B. Mills, P.T. Clayton, N. Mian, A.W. Johnson, B.G. Winchester, The underglycosylation of plasma α 1-antitrypsin in congenital disorders of glycosylation type I is not random, *Glycobiology*, 13 (2003) 73-85.
- [80] D.M. Krasnewich, G.D. Holt, M. Brantly, F. Skovby, J. Redwine, W.A. Gahl, Abnormal synthesis of dolichol-linked oligosaccharides in carbohydrate-deficient glycoprotein syndrome, *Glycobiology*, 5 (1995) 503-510.
- [81] C. Thiel, D. Meßner-Schmitt, G.F. Hoffmann, C. Körner, Screening for congenital disorders of glycosylation in the first weeks of life, *Journal of Inherited Metabolic Disease*, 36 (2013) 887-892.
- [82] A. Bruneel, F. Habarou, T. Stojkovic, G. Plouviez, L. Bougas, F. Guillemet, N. Brient, D. Henry, T. Dupré, S. Vuillaumier-Barrot, N. Seta, Two-dimensional electrophoresis highlights haptoglobin beta chain as an additional biomarker of congenital disorders of glycosylation, *Clinica Chimica Acta*, 470 (2017) 70-74.
- [83] N. Seta, A. Barnier, F. Hochedez, M.-A. Besnard, G. Durand, Diagnostic value of Western blotting in carbohydrate-deficient glycoprotein syndrome, *Clinica Chimica Acta*, 254 (1996) 131-140.

- [84] M.A. Sadat, S. Moir, T.W. Chun, P. Lusso, G. Kaplan, L. Wolfe, M.J. Memoli, M. He, H. Vega, L.J.Y. Kim, Y. Huang, N. Hussein, E. Nievas, R. Mitchell, M. Garofalo, A. Louie, D.C. Ireland, C. Grunes, R. Cimbro, V. Patel, G. Holzapfel, D. Salahuddin, T. Bristol, D. Adams, B.E. Marciano, M. Hegde, Y. Li, K.R. Calvo, J. Stoddard, J.S. Justement, J. Jacques, D.A.L. Priel, D. Murray, P. Sun, D.B. Kuhns, C.F. Boerkoel, J.A. Chiorini, G. Di Pasquale, D. Verthelyi, S.D. Rosenzweig, Glycosylation, hypogammaglobulinemia, and resistance to viral infections, *The New England journal of medicine*, 370 (2014) 1615-1625.
- [85] A. Bruneel, S. Cholet, V. Drouin-Garraud, M.L. Jacquemont, A. Cano, A. Megarbane, C. Ruel, D. Cheillan, T. Dupre, S. Vuillaumier-Barrot, N. Seta, F. Fenaille, Complementarity of electrophoretic, mass spectrometric, and gene sequencing techniques for the diagnosis and characterization of congenital disorders of glycosylation, *Electrophoresis*, 39 (2018) 3123-3132.
- [86] J. Chen, X. Li, A. Edmondson, G.D. Meyers, K. Izumi, A.M. Ackermann, E. Morava, C. Ficicioglu, M.J. Bennett, M. He, Increased Clinical Sensitivity and Specificity of Plasma Protein N-Glycan Profiling for Diagnosing Congenital Disorders of Glycosylation by Use of Flow Injection-Electrospray Ionization-Quadrupole Time-of-Flight Mass Spectrometry, *Clinical chemistry*, 65 (2019) 653-663.
- [87] B. Ramms, P.L.S.M. Gordts, Apolipoprotein C-III in triglyceride-rich lipoprotein metabolism, *Current Opinion in Lipidology*, 29 (2018) 171-179.
- [88] A. Bruneel, T. Robert, D.J. Lefeber, G. Benard, E. Loncle, A. Djedour, G. Durand, N. Seta, Two-dimensional gel electrophoresis of apolipoprotein C-III and other serum glycoproteins for the combined screening of human congenital disorders of O- and N-glycosylation, *PROTEOMICS – Clinical Applications*, 1 (2007) 321-324.
- [89] S.B. Harvey, Y. Zhang, J. Wilson-Grady, T. Monkkonen, G.L. Nelsestuen, R.S. Kasthuri, M.R. Verneris, T.C. Lund, E.W. Ely, G.R. Bernard, H. Zeisler, M. Homoncik, B. Jilma, T. Swan, T.A. Kellogg, O-Glycoside Biomarker of Apolipoprotein C3: Responsiveness to Obesity, Bariatric Surgery, and Therapy with Metformin, to Chronic or Severe Liver Disease and to Mortality in Severe Sepsis and Graft vs Host Disease, *Journal of Proteome Research*, 8 (2009) 603-612.
- [90] S. Nicolardi, Y.E.M. van der Burgt, I. Dragan, P.J. Hensbergen, A.M. Deelder, Identification of New Apolipoprotein-CIII Glycoforms with Ultrahigh Resolution MALDI-FTICR Mass Spectrometry of Human Sera, *Journal of Proteome Research*, 12 (2013) 2260-2268.
- [91] A. Bruneel, J. Dubail, C. Roseau, P. Prada, W. Haouari, C. Huber, T. Dupré, C. Poüs, V. Cormier-Daire, N. Seta, Serum bikunin is a biomarker of linkeropathies, *Clinica Chimica Acta*, 485 (2018) 178-180.
- [92] J.M. Ervasti, K.P. Campbell, A role for the dystrophin-glycoprotein complex as a transmembrane linker between laminin and actin, *The Journal of cell biology*, 122 (1993) 809-823.

- [93] C. Bouchet-Séraphin, S. Vuillaumier-Barrot, N. Seta, Dystroglycanopathies: About Numerous Genes Involved in Glycosylation of One Single Glycoprotein, *Journal of Neuromuscular Diseases*, 2 (2015) 27-38.
- [94] D.J. Lefeber, J. Schönberger, E. Morava, M. Guillard, K.M. Huyben, K. Verrijp, O. Grafakou, A. Evangelidou, F.W. Preijers, P. Manta, J. Yildiz, S. Grünwald, M. Spilioti, C. van den Elzen, D. Klein, D. Hess, H. Ashida, J. Hofsteenge, Y. Maeda, L. van den Heuvel, M. Lammens, L. Lehle, R.A. Wevers, Deficiency of Dol-P-Man Synthase Subunit DPM3 Bridges the Congenital Disorders of Glycosylation with the Dystroglycanopathies, *The American Journal of Human Genetics*, 85 (2009) 76-86.
- [95] J. Svahn, P. Laforêt, C. Vial, N. Streichenberger, N. Romero, C. Bouchet-Séraphin, A. Bruneel, T. Dupré, N. Seta, R. Menassa, L. Michel-Calemard, T. Stojkovic, Dilated cardiomyopathy and limb-girdle muscular dystrophy-dystroglycanopathy due to novel pathogenic variants in the DPM3 gene, *Neuromuscular Disorders*, 29 (2019) 497-502.
- [96] H. Geyer, R. Geyer, Strategies for analysis of glycoprotein glycosylation, *Biochimica et Biophysica Acta (BBA) - Proteins and Proteomics*, 1764 (2006) 1853-1869.
- [97] H. Desaire, Glycopeptide Analysis, Recent Developments and Applications *, *Molecular & Cellular Proteomics*, 12 (2013) 893-901.
- [98] L.R. Ruhaak, G. Zauner, C. Huhn, C. Bruggink, A.M. Deelder, M. Wuhrer, Glycan labeling strategies and their use in identification and quantification, *Analytical and Bioanalytical Chemistry*, 397 (2010) 3457-3481.
- [99] K. Mariño, J. Bones, J.J. Kattla, P.M. Rudd, A systematic approach to protein glycosylation analysis: a path through the maze, *Nature chemical biology*, 6 (2010) 713-723.
- [100] D. Liu, W. Tang, J.-Y. Yin, S.-P. Nie, M.-Y. Xie, Monosaccharide composition analysis of polysaccharides from natural sources: Hydrolysis condition and detection method development, *Food Hydrocolloids*, 116 (2021) 106641.
- [101] A. Bruneel, S. Cholet, V. Drouin-Garraud, M.L. Jacquemont, A. Cano, A. Mégarbané, C. Ruel, D. Cheillan, T. Dupré, S. Vuillaumier-Barrot, Complementarity of electrophoretic, mass spectrometric, and gene sequencing techniques for the diagnosis and characterization of congenital disorders of glycosylation, *Electrophoresis*, 39 (2018) 3123-3132.
- [102] A. Helander, A. Husa, J.-O. Jeppsson, Improved HPLC Method for Carbohydrate-deficient Transferrin in Serum, *Clinical Chemistry*, 49 (2003) 1881-1890.
- [103] E. Quintana, A. Navarro-Sastre, J.M. Hernández-Pérez, J. García-Villoria, R. Montero, R. Artuch, A. Ribes, P. Briones, Screening for congenital disorders of glycosylation (CDG): Transferrin HPLC versus isoelectric focusing (IEF), *Clinical Biochemistry*, 42 (2009) 408-415.
- [104] E. Quintana, R. Montero, M. Casado, A. Navarro-Sastre, M.A. Vilaseca, P. Briones, R. Artuch, Comparison between high performance liquid chromatography

- and capillary zone electrophoresis for the diagnosis of congenital disorders of glycosylation, *Journal of Chromatography B*, 877 (2009) 2513-2518.
- [105] R. Hackler, T. Arndt, T.O. Kleine, A.M. Gressner, Effect of Separation Conditions on Automated Isoelectric Focusing of Carbohydrate-Deficient Transferrin and Other Human Isotransferrins Using the PhastSystem, *Analytical Biochemistry*, 230 (1995) 281-289.
- [106] T. Rabilloud, Two-dimensional gel electrophoresis in proteomics: Old, old fashioned, but it still climbs up the mountains, *PROTEOMICS*, 2 (2002) 3-10.
- [107] H. Henry, F. Froehlich, R. Perret, J.-D. Tissot, B. Eilers-Messerli, D. Lavanchy, C. Dionisi-Vici, J.-J. Gonvers, C. Bachmann, Microheterogeneity of Serum Glycoproteins in Patients with Chronic Alcohol Abuse Compared with Carbohydrate-deficient Glycoprotein Syndrome Type I, *Clinical Chemistry*, 45 (1999) 1408-1413.
- [108] J. Joneli, U. Wanzenried, J. Schiess, C. Lanz, J. Caslavská, W. Thormann, Determination of carbohydrate-deficient transferrin in human serum by capillary zone electrophoresis: Evaluation of assay performance and quality assurance over a 10-year period in the routine arena, *ELECTROPHORESIS*, 34 (2013) 1563-1571.
- [109] H.A. Carchon, R. Chevigné, J.-B. Falmagne, J. Jaeken, Diagnosis of Congenital Disorders of Glycosylation by Capillary Zone Electrophoresis of Serum Transferrin, *Clinical Chemistry*, 50 (2004) 101-111.
- [110] H. Kingma, F. van der Sluijs, M. Heiner-Fokkema, Fast screening of N-glycosylation disorders by sialotransferrin profiling with capillary zone electrophoresis, *Annals of Clinical Biochemistry*, 55 (2018) 693-701.
- [111] M. Tobler, J. Caslavská, P. Burda, W. Thormann, High-resolution capillary zone electrophoresis for transferrin glycoform analysis associated with congenital disorders of glycosylation, *Journal of Separation Science*, 41 (2018) 2808-2818.
- [112] D.C. Frost, L. Li, Chapter Three - Recent Advances in Mass Spectrometry-Based Glycoproteomics, in: R. Donev (Ed.) *Advances in Protein Chemistry and Structural Biology*, Academic Press 2014, pp. 71-123.
- [113] S. Yamamoto, M. Kinoshita, S. Suzuki, Current landscape of protein glycosylation analysis and recent progress toward a novel paradigm of glycoscience research, *Journal of pharmaceutical and biomedical analysis*, 130 (2016) 273-300.
- [114] K. Tanaka, H. Waki, Y. Ido, S. Akita, Y. Yoshida, T. Yoshida, T. Matsuo, Protein and polymer analyses up to m/z 100 000 by laser ionization time-of-flight mass spectrometry, *Rapid Communications in Mass Spectrometry*, 2 (1988) 151-153.
- [115] F. Hillenkamp, M. Karas, R.C. Beavis, B.T. Chait, Matrix-assisted laser desorption/ionization mass spectrometry of biopolymers, *Analytical Chemistry*, 63 (1991) 1193A-1203A.
- [116] F. Hillenkamp, M. Karas, [12] Mass spectrometry of peptides and proteins by matrix-assisted ultraviolet laser desorption/ionization, *Methods in Enzymology*, Academic Press 1990, pp. 280-295.
- [117] E. Giménez, F. Benavente, J. Barbosa, V. Sanz-Nebot, Towards a reliable molecular mass determination of intact glycoproteins by matrix-assisted laser

- desorption/ionization time-of-flight mass spectrometry, *Rapid Communications in Mass Spectrometry*, 21 (2007) 2555-2563.
- [118] E. Giménez, F. Benavente, J. Barbosa, V. Sanz-Nebot, Ionic liquid matrices for MALDI-TOF-MS analysis of intact glycoproteins, *Analytical and Bioanalytical Chemistry*, 398 (2010) 357-365.
- [119] S. Yen-Nicolaÿ, C. Boursier, M. Rio, D.J. Lefeber, A. Pilon, N. Seta, A. Bruneel, MALDI-TOF MS applied to apoC-III glycoforms of patients with congenital disorders affecting O-glycosylation. Comparison with two-dimensional electrophoresis, *PROTEOMICS – Clinical Applications*, 9 (2015) 787-793.
- [120] Y. Wada, M. Kadoya, N. Okamoto, Mass spectrometry of apolipoprotein C-III, a simple analytical method for mucin-type O-glycosylation and its application to an autosomal recessive cutis laxa type-2 (ARCL2) patient, *Glycobiology*, 22 (2012) 1140-1144.
- [121] S. Nicolardi, L. Switzar, A.M. Deelder, M. Palmblad, Y.E.M. van der Burgt, Top-Down MALDI-In-Source Decay-FTICR Mass Spectrometry of Isotopically Resolved Proteins, *Analytical Chemistry*, 87 (2015) 3429-3437.
- [122] C.S. Ho, C. Lam, M. Chan, R. Cheung, L. Law, L. Lit, K. Ng, M. Suen, H. Tai, Electrospray ionisation mass spectrometry: principles and clinical applications, *The Clinical Biochemist Reviews*, 24 (2003) 3.
- [123] S. Banerjee, S. Mazumdar, Electrospray ionization mass spectrometry: a technique to access the information beyond the molecular weight of the analyte, *International journal of analytical chemistry*, 2012 (2012).
- [124] N. Abu Bakar, D.J. Lefeber, M. van Scherpenzeel, Clinical glycomics for the diagnosis of congenital disorders of glycosylation, *Journal of inherited metabolic disease*, 41 (2018) 499-513.
- [125] O. Aizpurua-Olaizola, J.S. Toraño, J.M. Falcon-Perez, C. Williams, N. Reichardt, G.-J. Boons, Mass spectrometry for glycan biomarker discovery, *TrAC Trends in Analytical Chemistry*, 100 (2018) 7-14.
- [126] A. Bruneel, F. Fenaille, Integrating mass spectrometry-based plasma (or serum) protein N-glycan profiling into the clinical practice?, *Ann Transl Med*, 7 (2019) S225-S225.
- [127] J. Etxebarria, N.-C. Reichardt, Methods for the absolute quantification of N-glycan biomarkers, *Biochimica et Biophysica Acta (BBA) - General Subjects*, 1860 (2016) 1676-1687.
- [128] H.R. Rabanes, A.M. Guidote Jr., J.P. Quirino, Capillary electrophoresis of natural products: Highlights of the last five years (2006–2010), *ELECTROPHORESIS*, 33 (2012) 180-195.
- [129] A. Guttman, L. Hajba, *Capillary Gel Electrophoresis*, 1st Edition, Elsevier 2021.
- [130] R. Freitag, *ELECTROPHORESIS | Capillary Gel Electrophoresis*, in: I.D. Wilson (Ed.) *Encyclopedia of Separation Science*, Academic Press, Oxford, 2000, pp. 1201-1208.

- [131] G. Lu, C.L. Crieffield, S. Gattu, L.M. Veltri, L.A. Holland, Capillary Electrophoresis Separations of Glycans, *Chemical Reviews*, 118 (2018) 7867-7885.
- [132] B. Reider, M. Szigeti, A. Guttman, Evaporative fluorophore labeling of carbohydrates via reductive amination, *Talanta*, 185 (2018) 365-369.
- [133] A. Guttman, F.-T.A. Chen, R.A. Evangelista, Separation of 1-aminopyrene-3,6,8-trisulfonate-labeled asparagine-linked fetuin glycans by capillary gel electrophoresis, *ELECTROPHORESIS*, 17 (1996) 412-417.
- [134] D. Sarkozy, B. Borza, A. Domokos, E. Varadi, M. Szigeti, A. Meszaros-Matwiejuk, D. Molnar-Gabor, A. Guttman, Ultrafast high-resolution analysis of human milk oligosaccharides by multicapillary gel electrophoresis, *Food Chemistry*, 341 (2021) 128200.
- [135] Á. Szekrényes, S.S. Park, M. Santos, C. Lew, A. Jones, T. Haxo, M. Kimzey, S. Pourkaveh, Z. Szabó, Z. Sosic, P. Feng, C. Váradi, F. de l'Escaille, J.-B. Falmagne, P. Sejwal, T. Niedringhaus, D. Michels, G. Freckleton, M. Hamm, A. Manuilov, M. Schwartz, J.-K. Luo, J. van Dyck, P.-K. Leung, M. Olajos, Y. Gu, K. Gao, W. Wang, J. Wegstein, S. Tep, A. Guttman, Multi-Site N-glycan mapping study 1: Capillary electrophoresis – laser induced fluorescence, *mAbs*, 8 (2016) 56-64.
- [136] Á. Szekrényes, J. Partyka, C. Varadi, J. Krenkova, F. Foret, A. Guttman, Sample Preparation for N-Glycosylation Analysis of Therapeutic Monoclonal Antibodies by Electrophoresis, in: A. Van Schepdael (Ed.) *Microchip Capillary Electrophoresis Protocols*, Springer New York, New York, NY, 2015, pp. 183-195.
- [137] S. Weiz, M. Wieczorek, C. Schwedler, M. Kaup, E.I. Braicu, J. Sehouli, R. Tauber, V. Blanchard, Acute-phase glycoprotein N-glycome of ovarian cancer patients analyzed by CE-LIF, *ELECTROPHORESIS*, 37 (2016) 1461-1467.
- [138] C. Váradi, S. Mittermayr, Á. Szekrényes, J. Kádas, L. Takacs, I. Kurucz, A. Guttman, Analysis of haptoglobin N-glycome alterations in inflammatory and malignant lung diseases by capillary electrophoresis, *ELECTROPHORESIS*, 34 (2013) 2287-2294.
- [139] Z. Kovacs, A. Simon, Z. Szabo, Z. Nagy, L. Varoczy, I. Pal, E. Csanky, A. Guttman, Capillary electrophoresis analysis of N-glycosylation changes of serum paraproteins in multiple myeloma, *Electrophoresis*, 38 (2017) 2115-2123.
- [140] M. Szigeti, C. Lew, K. Roby, A. Guttman, Fully automated sample preparation for ultrafast N-glycosylation analysis of antibody therapeutics, *Journal of Laboratory Automation*, 21 (2016) 281-286.
- [141] L.R. Ruhaak, R. Hennig, C. Huhn, M. Borowiak, R.J. Dolhain, A.M. Deelder, E. Rapp, M. Wuhrer, Optimized workflow for preparation of APTS-labeled N-glycans allowing high-throughput analysis of human plasma glycomes using 48-channel multiplexed CGE-LIF, *Journal of proteome research*, 9 (2010) 6655-6664.
- [142] L.R. Ruhaak, C.A. Koeleman, H.-W. Uh, J.C. Stam, D. van Heemst, A.B. Maier, J.J. Houwing-Duistermaat, P.J. Hensbergen, P.E. Slagboom, A.M. Deelder, Targeted biomarker discovery by high throughput glycosylation profiling of human plasma alpha1-antitrypsin and immunoglobulin A, *PloS one*, 8 (2013) e73082.

- [143] Y. Mechref, Analysis of glycans derived from glycoconjugates by capillary electrophoresis-mass spectrometry, *Electrophoresis*, 32 (2011) 3467-3481.
- [144] P. Pantůčková, P. Gebauer, P. Boček, L. Křivánková, Electrolyte systems for on-line CE-MS: Detection requirements and separation possibilities, *Electrophoresis*, 30 (2009) 203-214.
- [145] J. Zaia, *Capillary Electrophoresis-Mass Spectrometry of Carbohydrates, Capillary Electrophoresis of Biomolecules*, (2013) 13-25.
- [146] C.W. Klampfl, M. Himmelsbach, Sheath Liquids in CE-MS: Role, Parameters, and Optimization, *Capillary Electrophoresis-Mass Spectrometry (CE-MS)2016*, pp. 41-65.
- [147] C.M. Snyder, X. Zhou, J.A. Karty, B.R. Fonslow, M.V. Novotny, S.C. Jacobson, Capillary electrophoresis-mass spectrometry for direct structural identification of serum N-glycans, *Journal of chromatography A*, 1523 (2017) 127-139.
- [148] L.R. Ruhaak, A.M. Deelder, M. Wuhrer, Oligosaccharide analysis by graphitized carbon liquid chromatography-mass spectrometry, *Analytical and bioanalytical chemistry*, 394 (2009) 163-174.
- [149] M. Pabst, F. Altmann, Influence of electrosorption, solvent, temperature, and ion polarity on the performance of LC-ESI-MS using graphitic carbon for acidic oligosaccharides, *Analytical chemistry*, 80 (2008) 7534-7542.
- [150] K. Stavenhagen, D. Kolarich, M. Wuhrer, Clinical Glycomics Employing Graphitized Carbon Liquid Chromatography-Mass Spectrometry, *Chromatographia*, 78 (2015) 307-320.
- [151] G. Palmisano, M.R. Larsen, N.H. Packer, M. Thaysen-Andersen, Structural analysis of glycoprotein sialylation-part II: LC-MS based detection, *Rsc Advances*, 3 (2013) 22706-22726.
- [152] M. Pabst, F. Altmann, Glycan analysis by modern instrumental methods, *Proteomics*, 11 (2011) 631-643.
- [153] A.J. Alpert, Hydrophilic-interaction chromatography for the separation of peptides, nucleic acids and other polar compounds, *Journal of Chromatography A*, 499 (1990) 177-196.
- [154] M. Wuhrer, A.R. de Boer, A.M. Deelder, Structural glycomics using hydrophilic interaction chromatography (HILIC) with mass spectrometry, *Mass spectrometry reviews*, 28 (2009) 192-206.
- [155] I. Gudelj, P.P. Salo, I. Trbojević-Akmačić, M. Albers, D. Primorac, M. Perola, G. Lauc, Low galactosylation of IgG associates with higher risk for future diagnosis of rheumatoid arthritis during 10 years of follow-up, *Biochimica et Biophysica Acta (BBA) - Molecular Basis of Disease*, 1864 (2018) 2034-2039.
- [156] H. Deriš, D. Kifer, A. Cindrić, T. Petrović, A. Cvetko, I. Trbojević-Akmačić, I. Kolčić, O. Polašek, L. Newson, T. Spector, C. Menni, G. Lauc, Immunoglobulin G glycome composition in transition from premenopause to postmenopause, *iScience*, 25 (2022) 103897.

- [157] B. Cowper, X. Li, L. Yu, Y. Zhou, W. Fan, C. Rao, Comprehensive glycan analysis of twelve recombinant human erythropoietin preparations from manufacturers in China and Japan, *Journal of Pharmaceutical and Biomedical Analysis*, 153 (2018) 214-220.
- [158] T.Q. Shang, A. Saati, K.N. Toler, J. Mo, H. Li, T. Matlosz, X. Lin, J. Schenk, C.K. Ng, T. Duffy, Development and application of a robust N-glycan profiling method for heightened characterization of monoclonal antibodies and related glycoproteins, *Journal of pharmaceutical sciences*, 103 (2014) 1967-1978.
- [159] S. Tao, Y. Huang, B.E. Boyes, R. Orlando, Liquid chromatography-selected reaction monitoring (LC-SRM) approach for the separation and quantitation of sialylated N-glycans linkage isomers, *Analytical chemistry*, 86 (2014) 10584-10590.
- [160] L.R. Ruhaak, G. Xu, Q. Li, E. Goonatileke, C.B. Lebrilla, Mass spectrometry approaches to glycomic and glycoproteomic analyses, *Chemical reviews*, 118 (2018) 7886-7930.
- [161] M. Kinoshita, K. Yamada, Recent advances and trends in sample preparation and chemical modification for glycan analysis, *Journal of Pharmaceutical and Biomedical Analysis*, 207 (2022) 114424.
- [162] G. Zauner, R. Kozak, Protein O-glycosylation analysis *Biol. Chem*, 393 (2012) 687-708.
- [163] R.A. O'Neill, Enzymatic release of oligosaccharides from glycoproteins for chromatographic and electrophoretic analysis, *Journal of Chromatography A*, 720 (1996) 201-215.
- [164] Y. Wada, P. Azadi, C.E. Costello, A. Dell, R.A. Dwek, H. Geyer, R. Geyer, K. Kakehi, N.G. Karlsson, K. Kato, N. Kawasaki, K.-H. Khoo, S. Kim, A. Kondo, E. Lattova, Y. Mechref, E. Miyoshi, K. Nakamura, H. Narimatsu, M.V. Novotny, N.H. Packer, H. Perreault, J. Peter-Katalinić, G. Pohlentz, V.N. Reinhold, P.M. Rudd, A. Suzuki, N. Taniguchi, Comparison of the methods for profiling glycoprotein glycans—HUPO Human Disease Glycomics/Proteome Initiative multi-institutional study, *Glycobiology*, 17 (2007) 411-422.
- [165] M. Szigeti, A. Guttman, Sample preparation scale-up for deep N-glycomic analysis of human serum by capillary electrophoresis and CE-ESI-MS, *Molecular & Cellular Proteomics*, 18 (2019) 2524-2531.
- [166] B. Mészáros, G. Járvas, A. Farkas, M. Szigeti, Z. Kovács, R. Kun, M. Szabó, E. Csánky, A. Guttman, Comparative analysis of the human serum N-glycome in lung cancer, COPD and their comorbidity using capillary electrophoresis, *Journal of Chromatography B*, 1137 (2020) 121913.
- [167] Y. Wada, P. Azadi, C.E. Costello, A. Dell, R.A. Dwek, H. Geyer, R. Geyer, K. Kakehi, N.G. Karlsson, K. Kato, Comparison of the methods for profiling glycoprotein glycans—HUPO Human Disease Glycomics/Proteome Initiative multi-institutional study, *Glycobiology*, 17 (2007) 411-422.

- [168] J. Bodnar, A. Szekrenyes, M. Szigeti, G. Jarvas, J. Krenkova, F. Foret, A. Guttman, Enzymatic removal of N-glycans by PNGase F coated magnetic microparticles, *Electrophoresis*, 37 (2016) 1264-1269.
- [169] J. Kamerling, G. Gerwig, *Strategies for the structural analysis of carbohydrates*, (2007).
- [170] C. Váradi, C. Lew, A.s. Guttman, Rapid magnetic bead based sample preparation for automated and high throughput N-glycan analysis of therapeutic antibodies, *Analytical chemistry*, 86 (2014) 5682-5687.
- [171] A.L. Tarentino, A. Phelan, T.H. Plummer Jr, 2-Iminothiolane: a reagent for the introduction of sulphhydryl groups into oligosaccharides derived from asparagine-linked glycans, *Glycobiology*, 3 (1993) 279-285.
- [172] P. Jiang, F. Li, J. Ding, Development of an efficient LC-MS peptide mapping method using accelerated sample preparation for monoclonal antibodies, *Journal of Chromatography B*, 1137 (2020) 121895.
- [173] W.N. Sandoval, F. Arellano, D. Arnott, H. Raab, R. Vandlen, J.R. Lill, Rapid removal of N-linked oligosaccharides using microwave assisted enzyme catalyzed deglycosylation, *International Journal of Mass Spectrometry*, 259 (2007) 117-123.
- [174] H. Zhou, A.C. Briscoe, J.W. Froehlich, R.S. Lee, PNGase F catalyzes de-N-glycosylation in a domestic microwave, *Analytical biochemistry*, 427 (2012) 33-35.
- [175] M. Szigeti, J. Bondar, D. Gjerde, Z. Keresztessy, A. Szekrenyes, A. Guttman, Rapid N-glycan release from glycoproteins using immobilized PNGase F microcolumns, *Journal of Chromatography B*, 1032 (2016) 139-143.
- [176] J. Krenkova, A. Szekrenyes, Z. Keresztessy, F. Foret, A. Guttman, Oriented immobilization of peptide-N-glycosidase F on a monolithic support for glycosylation analysis, *Journal of Chromatography A*, 1322 (2013) 54-61.
- [177] X. Ren, H. Bai, Y. Pan, W. Tong, P. Qin, H. Yan, S. Deng, R. Zhong, W. Qin, X. Qian, A graphene oxide-based immobilized PNGase F reagent for highly efficient N-glycan release and MALDI-TOF MS profiling, *Analytical Methods*, 6 (2014) 2518-2525.
- [178] A. Kameyama, S.K. Dissanayake, W.W. Thet Tin, Rapid chemical de-N-glycosylation and derivatization for liquid chromatography of immunoglobulin N-linked glycans, *PloS one*, 13 (2018) e0196800.
- [179] X. Song, H. Ju, Y. Lasanajak, M.R. Kudelka, D.F. Smith, R.D. Cummings, Oxidative release of natural glycans for functional glycomics, *Nat Methods*, 13 (2016) 528-534.
- [180] R.A. Evangelista, M.-S. Liu, F.-T.A. Chen, Characterization of 9-aminopyrene-1, 4, 6-trisulfonate derivatized sugars by capillary electrophoresis with laser-induced fluorescence detection, *Analytical Chemistry*, 67 (1995) 2239-2245.
- [181] D.J. Harvey, Derivatization of carbohydrates for analysis by chromatography; electrophoresis and mass spectrometry, *Journal of Chromatography B*, 879 (2011) 1196-1225.
- [182] L.R. Ruhaak, E. Steenvoorden, C.A. Koeleman, A.M. Deelder, M. Wuhrer, 2-Picoline-borane: A non-toxic reducing agent for oligosaccharide labeling by reductive amination, *Proteomics*, 10 (2010) 2330-2336.

- [183] D.S. Dalpathado, H. Jiang, M.A. Kater, H. Desaire, Reductive amination of carbohydrates using NaBH (OAc) 3, *Analytical and bioanalytical chemistry*, 381 (2005) 1130-1137.
- [184] E. Maeda, S. Kita, M. Kinoshita, K. Urakami, T. Hayakawa, K. Kakehi, Analysis of nonhuman N-glycans as the minor constituents in recombinant monoclonal antibody pharmaceuticals, *Analytical chemistry*, 84 (2012) 2373-2379.
- [185] M. Yodoshi, N. Ikeda, N. Yamaguchi, M. Nagata, N. Nishida, K. Kakehi, T. Hayakawa, S. Suzuki, A novel condition for capillary electrophoretic analysis of reductively aminated saccharides without removal of excess reagents, *Electrophoresis*, 34 (2013) 3198-3205.
- [186] T. Matsumoto, S. Hatakeyama, T. Yoneyama, Y. Tobisawa, Y. Ishibashi, H. Yamamoto, T. Yoneyama, Y. Hashimoto, H. Ito, S.-I. Nishimura, C. Ohyama, Serum N-glycan profiling is a potential biomarker for castration-resistant prostate cancer, *Scientific Reports*, 9 (2019) 16761.
- [187] H. Kodama, T. Yoneyama, T. Tanaka, D. Noro, Y. Tobisawa, H. Yamamoto, S. Suto, S. Hatakeyama, K. Mori, T. Yoneyama, N-glycan signature of serum immunoglobulins as a diagnostic biomarker of urothelial carcinomas, *Cancer Medicine*, 10 (2021) 1297-1313.
- [188] C. Filep, M. Szigeti, R. Farsang, M. Habberger, D. Reusch, A. Guttman, Multilevel capillary gel electrophoresis characterization of new antibody modalities, *Analytica Chimica Acta*, 1166 (2021) 338492.
- [189] J. Kieleczawa, DNA sequencing. . Vol. 2, Vol. 2, Jones and Bartlett Publishers, Sudbury, Mass., 2006.
- [190] Y.Q. Yu, M. Gilar, J. Kaska, J.C. Gebler, A rapid sample preparation method for mass spectrometric characterization of N-linked glycans, *Rapid Communications in Mass Spectrometry: An International Journal Devoted to the Rapid Dissemination of Up-to-the-Minute Research in Mass Spectrometry*, 19 (2005) 2331-2336.
- [191] Y.Q. Yu, J. Fournier, M. Gilar, J.C. Gebler, Identification of N-linked glycosylation sites using glycoprotein digestion with pronase prior to MALDI tandem time-of-flight mass spectrometry, *Analytical chemistry*, 79 (2007) 1731-1738.
- [192] C.C. Nwosu, R.R. Seipert, J.S. Strum, S.S. Hua, H.J. An, A.M. Zivkovic, B.J. German, C.B. Lebrilla, Simultaneous and extensive site-specific N-and O-glycosylation analysis in protein mixtures, *Journal of proteome research*, 10 (2011) 2612-2624.
- [193] C. Wang, W. Fan, P. Zhang, Z. Wang, L. Huang, One-pot nonreductive O-glycan release and labeling with 1-phenyl-3-methyl-5-pyrazolone followed by ESI-MS analysis, *Proteomics*, 11 (2011) 4229-4242.
- [194] M. Yodoshi, T. Ikuta, Y. Mouri, S. Suzuki, Specific extraction of sialic-acid-containing glycans and glycopeptides using serotonin-bonded silica, *Analytical Sciences*, 26 (2010) 75-81.
- [195] R. Naka, S. Kamoda, A. Ishizuka, M. Kinoshita, K. Kakehi, Analysis of total N-glycans in cell membrane fractions of cancer cells using a combination of serotonin

- affinity chromatography and normal phase chromatography, *Journal of proteome research*, 5 (2006) 88-97.
- [196] M.R. Larsen, S.S. Jensen, L.A. Jakobsen, N.H. Heegaard, Exploring the sialome using titanium dioxide chromatography and mass spectrometry, *Molecular & cellular proteomics*, 6 (2007) 1778-1787.
- [197] S. Kamoda, M. Nakano, R. Ishikawa, S. Suzuki, K. Kakehi, Rapid and sensitive screening of N-glycans as 9-fluorenylmethyl derivatives by high-performance liquid chromatography: a method which can recover free oligosaccharides after analysis, *Journal of Proteome Research*, 4 (2005) 146-152.
- [198] M. Kinoshita, Y. Nakatani, K. Yamada, S. Yamamoto, S. Suzuki, A rapid and facile preparation of APTS-labeled N-glycans by combination of ion pair-assisted extraction and HILIC-SPE for routine glycan analysis, *Journal of Pharmaceutical and Biomedical Analysis*, 195 (2021) 113875.
- [199] U. Aich, A. Liu, J. Lakub, J. Mozdzanowski, M. Byrne, N. Shah, S. Galosy, P. Patel, N. Bam, An integrated solution-based rapid sample preparation procedure for the analysis of N-glycans from therapeutic monoclonal antibodies, *Journal of Pharmaceutical Sciences*, 105 (2016) 1221-1232.
- [200] J.-i. Furukawa, Y. Shinohara, H. Kuramoto, Y. Miura, H. Shimaoka, M. Kurogochi, M. Nakano, S.-I. Nishimura, Comprehensive approach to structural and functional glycomics based on chemoselective glycoblotting and sequential tag conversion, *Analytical Chemistry*, 80 (2008) 1094-1101.
- [201] B.B. VanOrman, G.G. Liversidge, G.L. McIntire, T.M. Olefirowicz, A.G. Ewing, Effects of buffer composition on electroosmotic flow in capillary electrophoresis, *Journal of Microcolumn Separations*, 2 (1990) 176-180.
- [202] G. Jarvas, M. Szigeti, J. Chapman, A. Guttman, Triple-internal standard based glycan structural assignment method for capillary electrophoresis analysis of carbohydrates, *Analytical chemistry*, 88 (2016) 11364-11367.
- [203] G. Jarvas, M. Szigeti, A. Guttman, GUcal: An integrated application for capillary electrophoresis based glycan analysis, *Electrophoresis*, 36 (2015) 3094-3096.
- [204] M.P. Campbell, L. Royle, C.M. Radcliffe, R.A. Dwek, P.M. Rudd, GlycoBase and autoGU: tools for HPLC-based glycan analysis, *Bioinformatics (Oxford, England)*, 24 (2008) 1214-1216.
- [205] S. Zhao, I. Walsh, J.L. Abrahams, L. Royle, T. Nguyen-Khuong, D. Spencer, D.L. Fernandes, N.H. Packer, P.M. Rudd, M.P. Campbell, GlycoStore: a database of retention properties for glycan analysis, *Bioinformatics (Oxford, England)*, 34 (2018) 3231-3232.
- [206] C.A. Cooper, M.J. Harrison, M.R. Wilkins, N.H. Packer, GlycoSuiteDB: a new curated relational database of glycoprotein glycan structures and their biological sources, *Nucleic acids research*, 29 (2001) 332-335.
- [207] S. Mittermayr, A. Guttman, Influence of molecular configuration and conformation on the electromigration of oligosaccharides in narrow bore capillaries, *Electrophoresis*, 33 (2012) 1000-1007.

- [208] M. Kinoshita, K. Kakehi, Capillary-based lectin affinity electrophoresis for interaction analysis between lectins and glycans, *Lectins*, Springer2014, pp. 131-146.
- [209] K. Yamashita, T. Ohkura, Determination of glycan motifs using serial lectin affinity chromatography, *Lectins*, Springer2014, pp. 79-92.
- [210] E.K. Sackmann, A.L. Fulton, D.J. Beebe, The present and future role of microfluidics in biomedical research, *Nature*, 507 (2014) 181-189.
- [211] U. Aich, J. Lakub, A. Liu, State-of-the-art technologies for rapid and high-throughput sample preparation and analysis of N-glycans from antibodies, *Electrophoresis*, 37 (2016) 1468-1488.
- [212] S. Sohrabi, M.K. Moraveji, Droplet microfluidics: Fundamentals and its advanced applications, *RSC advances*, 10 (2020) 27560-27574.
- [213] P. Tabeling, *Introduction to microfluidics*, Oxford University Press on Demand2005.
- [214] L. Shang, Y. Cheng, Y. Zhao, Emerging droplet microfluidics, *Chemical reviews*, 117 (2017) 7964-8040.
- [215] H.N. Joensson, H. Andersson Svahn, Droplet microfluidics—A tool for single-cell analysis, *Angewandte Chemie International Edition*, 51 (2012) 12176-12192.
- [216] H. Yin, D. Marshall, Microfluidics for single cell analysis, *Current opinion in biotechnology*, 23 (2012) 110-119.
- [217] O. Reynolds, XXIX. An experimental investigation of the circumstances which determine whether the motion of water shall be direct or sinuous, and of the law of resistance in parallel channels, *Philosophical Transactions of the Royal society of London*, (1883) 935-982.
- [218] J. Cottet, P. Renaud, Chapter 1 - Introduction to microfluidics, in: E. Chappel (Ed.) *Drug Delivery Devices and Therapeutic Systems*, Academic Press2021, pp. 3-17.
- [219] Y.K. Suh, S. Kang, A Review on Mixing in Microfluidics, *Micromachines*, 1 (2010) 82-111.
- [220] K. Ward, Z.H. Fan, Mixing in microfluidic devices and enhancement methods, *Journal of Micromechanics and Microengineering*, 25 (2015) 094001.
- [221] S. Preetam, B.K. Nahak, S. Patra, D.C. Toncu, S. Park, M. Syväjärvi, G. Orive, A. Tiwari, Emergence of microfluidics for next generation biomedical devices, *Biosensors and Bioelectronics: X*, (2022) 100106.
- [222] Y.-J. Juang, Y.-J. Chiu, Fabrication of Polymer Microfluidics: An Overview, *Polymers*, 14 (2022) 2028.
- [223] O. Sartipzadeh, S.M. Naghib, A. Seyfoori, M. Rahmanian, F.S. Fateminia, Controllable size and form of droplets in microfluidic-assisted devices: Effects of channel geometry and fluid velocity on droplet size, *Materials Science and Engineering: C*, 109 (2020) 110606.
- [224] J. Yao, F. Lin, H.S. Kim, J. Park, The effect of oil viscosity on droplet generation rate and droplet size in a T-junction microfluidic droplet generator, *Micromachines*, 10 (2019) 808.

- [225] M.Y.A. Jamalabadi, M. DaqiqShirazi, A. Kosar, M.S. Shadloo, Effect of injection angle, density ratio, and viscosity on droplet formation in a microfluidic T-junction, *Theoretical and Applied Mechanics Letters*, 7 (2017) 243-251.
- [226] C.N. Baroud, F. Gallaire, R. Dangla, Dynamics of microfluidic droplets, *Lab on a Chip*, 10 (2010) 2032-2045.
- [227] P. Zhu, L. Wang, Passive and active droplet generation with microfluidics: a review, *Lab on a Chip*, 17 (2017) 34-75.
- [228] F.P. Bretherton, The motion of long bubbles in tubes, *Journal of Fluid Mechanics*, 10 (1961) 166-188.
- [229] L. Schwartz, H. Princen, A. Kiss, On the motion of bubbles in capillary tubes, *Journal of Fluid Mechanics*, 172 (1986) 259-275.
- [230] D. Reinelt, P. Saffman, The penetration of a finger into a viscous fluid in a channel and tube, *SIAM Journal on Scientific and Statistical Computing*, 6 (1985) 542-561.
- [231] A.L. Hazel, M. Heil, The steady propagation of a semi-infinite bubble into a tube of elliptical or rectangular cross-section, *Journal of fluid mechanics*, 470 (2002) 91-114.
- [232] H. Wong, C. Radke, S. Morris, The motion of long bubbles in polygonal capillaries. Part 2. Drag, fluid pressure and fluid flow, *Journal of Fluid Mechanics*, 292 (1995) 95-110.
- [233] F. Sarrazin, T. Bonometti, L. Prat, C. Gourdon, J. Magnaudet, Hydrodynamic structures of droplets engineered in rectangular micro-channels, *Microfluidics and Nanofluidics*, 5 (2008) 131-137.
- [234] J. Boussinesq, Mémoire sur l'influence des frottements dans les mouvements réguliers des fluids, *Journal de mathématiques pures et appliquées*, 13 (1868) 377-424.
- [235] H. Song, J.D. Tice, R.F. Ismagilov, A microfluidic system for controlling reaction networks in time, *Angewandte Chemie*, 115 (2003) 792-796.
- [236] M.L. Cordero, H.O. Rolfsnes, D.R. Burnham, P.A. Campbell, D. McGloin, C.N. Baroud, Mixing via thermocapillary generation of flow patterns inside a microfluidic drop, *New Journal of Physics*, 11 (2009) 075033.
- [237] A. Günther, M. Jhunjhunwala, M. Thalmann, M.A. Schmidt, K.F. Jensen, Micromixing of miscible liquids in segmented gas- liquid flow, *Langmuir*, 21 (2005) 1547-1555.
- [238] N. Bremond, A.R. Thiam, J. Bibette, Decompressing emulsion droplets favors coalescence, *Physical review letters*, 100 (2008) 024501.
- [239] C. Priest, S. Herminghaus, R. Seemann, Controlled electrocoalescence in microfluidics: Targeting a single lamella, *Applied Physics Letters*, 89 (2006) 134101.
- [240] E. Verneuil, M.a. Cordero, F. Gallaire, C.N. Baroud, Laser-induced force on a microfluidic drop: origin and magnitude, *Langmuir*, 25 (2009) 5127-5134.
- [241] D. Link, S.L. Anna, D. Weitz, H. Stone, Geometrically mediated breakup of drops in microfluidic devices, *Physical review letters*, 92 (2004) 054503.

- [242] Y. Chen, W. Gao, C. Zhang, Y. Zhao, Three-dimensional splitting microfluidics, *Lab on a Chip*, 16 (2016) 1332-1339.
- [243] J.H. Jung, G. Destgeer, B. Ha, J. Park, H.J. Sung, On-demand droplet splitting using surface acoustic waves, *Lab on a Chip*, 16 (2016) 3235-3243.
- [244] L. Mazutis, A.D. Griffiths, Preparation of monodisperse emulsions by hydrodynamic size fractionation, *Applied Physics Letters*, 95 (2009) 204103.
- [245] K. Ahn, C. Kerbage, T.P. Hunt, R. Westervelt, D.R. Link, D.A. Weitz, Dielectrophoretic manipulation of drops for high-speed microfluidic sorting devices, *Applied Physics Letters*, 88 (2006) 024104.
- [246] J.-Y. Kim, S.-W. Cho, D.-K. Kang, J.B. Edel, S.-I. Chang, A.J. deMello, D. O'Hare, Lab-chip HPLC with integrated droplet-based microfluidics for separation and high frequency compartmentalisation, *Chemical Communications*, 48 (2012) 9144-9146.
- [247] A.B. Theberge, G. Whyte, W.T. Huck, Generation of picoliter droplets with defined contents and concentration gradients from the separation of chemical mixtures, *Analytical chemistry*, 82 (2010) 3449-3453.
- [248] F. Pereira, X. Niu, A.J. deMello, A nano LC-MALDI mass spectrometry droplet interface for the analysis of complex protein samples, *PLoS One*, 8 (2013) e63087.
- [249] J. Ji, L. Nie, L. Qiao, Y. Li, L. Guo, B. Liu, P. Yang, H.H. Girault, Proteolysis in microfluidic droplets: an approach to interface protein separation and peptide mass spectrometry, *Lab on a Chip*, 12 (2012) 2625-2629.
- [250] A. Ochoa, E. Álvarez-Bohórquez, E. Castellero, L.F. Olguin, Detection of Enzyme Inhibitors in Crude Natural Extracts Using Droplet-Based Microfluidics Coupled to HPLC, *Analytical Chemistry*, 89 (2017) 4889-4896.
- [251] Q. Li, J. Pei, P. Song, R.T. Kennedy, Fraction collection from capillary liquid chromatography and off-line electrospray ionization mass spectrometry using oil segmented flow, *Analytical chemistry*, 82 (2010) 5260-5267.
- [252] R.F. Gerhardt, A.J. Peretzki, S.K. Piendl, D. Belder, Seamless combination of high-pressure chip-HPLC and droplet microfluidics on an integrated microfluidic glass chip, *Analytical chemistry*, 89 (2017) 13030-13037.
- [253] A.J. Peretzki, D. Belder, On-chip integration of normal phase high-performance liquid chromatography and droplet microfluidics introducing ethylene glycol as polar continuous phase for the compartmentalization of n-heptane eluents, *Journal of Chromatography A*, 1612 (2020) 460653.
- [254] S.K. Piendl, T. Schönfelder, M. Polack, L. Weigelt, T. van der Zwaag, T. Teutenberg, E. Beckert, D. Belder, Integration of segmented microflow chemistry and online HPLC/MS analysis on a microfluidic chip system enabling enantioselective analyses at the nanoliter scale, *Lab on a Chip*, 21 (2021) 2614-2624.
- [255] S. Sun, R.T. Kennedy, Droplet electrospray ionization mass spectrometry for high throughput screening for enzyme inhibitors, *Analytical chemistry*, 86 (2014) 9309-9314.
- [256] X.W. Diefenbach, I. Farasat, E.D. Guetschow, C.J. Welch, R.T. Kennedy, S. Sun, J.C. Moore, Enabling Biocatalysis by High-Throughput Protein Engineering Using

- Droplet Microfluidics Coupled to Mass Spectrometry, *ACS Omega*, 3 (2018) 1498-1508.
- [257] D.J. Steyer, R.T. Kennedy, High-Throughput Nanoelectrospray Ionization-Mass Spectrometry Analysis of Microfluidic Droplet Samples, *Analytical Chemistry*, 91 (2019) 6645-6651.
- [258] D.A. Holland-Moritz, M.K. Wismer, B.F. Mann, I. Farasat, P. Devine, E.D. Guetschow, I. Mangion, C.J. Welch, J.C. Moore, S. Sun, Mass Activated Droplet Sorting (MADS) Enables High-Throughput Screening of Enzymatic Reactions at Nanoliter Scale, *Angewandte Chemie International Edition*, 59 (2020) 4470-4477.
- [259] D. Haidas, M. Napiorkowska, S. Schmitt, P.S. Dittrich, Parallel sampling of nanoliter droplet arrays for noninvasive protein analysis in discrete yeast cultivations by MALDI-MS, *Analytical chemistry*, 92 (2020) 3810-3818.
- [260] S.K. Küster, M. Pabst, K. Jefimovs, R. Zenobi, P.S. Dittrich, High-Resolution Droplet-Based Fractionation of Nano-LC Separations onto Microarrays for MALDI-MS Analysis, *Analytical Chemistry*, 86 (2014) 4848-4855.
- [261] P. Elmer, Rapid Analysis of N-Glycans on the LabChip GXII Touch Microchip-CE Platform, 2019.
- [262] J.N. Arnold, M.R. Wormald, R.B. Sim, P.M. Rudd, R.A. Dwek, The impact of glycosylation on the biological function and structure of human immunoglobulins, *Annual review of immunology*, 25 (2007) 21-50.
- [263] T. Liénard, B. Yang, N.T. Tran, A. Bruneel, A. Guttman, M. Taverna, T.D. Mai, High sensitivity capillary electrophoresis with fluorescent detection for glycan mapping, *Journal of Chromatography A*, 1657 (2021) 462593.
- [264] M.A. Bynum, H. Yin, K. Felts, Y.M. Lee, C.R. Monell, K. Killeen, Characterization of IgG N-glycans employing a microfluidic chip that integrates glycan cleavage, sample purification, LC separation, and MS detection, *Analytical chemistry*, 81 (2009) 8818-8825.
- [265] S. Mohammed, K. Kraiczek, M.W. Pinkse, S. Lemeer, J.J. Benschop, A.J. Heck, Chip-Based Enrichment and NanoLC-MS/MS Analysis of Phosphopeptides from Whole Lysates, *Journal of proteome research*, 7 (2008) 1565-1571.
- [266] W.R. Alley Jr, M. Madera, Y. Mechref, M.V. Novotny, Chip-based reversed-phase liquid chromatography- mass spectrometry of permethylated N-linked glycans: a potential methodology for cancer-biomarker discovery, *Analytical chemistry*, 82 (2010) 5095-5106.
- [267] S. Hua, H.J. An, S. Ozcan, G.S. Ro, S. Soares, R. DeVere-White, C.B. Lebrilla, Comprehensive native glycan profiling with isomer separation and quantitation for the discovery of cancer biomarkers, *Analyst*, 136 (2011) 3663-3671.
- [268] C.S. Chu, M.R. Niñonuevo, B.H. Clowers, P.D. Perkins, H.J. An, H. Yin, K. Killeen, S. Miyamoto, R. Grimm, C.B. Lebrilla, Profile of native N-linked glycan structures from human serum using high performance liquid chromatography on a microfluidic chip and time-of-flight mass spectrometry, *Proteomics*, 9 (2009) 1939-1951.

- [269] C.C. Nwosu, D.L. Aldredge, H. Lee, L.A. Lerno, A.M. Zivkovic, J.B. German, C.B. Lebrilla, Comparison of the human and bovine milk N-glycome via high-performance microfluidic chip liquid chromatography and tandem mass spectrometry, *Journal of proteome research*, 11 (2012) 2912-2924.
- [270] H. Yin, K. Killeen, The fundamental aspects and applications of Agilent HPLC-Chip, *Journal of separation science*, 30 (2007) 1427-1434.
- [271] S. Yang, S. Toghi Eshghi, H. Chiu, D.L. DeVoe, H. Zhang, Glycomic analysis by glycoprotein immobilization for glycan extraction and liquid chromatography on microfluidic chip, *Analytical chemistry*, 85 (2013) 10117-10125.
- [272] Y. Wu, Y. Zhang, W. Li, Y. Xu, Y. Liu, X. Liu, Y. Xu, W. Liu, Flowing on-line preparation of deglycosylation, labeling and purification for N-glycan analysis, *Talanta*, (2022) 123652.
- [273] A.K. Palm, M.V. Novotny, A monolithic PNGase F enzyme microreactor enabling glycan mass mapping of glycoproteins by mass spectrometry, *Rapid Communications in Mass Spectrometry: An International Journal Devoted to the Rapid Dissemination of Up-to-the-Minute Research in Mass Spectrometry*, 19 (2005) 1730-1738.
- [274] J. Krenkova, N.A. Lacher, F. Svec, Multidimensional system enabling deglycosylation of proteins using a capillary reactor with peptide-N-glycosidase F immobilized on a porous polymer monolith and hydrophilic interaction liquid chromatography–mass spectrometry of glycans, *Journal of Chromatography A*, 1216 (2009) 3252-3259.
- [275] Y. Wu, Q. Sha, J. Du, C. Wang, L. Zhang, B.-F. Liu, Y. Lin, X. Liu, Determination of N-glycans by high performance liquid chromatography using 6-aminoquinolyl-N-hydroxysuccinimidyl carbamate as the glycosylamine labeling reagent, *Journal of Chromatography A*, 1535 (2018) 114-122.
- [276] M. Serra, D. Ferraro, I. Pereiro, J.-L. Viovy, S. Descroix, The power of solid supports in multiphase and droplet-based microfluidics: towards clinical applications, *Lab on a Chip*, 17 (2017) 3979-3999.
- [277] C. Lim, Y. Zhang, Bead-based microfluidic immunoassays: the next generation, *Biosensors and Bioelectronics*, 22 (2007) 1197-1204.
- [278] M.F. Elshal, J.P. McCoy, Multiplex bead array assays: performance evaluation and comparison of sensitivity to ELISA, *Methods*, 38 (2006) 317-323.
- [279] M. Shikida, K. Takayanagi, K. Inouchi, H. Honda, K. Sato, Using wettability and interfacial tension to handle droplets of magnetic beads in a micro-chemical-analysis system, *Sensors and Actuators B: Chemical*, 113 (2006) 563-569.
- [280] E. Al-Hetlani, O.J. Hatt, M. Vojtišek, M.D. Tarn, A. Iles, N. Pamme, Sorting and manipulation of magnetic droplets in continuous flow, *AIP Conference Proceedings*, American Institute of Physics, 2010, pp. 167-175.
- [281] D. Lombardi, P.S. Dittrich, Droplet microfluidics with magnetic beads: a new tool to investigate drug–protein interactions, *Analytical and bioanalytical chemistry*, 399 (2011) 347-352.

- [282] X. Pan, S. Zeng, Q. Zhang, B. Lin, J. Qin, Sequential microfluidic droplet processing for rapid DNA extraction, *Electrophoresis*, 32 (2011) 3399-3405.
- [283] R. Gao, Z. Cheng, A.J. deMello, J. Choo, Wash-free magnetic immunoassay of the PSA cancer marker using SERS and droplet microfluidics, *Lab on a Chip*, 16 (2016) 1022-1029.
- [284] H. Lee, L. Xu, K.W. Oh, Droplet-based microfluidic washing module for magnetic particle-based assays, *Biomicrofluidics*, 8 (2014) 044113.
- [285] E. Brouzes, T. Kruse, R. Kimmerling, H.H. Strey, Rapid and continuous magnetic separation in droplet microfluidic devices, *Lab on a Chip*, 15 (2015) 908-919.
- [286] B. Verbruggen, K. Leirs, R. Puers, J. Lammertyn, Selective DNA extraction with microparticles in segmented flow, *Microfluidics and Nanofluidics*, 18 (2015) 293-303.
- [287] B. Verbruggen, T. Tóth, M. Cornaglia, R. Puers, M.A. Gijs, J. Lammertyn, Separation of magnetic microparticles in segmented flow using asymmetric splitting regimes, *Microfluidics and Nanofluidics*, 18 (2015) 91-102.
- [288] A. Ali-Cherif, S. Begolo, S. Descroix, J.L. Viovy, L. Malaquin, Programmable Magnetic Tweezers and Droplet Microfluidic Device for High-Throughput Nanoliter Multi-Step Assays, *Angewandte Chemie*, 124 (2012) 10923-10927.
- [289] D. Ferraro, J. Champ, B. Teste, M. Serra, L. Malaquin, J.L. Viovy, P. de Cremoux, S. Descroix, Microfluidic platform combining droplets and magnetic tweezers: application to HER2 expression in cancer diagnosis, *Sci. Rep.*, 6 (2016).
- [290] T.D. Mai, D. Ferraro, N. Aboud, R. Renault, M. Serra, N.T. Tran, J.-L. Viovy, C. Smadja, S. Descroix, M. Taverna, Single-step immunoassays and microfluidic droplet operation: Towards a versatile approach for detection of amyloid- β peptide-based biomarkers of Alzheimer's disease, *Sens. Actuators B*, 255 (2018) 2126-2135.
- [291] S. Dumas, M. Richerd, M. Serra, S. Descroix, Magnetic Microtweezers: A Tool for High-Throughput Bioseparation in Sub-Nanoliter Droplets, *Advanced Materials Technologies*, (2022) 2200747.
- [292] K. Swinney, D.J. Bornhop, Detection in capillary electrophoresis, *ELECTROPHORESIS: An International Journal*, 21 (2000) 1239-1250.
- [293] M.G. Khaledi, High performance capillary electrophoresis, John Wiley & Sons, Inc., New York, 146 (1998) 303-401.
- [294] S. Mittermayr, J. Bones, A. Guttman, Unraveling the Glyco-Puzzle: Glycan Structure Identification by Capillary Electrophoresis, *Analytical Chemistry*, 85 (2013) 4228-4238.
- [295] S.L. Simpson Jr, J.P. Quirino, S. Terabe, On-line sample preconcentration in capillary electrophoresis: Fundamentals and applications, *Journal of Chromatography A*, 1184 (2008) 504-541.
- [296] E. Fukushima, Y. Yagi, S. Yamamoto, Y. Nakatani, K. Kakehi, T. Hayakawa, S. Suzuki, Partial filling affinity capillary electrophoresis using large-volume sample stacking with an electroosmotic flow pump for sensitive profiling of glycoprotein-derived oligosaccharides, *Journal of Chromatography A*, 1246 (2012) 84-89.

- [297] T. Kawai, M. Watanabe, K. Sueyoshi, F. Kitagawa, K. Otsuka, Highly sensitive oligosaccharide analysis in capillary electrophoresis using large-volume sample stacking with an electroosmotic flow pump, *Journal of chromatography A*, 1232 (2012) 52-58.
- [298] T. Kawai, M. Ueda, Y. Fukushima, K. Sueyoshi, F. Kitagawa, K. Otsuka, Toward 10 000-fold sensitivity improvement of oligosaccharides in capillary electrophoresis using large-volume sample stacking with an electroosmotic flow pump combined with field-amplified sample injection, *ELECTROPHORESIS*, 34 (2013) 2303-2310.
- [299] T. Kawai, N. Ota, A. Imasato, Y. Shirasaki, K. Otsuka, Y. Tanaka, Profiling of N-linked glycans from 100 cells by capillary electrophoresis with large-volume dual preconcentration by isotachopheresis and stacking, *Journal of Chromatography A*, 1565 (2018) 138-144.
- [300] F. Kitagawa, T. Kawai, K. Otsuka, On-line Sample Preconcentration by Large-volume Sample Stacking with an Electroosmotic Flow Pump (LVSEP) in Microscale Electrophoresis, *Analytical Sciences*, 29 (2013) 1129-1139.
- [301] C.d. Crosnier de Lassichère, T.D. Mai, M. Otto, M. Taverna, Online preconcentration in capillaries by multiple large-volume sample stacking: an alternative to immunoassays for quantification of amyloid beta peptides biomarkers in cerebrospinal fluid, *Analytical chemistry*, 90 (2018) 2555-2563.
- [302] P.L. Urban, Universal electronics for miniature and automated chemical assays, *Analyst*, 140 (2015) 963-975.
- [303] J.M. Pearce, Open-source lab: how to build your own hardware and reduce research costs, *Newnes*2013.
- [304] J. Sáiz, I.J. Koenka, C. García-Ruiz, B. Müller, T. Chwalek, P.C. Hauser, Microinjector for capillary electrophoresis, *Electrophoresis*, 36 (2015) 1941-1944.
- [305] J. Wang, P. Cai, J. Mo, Z. Chen, A Sample Introduction Method Based on Negative Pressure in Flow Injection-Capillary Electrophoresis System and Its Application to the Alkaline-Earth Metal Cation Separation, *Analytical letters*, 38 (2005) 857-867.
- [306] P. Kubán, Engström, A. Olsson, J.C. Thorsén, G. et al, *Anal. Chim. Acta*, 337 (1997) 117-124.
- [307] Z.-L. Fang, Z.-S. Liu, Q. Shen, Combination of flow injection with capillary electrophoresis. Part I. The basic system, *Analytica chimica acta*, 346 (1997) 135-143.
- [308] C.-H. Wu, L. Scampavia, J. Ruzicka, Microsequential injection: anion separations using 'Lab-on-Valve' coupled with capillary electrophoresis, *Analyst*, 127 (2002) 898-905.
- [309] D. Xiao, S. Zhao, H. Yuan, X. Yang, CE detector based on light-emitting diodes, *Electrophoresis*, 28 (2007) 233-242.
- [310] D. Xiao, L. Yan, H. Yuan, S. Zhao, X. Yang, M.M. Choi, CE with LED-based detection: An update, *Electrophoresis*, 30 (2009) 189-202.
- [311] O. Cybulski, S. Jakiela, P. Garstecki, Whole Teflon valves for handling droplets, *Lab on a Chip*, 16 (2016) 2198-2210.

[312] D. Ferraro, M. Serra, I. Ferrante, J.-L. Viowy, S. Descroix, Microfluidic valve with zero dead volume and negligible back-flow for droplets handling, *Sensors and Actuators B: Chemical*, 258 (2018) 1051-1059.

[313] T.D. Mai, S. Schmid, B. Müller, P.C. Hauser, Capillary electrophoresis with contactless conductivity detection coupled to a sequential injection analysis manifold for extended automated monitoring applications, *Analytica Chimica Acta*, 665 (2010) 1-6.